

**Dynamics of Crop Production and Greenhouse Gas Balance in a Changing Environment:
Data-Driven Systems Approach for Sustainable Agriculture in the United States**

by

Yongfa You

A dissertation submitted to the Graduate Faculty of
Auburn University
in partial fulfillment of the
requirements for the Degree of
Doctor of Philosophy

Auburn, Alabama
December 9, 2023

Keywords: Crop production, Greenhouse gas emission, Climate change, Climate-smart
agriculture practice, Dynamic Land Ecosystem Model, Sustainable agriculture

Copyright 2023 by Yongfa You

Approved by

Shufen Pan, Chair, Associate Professor of College of Forestry, Wildlife and Environment
Hanqin Tian, Co-Chair, Solon Dixon Professor of College of Forestry, Wildlife and Environment
William D. Batchelor, Professor of Biosystems Engineering Department
Stephen A. Prior, Lead Scientist and Plant Physiologist of USDA-ARS

Abstract

Contemporary agriculture faces multiple pressing challenges, particularly feeding a growing world population and mitigating climate change. During the past several decades, climate change has significantly impacted crop growth and production, undermining the resilience of food systems. Concurrently, management activities such as nitrogen fertilization and intensive tillage have in turn contributed to climate change through increased greenhouse gas (GHG) emissions. To address these challenges and promote sustainable agriculture, it is imperative to understand how historical climate change and human management activities have influenced crop production and agricultural GHG emissions, and the extent to which climate-smart agriculture (CSA) practices can help reduce net soil GHG emissions without compromising crop production. This dissertation delves into these aspects, employing a data-driven systems approach to quantify the impacts of multiple environmental forcings (e.g., climate change, atmospheric CO₂ concentration, and nitrogen deposition) and agricultural management practices (e.g., nitrogen fertilization, tillage, rotation, and cover cropping) on the magnitude and spatiotemporal variations of crop production, net GHG balance, and net GHG emissions intensity (GHGI, defined as net soil GHGs emissions per unit of crop production) in U.S. croplands under both historical and future climate scenarios.

We first developed a new agricultural module within the framework of the Dynamic Land Ecosystem Model (DLEM) v4.0 by better representing dynamic crop growth processes (e.g., crop-specific phenological development, carbon allocation, yield formation, and biological nitrogen fixation) and agricultural management practices (e.g., nitrogen fertilization, irrigation, tillage, rotation, manure application, and cover cropping). Evaluations against site- and regional-scale observations demonstrate that the newly developed agricultural model effectively simulates the

magnitude and spatial and temporal variations in both crop production and net GHG emissions.

Combining this new agricultural model and multi-source datasets, we used a data-driven systems approach to quantify U.S. crop yield losses caused by compound droughts and heatwaves. We also analyzed the temporal variations in the sensitivity of U.S. corn-soybean systems to these extreme climate events over the past decades. Results indicate that U.S. corn and soybean yields exhibited heightened sensitivity to short-term droughts (spanning 1-3 months) and heatwaves during their critical reproductive stages. The simultaneous occurrence of droughts and heatwaves exacerbates yield loss substantially, resulting in yield losses of 29.6% for corn and 25.4% for soybean, surpassing the effects of individual extreme events. U.S. corn-soybean systems also showed a decreased sensitivity to concurrent droughts and heatwaves over the past six decades.

We further quantified the impacts of natural and anthropogenic factors on the magnitude and spatiotemporal variations of the net soil GHG balance in U.S. croplands during 1960-2018. Results show that U.S. agricultural soils sequestered 13.2 ± 1.16 Tg CO₂-C yr⁻¹ in SOC (at a depth of 3.5 m) during 1960-2018 and emitted 0.39 ± 0.02 Tg N₂O-N yr⁻¹ and 0.21 ± 0.01 Tg CH₄-C yr⁻¹, respectively. Based on the GWP100 metric (global warming potential on a 100-year time horizon), the estimated national net GHG emission rate from agricultural soils was 121.9 ± 11.46 Tg CO₂-eq yr⁻¹, thus contributing to climate warming. The sequestered SOC offset ~28% of the climate-warming effects resulting from non-CO₂ GHG emissions, and this offsetting effect increased over time. Increased nitrogen fertilizer use was the dominant factor contributing to the increase in net GHG emissions during 1960-2018, explaining ~47% of total changes. In contrast, the adoption of agricultural conservation practices (e.g., reduced tillage) and rising atmospheric CO₂ attenuated net GHG emissions from U.S. croplands.

By integrating climate forcings from the CMIP6 climate model, we also predicted future crop

production, net GHG balance, and GHGI in U.S. croplands under three climate scenarios, including SSP126, SSP245, and SSP585. Results show a significant increase in the national net GHG balance for the SSP245 and SSP585 scenarios, with the most pronounced increase occurring under the high-emission trajectory SSP585, averaging 236 Tg CO₂-eq year⁻¹ during 2020-2100. In contrast, the net GHG balance under the 126 scenario remains relatively stable throughout the study period. Crop production shows significant interannual variations but does not exhibit significant trends across all three climate scenarios. This imbalance, where the net GHG balance increases disproportionately compared to crop production, results in an elevated GHGI. For the SSP126, SSP245, and SSP585 scenarios, the GHGI is estimated to be 0.26 CO₂-eq Tg⁻¹, 0.34 CO₂-eq Tg⁻¹, and 0.42 CO₂-eq Tg⁻¹, respectively. The significant increase in both net GHG balance and GHGI is mainly attributed to increased temperatures and atmospheric CO₂ concentrations.

Additionally, we further predicted the long-term impacts of four CSA practices—no tillage, crop rotation, cover cropping, and N fertilizer reduction—on crop production and net GHG balance in U.S. croplands across various future climate scenarios. Our results suggest that these CSA practices significantly reduced the net GHG balance in U.S. croplands, with average reductions of 18.9% for no tillage, 10.3% for N fertilizer reduction, 28.6% for cover cropping, and 17.8% for crop rotation across the three climate scenarios. Furthermore, while no tillage and N fertilizer reduction only marginally impacted crop production, cover cropping and crop rotation decreased crop production by approximately 14.7% and 18.5%, respectively. Consequently, our findings underscore the imperative for comprehensive, scenario-specific CSA strategies to meet the dual goals of climate change mitigation and food security.

This dissertation filled the knowledge gap by comprehensively assessing and predicting the impacts of multiple environmental forcings and human management practices on crop production

and net GHG balance in U.S. croplands under both historical and future climate scenarios. The derived results offer important implications for effectively implementing CSA practices to address both climate change and food security issues, which also aligns with carbon neutrality goals and supports the achievement of climate-resilient and sustainable agricultural systems.

Acknowledgments

I am so blessed to have the opportunity to study at Auburn University and to conduct my Ph.D. research within such an excellent team. The past four and a half years have been a very valuable experience for me. I am extremely grateful to all those who contributed to the successful completion of my doctoral journey. Their support, guidance, and encouragement have been instrumental in both my academic and personal growth.

First and foremost, I would like to express my deepest gratitude to my advisors, Dr. Shufen Pan and Dr. Hanqin Tian, whose exceptional academic insights and patient guidance have been the cornerstone of this dissertation. I would not have been able to complete my Ph.D. without their support. They continuously encouraged me to think and dream bigger, and provided me with not only academic mentorship but also valuable guidance for my personal growth that will benefit me throughout my life. I also extend my deepest appreciation to my dissertation committee members, Dr. William D. Batchelor and Dr. Stephen A. Prior, for their valuable suggestions, support, and kindness. I still vividly remember the valuable advice they provided for my academic and personal growth during my oral qualifying examination. In addition, I thank Dr. Ruiqing Miao for reviewing this dissertation and providing constructive feedback during the NSF project.

I am also grateful to the current and former members of the EDGE group. Special thanks go to my officemate, Dr. Naiqing Pan, for his kindness, help, and encouragement, and to Dr. Zihao Bian for his kind support, encouragement, and humor. I would also like to thank the current EDGE members who have brought me a lot of happiness and support: Mr. Xiaoyong Li, Mr. Yu Shi, Ms. Ya Li, Ms. Qiqi Liu, Ms. Chujie Liu, Ms. Huiqian Yu, Mr. Binyuan Xu, Ms. Xinyi Yang, and Mr. Thomas Lee. My gratitude also extends to previous group members who provide me with valuable

research suggestions and made pioneering contributions to the development of the Dynamic Land Ecosystem Model: Dr. Hao Shi, Dr. Rongting Xu, Dr. Zhuonan Wang, Dr. Yuanzhi Yao, Dr. Chaoqun Lu, Dr. Jia Yang, and Dr. Wei Ren. My thanks also extend to Dr. Chengcheng Gang, Dr. Jing Wang, Dr. Lei Zhang, Dr. Peipei Pan, Dr. Fangjie Mao, Mr. Zhao Jin, Mr. Hua Yan, Mr. Bo Cheng, Mr. Kai Ling, Mr. Hang Song, Mr. Liangyu Huang, and other group members.

I am also grateful for all the assistance provided by Ms. Audrey Grindle, Mr. James Fukai, and all the faculty and staff members of the College of Forestry, Wildlife and Environment. I am very glad to have become friends with Dr. Yufei Nan, Dr. Teng Zhao, Dr. Wenjing Ren, and Mr. Germany Leonard.

Lastly, I would like to express my deepest gratitude to my parents, Mr. Zongyang You and Ms. Dongmei Yin, as well as my sister, Ms. Qiong You, for their unwavering support, encouragement, and understanding. Their unconditional love has been an unwavering source of strength, propelling me forward in the face of every challenge. I miss you all so much!

Table of Contents

Abstract	II
Acknowledgments.....	VI
Table of Contents	VIII
List of Tables.....	XIV
List of Figures.....	XV
Chapter 1. Introduction	1
1.1 Background.....	1
1.2 Objectives	7
1.3 Dissertation structure	8
References.....	11
Chapter 2. Integrating a new agricultural module into DLEM v4.0: Toward a data-driven systems approach.....	15
2.1 The Dynamic Land Ecosystem Model (DLEM) v4.0.....	15
2.2 Development of the agricultural module of DLEM v4.0.....	16
2.2.1 Dynamic crop growth processes	19
2.2.2 Agricultural management practices.....	32
2.2.3 Vertical discretization of soil profile and soil biogeochemical processes.....	39
2.3 Model forcing data.....	45
2.4 Summary	47
References.....	48
Chapter 3. Multi-scale crop yield simulation in the United States using a data-driven systems	

approach: Parameterization, evaluation, and application	55
Abstract	55
3.1 Introduction.....	56
3.2 Materials and methods	60
3.2.1 Model descriptions.....	60
3.2.2 Input data	61
3.2.3 Model calibration and validation	65
3.2.4 Model implementation.....	68
3.2.5 Parameter sensitivity analysis.....	68
3.3 Results.....	69
3.3.1 Site-scale model performance.....	69
3.3.2 Spatial patterns of simulated crop production	72
3.3.3 Temporal variations of simulated crop production	75
3.4 Discussion	76
3.4.1 General performance of the agricultural module of DLEM	76
3.4.2 Parameter sensitivity analysis.....	81
3.4.3 Uncertainties	84
3.4.4 Future research opportunities.....	85
3.5 Conclusion	86
References.....	87
Chapter 4. Decreased sensitivity of corn and soybean yields to the concurrent droughts and heatwaves in the United States	92
Abstract	92

4.1 Introduction.....	93
4.2 Materials and methods	96
4.2.1 Model descriptions.....	96
4.2.2 Model forcing data and yield survey data.....	97
4.2.3 Calculation of yield anomaly, SPEI, and HWMIId.....	97
4.2.4 Impact of timing of drought and heatwave on crop yields	99
4.2.5 Quantifying crop yield loss caused by extreme drought and heatwave events....	100
4.2.6 Time trends in yield sensitivity to droughts and heatwaves and their combinations	102
4.3 Results.....	102
4.3.1 Impact of timing and duration of droughts and heatwaves on crop yields	102
4.3.2 Influence of extreme droughts and heatwaves on crop yield losses	104
4.3.3 Sensitivity of corn and soybean yields to concurrent drought and heatwave events	108
4.4 Discussion	111
4.4.1 Timescale and timing of drought and heatwave impacts	112
4.4.2 Crop yield responses to droughts and heatwaves	113
4.4.3 Sensitivity of crop yields to droughts and heatwaves	115
4.4.4 Model uncertainties.....	117
4.5 Conclusion	118
References.....	119
Chapter 5. Net greenhouse gas balance in U.S. croplands: How can soils be a part of the climate solution?.....	124

Abstract	124
5.1 Introduction.....	125
5.2 Materials and methods.....	130
5.2.1 Meta-data collection.....	130
5.2.2 Model and forcing datasets	131
5.2.3 Model calibration, validation, and uncertainty analysis	132
5.2.4 Model implementation and experimental design.....	135
5.2.5 Global warming potential calculation.....	137
5.3 Results.....	138
5.3.1 National budget and dynamics of net GHG balance in U.S. croplands.....	138
5.3.2 Spatial patterns of net GHG balance in U.S. croplands.....	141
5.3.3 Relative contributions of SOC sequestration and N ₂ O and CH ₄ emissions to net GHG balance.....	145
5.3.4 Factorial contributions of multi-driver changes to net GHG balance in U.S. croplands.....	146
5.4 Discussion	148
5.4.1 Comparison with previous studies	148
5.4.2 Impacts of agricultural management factors and environmental changes on net GHG balance	152
5.4.3 Uncertainty and future work	158
5.5 Conclusion	159
References.....	160

Chapter 6. Projected dynamics of crop production and greenhouse gas balance in U.S. croplands:

The imperative of sustainable agriculture.....	167
Abstract.....	167
6.1 Introduction.....	168
6.2 Materials and methods.....	172
6.2.1 Model descriptions.....	172
6.2.2 Future climate scenarios and other input data.....	172
6.2.3 Model implementation and experimental design.....	174
6.2.4 Global warming potential and GHGI calculation.....	176
6.3 Results.....	177
6.3.1 National budget and spatiotemporal variations in net GHG balance.....	177
6.3.2 Spatial and temporal variations in crop production.....	180
6.3.3 Spatial and temporal variations in net GHG emissions intensity.....	182
6.3.4 Factorial contributions of multi-driver changes to net GHG balance and crop production.....	184
6.4 Discussion.....	187
6.4.1 Impacts of future climate change on net GHG balance, crop production, and GHGI	187
6.4.2 Uncertainty and future work.....	192
6.5 Conclusion.....	193
References.....	194
Chapter 7. Impacts of climate-smart agricultural practices on crop production and greenhouse gas balance in U.S. croplands under future climate predictions.....	199
Abstract.....	199

7.1 Introduction.....	200
7.2 Materials and methods	205
7.2.1 Model and forcing datasets	205
7.2.2 CSA practices scenarios.....	206
7.2.3 Model implementation and experimental design.....	206
7.2.4 Global warming potential and GHGI calculation	208
7.3 Results.....	209
7.3.1 Impacts of no tillage on net GHG balance, crop production, and GHGI.....	209
7.3.2 Impacts of N fertilizer reduction on net GHG balance, crop production, and GHGI	212
7.3.3 Impacts of cover cropping on net GHG balance, crop production, and GHGI ...	215
7.3.4 Impacts of crop rotation on net GHG balance, crop production, and GHGI	218
7.4 Discussion	220
7.4.1 Comparison with previous studies.....	220
7.4.2 Uncertainty and implications	224
7.5 Conclusion	226
References.....	227
Chapter 8. Conclusions and future works	232

List of Tables

Table 2-1. Comparisons between the new agricultural module in the Dynamic Land Ecosystem Model v4.0 and previous versions.	18
Table 2-2. Phenological stages in the specific crop scheme of the Dynamic Land Ecosystem Model and the main growing tissues during these stages.	21
Table 2-3. Four tillage systems implemented in the Dynamic Land Ecosystem Model.....	33
Table 3-1. Input datasets to drive DLEM v4.0.....	62
Table 3-2. Major parameter values of the crop variety groups used in this study.	64
Table 3-3. General model parameters related to crop growth, development, and yield formation processes in the Dynamic Land Ecosystem Model.....	66
Table 3-4. Temporal changes in photosynthesis rate and nitrogen uptake capability due to crop genetic improvement.....	67
Table 4-1. Classification of droughts following the U.S. Drought Monitor (http://droughtmonitor.unl.edu/).	100
Table 4-2. Classification of heatwaves adapted from Ceccherini et al. (2017).	101
Table 5-1. Factorial experiments to quantify the relative contributions of different drivers to changes in carbon dioxide, nitrous oxide, and methane emissions from U.S. croplands.	137
Table 5-2. Comparisons of SOC sequestration rate and fluxes of N ₂ O and CH ₄ from other studies.	151
Table 6-1. Factorial experiments in this study.	175
Table 7-1. Comparative experiments of climate-smart agriculture practices in this study.	208

List of Figures

Figure 1-1. The structure of this dissertation.	9
Figure 2-1. Framework of the Dynamic Land Ecosystem Model (Tian et al. 2010b).....	16
Figure 2-2. Crop life cycle in the general crop scheme of the Dynamic Land Ecosystem Model v4.0. fCBD_emer, fCBD_juve, fCBD_fini, fCBD_flow, fCBD_bfill, fCBD_efill, and fCBD_matu denote the target fraction of Cumulative Biological Days required to reach the phenological stages of emergence, end of juvenile, floral initiation, flowering, beginning of grain filling, end of grain filling, and maturity, respectively.....	20
Figure 3-1. Boundaries of crop variety groups in the conterminous United States and the spatial distribution of cumulative biological days required for maturity for corn (a), soybean (b), and winter wheat (c). The blue lines are the boundaries of crop variety groups, and the labels denote the crop variety groups presented in Table 3-2.	63
Figure 3-2. Spatial distribution of field sites. The green, red and blue colors represent the sites of corn, soybean and winter wheat, respectively, and the size of symbols indicates the number of sites.	67
Figure 3-3. Site-scale comparisons between the simulated leaf area index (LAI) and field observations for corn (a), soybean (b), and winter wheat (c). Different colors indicate different crop sites.	70
Figure 3-4. The seasonal evolution of observed and simulated leaf area index (LAI) in a corn-soybean rotation rainfed site, US-Ne3, where corn is planted in odd years (2001, 2003, 2005, and 2007) and soybean is planted in even years (2002, 2004, 2006).	70
Figure 3-5. Site-scale comparisons between the simulated aboveground biomass and field observations for corn (a), soybean (b), and winter wheat (c). Different colors indicate different crop sites.	71
Figure 3-6. The seasonal evolution of observed and simulated aboveground biomass in a corn-soybean rotation rainfed site, US-Ne3, where corn is planted in odd years (2001, 2003, 2005, and 2007) and soybean is planted in even years (2002, 2004, 2006).	72

Figure 3-7. Site-scale comparisons between the simulated yield and field observations for corn (a), soybean (b) and winter wheat (c). Different colors indicate different crop sites..... 72

Figure 3-8. Comparisons between the spatial patterns of average annual crop production simulated by the Dynamic Land Ecosystem Model (DLEM) and derived from the United States Department of Agriculture-National Agricultural Statistics Service (USDA-NASS) during 1960-2018, as well as the differences between them. (a-c) Corn production obtained from the DLEM and the USDA-NASS and their difference; (d-f) Soybean production obtained from the DLEM and the USDA-NASS and their difference; (g-i) Winter wheat production obtained from the DLEM and the USDA-NASS and their difference. A negative value in the difference of production indicates an underestimation of production by the DLEM, and a positive value indicates an overestimation of production by the DLEM. 73

Figure 3-9. Correlation coefficient between the simulated and observed crop productions in each county during 1960-2018 for corn (a), soybean (b) and winter wheat (c). The inset shows the spatial distribution of the corresponding P value, in which green color denotes significant correlation (P value < 0.05), and gray color denotes non-significant correlation (P value > 0.05)..... 74

Figure 3-10. Quantitative comparisons between the average annual crop production during 1960-2018 simulated by the Dynamic Land Ecosystem Model (DLEM) and obtained from the United States Department of Agriculture-National Agricultural Statistics Service (USDA-NASS) survey data at county-scale for corn (a), soybean (b) and winter wheat (c), respectively. The number next to the color bar represents the normalized point density..... 75

Figure 3-11. Historical trends of national crop production simulated by the Dynamic Land Ecosystem Model (DLEM) and obtained from the United States Department of Agriculture-National Agricultural Statistics Service (USDA-NASS) for corn (a), soybean (b) and winter wheat (c), respectively. 76

Figure 3-12. The spatial distribution of the simulated average annual β (i.e., soil water availability) during the growing season of winter wheat from 1960 to 2018. 78

Figure 3-13. Comparisons between the winter wheat production simulated by the Dynamic Land Ecosystem Model (DLEM) under real irrigation (a) and full irrigation (b), and obtained from the United States Department of Agriculture-National Agricultural Statistics Service (USDA-NASS)

(c).....	79
Figure 3-14. Comparisons between the historical trends of national crop production simulated by the Dynamic Land Ecosystem Model v4.0 (DLEM v4.0) and DLEM-Ag2, as well as obtained from the United States Department of Agriculture-National Agricultural Statistics Service (USDA-NASS) for corn (a), soybean (b) and winter wheat (c), respectively.....	81
Figure 3-15. The first-order and total-order sensitivity indices of corn-related parameters calculated by the Sobol’ global sensitivity analysis method, in which the error bars indicate the corresponding standard deviations derived from the resampling analysis.	82
Figure 3-16. The first-order and total-order sensitivity indices of soybean-related parameters calculated by the Sobol’ global sensitivity analysis method, in which the error bars indicate the corresponding standard deviations derived from the resampling analysis.	83
Figure 3-17. The first-order and total-order sensitivity indices of winter wheat-related parameters calculated by the Sobol’ global sensitivity analysis method, in which the error bars indicate the corresponding standard deviations derived from the resampling analysis.	84
Figure 4-1. Histograms showing the timing (a) and duration (timescale) (b) of droughts with the strongest correlation for the relationship between crop yield anomalies and the Standardized Precipitation-Evapotranspiration Index (SPEI) across U.S. counties.....	104
Figure 4-2. Histogram showing the timing of heatwaves with the strongest correlation for the relationship between crop yield anomalies and the Heatwave Magnitude Index daily (HWMId) across U.S. counties.....	104
Figure 4-3. The percentage of counties experiencing concurrent droughts and heatwaves in corn and soybean planting regions during 1964-2018.....	105
Figure 4-4. Influence of extreme droughts, heatwaves, and their co-occurrence on observed (i.e., USDA) and simulated (i.e., DLEM) crop yields. Composites are based on 7-year time windows of county-level yields centered on the respective event.....	106
Figure 4-5. Influence of extreme droughts, heatwaves, and their co-occurrence on observed (i.e., USDA) and simulated (i.e., DLEM) corn yields over different climate hubs.	107
Figure 4-6. Influence of extreme droughts, heatwaves, and their co-occurrence on observed (i.e.,	

USDA) and simulated (i.e., DLEM) soybean yields across different climate hubs.	108
Figure 4-7. Nonlinear responses of crop yields to droughts and heatwaves from multivariate adaptive regression splines analysis for corn and soybean, where shaded areas show 10–90% confidence interval.....	109
Figure 4-8. Time trends in yield sensitivity to heatwaves, droughts, and their combinations (i.e., concurrent droughts and heatwaves). The panel model estimates the time trend in sensitivity to SPEI (Standardized Precipitation Evapotranspiration Index) and HWMId (Heat Wave Magnitude Index daily), using county-level data during 1964-2018 in the conterminous US. Trends are expressed as a percentage of the value at the start of the time period. Vertical lines show the median estimate, boxes represent the 25th–75th percentiles, and whiskers show the range of bootstrap estimates, with block bootstrapping conducted by year.....	110
Figure 4-9. Time trends in yield sensitivity to heatwaves, droughts, and their combinations (i.e., concurrent droughts and heatwaves) across different climate hubs.....	111
Figure 5-1. Spatial distribution of field sites included in this study. Different colors represent different crop types, in which “others” represent crop types not listed in the legend (e.g., barley, cotton, and sorghum). Point size represents the number of replications/observations at each site.	131
Figure 5-2. Site-scale comparisons of model estimates and field observations of N ₂ O (a), CH ₄ (b), SOC sequestration rate (c), and SOC stocks (d) across different crop types. Dashed line is the regression of observed data and modeled results, and the solid line is the 1:1 line. Note that the SOC sequestration rates and SOC stocks here were reported by studies at various soil depths (e.g., 0~20 cm or 0~30 cm), thus we outputted simulation results at corresponding soil depths for validation. “Others” represent all crop types not listed in the legend (e.g., barley, cotton, and sorghum). Additionally, due to the small amount of N ₂ O and CH ₄ emissions (close to 0) at many sites, these datapoints are stacked near the origin, resulting in the number of datapoints on the graph appearing to be fewer than the actual number of datapoints involved in the statistical analysis.	134
Figure 5-3. Temporal variations in national SOC sequestration rate (a) and fluxes of N ₂ O (b) and CH ₄ (c) in U.S. agricultural soils from 1960 to 2018. Shaded area denotes the uncertainty ranges	

of SOC sequestration rate and N₂O and CH₄ fluxes (represented by ± 1 standard deviation). 139

Figure 5-4. Temporal variations in national net greenhouse gas balance of U.S. croplands from the 1960s to the 2010s. Note that error bars represent ± 1 standard deviation of net greenhouse gas balance in each decade..... 140

Figure 5-5. Spatial patterns of average annual SOC sequestration rate (a) and fluxes of N₂O (b) and CH₄ (c) in U.S. agricultural soils from 1960 to 2018. Note that negative values in soil fluxes represent uptake and positive values represent release. Therefore, negative soil CO₂ flux indicates SOC sequestration..... 142

Figure 5-6. Spatial pattern of average annual net greenhouse gas balance of U.S. croplands from the 1960s to the 2010s. Note that error bars in insets represent ± 1 standard deviation of the net greenhouse gas balance in each decade. NW, NP, MW, NE, SW, SP, and SE represent the Northwest, Northern Plains, Midwest, Northeast, Southwest, Southern Plains, and Southeast climate hubs, respectively. 144

Figure 5-7. Spatial distributions of the relative contribution of SOC sequestration and emissions of N₂O and CH₄ to the net greenhouse gas balance of U.S. croplands from the 1960s to the 2010s. 146

Figure 5-8. Factorial contributions of multiple agricultural management practices and environmental forcings to changes in the net greenhouse gas balance of U.S. croplands from the 1960s to the 2010s, in comparison to the average state in the 1950s. Nfer represents nitrogen fertilizer use; Ndep represents atmospheric nitrogen deposition; LULC represents land use and land cover change (reflecting both cropland abandonment and expansion, as well as interannual crop rotation changes); and CO₂ represents atmospheric carbon dioxide concentration. Note that the sum of factorial contributions of individual drivers (i.e., stacked bars) does not equal net changes in the net greenhouse gas balance (i.e., black line) due to interaction effects. 147

Figure 5-9. Factorial contributions of multiple agricultural management practices and environmental forcings to changes in CO₂ emission, N₂O emission, and CH₄ emission in U.S. croplands from the 1960s to the 2010s, in comparison to the average state in the 1950s. Noted that the negative impact on CO₂ emissions indicates a positive impact on soil organic carbon sequestration. Nfer represents nitrogen fertilizer use; Ndep represents atmospheric nitrogen

deposition; LULC represents land use and land cover change (reflecting both cropland abandonment and expansion, as well as interannual crop rotation changes); and CO₂ represents atmospheric carbon dioxide concentration. 155

Figure 5-10. Temporal changes in nitrogen fertilization amount (a), cropland area (b), tillage intensity (c), manure production (d), irrigated cropland acreage (e), atmospheric CO₂ concentration (f), atmospheric nitrogen deposition (g), temperature (h), and precipitation (i) over the study period. 156

Figure 5-11. Decadal changes in various factors relative to the 1950s, including nitrogen fertilization amount (a), cropland area (b), tillage intensity (c), manure production (d), irrigated cropland acreage (e), atmospheric CO₂ concentration (f), atmospheric nitrogen deposition (g), temperature (h), and precipitation (i). 157

Figure 6-1. Temporal variations in national SOC sequestration rate (a) and fluxes of N₂O (b) and CH₄ (c) in U.S. agricultural soils from 2020 to 2100. Note that negative values in SOC sequestration rate represent carbon release. 178

Figure 6-2. Temporal variations in national net greenhouse gas balance of U.S. croplands from the 2020s to the 2090s. 179

Figure 6-3. Spatial pattern of the average annual net greenhouse gas balance of U.S. croplands during 2020-2100 under the SSP126 (a), SSP245 (b), and SSP585 (c) scenarios. 180

Figure 6-4. Temporal variations in national crop production in U.S. croplands from 2020 to 2100 under the SSP126, SSP245, and SSP585 scenarios. 181

Figure 6-5. Spatial pattern of the average annual crop production in U.S. croplands during 2020-2100 under the SSP126 (a), SSP245 (b), and SSP585 (c) scenarios. 182

Figure 6-6. Temporal variations in greenhouse gas emissions intensity in U.S. croplands from the 2020s to the 2090s under the SSP126, SSP245, and SSP585 scenarios. 183

Figure 6-7. Spatial pattern of net greenhouse gas emissions intensity in U.S. croplands during 2020-2100 under the SSP126 (a), SSP245 (b), and SSP585 (c) scenarios. 184

Figure 6-8. Factorial contributions of climate change, atmospheric CO₂, and N deposition to the changes in net soil GHG balance of U.S. croplands during 2020-2100 under the SSP126 (a),

SSP245 (b), and SSP585 (c) scenarios.	185
Figure 6-9. Factorial contributions of climate change, atmospheric CO ₂ , and N deposition to the changes in crop production of U.S. croplands during 2020-2100 under the SSP126 (a), SSP245 (b), and SSP585 (c) scenarios.....	186
Figure 6-10. Temporal changes in temperature (a), precipitation (b), atmospheric carbon dioxide concentration (c), and atmospheric nitrogen deposition (d) under the SSP126, SSP245, and SSP585 scenarios during the 2020-2100 period.....	188
Figure 6-11. Factorial contributions of climate change, atmospheric CO ₂ , and N deposition to the changes in CO ₂ emission (a-c), N ₂ O emission (d-f), and CH ₄ emission (g-i) from U.S. croplands during 2020-2100 under the SSP126, SSP245, and SSP585 scenarios.....	190
Figure 7-1. Temporal variations in national net greenhouse gas balance of U.S. croplands from the 2020s to the 2090s under the implementation of no tillage and conventional tillage across various future scenarios (i.e., SSP126, SSP245, and SSP585). Note that NT and CT represent no tillage and conventional tillage, respectively.....	210
Figure 7-2. Temporal variations in national crop production of U.S. croplands from the 2020s to the 2090s under the implementation of no tillage and conventional tillage across various future scenarios (i.e., SSP126, SSP245, and SSP585). Note that NT and CT represent no tillage and conventional tillage, respectively.....	211
Figure 7-3. Temporal variations in national greenhouse gas emissions intensity of U.S. croplands from the 2020s to the 2090s under the implementation of no tillage and conventional tillage across various future scenarios (i.e., SSP126, SSP245, and SSP585). Note that NT and CT represent no tillage and conventional tillage, respectively.....	212
Figure 7-4. Temporal variations in national net greenhouse gas balance of U.S. croplands from the 2020s to the 2090s under a 25% reduction in nitrogen fertilizer (i.e., 75% Nfer) and no nitrogen fertilizer reduction (i.e., 100% Nfer) across various future scenarios (i.e., SSP126, SSP245, and SSP585).....	213
Figure 7-5. Temporal variations in national crop production of U.S. croplands from the 2020s to the 2090s under a 25% reduction in nitrogen fertilizer (i.e., 75% Nfer) and no nitrogen fertilizer reduction (i.e., 100% Nfer) across various future scenarios (i.e., SSP126, SSP245, and SSP585).	

..... 214

Figure 7-6. Temporal variations in national greenhouse gas emissions intensity of U.S. croplands from the 2020s to the 2090s under a 25% reduction in nitrogen fertilizer (i.e., 75% Nfer) and no nitrogen fertilizer reduction (i.e., 100% Nfer) across various future scenarios (i.e., SSP126, SSP245, and SSP585). 215

Figure 7-7. Temporal variations in national net greenhouse gas balance of U.S. croplands from the 2020s to the 2090s with cover cropping and without cover cropping practices across various future scenarios (i.e., SSP126, SSP245, and SSP585). Note that CC represents cover cropping. 216

Figure 7-8. Temporal variations in national crop production of U.S. croplands from the 2020s to the 2090s with cover cropping and without cover cropping practices across various future scenarios (i.e., SSP126, SSP245, and SSP585). Note that CC represents cover cropping. 217

Figure 7-9. Temporal variations in national greenhouse gas emissions intensity of U.S. croplands from the 2020s to the 2090s with cover cropping and without cover cropping practices across various future scenarios (i.e., SSP126, SSP245, and SSP585). Note that CC represents cover cropping. 218

Figure 7-10. Temporal variations in national net greenhouse gas balance of U.S. croplands from the 2020s to the 2090s with crop rotation (i.e., corn-soybean rotation) and without crop rotation (i.e., continuous corn) practices across various future scenarios (i.e., SSP126, SSP245, and SSP585). 218

Figure 7-11. Temporal variations in national crop production of U.S. croplands from the 2020s to the 2090s with crop rotation (i.e., corn-soybean) and without crop rotation (i.e., continuous corn) practices across various future scenarios (i.e., SSP126, SSP245, and SSP585). 219

Figure 7-12. Temporal variations in national greenhouse gas emissions intensity of U.S. croplands from the 2020s to the 2090s with crop rotation (i.e., corn-soybean) and without crop rotation (i.e., continuous corn) practices across various future scenarios (i.e., SSP126, SSP245, and SSP585). 220

Chapter 1. Introduction

1.1 Background

Contemporary agriculture is facing multiple challenges such as feeding a growing world population and mitigating climate change (Chen et al. 2014; Foley et al. 2011; Pittelkow et al. 2015a). During the past several decades, climate change and concomitant environmental stressors (e.g., water scarcity, pest prevalence, and soil degradation) have significantly impacted crop growth and production and are likely to reduce the resilience of global food systems (Bezner Kerr et al. 2022; Lesk et al. 2016; Wheeler and von Braun 2013b). Agricultural activities (e.g., fertilization, irrigation, and cropland expansion) have, in turn, exacerbated climatic and environmental changes through pathways such as greenhouse gas (GHG) emissions, groundwater extraction, and nutrient pollution (Giordano and Villholth 2007; Tian et al. 2016; Tian et al. 2020a). In view of the increasing uncertainty in the agriculture-climate-environment system caused by complex cross-sector interactions, effective climate change mitigation and adaptation strategies in the agricultural sector are needed to limit further changes in the climate system and reduce the negative impacts of climate change on food production (Howden et al. 2007; Vermeulen et al. 2012). This could further contribute to achieving sustainable agriculture and the Sustainable Development Goals, including “Climate Action” and “Zero Hunger”.

As a leading global producer of staple crops such as corn, soybean, and wheat, the United States (U.S.) plays a crucial role in global food systems (Dohlman et al. 2020). Nonetheless, climate change has significantly impacted its agricultural system (Lobell et al. 2014; Ortiz-Bobea et al. 2019; Schlenker and Roberts 2009b). Estimates indicate that rising temperatures decrease corn, soybean, and wheat productions in the U.S. by 10.3%, 6.8%, and 5.5% per degree Celsius, respectively (Zhao et al. 2017). Moreover, the frequency and intensity of extreme climate events

like droughts and heatwaves are projected to rise due to climate change (Janssen et al. 2014; Mazdidasni and AghaKouchak 2015), adversely affecting crop production (Lobell et al. 2013; Lobell et al. 2014; Troy et al. 2015; Zipper et al. 2016). In light of the increasing climate-related risks in the future coupled with the U.S.'s pivotal role in global food supply, a comprehensive analysis of how historical and future climate change, as well as extreme climate events, have affected the magnitude and spatiotemporal variations in U.S. crop yields becomes indispensable for informing policy-making ranging from localized farm management strategies to international trade accords.

Under conventional intensive farming (e.g., excessive nitrogen (N) fertilizer use and intensive tillage), agricultural activities have led to tremendous environmental impacts such as accelerated soil organic carbon (SOC) decomposition and increased GHG emissions (Davidson 2009; Zhang et al. 2020a). To date, agriculture has been a major force in anthropogenic global warming, contributing about 25%-30% and 35%-50% of global land biogenic emissions of nitrous oxide (N₂O) and methane (CH₄), respectively (Tian et al. 2016), and these emissions are projected to continue to rise as global fertilizer use increases (Cavigelli et al. 2012; Thompson et al. 2019). This constitutes a great challenge to achieve the Paris climate goal of limiting global warming to well below 2°C by the end of this century (Tian et al. 2020a). In the U.S., agriculture emitted ~10% of the national total GHG emissions in 2019 and was the largest source of N₂O emissions (~75%) (EPA 2021). Therefore, reducing GHG emissions from agriculture is an imminent need for climate change mitigation. On the other hand, under conservative agriculture practices (e.g., reduced tillage and cover cropping), croplands can significantly mitigate climate change by enhancing SOC sequestration (Bai et al. 2019; Hutchinson et al. 2007; Sun et al. 2020). Global croplands account for about 10% of the terrestrial soil organic carbon (SOC) stock (IPCC 2019; Watson et al. 2000)

and could potentially sequester 0.90~1.85 Pg C/yr in the top 0.3 m of soils, which is equivalent to 26-53% of the soil carbon sequestration target of 3.5 Pg C/yr established by the 4p1000 Initiative for climate mitigation (Zomer et al. 2017). In the U.S., agricultural soils could potentially sequester 45 to 98 Tg C/yr with the adoption of conservation management practices (Chambers et al. 2016; Kimble et al. 1998). Increasing SOC stock is considered to be the most important countermeasure for GHG mitigation in agriculture (Mosier et al. 2006; Smith et al. 2010). Besides sequestering atmospheric CO₂, enhancing SOC stocks can also provide multiple co-benefits, such as reducing soil erosion, strengthening climate resilience, and improving soil fertility and health (Lal 2018; Sohi 2012). Thus, advancing our understanding of the magnitude and spatiotemporal variations of the net GHG balance (i.e., sum of SOC sequestration of CO₂ and emissions of N₂O and CH₄) in U.S. croplands under both historical and future climate scenarios, as well as understanding the drivers behind these changes, are critical, which is essential for developing robust, data-driven policy interventions aimed at mitigating climate change while maintaining food security.

Climate-smart agriculture (CSA) management practices, such as reduced tillage, optimized N fertilizer use, and cover cropping, have been advocated to mitigate GHG emissions without compromising crop yield (FAO 2013; Miralles-Wilhelm 2021). Various field investigations and meta-analyses have explored the effects and efficacy of these practices on various agricultural components (i.e., SOC, N₂O, CH₄, and yield) (Bai et al. 2019; Gerber et al. 2016; Shang et al. 2021; Sun et al. 2020). However, most existing work has primarily focused on single management practices, examining one or two agricultural components (e.g., yield, CO₂, or N₂O) at a time (Huang et al. 2022; Lu et al. 2022; Yu et al. 2020). Relatively few studies have simultaneously quantified the integrated effects of multiple management practices on all agricultural components (including yield, SOC sequestration and non-CO₂ GHG emissions), especially at broader spatial

scales like national and continental scales. Given that some CSA management practices may have antagonistic effects on yields, SOC sequestration, and non-CO₂ GHG emissions (Guenet et al. 2021), and the resulting effects of different practices typically have large variations and may be non-additive (Yue et al. 2019), studies that fail to combine these components (as well as multiple practices together) may lead to inconsistencies when making comparisons that would not provide effective assessments (Shang et al. 2021).

Greenhouse gas emission intensity (GHGI), a CO₂ equivalents-based metric defined as net soil GHG emissions per unit of crop production (Grassini and Cassman 2012; Mosier et al. 2006), can be used to measure the balance between net soil GHG emissions and crop yields. However, there is still a lack of long-term and spatially explicit assessments examining the effects of multiple CSA practices (e.g., no tillage, cover cropping, and N fertilizer reduction) on GHGI at the regional scale—information that is critical for developing effective mitigation strategies. Therefore, identifying appropriate CSA practices that can reduce net soil GHG emissions while sustaining or boosting food production, ultimately reducing GHGI, is imperative, which could contribute to a win-win outcome between stabilizing the global climate system and safeguarding food security.

Global environmental changes such as climate change, rising atmospheric CO₂ concentration, and N deposition have also substantially affected agricultural GHG emissions (Ren et al. 2020; Ren et al. 2011). These factors vary over space and time in a highly heterogeneous geographical environment (e.g., diverse soil types and cropping systems) that can affect the effectiveness of CSA practices (Abdalla et al. 2013; Sun et al. 2020). This implies that a mitigation practice effective in one location or under certain conditions may not be effective elsewhere or under other conditions (Shang et al. 2021). In an example illustrating the importance of considering interactions between environmental factors and agricultural management practices, Huang et al.

(2018) found that conversion from conventional tillage to no-tillage reduced GHG emissions in dry but not in humid climates. However, relatively few studies have quantitatively attributed changes in the crop yield, net soil GHG balance, and GHGI of U.S. croplands to different drivers (including both management practices and environmental factors) over long-term periods (Moore et al., 2022). As the climate continues to change, it is therefore imperative to comprehend and predict the impacts of CSA practices on food production and GHG emissions (i.e., changes in GHGI) under future environmental changes scenarios (including variations in climate conditions, CO₂ concentration, and N deposition). This prediction could provide farmers and policymakers with valuable insights to mitigate the negative effects of climate change on food security and to ensure environmental sustainability (IPCC 2019; Rosenzweig et al. 2014; Wheeler and von Braun 2013a).

Field experiments provide feasible and reliable means of elucidating complex relationships of agricultural management practices and crop yield, net GHG balance, and GHGI under multiple environmental changes (Plaza-Bonilla et al. 2018). However, directly extrapolating site-specific findings to large spatial areas is difficult due to unique environmental and management conditions of each site (Huang et al. 2022). Meanwhile, effective mitigation and adaptation actions usually occur on multiple scales and are intertwined in intricate ways (Beveridge et al. 2018; Klein et al. 2007; Tol 2005). Specifically, stakeholders' adaptation decisions to sustain food production are usually carried out on a small scale (e.g., field-farm-landscape scales) and benefit local communities, as the influences of climate change on crop growth and production are largely mediated by local environments and local-specific adaptation strategies would be more effective (Hammer et al. 2014; Ofgeha and Abshare 2021). In contrast, agricultural mitigation measures (e.g., SOC sequestration and GHG mitigation) and their potential feedbacks to the environment and climate are often implemented and assessed on a broader scale (e.g., regional-national-global

scales), because effective mitigation requires the participation of major GHG emitters globally and is primarily driven by international agreements and ensuing national public policies (Hansen and Jones 2000; Klein et al. 2007; Locatelli 2011). Therefore, a unified tool that is capable of addressing cross-scale agricultural application demands is needed (Beveridge et al. 2018; Peng et al. 2020). Such a tool would enable a more consistent and robust prediction and assessment of crop production and the concomitant environmental and climatic tradeoffs.

Process-based terrestrial biosphere models (TBMs) with detailed hydrological, biophysical, and biogeochemical processes unlock an opportunity for agricultural climate change mitigation and adaptation (Bondeau et al. 2007; Lombardozzi et al. 2020; McDermid et al. 2017). When integrated with general circulation models, they can simulate regional crop production under historical and future climate scenarios, assess the mitigation potential of agricultural management options, and quantify the exchange of carbon, water, nutrient and energy fluxes within the agriculture-climate-environment system. However, the representation of agriculture in most TBMs is relatively simple (e.g., lacking or simplifying dynamic crop growth processes and management practices), with some TBMs even treating crops as natural grasses though using different eco-physiological parameters as a distinction (Betts 2005; McDermid et al. 2017). Since crops have rather different phenological development processes compared with natural vegetation and often involve implementation of management practices (e.g., irrigation and fertilization), such simplified schemes are unlikely to be able to closely replicate observed yields under varying climatic and environmental conditions across different spatiotemporal scales, which limit their use for agricultural adaptation and mitigation assessments. Therefore, it is highly desirable to incorporate mechanistic representations of dynamic crop growth processes and critical agricultural management practices (e.g., N fertilization, tillage, irrigation, and rotation) into TBMs to quantify

and predict the effects of different CSA practices (e.g., reduced tillage, N fertilizer reduction, cover cropping, and crop rotation) in crop yield, net GHG balance, and GHGI under both historical and future climate scenarios.

In summary, there are several major gaps in current studies addressing climate impacts, adaptation, and mitigation within the agricultural sector. First, there is still a lack of effective tools capable of addressing the cross-scale agricultural application demands, such as predicting regional crop production, assessing the mitigation potential of CSA practices, and evaluating the environmental impacts of agricultural management activities. Second, whether the sensitivity of U.S. agricultural systems to compound climate extremes has evolved during the past decades remains unclear. Third, large uncertainties persist regarding the magnitude, spatial, and temporal variations in crop yields, net GHG balance, and GHGI in U.S. croplands under both historical and future climate scenarios. Lastly, the long-term impacts of CSA practices on crop yields, net GHG balance, and GHGI in U.S. croplands under future climate scenarios remain uncertain. Bridging these gaps is critical for providing accurate, comprehensive, and actionable insights that can effectively inform agricultural policies, management strategies, and mitigation measures.

1.2 Objectives

The overarching goal of this study is to comprehensively quantify the impacts of multiple environmental forcings and CSA practices on the magnitude and spatiotemporal variations of crop production, net GHG balance, and GHGI in U.S. croplands, thereby promoting sustainable agriculture. The specific objectives are to:

- (1) develop a data-driven systems approach by integrating a process-based agricultural model with multi-source datasets to fulfill cross-scale agricultural application needs (e.g., management guidance, adaptation, and mitigation);

- (2) estimate crop yield losses caused by compound climate extremes and analyze whether the sensitivity of U.S. agricultural systems to compound extremes has changed over the past decades;
- (3) quantify the combined impacts of multiple agricultural management practices and environmental changes on the magnitude and spatiotemporal variations of net soil GHG balance in U.S. croplands;
- (4) predict future crop production, net GHG balance, and GHGI in U.S. croplands under various future climate scenarios, including SSP126, SSP245, and SSP585;
- (5) evaluate the impacts of four CSA practices—namely, no tillage, crop rotation, cover cropping, and reduced N fertilization—on crop production, net GHG balance, and GHGI in U.S. croplands across various future climate scenarios.

1.3 Dissertation structure

This dissertation is organized according to the structure showing below (Figure 1-1):

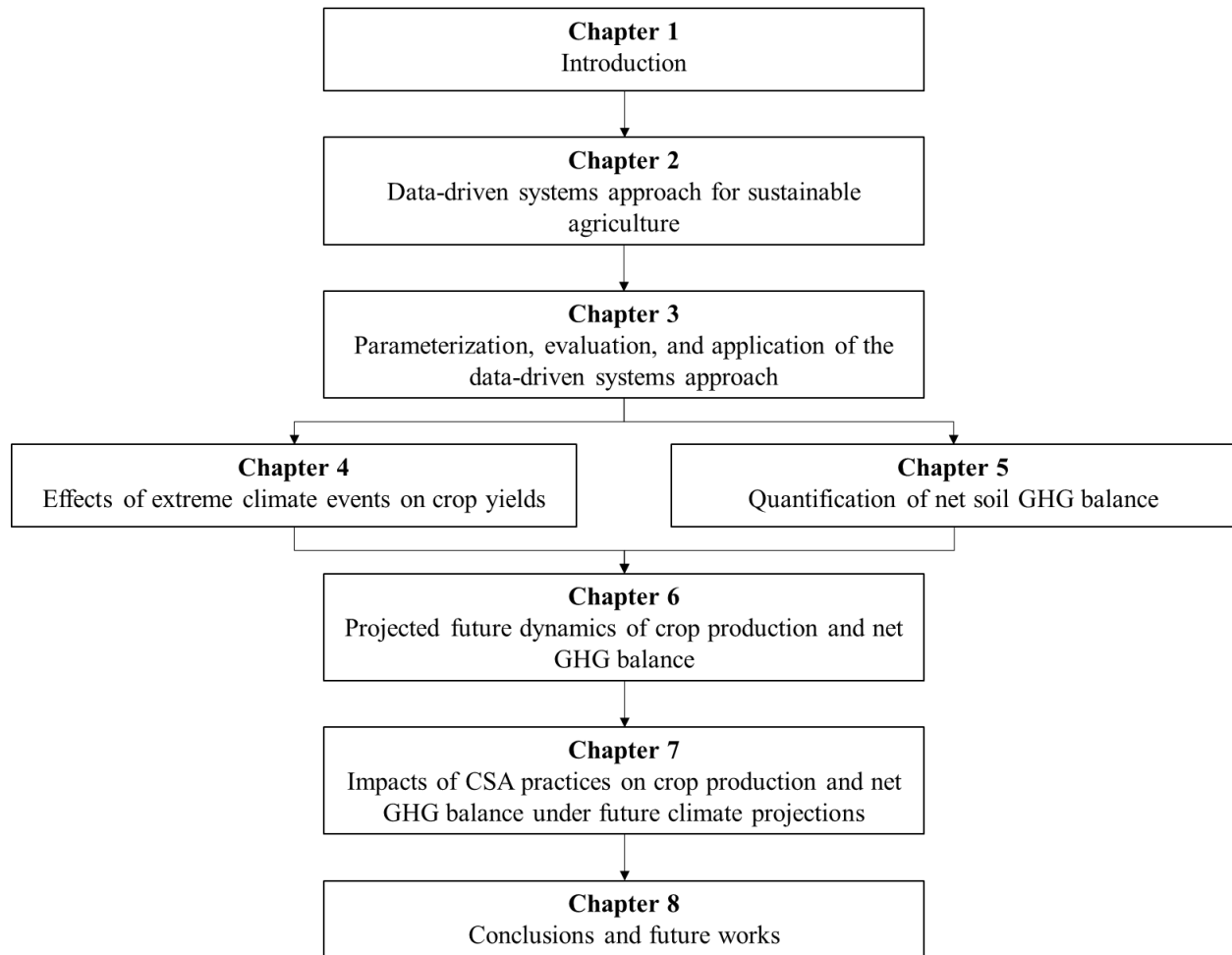


Figure 1-1. The structure of this dissertation.

Chapter 1 presents a brief introduction to the background, significance, current research gaps, and the objectives of this study.

Chapter 2 describes the data-driven systems approach (i.e., integrating a process-based agricultural model with multi-source data) used in this study. The processes incorporated into the new agricultural module of Dynamic Land Ecosystem Model v4.0 (DLEM v4.0) include but are not limited to dynamic crop growth processes such as crop-specific phenological development, carbon allocation, yield formation, and biological N fixation, and agricultural management practices such as tillage, cover cropping, N fertilization, irrigation, and crop genetic improvements,

as well as vertical discretization of soil profile and soil biogeochemical processes. Additionally, long-term model forcing datasets used to drive DLEM v4.0 are presented.

Chapter 3 describes the parameterization, evaluation and application details of the data-driven systems approach for simulating leaf area index, aboveground biomass, and crop yield from site to regional scales.

Chapter 4 estimates crop yield losses due to concurrent drought and heatwave events and evaluates whether the sensitivity of crop yields to extreme climate events has changed over the past decades.

Chapter 5 quantifies the combined effects of multiple agricultural management practices and environmental changes on the magnitude and spatiotemporal variations of the net soil GHG balance in U.S. croplands. It also examines the relative contributions of SOC sequestration of CO₂ and non-CO₂ GHG emissions to the net soil GHG balance.

Chapter 6 predicts crop production, net GHG balance, and GHGI in U.S. croplands under various future climate scenarios, including SSP126, SSP245, and SSP585. It also quantifies the factorial contributions of different climate drivers (i.e., climate change, atmospheric CO₂, and N deposition) to the spatial and temporal variations in future net GHG balance and crop production.

Chapter 7 assesses the long-term impacts of four CSA practices—namely, no tillage, crop rotation with legume crops, cover cropping, and reduced N fertilization—on crop production, net GHG balance, and GHGI in U.S. croplands across various future climate scenarios.

Chapter 8 summarizes the major findings of this study and discusses potential future works.

References

- Abdalla, M., Osborne, B., Lanigan, G., Forristal, D., Williams, M., Smith, P., & Jones, M.B. (2013). Conservation tillage systems: a review of its consequences for greenhouse gas emissions. *Soil Use and Management*, 29, 199-209
- Bai, X., Huang, Y., Ren, W., Coyne, M., Jacinthe, P.A., Tao, B., Hui, D., Yang, J., & Matocha, C. (2019). Responses of soil carbon sequestration to climate-smart agriculture practices: A meta-analysis. *Global Change Biology*, 25, 2591-2606
- Betts, R.A. (2005). Integrated approaches to climate-crop modelling: needs and challenges. *Philosophical transactions of the Royal Society of London. Series B, Biological sciences*, 360, 2049-2065
- Beveridge, L., Whitfield, S., & Challinor, A. (2018). Crop modelling: towards locally relevant and climate-informed adaptation. *Climatic Change*, 147, 475-489
- Bezner Kerr, R., Hasegawa, T., Lasco, R., Bhatt, I., Deryng, D., Farrell, A., Gurney-Smith, H., Ju, H., Lluch-Cota, S., Meza, F., Nelson, G., Neufeldt, H., & Thornton, P. (2022). *Food, Fibre, and Other Ecosystem Products. In: Climate Change 2022: Impacts, Adaptation, and Vulnerability. Contribution of Working Group II to the Sixth Assessment Report of the Intergovernmental Panel on Climate Change [H.-O. Pörtner, D.C. Roberts, M. Tignor, E.S. Poloczanska, K. Mintenbeck, A. Alegría, M. Craig, S. Langsdorf, S. Lösschke, V. Möller, A. Okem, B. Rama (eds.)]. Cambridge University Press.*
- Bondeau, A., Smith, P.C., Zaehle, S., Schaphoff, S., Lucht, W., Cramer, W., Gerten, D., Lotze-Campen, H., Müller, C., & Reichstein, M. (2007). Modelling the role of agriculture for the 20th century global terrestrial carbon balance. *Global Change Biology*, 13, 679-706
- Cavigelli, M.A., Grosso, S.J.D., Liebig, M.A., Snyder, C.S., Fixen, P.E., Venterea, R.T., Leytem, A.B., McLain, J.E., & Watts, D.B. (2012). US agricultural nitrous oxide emissions: context, status, and trends. *Frontiers in Ecology and the Environment*, 10, 537-546
- Chambers, A., Lal, R., & Paustian, K. (2016). Soil carbon sequestration potential of US croplands and grasslands: Implementing the 4 per Thousand Initiative. *Journal of Soil and Water Conservation*, 71, 68A-74A
- Chen, X., Cui, Z., Fan, M., Vitousek, P., Zhao, M., Ma, W., Wang, Z., Zhang, W., Yan, X., & Yang, J. (2014). Producing more grain with lower environmental costs. *Nature*, 514, 486-489
- Davidson, E.A. (2009). The contribution of manure and fertilizer nitrogen to atmospheric nitrous oxide since 1860. *Nature Geoscience*, 2, 659-662
- Dohlman, E., Hansen, J., & Boussios, D. (2020). USDA agricultural projections to 2029. *USDA agricultural projections to 2029*.
- EPA (2021). Inventory of US greenhouse gas emissions and sinks: 1990–2019. *Tech. Rep. EPA 430-R-21-003*
- FAO (2013). *Climate-smart agriculture: sourcebook*. Rome, Italy: Food and Agriculture Organization of the United Nations (FAO)
- Foley, J.A., Ramankutty, N., Brauman, K.A., Cassidy, E.S., Gerber, J.S., Johnston, M., Mueller, N.D., O'Connell, C., Ray, D.K., West, P.C., Balzer, C., Bennett, E.M., Carpenter, S.R., Hill, J., Monfreda, C., Polasky, S., Rockström, J., Sheehan, J., Siebert, S., Tilman, D., & Zaks, D.P.M. (2011). Solutions for a cultivated planet. *Nature*, 478, 337-342
- Gerber, J.S., Carlson, K.M., Makowski, D., Mueller, N.D., Garcia de Cortazar-Atauri, I., Havlik, P., Herrero, M., Launay, M., O'Connell, C.S., & Smith, P. (2016). Spatially explicit estimates of N₂O emissions from croplands suggest climate mitigation opportunities from improved fertilizer management. *Global Change Biology*, 22, 3383-3394
- Giordano, M., & Villholth, K.G. (2007). *The agricultural groundwater revolution: opportunities and threats to development*. CABI
- Grassini, P., & Cassman, K.G. (2012). High-yield maize with large net energy yield and small global warming intensity. *Proceedings of the National Academy of Sciences*, 109, 1074-1079
- Guenet, B., Gabrielle, B., Chenu, C., Arrouays, D., Balesdent, J., Bernoux, M., Bruni, E., Caliman, J.-P., Cardinael, R., Chen, S., Ciais, P., Desbois, D., Fouche, J., Frank, S., Henault, C., Lugato, E., Naipal, V., Nesme, T., Obersteiner, M., Pellerin, S., Powelson, D.S., Rasse, D.P., Rees, F., Soussana, J.-F., Su, Y., Tian, H., Valin, H., & Zhou, F. (2021). Can N₂O emissions offset the benefits from soil organic carbon storage? *Global Change Biology*, 27, 237-256
- Hammer, G.L., McLean, G., Chapman, S., Zheng, B., Doherty, A., Harrison, M.T., van Oosterom, E., & Jordan, D. (2014). Crop design for specific adaptation in variable dryland production environments. *Crop and Pasture Science*, 65, 614-626

- Hansen, J.W., & Jones, J.W. (2000). Scaling-up crop models for climate variability applications. *Agricultural systems*, 65, 43-72
- Howden, S.M., Soussana, J.-F., Tubiello, F.N., Chhetri, N., Dunlop, M., & Meinke, H. (2007). Adapting agriculture to climate change. *Proceedings of the National Academy of Sciences*, 104, 19691
- Huang, Y., Ren, W., Wang, L., Hui, D., Grove, J.H., Yang, X., Tao, B., & Goff, B. (2018). Greenhouse gas emissions and crop yield in no-tillage systems: A meta-analysis. *Agriculture, Ecosystems & Environment*, 268, 144-153
- Huang, Y., Tao, B., Yang, Y., Zhu, X., Yang, X., Grove, J.H., & Ren, W. (2022). Simulating no-tillage effects on crop yield and greenhouse gas emissions in Kentucky corn and soybean cropping systems: 1980–2018. *Agricultural systems*, 197, 103355
- Hutchinson, J.J., Campbell, C.A., & Desjardins, R.L. (2007). Some perspectives on carbon sequestration in agriculture. *Agricultural and Forest Meteorology*, 142, 288-302
- IPCC (2019). Climate Change and Land: an IPCC special report on climate change, desertification, land degradation, sustainable land management, food security, and greenhouse gas fluxes in terrestrial ecosystems [P.R. Shukla, J. Skea, E. Calvo Buendia, V. Masson-Delmotte, H.-O. Pörtner, D. C. Roberts, P. Zhai, R. Slade, S. Connors, R. van Diemen, M. Ferrat, E. Haughey, S. Luz, S. Neogi, M. Pathak, J. Petzold, J. Portugal Pereira, P. Vyas, E. Huntley, K. Kissick, M. Belkacemi, J. Malley, (eds.)]
- Janssen, E., Wuebbles, D.J., Kunkel, K.E., Olsen, S.C., & Goodman, A. (2014). Observational- and model-based trends and projections of extreme precipitation over the contiguous United States. *Earth's Future*, 2, 99-113
- Kimble, J.M., Follett, R.F., & Cole, C.V. (1998). *The Potential of U.S. Cropland to Sequester Carbon and Mitigate the Greenhouse Effect*. CRC Press
- Klein, R.J.T., Huq, S., Denton, F., Downing, T.E., Richels, R.G., Robinson, J.B., & Toth, F.L. (2007). Inter-relationships between adaptation and mitigation. Climate Change 2007: impacts, adaptation and vulnerability. In: Parry ML, Canziani OF, Palutikof JP, van der Linden PJ, Hanson CE (eds) Contribution of working group II to the fourth assessment report of the intergovernmental panel on climate change. Cambridge, UK: Cambridge University Press, Cambridge
- Lal, R. (2018). Digging deeper: A holistic perspective of factors affecting soil organic carbon sequestration in agroecosystems. *Global Change Biology*, 24, 3285-3301
- Lesk, C., Rowhani, P., & Ramankutty, N. (2016). Influence of extreme weather disasters on global crop production. *Nature*, 529, 84-87
- Lobell, D.B., Hammer, G.L., McLean, G., Messina, C., Roberts, M.J., & Schlenker, W. (2013). The critical role of extreme heat for maize production in the United States. *Nature Climate Change*, 3, 497-501
- Lobell, D.B., Roberts, M.J., Schlenker, W., Braun, N., Little, B.B., Rejesus, R.M., & Hammer, G.L. (2014). Greater Sensitivity to Drought Accompanies Maize Yield Increase in the U.S. Midwest. *Science*, 344, 516
- Locatelli, B. (2011). *Synergies between adaptation and mitigation in a nutshell*. CIFOR
- Lombardozi, D.L., Lu, Y., Lawrence, P.J., Lawrence, D.M., Swenson, S., Oleson, K.W., Wieder, W.R., & Ainsworth, E.A. (2020). Simulating Agriculture in the Community Land Model Version 5. *Journal of Geophysical Research: Biogeosciences*, 125, e2019JG005529
- Lu, C., Yu, Z., Hennessy, D.A., Feng, H., Tian, H., & Hui, D. (2022). Emerging weed resistance increases tillage intensity and greenhouse gas emissions in the US corn–soybean cropping system. *Nature Food*, 3, 266-274
- Mazdiyasi, O., & AghaKouchak, A. (2015). Substantial increase in concurrent droughts and heatwaves in the United States. *Proceedings of the National Academy of Sciences*, 112, 11484
- McDermid, S.S., Mearns, L.O., & Ruane, A.C. (2017). Representing agriculture in Earth System Models: Approaches and priorities for development. *Journal of Advances in Modeling Earth Systems*, 9, 2230-2265
- Miralles-Wilhelm, F. (2021). Nature-based solutions in agriculture: Sustainable management and conservation of land, water and biodiversity. In. Rome, Italy: Food and Agriculture Organization of the United Nations
- Mosier, A.R., Halvorson, A.D., Reule, C.A., & Liu, X.J. (2006). Net global warming potential and greenhouse gas intensity in irrigated cropping systems in northeastern Colorado. *Journal of environmental quality*, 35, 1584-1598
- Ofgeha, G.Y., & Abshare, M.W. (2021). Local adaptation and coping strategies to global environmental changes: Portraying agroecology beyond production functions in southwestern Ethiopia. *Plos One*, 16, e0255813
- Ortiz-Bobea, A., Wang, H., Carrillo, C.M., & Ault, T.R. (2019). Unpacking the climatic drivers of US agricultural yields. *Environmental Research Letters*, 14, 064003
- Peng, B., Guan, K., Tang, J., Ainsworth, E.A., Asseng, S., Bernacchi, C.J., Cooper, M., Delucia, E.H., Elliott, J.W., Ewert, F., Grant, R.F., Gustafson, D.I., Hammer, G.L., Jin, Z., Jones, J.W., Kimm, H., Lawrence, D.M., Li, Y., Lombardozi, D.L., Marshall-Colon, A., Messina, C.D., Ort, D.R., Schnable, J.C., Vallejos, C.E., Wu,

- A., Yin, X., & Zhou, W. (2020). Towards a multiscale crop modelling framework for climate change adaptation assessment. *Nature Plants*, 6, 338-348
- Pittelkow, C.M., Liang, X., Linnquist, B.A., van Groenigen, K.J., Lee, J., Lundy, M.E., van Gestel, N., Six, J., Venterea, R.T., & van Kessel, C. (2015). Productivity limits and potentials of the principles of conservation agriculture. *Nature*, 517, 365-368
- Plaza-Bonilla, D., Álvaro-Fuentes, J., Bareche, J., Pareja-Sánchez, E., Justes, É., & Cantero-Martínez, C. (2018). No-tillage reduces long-term yield-scaled soil nitrous oxide emissions in rainfed Mediterranean agroecosystems: A field and modelling approach. *Agriculture, Ecosystems & Environment*, 262, 36-47
- Ren, W., Banger, K., Tao, B., Yang, J., Huang, Y., & Tian, H. (2020). Global pattern and change of cropland soil organic carbon during 1901-2010: Roles of climate, atmospheric chemistry, land use and management. *Geography and Sustainability*, 1, 59-69
- Ren, W., Tian, H., Xu, X., Liu, M., Lu, C., Chen, G., Melillo, J., Reilly, J., & Liu, J. (2011). Spatial and temporal patterns of CO₂ and CH₄ fluxes in China's croplands in response to multifactor environmental changes. *Tellus B: Chemical and Physical Meteorology*, 63, 222-240
- Rosenzweig, C., Elliott, J., Deryng, D., Ruane, A.C., Müller, C., Arneth, A., Boote, K.J., Folberth, C., Glotter, M., & Khabarov, N. (2014). Assessing agricultural risks of climate change in the 21st century in a global gridded crop model intercomparison. *Proceedings of the National Academy of Sciences*, 111, 3268-3273
- Schlenker, W., & Roberts, M.J. (2009). Nonlinear temperature effects indicate severe damages to US crop yields under climate change. *Proceedings of the National Academy of Sciences*, 106, 15594-15598
- Shang, Z., Abdalla, M., Xia, L., Zhou, F., Sun, W., & Smith, P. (2021). Can cropland management practices lower net greenhouse emissions without compromising yield? *Global Change Biology*, 27, 4657–4670
- Smith, P., Lanigan, G., Kutsch, W.L., Buchmann, N., Eugster, W., Aubinet, M., Ceschia, E., Béziat, P., Yeluripati, J.B., & Osborne, B. (2010). Measurements necessary for assessing the net ecosystem carbon budget of croplands. *Agriculture, Ecosystems & Environment*, 139, 302-315
- Sohi, S.P. (2012). Carbon storage with benefits. *Science*, 338, 1034-1035
- Sun, W., Canadell, J.G., Yu, L., Yu, L., Zhang, W., Smith, P., Fischer, T., & Huang, Y. (2020). Climate drives global soil carbon sequestration and crop yield changes under conservation agriculture. *Global Change Biology*, 26, 3325-3335
- Thompson, R.L., Lassaletta, L., Patra, P.K., Wilson, C., Wells, K.C., Gressent, A., Koffi, E.N., Chipperfield, M.P., Winiwarter, W., Davidson, E.A., Tian, H., & Canadell, J.G. (2019). Acceleration of global N₂O emissions seen from two decades of atmospheric inversion. *Nature Climate Change*, 9, 993-998
- Tian, H., Lu, C., Ciais, P., Michalak, A.M., Canadell, J.G., Saikawa, E., Huntzinger, D.N., Gurney, K.R., Sitch, S., Zhang, B., Yang, J., Bousquet, P., Bruhwiler, L., Chen, G., Dlugokencky, E., Friedlingstein, P., Melillo, J., Pan, S., Poulter, B., Prinn, R., Saunio, M., Schwalm, C.R., & Wofsy, S.C. (2016). The terrestrial biosphere as a net source of greenhouse gases to the atmosphere. *Nature*, 531, 225-228
- Tian, H., Xu, R., Canadell, J.G., Thompson, R.L., Winiwarter, W., Suntharalingam, P., Davidson, E.A., Ciais, P., Jackson, R.B., Janssens-Maenhout, G., Prather, M.J., Regnier, P., Pan, N., Pan, S., Peters, G.P., Shi, H., Tubiello, F.N., Zaehle, S., Zhou, F., Arneth, A., Battaglia, G., Berthet, S., Bopp, L., Bouwman, A.F., Buitenhuis, E.T., Chang, J., Chipperfield, M.P., Dangal, S.R.S., Dlugokencky, E., Elkins, J.W., Eyre, B.D., Fu, B., Hall, B., Ito, A., Joos, F., Krummel, P.B., Landolfi, A., Laruelle, G.G., Lauerwald, R., Li, W., Lienert, S., Maavara, T., MacLeod, M., Millet, D.B., Olin, S., Patra, P.K., Prinn, R.G., Raymond, P.A., Ruiz, D.J., van der Werf, G.R., Vuichard, N., Wang, J., Weiss, R.F., Wells, K.C., Wilson, C., Yang, J., & Yao, Y. (2020). A comprehensive quantification of global nitrous oxide sources and sinks. *Nature*, 586, 248-256
- Tol, R.S.J. (2005). Adaptation and mitigation: trade-offs in substance and methods. *Environmental Science & Policy*, 8, 572-578
- Troy, T.J., Kipgen, C., & Pal, I. (2015). The impact of climate extremes and irrigation on US crop yields. *Environmental Research Letters*, 10, 054013
- Vermeulen, S.J., Campbell, B.M., & Ingram, J.S.I. (2012). Climate change and food systems. *Annual review of environment and resources*, 37, 195-222
- Watson, R.T., Noble, I.R., Bolin, B., Ravindranath, N.H., Verardo, D.J., & Dokken, D.J. (2000). *Land use, land-use change and forestry: a special report of the Intergovernmental Panel on Climate Change*. Cambridge University Press
- Wheeler, T., & von Braun, J. (2013a). Climate Change Impacts on Global Food Security. *Science*, 341, 508
- Wheeler, T., & von Braun, J. (2013b). Climate Change Impacts on Global Food Security. *Science*, 341, 508-513
- Yu, Z., Lu, C., Hennessy, D.A., Feng, H., & Tian, H. (2020). Impacts of tillage practices on soil carbon stocks in the US corn-soybean cropping system during 1998 to 2016. *Environmental Research Letters*, 15, 014008

- Yue, K., Peng, Y., Fornara, D.A., Van Meerbeek, K., Vesterdal, L., Yang, W., Peng, C., Tan, B., Zhou, W., & Xu, Z. (2019). Responses of nitrogen concentrations and pools to multiple environmental change drivers: A meta-analysis across terrestrial ecosystems. *Global Ecology and Biogeography*, *28*, 690-724
- Zhang, J., Tian, H., Shi, H., Zhang, J., Wang, X., Pan, S., & Yang, J. (2020). Increased greenhouse gas emissions intensity of major croplands in China: Implications for food security and climate change mitigation. *Global Change Biology*, *26*, 6116-6133
- Zhao, C., Liu, B., Piao, S., Wang, X., Lobell, D.B., Huang, Y., Huang, M., Yao, Y., Bassu, S., Ciais, P., Durand, J.-L., Elliott, J., Ewert, F., Janssens, I.A., Li, T., Lin, E., Liu, Q., Martre, P., Müller, C., Peng, S., Peñuelas, J., Ruane, A.C., Wallach, D., Wang, T., Wu, D., Liu, Z., Zhu, Y., Zhu, Z., & Asseng, S. (2017). Temperature increase reduces global yields of major crops in four independent estimates. *Proceedings of the National Academy of Sciences*, *114*, 9326
- Zipper, S.C., Qiu, J., & Kucharik, C.J. (2016). Drought effects on US maize and soybean production: spatiotemporal patterns and historical changes. *Environmental Research Letters*, *11*, 094021
- Zomer, R.J., Bossio, D.A., Sommer, R., & Verchot, L.V. (2017). Global Sequestration Potential of Increased Organic Carbon in Cropland Soils. *Scientific Reports*, *7*, 15554

Chapter 2. Integrating a new agricultural module into DLEM v4.0: Toward a data-driven systems approach

2.1 The Dynamic Land Ecosystem Model (DLEM) v4.0

Dynamic Land Ecosystem Model (DLEM) v4.0 is a highly integrated terrestrial biosphere model (TBM) that is capable of quantifying daily, spatially explicit carbon, water, and nutrient stocks and fluxes in terrestrial ecosystems and inland water systems across site, regional, and global scales (Pan et al. 2021; Tian et al. 2010a; Tian et al. 2020b; Yao et al. 2020). Five core components are included in DLEM v4.0 to simulate the biogeochemical and biogeophysical processes within terrestrial ecosystems: biophysics, plant physiology, dynamic vegetation, soil biogeochemistry, and natural and anthropogenic disturbances (Figure 2-1). Through coupling major biogeochemical-hydrological processes, DLEM is able to simultaneously depict the biosphere-atmosphere exchanges of carbon dioxide (CO₂), nitrous oxide (N₂O) and methane (CH₄) as driven by multiple environmental forcings (e.g., climate, atmospheric CO₂ concentration, nitrogen (N) deposition, tropospheric ozone pollution, and land use and land cover change). This capability provides a powerful tool for supporting the development of effective greenhouse gas (GHG) mitigation options. DLEM has been widely evaluated and applied to estimate CO₂, CH₄ and N₂O fluxes at multiple sites and regions like China (Ren et al. 2011; Tian et al. 2011), the United States (Tian et al. 2012a; Zhang et al. 2012), North America (Tian et al. 2015b; Xu et al. 2012; Xu et al. 2010), and across the globe (Friedlingstein et al. 2020a; Saunio et al. 2020b; Tian et al. 2020a). In addition, a land-aquatic interface has also been coupled to DLEM (Pan et al. 2021; Yao et al. 2020), which enhances its ability to simulate nutrient loading from agroecosystems and investigate potential mitigation strategies.

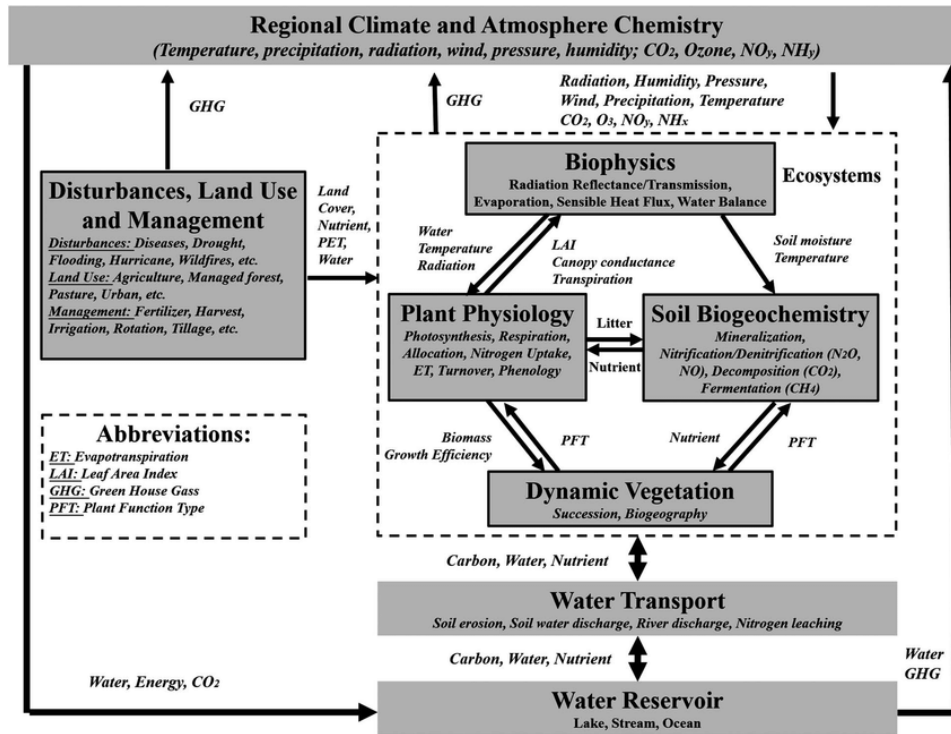


Figure 2-1. Framework of the Dynamic Land Ecosystem Model (Tian et al. 2010b).

2.2 Development of the agricultural module of DLEM v4.0

The new agricultural module is developed based on previous agricultural versions of DLEM (DLEM-Ag and DLEM-Ag2), which included simplified crop growth processes and basic management practices (e.g., N fertilization, irrigation, and rotation) (Ren et al. 2012; Tian et al. 2012c; Zhang et al. 2018). While DLEM-Ag and DLEM-Ag2 can achieve a good performance at specific sites, their performance in regional-scale simulations has been relatively poor (especially when simulating long-term series of regional crop production) (Zhang et al. 2018). Moreover, their ability to quantify impacts of agricultural activities on biosphere-atmosphere feedback is also limited.

To overcome the above shortcomings, the new agricultural module in DLEM v4.0 has major improvements in five aspects: crop phenological development, carbon allocation, yield formation,

biological N fixation, and management practices (Table 2-1). First, we included crop-specific phenological development schemes, with phenology-stage-dependent environmental stresses explicitly considered. Second, a new dynamic carbon allocation scheme was implemented, where the allocation fraction of net assimilates to different vegetation pools is determined by a prescribed growth-stage dependent carbon allocation curve and modified by water, light, and N stresses. Third, the yield formation process was improved by calculating crop yield as the balance between available carbon supply to the reproduction pool and the actual carbon demand for grain filling. The actual carbon demand for grain filling of different crops was calculated using crop-specific methods derived from relevant studies (Gaspar et al. 2017; Gregory and Atwell 1991; Gregory et al. 1995; Lei et al. 2010; Lokupitiya et al. 2009; Peart and Shoup 2018; Ritchie 1991; Srivastava et al. 2006; Taylor et al. 1982; Wilhelm 1998; Yamagata et al. 1987). Meanwhile, the translocation of dry matter between the stem tissue and the reproduction pool to supplement grain filling was also considered. Fourth, a new biological N fixation scheme was included, where the N fixation rate is dependent on soil temperature, soil moisture, N availability, substrate concentration, and crop phenological stage. Finally, we incorporated several important management practices (i.e., tillage, cover cropping, and crop genetic improvements) in the new model and implemented a dynamic crop rotation scheme through introducing time-varying crop rotation maps to better reflect the interannual changes in distributions of different crop types.

In addition, we have also improved the soil module in the DLEM by better representing soil organic carbon (SOC) distribution along the soil column down to a depth of 3.5m, partitioned into 10 layers following a biome-specific exponential vertical discretization scheme. Subsequently, the relevant soil biogeochemical processes were individually calculated within each soil layer and then integrated together to improve the simulation of soil dynamics processes.

Table 2-1. Comparisons between the new agricultural module in the Dynamic Land Ecosystem Model v4.0 and previous versions.

	Process	DLEM-Ag	DLEM-Ag2	Agricultural module in DLEM v4.0
Crop growth processes	Phenological development	(1) Use prescribed static leaf area index curve derived from satellite images to determine phenology (growing or senescence); (2) Sowing date is prescribed and remains unchanged.	(1) Divide the life cycle of all crops into the same eight phenological stages; (2) Does not consider the impacts of environmental stresses on phenological development; (3) Sowing date is prescribed and remains unchanged.	(1) Include more detailed phenological stages, and explicitly consider the phenological differences of various crop types and use the Biological Days-based phenological development scheme to determine the initiation and duration of different phenological stages; (2) Include the effects of phenology-stage-dependent environmental stresses on crop phenological development; (3) Sowing date is automatically simulated and changes with climatic conditions.
	Carbon allocation	(1) Crop phenological stage has no effect on carbon allocation; (2) Does not consider the impacts of environmental stresses when allocating net carbon assimilates to the leaf, stem, and reproduction pools	(1) Allocation fraction varied with phenological stages; (2) Does not consider the impacts of environmental stresses when allocating net carbon assimilates to the leaf, stem, and reproduction pools.	(1) Include a new dynamic carbon allocation scheme, where the allocation fraction of net assimilates to different vegetation pools is varied across phenological stages and is simultaneously adjusted by multiple environmental stresses; (2) Include a new enzyme-driven C4 photosynthesis routine to improve the representation of C4 plant responses to environmental factors.
	Yield formation	(1) Yield is estimated as the product of total aboveground biomass and a constant harvest index; (2) Does not consider dry matter translocation process.	(1) Yield is determined by the actual carbon demand for grain filling, where a single empirical equation related to stem dry weight is used to calculate the actual carbon demand of all crops, even though the grain filling characteristics differ by crop (2) Does not consider dry matter translocation process	(1) Yield is estimated as the balance between available carbon and grain demand, in which the actual grain demand for different crop types is calculated using crop-specific methods; (2) Consider the translocation process of dry matter from non-structural tissues to reproduction pool to supplement grain filling.
	Biological N fixation	Biological N fixation is determined by the annual N fixation amount and CO ₂ concentration, which does not consider the impacts of environmental stresses and phenological stages.	Same as DLEM-Ag	Biological N fixation is jointly controlled by soil temperature, soil moisture, soil mineral N concentration, substrate carbon concentration, and crop phenological stage.
Management practices	Tillage	Included	Not included	Included
	Cover cropping	Included	Not included	Included
	Rotation	Static prescribed rotation map	Same as DLEM-Ag	Incorporate a new dynamic rotation scheme through introducing time-varying rotation maps.
	Genetic improvements	Not included	Not included	Included

2.2.1 Dynamic crop growth processes

2.2.1.1 Crop phenological development

The life cycle of a crop can be divided into several phenological stages that influence the development of crop canopy structure (e.g., leaf area index (LAI) and canopy height), the allocation of carbon and nutrients among crop tissues, and the biological N fixation process. Some of these phenological stages are general to all crops, such as sowing, germination, emergence, physiological maturity, and harvest; while other stages are crop-specific such as the tassel initiation and silking stages of corn. DLEM-Ag uses prescribed static LAI curves derived from satellite images to determine phenology (Ren et al. 2012). DLEM-Ag2 divides the life cycle of all crops into the same eight stages and does not consider environmental stresses on phenological development (Zhang et al. 2018), which have been shown to be critical for determining phenological stages (Gungula et al. 2003; Uhart and Andrade 1995; Wilhelm et al. 1993). Our new model explicitly considers the phenological differences among crops as well as phenology-stage-dependent environmental stresses. It also adopts two separate schemes to determine phenological stages of various crop types: a general crop scheme (GCS) for some crops (currently including rice, peanuts, cotton, sorghum, barley, rye, cassava, potato, rapeseed, sugarbeet and sugarcane, but can be flexibly expanded if needed) and a specific crop scheme (SCS) for other crops (currently including corn, soybean, and wheat). For the GCS, we used a unified phenological development cycle similar to that in DLEM-Ag2 but included more detailed phenological stages and the environmental stresses (e.g., water and N) on phenological development. Crop life cycle in the GCS is divided into ten stages: sowing, germination, emergence, end of juvenile, floral initiation, flowering, beginning of grain filling, end of grain filling, maturity, and harvest (Figure 2-2). Each crop type using the GCS is specifically parameterized. The SCS has the same basic characteristics

as the GCS, but it additionally includes crop-specific phenological stages (Table 2-2), such as the tassel initiation and silking stages for corn, beginning of pod growth and end of pod growth stages for soybean, and terminal spikelet and end of ear growth stages for winter wheat, and the main growth tissues also differ across the crops' various phenological stages. Moreover, the SCS also includes crop-specific physiological characteristics, such as photoperiodism and biological N fixation for soybean, and vernalization for winter wheat.

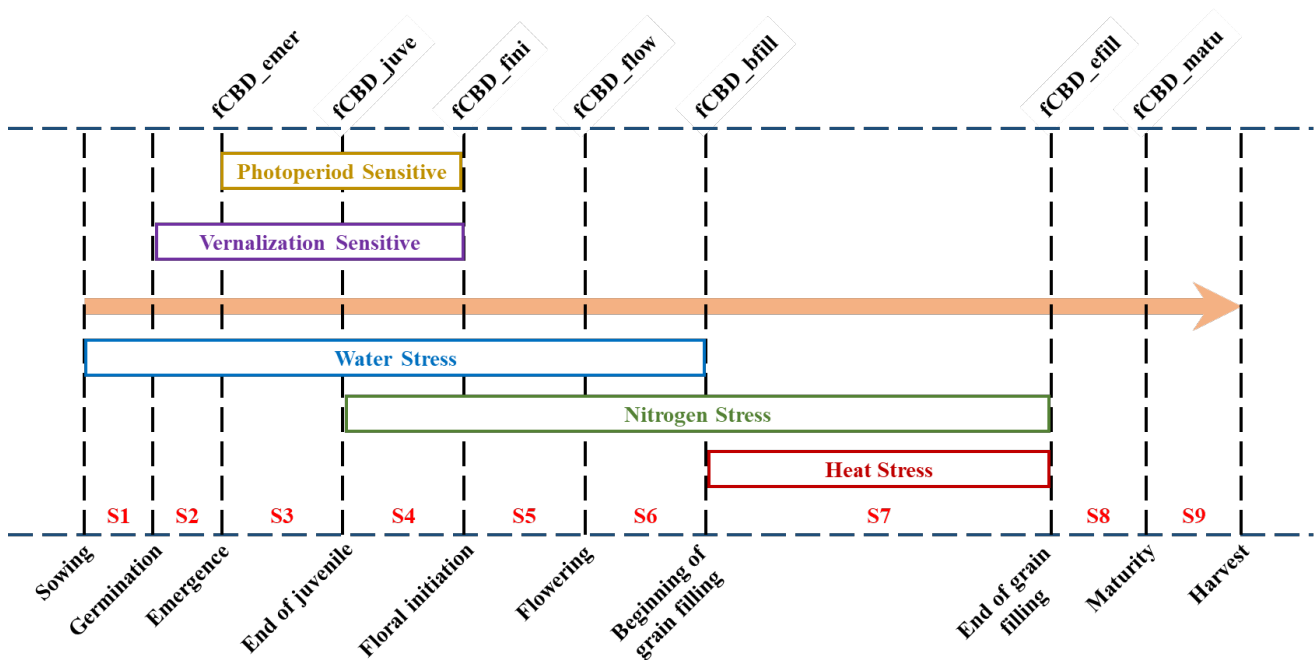


Figure 2-2. Crop life cycle in the general crop scheme of the Dynamic Land Ecosystem Model v4.0. fCBD_emer, fCBD_juve, fCBD_fini, fCBD_flow, fCBD_bfill, fCBD_efill, and fCBD_matu denote the target fraction of Cumulative Biological Days required to reach the phenological stages of emergence, end of juvenile, floral initiation, flowering, beginning of grain filling, end of grain filling, and maturity, respectively.

Table 2-2. Phenological stages in the specific crop scheme of the Dynamic Land Ecosystem Model and the main growing tissues during these stages.

Phase	Duration	Crop	Main growth tissues
1	Sowing to germination	All	None
2	Germination to emergence	All	Root, leaf
3	Emergence to end of juvenile	Corn	Root, leaf
	Emergence to flowering (R1)	Soybean	Root, leaf, stem
4	Emergence to terminal spikelet	Winter wheat	Root, leaf
	End of juvenile to tassel initiation	Corn	Root, leaf, stem
5	Flowering (R1) to beginning of pod growth (R3)	Soybean	Root, leaf, stem
	Terminal spikelet to end of leaf growth	Winter wheat	Root, leaf, stem
6	Tassel initiation to silking	Corn	Root, leaf, stem
	Beginning of pod growth (R3) to beginning of grain filling (R5)	Soybean	Root, leaf, stem
	End of leaf growth to end of ear growth	Winter wheat	Root, stem
7	Silking to beginning of grain filling	Corn	Root, stem
	Beginning of grain filling (R5) to end of pod growth	Soybean	Root, stem, grain
8	End of ear growth to beginning of grain filling	Winter wheat	Root, stem
	Beginning of grain filling to end of grain filling	Corn, winter wheat	Stem, grain
9	End of pod growth to end of grain filling	Soybean	Stem, grain
	End of grain filling to physiological maturity	All	None
9	Physiological maturity to harvest	All	None

The crop life cycle begins with seed sowing or planting. In DLEM-Ag and DLEM-Ag2, crop sowing dates have been prescribed and remain unchanged, which may lead to large errors in the simulated yields considering that crop planting dates vary annually due to changing weather conditions (Kucharik 2006; Laux et al. 2010; Yang et al. 2020). In contrast, sowing dates in the new model are dynamically simulated rather than prescribed. To determine crop sowing dates,

sowing trigger criteria modified from CLM4.5 were used (Levis et al. 2012). The original sowing trigger criteria in CLM4.5 include: (1) a 10-day running average of mean air temperature that exceeds a threshold; (2) a 10-day running average of minimum air temperature that exceeds a threshold; and (3) a 20-year running average of 8°C-based growing degree-days (GDD) from April to September that exceeds a threshold. However, these criteria have been found to lead to earlier sowing dates than the actual, because the GDD criterion is easily met and thus the sowing date is in fact determined by the first two criteria (Chen et al. 2015; Chen et al. 2018). To this end, we have modified the GDD criterion to be the cumulative thermal time from the earliest sowing date (defined by input data) that is greater than the crop-specific threshold (Peng et al. 2018). Summarizing, the revised sowing trigger criteria used in DLEM v4.0 are as follows:

$$\left\{ \begin{array}{l} SDate_{earliest} \leq SDate \leq SDate_{latest} \\ T_{avg}^p < T_{avg}^{10d} \\ T_{min}^p < T_{min}^{10d} \\ ATT_{min} < ATT \end{array} \right. \quad (1)$$

where $SDate_{earliest}$ and $SDate_{latest}$ denote the crop-specific prescribed earliest and latest sowing dates, respectively, which are obtained from input data; $SDate$ denotes the simulated sowing date; T_{avg}^p and T_{min}^p denote the crop-specific thresholds of the 10-day running average and minimum temperatures for sowing; T_{avg}^{10d} and T_{min}^{10d} denote the actual 10-day running average and minimum air temperatures, respectively; ATT_{min} denotes the crop-specific threshold of minimum thermal time for sowing; ATT denotes the accumulated thermal time from the earliest sowing date to the current day, which is calculated using Equations (2) and (3). If the above criteria are not met, crops will be sown at the prescribed latest sowing date.

$$ATT = \sum_{earliest\ day}^{current\ day} dailyTT \quad (2)$$

$$dailyTT = \begin{cases} 0, & \text{if } T_{avg} \leq Card_{min} \text{ or } T_{avg} \geq Card_{max} \\ T_{avg} - Card_{min}, & \text{if } Card_{min} < T_{avg} \leq Card_{opt1} \\ Card_{opt1} - Card_{min}, & \text{if } Card_{opt1} < T_{avg} < Card_{opt2} \\ \frac{(Card_{max} - T_{avg}) \times (Card_{opt1} - Card_{min})}{Card_{max} - Card_{opt2}}, & \text{if } Card_{opt2} < T_{avg} < Card_{max} \end{cases} \quad (3)$$

where $dailyTT$ is the daily thermal time; T_{avg} is the average air temperature; $Card_{min}$, $Card_{opt1}$, $Card_{opt2}$, and $Card_{max}$ are the crop-specific minimum, lower optimal, upper optimal, and maximum air temperatures required for photosynthesis, respectively.

Seed germination is triggered if the number of days after the simulated sowing date is larger than the crop-specific threshold. The initiation and duration of the subsequent phenological stages (i.e., from emergence to maturity) are determined according to the Biological Days (BD)-based phenological development scheme (Soltani and Sinclair 2012). Specifically, we first calculate the daily BD (i.e., an indicator of daily development rate) using a 3-segment temperature response function, with the vernalization and photoperiod effects as well as environmental stresses considered (Equation (4)); then the fraction of Cumulative Biological Days (fCBD), an indicator of cumulative crop development rate updated at a daily time-step, is calculated as the actual accumulated BD from germination to the current day divided by the total BD required for maturity (Equation (5)). A phenological stage is predicted to occur when the calculated fCBD reaches the target fCBD of that stage.

$$dailyBD = tempfun \times ppfun \times verfun \times f_{stress} \quad (4)$$

$$fCBD = \frac{\sum_{germination}^{current\ day} dailyBD}{\sum_{germination}^{maturity} dailyBD} \quad (5)$$

where $dailyBD$ denotes daily crop development rate; $tempfun$, $ppfun$, $verfun$, and f_{stress} denote the inhibition of the potential crop development rate by temperature, photoperiod,

vernalization, and environmental stresses, respectively, and are calculated using Equations (6)-(11); $fCBD$ denotes the fraction of accumulated $dailyBD$ (i.e., from germination to the current day) to total BD required for maturity, in which $fCBD$ is equal to 0 at the germination stage and equal to 1 at the maturity stage. The crop is harvested immediately after maturity or when the growing season length of crops exceeds the crop-specific longest growing days.

$$tempfun = \frac{dailyTT}{Card_{opt1} - Card_{min}} \quad (6)$$

$$ppfun = \begin{cases} \begin{cases} 1 - ppsen \times (CPP - PP), & \text{if } PP < CPP \\ 1, & \text{if } PP \geq CPP \end{cases} & \text{(for long day crop)} \\ \begin{cases} 1, & \text{if } PP < CPP \\ 1 - ppsen \times (PP - CPP), & \text{if } PP \geq CPP \end{cases} & \text{(for short day crop)} \end{cases} \quad (7)$$

$$verfun = \begin{cases} 1 - vsen \times (VDSAT - CUMVER_i), & \text{if } CUMVER_i < VDSAT \\ 1, & \text{if } CUMVER_i \geq VDSAT \end{cases} \quad (8)$$

$CUMVER_i$

$$= \begin{cases} CUMVER_{i-1} + VERDAY - 0.5 \times (T_{max} - 30), & \text{if } CUMVER_{i-1} < 10 \text{ and } T_{max} > 30 \\ CUMVER_{i-1} + VERDAY, & \text{other conditions} \end{cases} \quad (9)$$

$$VERDAY = \begin{cases} 0, & \text{if } T_{avg} \leq Ver_{min} \text{ or } T_{avg} \geq Ver_{max} \\ \frac{T_{avg} - Ver_{min}}{Ver_{opt1} - Ver_{min}}, & \text{if } Ver_{min} < T_{avg} \leq Ver_{opt1} \\ 1, & \text{if } Ver_{opt1} < T_{avg} < Ver \\ \frac{Ver_{max} - T_{avg}}{Ver_{max} - Ver_{opt2}}, & \text{if } Ver_{opt2} < T_{avg} < Ver_{max} \end{cases} \quad (10)$$

$$f_{stress} = \begin{cases} \max(f_W, f_W^{min}), & \text{if sowing} \leq \text{stage} \leq \text{end juvenile} \\ \min(f_W, \max(f_N, f_N^{min})), & \text{if end juvenile} \leq \text{stage} \leq \text{flowering} \\ 1, & \text{for other stages} \end{cases} \quad (11)$$

where $dailyTT$ denotes the daily thermal time, which is calculated using Equation (3); $Card_{min}$ and $Card_{opt1}$ denote the minimum and lower optimal air temperatures required for

photosynthesis, respectively; $ppsen$ is a cultivar-specific photoperiod sensitivity coefficient; PP is daylength; CPP is a cultivar-specific critical daylength parameter at which the rate of phenological development began to be restricted by daylength; $vsen$ is a cultivar-specific vernalization sensitivity coefficient; $VDSAT$ is the number of vernalization days needed to saturate the vernalization response; $CUMVER$ denotes cumulative vernalization days; $VERDAY$ denotes vernalization day, representing the contribution of each day to vernalization; T_{max} denotes the maximum air temperature; Ver_{min} , Ver_{opt1} , Ver_{opt2} , and Ver_{max} are the minimum, lower optimal, upper optimal, and maximum air temperatures required for vernalization, respectively; f_W and f_N denote drought and N stresses, respectively, which are calculated using Equation (15); and f_W^{min} and f_N^{min} denote the minimum drought and N stresses, respectively (here set to be 0.5 (Peng et al. 2018)). In addition, the devernalization process is also considered in DLEM v4.0 when winter crops are exposed to high temperature, namely, if $CUMVER$ is less than 10 days and the maximum air temperature is higher than 30 °C, then $CUMVER$ is decreased by 0.5 days per degree above 30 °C; however, if $CUMVER$ is larger than 10 days, no devernalization will occur.

Along with the development of phenology, crop LAI is updated at a daily time step and ceases increase at the beginning of the reproductive phase. The daily LAI is calculated as a function of leaf carbon content and specific leaf area (SLA; the ratio of leaf area to leaf dry mass) (Equation (12)). Meanwhile, following CLM 4.5 (Levis et al. 2012), crop canopy height (H_{canopy}) also varied with phenological stages and is obtained by scaling the maximum canopy height ($H_{canopy,max}$) by the daily LAI (Equation (13)).

$$LAI = \min(C_{leaf} \times SLA, LAI_{max}) \quad (12)$$

$$H_{canopy} = H_{canopy,max} \times \min \left[\left(\frac{LAI}{LAI_{max} - 1} \right), 1 \right]^2 \quad (13)$$

where C_{leaf} denotes leaf carbon content; SLA is a cultivar-specific parameter representing the ratio of leaf area to leaf dry mass; and LAI_{max} denotes the maximum LAI.

2.2.1.2 Carbon assimilation and allocation

Photosynthesis processes in the agricultural module of DLEM v4.0 are inherited from a previous DLEM version (Tian et al. 2010a). However, to improve the representation of C4 plant (e.g., corn and sorghum) responses to environmental stresses (e.g., temperature, moisture, and radiation), we further incorporated an enzyme-driven C4 photosynthesis routine (Di Vittorio et al. 2010), which uses an enzyme-driven bundle sheath CO₂ concentration to substitute the diffusion-driven internal CO₂ concentration available to ribulose-1,5-bisphosphate carboxylase-oxygenase (Rubisco) for carbon assimilation.

For daily carbon allocation, DLEM-Ag and DLEM-Ag2 do not consider environmental stresses when allocating net carbon assimilates to the leaf, stem, and reproduction pools. To overcome this limitation, we implemented a new dynamic carbon allocation scheme in the agricultural module of DLEM v4.0. The potential allocation ratios followed a crop-specific dynamic carbon allocation curve across phenological stages (Gaspar et al. 2017; Gregory and Atwell 1991; Gregory et al. 1995; Lei et al. 2010; Lokupitiya et al. 2009; Peart and Shoup 2018; Ritchie 1991; Srivastava et al. 2006; Taylor et al. 1982; Wilhelm 1998; Yamagata et al. 1987), which were further regulated by light, N, and water stresses (Song et al. 2013) to obtain the actual ratios:

$$\left\{ \begin{array}{l} A_{leaf} = \frac{A_{leaf,p}}{1 + \omega \times (3 - f_L - f_N - f_W)} \\ A_{stem} = \frac{A_{stem,p} + \omega \times (1 - f_L)}{1 + \omega \times (3 - f_L - f_N - f_W)} \\ A_{root} = \frac{A_{root,p} + \omega \times (2 - f_N - f_W)}{1 + \omega \times (3 - f_L - f_N - f_W)} \\ A_{repr} = \frac{\min(C_{avail} \times A_{repr,p}, C_{demand})}{C_{avail} \times (1 + \omega \times (3 - f_L - f_N - f_W))} \end{array} \right. \quad (14)$$

where A_{leaf} , A_{stem} , A_{root} , and A_{repr} denote the actual carbon allocation ratios for leaf, stem, root, and reproduction pools modified by environmental stresses, respectively; $A_{leaf,p}$, $A_{stem,p}$, $A_{root,p}$, and $A_{repr,p}$ denote the potential carbon allocation ratios for leaf, stem, root, and reproduction pools, respectively, which are derived from the prescribed growth-stage dependent carbon allocation curve; ω is a scaling parameter representing the sensitivity of an allocation ratio to changes in light, N, and water stresses; f_L , f_N , and f_W denote the light, N, and water stresses, respectively, which are calculated as follows:

$$\left\{ \begin{array}{l} f_L = \exp(-ext_{coef} \times LAI) \\ f_N = \min\left(\frac{N_{act}}{N_{max}}, 1\right) \\ f_W = \sum_{i=1}^{10} f_{root_i} \times \beta_i \\ \beta_i = \begin{cases} 0, & \text{if } \psi_i \leq \psi_{close} \\ \frac{\psi_{max} - \psi_i}{\psi_{max} - \psi_{sat,i}}, & \text{if } \psi_{close} < \psi_i < \psi_{open} \\ 1, & \text{if } \psi_i \geq \psi_{open} \end{cases} \end{array} \right. \quad (15)$$

where ext_{coef} denotes the canopy light extinction coefficient; LAI denotes the leaf area index; N_{act} denotes the actual N content in the vegetation pool; N_{max} denotes the maximum N content in the vegetation pool; f_{root_i} denotes the root fraction in the soil layer i ; β_i is a soil matric potential-related factor; ψ_{max} denotes the maximum water potential, which represents the wilting

point potential of leaves (currently set to be -1.5×10^5); ψ_i denotes the water potential of layer i (mm H₂O); and ψ_{open} and ψ_{close} denote the water potential under which the stomata fully opens and closes, respectively (mm H₂O).

In addition, C_{avail} is the net carbon assimilates available for allocation, and C_{demand} is the actual carbon demand for fulfilling grain filling, which is calculated as:

$$C_{demand} = AKW \times GN \times P_{density} \quad (16)$$

where $P_{density}$ denotes planting density (i.e., number of plants per square meter), and AKW denotes the actual kernel weight at physiological maturity, which is determined as the product of daily BD and potential kernel growth rate (pKGR) and is subject to heat and N stresses:

$$\left\{ \begin{array}{l} AKW = dailyBD \times pKGR \times f_N \times f_{heat} \\ pKGR = \frac{pKW}{\sum_{start\ grain\ fill}^{end\ grain\ fill} dailyBD} \\ f_{heat} = \begin{cases} 1, & \text{if } T_{avg} \leq HeatTemp_{min} \\ 1 - \frac{T_{avg} - HeatTemp_{min}}{HeatTemp_{max} - HeatTemp_{min}}, & \text{if } HeatTemp_{min} < T_{avg} \leq HeatTemp_{max} \\ 0, & \text{if } T_{avg} > HeatTemp_{max} \end{cases} \end{array} \right. \quad (17)$$

where $dailyBD$ is calculated from Equation (4); f_N and f_{heat} denote the N and heat stresses, respectively; pKW denotes the potential kernel weight, which is estimated as the ratio of potential kernel weight to the target BD during the grain filling period; $HeatTemp_{min}$ and $HeatTemp_{max}$ denote the minimum and maximum cardinal temperatures at which heat stress occurs.

In terms of grain number (GN), previous studies have demonstrated that GN is strongly associated with the physiological status of a crop (e.g., plant growth rate and tissue biomass) during a critical period for seed set, in which the critical period for corn and wheat are around the flowering stage (Aluko and Fischer 1988; Andrade et al. 1999; Bindraban et al. 1998; Early et al. 1967; Fischer 1985; Zheng et al. 2014). For soybean, this period extends from the flowering stage

to the beginning or middle grain filling stage (Board and Tan 1995; Egli 1998; Jiang and Egli 1995; Vega et al. 2001). In our model, GN of corn is calculated based on an exponential function related to plant growth rate from the end of juvenile stage to the silking stage, similar to the methods implemented in the APSIM model (Keating et al. 2003); GN of soybean is calculated based on an empirical linear model related to plant growth rate from the flowering stage to the start of grain filling stage (Vega et al. 2001); and GN of wheat and other crops are calculated from an empirical equation related to stem dry matter at anthesis (Fischer 1985; Zheng et al. 2014):

$$\left\{ \begin{array}{l} GN = \begin{cases} GN_{max} \times \left(1 - \exp(-GNk \times (PGR - PGR_{base}))\right), & \text{for corn} \\ \max(k_1 + k_2 \times PGR, GN_{max}), & \text{for soybean} \\ \max(DM_{stem} \times GNg_{stem}, GN_{max}), & \text{for wheat and other crops} \end{cases} \\ PGR = \frac{DM_{t1} - DM_{t0}}{Nday} \end{array} \right. \quad (18)$$

where GN_{max} is a cultivar-specific parameter representing the maximum grain number per plant; GNk and PGR_{base} are genotype parameters related to the GN of corn, which are set to 0.83 and 1.2, respectively (derived from the APSIM model); k_1 and k_2 denote the intercept and slope of the empirical linear model used to calculate the GN of soybean, which are set to 4.5 and 123.9, respectively (derived from Vega et al. (2001)); DM_{stem} denotes the stem dry weight at anthesis; GNg_{stem} denotes the number of kernels per gram stem; PGR denotes the plant growth rate during the critical period for seed set and is calculated by dividing the accumulated shoot dry matter during this critical period ($DM_{t1} - DM_{t0}$) by the number of days of this period ($Nday$), in which DM_{t1} and DM_{t0} denote the shoot dry matter at the end and beginning of this period, respectively.

This dynamic carbon allocation scheme allows optimizing crop growth processes across its phenological stages. During the emergence stage, carbon stored in the seeds is allocated to the leaf pool and root pool at a fixed ratio of 0.6 and 0.4, respectively; during the vegetative phase, net

assimilates are preferentially allocated to leaf, root, and then stem to facilitate capture of solar radiation and uptake of nutrients and water; during the reproductive phase, the reproduction pool has the highest priority of carbon allocation to fulfill grain filling.

2.2.1.3 Yield formation

In DLEM v4.0, the estimation of crop yield adopts a different algorithm from DLEM-Ag and DLEM-Ag2. Specifically, in DLEM-Ag, crop yield is estimated as the product of total aboveground biomass and a constant harvest index, which may lead to deviation in the simulated yields considering that harvest index actually varies with climate conditions, farming practices, and environmental factors (Hay 1995; Porker et al. 2020; Sinclair 1998). In DLEM-Ag2, crop yield is determined by the actual carbon demand for grain filling, where a single empirical equation related to stem dry weight is used to calculate the actual carbon demand of all crops, even though the grain filling characteristics differ by crops. In DLEM v4.0, yield formation follows a supply-demand relationship. That is, it is estimated as the balance between the available carbon assimilates supply to the reproduction pool and the actual carbon demand for crop to fulfill grain filling (Jones et al. 2003; Villalobos et al. 1996). Moreover, we use various methods derived from relevant studies, with crop-specific grain filling characteristics considered, to calculate the actual carbon demand of different crops (Equation (16)). The translocation of dry matter between the stem tissue and the reproduction pool is also considered in the new model, allowing up to 20% of carbon to be translocated from the stem pool to the reproduction pool to supplement grain filling if the available carbon assimilates cannot satisfy the actual carbon demand. If excess assimilates are available, the carbon that exceeds the actual carbon demand will be re-translocated from the reproduction pool to the stem pool to ensure mass balance.

2.2.1.4 Biological nitrogen fixation

Crops like soybeans are able to fix N to meet nutrient requirements for growth. In DLEM-Ag and DLEM-Ag2, the biological N fixation is determined by the prescribed PFT-specific annual N fixation rate and CO₂ concentration, which does not consider environmental stresses and the effects of crop growth stages. In DLEM v4.0, the biological N fixation process has been improved, which is calculated as a function of potential N fixation rate, soil temperature, soil moisture, soil mineral N concentration, substrate carbon concentration, and crop phenological stage (Liu et al. 2011):

$$N_{fix} = N_{fix,pot} \times f_{soilT} \times f_{soilW} \times f_{soilN} \times f_{soilC} \times f_{phen} \quad (19)$$

where N_{fix} is the actual biological N fixation rate; $N_{fix,pot}$ is the potential N fixation rate; f_{soilT} is a soil temperature factor; f_{soilW} is a soil moisture factor; f_{soilN} is a soil mineral N factor; f_{soilC} is a function of substrate carbon concentration; and f_{phen} is a factor of crop phenological stage (calculated using Equation (20)).

$$\left\{ \begin{array}{l} f_{soilT} = \begin{cases} f_{max}(0, T_{soil} \times T_{soil} \times (45 - T_{soil}) \times 0.0001), & \text{if } T_{soil} > 0 \\ 0, & \text{if } T_{soil} \leq 0 \end{cases} \\ f_{soilW} = f_{min}\left(1.82 * \frac{\theta}{\theta_{sat}}, 1\right) \\ f_{soilN} = f_{min}(f_{max}(1 - 0.0784 \times \log(avn), 0), 1) \\ f_{soilC} = f_{max}\left(\frac{C_{sub}}{C_{sub} + kc}, 0.01\right) \\ f_{phen} = \begin{cases} 0, & \text{for } f_{CBD} < f_{Phen_{min}} \\ \frac{f_{CBD} - f_{Phen_{min}}}{f_{Phen_{optL}} - f_{Phen_{min}}}, & \text{for } f_{Phen_{min}} < f_{CBD} < f_{Phen_{optL}} \\ 1, & \text{for } f_{Phen_{optL}} < f_{CBD} < f_{Phen_{optH}} \\ \frac{f_{Phen_{max}} - f_{CBD}}{f_{Phen_{max}} - f_{Phen_{optH}}}, & \text{for } f_{Phen_{optH}} < f_{CBD} < f_{Phen_{max}} \\ 0, & \text{for } f_{CBD} > f_{Phen_{max}} \end{cases} \end{array} \right. \quad (20)$$

where T_{soil} denotes the soil temperature; θ and θ_{sat} denote the actual and saturated soil moisture contents, respectively; avn denotes the available soil N; C_{sub} denotes the substrate carbon; kc denotes the Michaelis–Menten constant for CO_2 ; $fCBD$ denotes the cumulative crop development rate from germination to the current day; $fPhen_{min}$ denotes the time before which no N fixation happens; $fPhen_{optL}$ and $fPhen_{optH}$ denote the beginning and end time within which the N fixation rate is not limited by crop phenological stage; $fPhen_{max}$ denotes the time after which the N fixation ceases. The values of $fPhen_{min}$, $fPhen_{optL}$, $fPhen_{optH}$, and $fPhen_{max}$ are set to 15%, 30%, 55%, and 75% of the crop life cycle (Cabelguenne et al. 1999).

2.2.2 Agricultural management practices

Previous DLEM versions have incorporated common management practices, including N fertilization, irrigation, and crop rotation. N fertilization practice is represented by adding N directly to the soil ammonium and nitrate pools to meet crop N demands through both industrial fertilizer and manure application. Irrigation practice is implemented by assuming that soil moisture would reach field capacity when irrigated, in which irrigation timing is determined as the point when soil moisture of the top layer dropped to 30% of maximum available water (i.e., field capacity minus wilting point) during the growing season (Ren et al. 2011). Crop rotation is implemented by allowing different crop types to exist on the same soil during different periods of growing/planting cycles (e.g., rotation of winter and summer crops).

In the new model, besides including more management practices like tillage and cover cropping, we also incorporated genetic improvement options, as increased crop yields in the past decades can be largely attributed to improvements in both management practices and crop genetic breeding (Duvick 1984, 2005; Hammer et al. 2009; Pingali 2012). Four types of tillage practices (i.e., no-tillage, conservation tillage, reduced tillage, and conventional tillage) are considered in

our model, based on the differences in tillage depth, mixing efficiency, and the proportion of soil surface covered by residues after tillage (Table 2-3) (Porwollik et al. 2019). Three aspects of tillage impacts on the agroecosystem are represented: (1) changes in surface residue coverage and the subsequent redistribution of soil organic matter (SOM) and nutrients within the tilled soil layers due to tillage mixing (Section 2.2.2.1); (2) changes in litter interception, bulk density, soil moisture and other water-related effects on processes such as nitrification, denitrification, and leaching (Section 2.2.2.2); and (3) changes in the soil decomposition rate (Section 2.2.2.3). Cover cropping is represented in the new model through planting crops (e.g., winter rye and peas) during the normal fallow period and leaving crop biomass in the field at the beginning of the following main crop growing season (Huang et al. 2020). The impacts of crop genetic improvements on yields are represented through two mechanisms: (1) increasing the photosynthesis rate of crops (Long et al. 2015; Parry et al. 2011; Wu et al. 2019), and (2) enhancing crop N uptake ability (Lu et al. 2018). Besides these new considerations, we have also improved the representation of the existing rotation practice, where a dynamic rotation scheme is incorporated into the new model through introducing time-varying crop rotation maps, rather than the static rotation map in previous versions.

Table 2-3. Four tillage systems implemented in the Dynamic Land Ecosystem Model.

Tillage Type	No-tillage	Conservation tillage	Reduced tillage	Conventional tillage
Depth (cm)	5	10	20	20
Mixing efficiency (%)	5	50	90	90
Soil layer inversion	No	Yes	Yes	Yes
Soil surface covered by residues after planting (%)	> 30	15 ~ 30	15 ~ 30	< 15

2.2.2.1 Effects of tillage implement on soil organic matter and nutrients contents

The effects of tillage practice on litter pools include the incorporation of surface residues into the soil and the redistribution of SOM and nutrients in the tilled soil layers. In DLEM v4.0, litter pool can be classified into two categories: aboveground litter pool ($Litter_{ag}$) and belowground litter pool ($Litter_{bg}$). Both of the dead shoot biomass of crops due to turnover and the crop residues not removed from the field are directly added to $Litter_{ag}$, and the dead root biomass as well as the root residue are added to the $Litter_{bg}$. Besides, part of $Litter_{ag}$ will be transferred to $Litter_{bg}$ through bioturbation and tillage mixing practice, which is the same as that implemented in LPJmL5 (Lutz et al. 2019a). For the bioturbation pathway, we assumed that 0.1897% of the $Litter_{ag}$ is transferred to $Litter_{bg}$ per day to account for the vertical displacement of litter under no-tillage and natural vegetation conditions (Lutz et al. 2019a); and for the tillage pathway, the amount of transfer depends on tillage intensity:

$$Litter_{bg,t+1} = Litter_{bg,t} + Litter_{ag,t} \times f_{mix} \quad (21)$$

$$Litter_{ag,t+1} = Litter_{ag,t} \times (1 - EF_{mix}) \quad (22)$$

where $Litter_{bg,t+1}$ and $Litter_{ag,t+1}$ denote the belowground and aboveground litter pools in the $(t + 1)$ th day, respectively; $Litter_{bg,t}$ and $Litter_{ag,t}$ denote the belowground and aboveground litter pools in the t th day, respectively; and EF_{mix} denotes the mixing efficiency, with a value between 0 and 1.

The redistribution of SOM and nutrients among the tilled soil layers is calculated based on the methods adopted in the Agricultural Policy Environmental EXTender (APEX) model (Williams et al. 2008):

$$X_l = X_{ol} \times (1 - EF_{mix}) + \frac{Z_l - Z_{l-1}}{D_t} \times EF_{mix} \times \sum_{k=1}^M X_{ok} \quad (23)$$

where X_l is the amount of SOM/nutrients in layer l after mixing; X_{ol} is the original amount of SOM/nutrients in layer l before mixing; EF_{mix} denotes the mixing efficiency; Z is the depth to the bottom of the tilled layer; D_t is the tillage depth; M is the total number of soil layers affected by tillage operation; and X_{ok} is the original amount of SOM/nutrients in layer k before mixing.

2.2.2.2 Effects of tillage implement on soil water processes

The impacts of tillage operation on soil water processes in DLEM are mainly reflected in two aspects: (1) changes in litter interception due to reduced surface residue coverage and the accompanying changes in litter evaporation, soil evaporation and infiltration, as well as soil moisture content; (2) changes in soil bulk density due to tillage mixing and the accompanying changes in soil moisture content at saturation and field capacity.

In DLEM, precipitation and irrigation water are either intercepted by crop canopy and surface litter or falls to the ground as throughfall, and will be lost through evapotranspiration, soil infiltration and surface runoff. Crop canopy interception is calculated as the same process as in the natural vegetation module of DLEM, which is estimated as the minimum of input water content and canopy water holding capacity (Tian et al. 2010a). Litter interception is determined as the balance of available input water content after canopy interception and actual water holding capacity of surface litter ($whc_{lit,act}$), in which $whc_{lit,act}$ is calculated as:

$$whc_{lit,act} = whc_{lit,max} \times f_{lit} \quad (24)$$

where $whc_{lit,max}$ denotes the maximum water holding capacity of surface litter, which is obtained by multiplying $Litter_{ag}$ with a conversion factor of $2 \times 10^{-3} mmkg^{-1}$, following Lutz

et al. (2019a) and Enrique et al. (1999); and f_{lit} denotes the fraction of soil surface covered by litter, which is calculated through adapting the equation from Gregory (1982):

$$f_{lit} = 1 - e^{-A_m \times Litter_{ag}} \quad (25)$$

where A_m denotes the area covered per dry matter of surface litter and is set to 0.004 in DLEM (Dadoun 1993).

The calculation of litter evaporation ($EVAP_{lit}$) is similar to the calculation of soil evaporation ($EVAP_{soil}$) in DLEM, which is obtained by multiplying the potential evaporation (PET) estimated from the Penman–Monteith equation with a LAI-adjusted item (Pan et al. 2020; Pan et al. 2015). Here, f_{lit} is also included in the calculation process of $EVAP_{lit}$ and $EVAP_{soil}$ to account for the impacts of changes in surface litter coverage on evaporation:

$$EVAP_{lit} = PET_{lit} \times e^{-0.6 \times LAI} \times f_{lit} \quad (26)$$

$$EVAP_{soil} = PET_{soil} \times e^{-0.6 \times LAI} \times (1 - f_{lit}) \quad (27)$$

Tillage practice generally leads to a reduction in bulk density through incorporating surface residues into the soil and promoting soil fragmentation (Guérif et al. 2001; Maharjan et al. 2018), which further results in the changes in soil moisture content at saturation and field capacity. Here, the impacts of tillage implement on bulk density and the subsequent soil moisture effects are calculated as (Lutz et al. 2019a):

$$f_{BDtill,l,aft} = f_{BDtill,l,pri} - (f_{BDtill,l,pri} - 0.667) \times EF_{mix} \quad (28)$$

$$\theta_{sat,l,aft} = 1 - (1 - \theta_{sat,l,pri}) \times f_{BDtill,l,aft} \quad (29)$$

$$\theta_{fc,l,aft} = \theta_{fc,l,pri} - 0.2 \times (\theta_{sat,l,pri} - \theta_{sat,l,aft}) \quad (30)$$

where $f_{BDtill,l,aft}$ denotes the fraction of bulk density change after tillage in layer l ; and $f_{BDtill,prior}$ denotes the density effect before tillage in layer l ; $\theta_{sat,l,aft}$ and $\theta_{fc,l,aft}$ are the modified soil moisture content at saturation and field capacity after tillage in layer l ; $\theta_{sat,l,pri}$ and $\theta_{fc,l,pri}$ are the original soil moisture content at saturation and field capacity before tillage in layer l . In DLEM v4.0, the vertical soil profile is described by a ten-layer discretization of a 3.5 m soil profile, and the layer thickness increases geometrically from top to bottom with values of 0.05 m, 0.05 m, 0.1 m, 0.2 m, 0.2 m, 0.3 m, 0.3 m, 0.5 m, 0.8 m, and 1 m, respectively. Soil water flow between different soil layers is calculated using the Darcy's law, in which the water flow rate q (mm/s) in layer l can be approximated as:

$$q_l = -k[z_{h,l}] \left[\frac{(\Psi_l - \Psi_{l+1}) + (z_{l+1} - z_l)}{(z_{l+1} - z_l)} \right] \quad (31)$$

where $k[z_{h,l}]$ is the hydraulic conductivity at the depth of the interface of two adjacent layers ($z_{h,l}$), z_l is the depth of soil layer l , and Ψ_l is the soil matric potential (mm).

2.2.2.3 Effects of tillage implement on decomposition

In DLEM, the direct effect of tillage implement on the decomposition rate of litter pools is represented by a tillage scalar (f_{till}), which has a value greater than 1, indicating the promoting effect of tillage on decomposition (Huang et al. 2020). In addition, the indirect effect of tillage implement on decomposition is also included, which is mainly reflected in its impacts on the amount of SOM, nutrient availability, actual soil moisture content, and soil moisture content at saturation and field capacity. The actual decomposition rate of each litter pool (k_{pool}) within the tilled soil layers is calculated as:

$$k_{pool} = kmax_{pool} \times f(T) \times f(W) \times f(clay) \times f(N) \times f_{till} \quad (32)$$

$$f(T) = 4.89 \times e^{-3.432+0.1 \times T_{soil} \times (1-0.5 \times T_{soil}/36.9)} \quad (33)$$

$$f(W) = \begin{cases} \frac{1 - e^{-\theta/\theta_{sat}}}{1 - e^{-\theta_{fc}/\theta_{sat}}}, & \text{if } \theta \leq \theta_{fc} \\ 1.0044 - \frac{0.0044}{e^{-5 \times \left(\frac{\theta/\theta_{sat} - \theta_{fc}/\theta_{sat}}{1 - \theta_{fc}/\theta_{sat}} \right)}}, & \text{if } \theta > \theta_{fc} \end{cases} \quad (34)$$

$$f(clay) = 1 - 0.75 \times P_{clay}/100 \quad (35)$$

$$f(N) = \begin{cases} f(N_{mi}), & \text{if mineralization occurs} \\ f(N_{im}), & \text{if immobilization occurs} \end{cases} \quad (36)$$

$$f(N_{mi}) = \begin{cases} 1 - \frac{avn - avn_{opt}}{avn_{opt}}, & \text{if } avn > avn_{opt} \\ 1, & \text{if } avn_{opt}/2 \leq avn \leq avn_{opt} \\ 1 + \frac{0.5avn_{opt} - avn}{avn_{opt}}, & \text{if } avn \leq avn_{opt}/2 \end{cases} \quad (37)$$

$$f(N_{im}) = avn/n_{imm} \quad (38)$$

$$f_{till,i} = 1 + f_{cm,i} \quad (39)$$

$$f_{cm,i} = \begin{cases} (3 + 5 \times e^{-5.5 \times P_{clay}}) \times \frac{EF_{mix}}{EF_{mix} + e^{1-2 \times EF_{mix}}}, & i = 1 \\ f_{cm,i-1} \times \left(1 - 0.02 \times \frac{\theta}{\theta_{sat}} \right), & i > 1 \end{cases} \quad (40)$$

where $kmax_{pool}$ denotes the potential decomposition rate of each pool; $f(T)$, $f(W)$, $f(clay)$, and $f(N)$ denote the limitation of soil temperature, soil moisture, soil texture, and N on decomposition; f_{till} is a tillage scalar; T_{soil} is soil temperature; θ , θ_{sat} and θ_{fc} denote the actual soil moisture content, soil moisture content at saturation, and soil moisture content at field

capacity, respectively; P_{clay} denotes the percentage of clay content; $f(N_{mi})$ and $f(N_{im})$ denote the limitation of N availability when mineralization and immobilization occur, respectively; avn and avn_{opt} denote the actual and optimum available soil N, respectively; n_{imm} denotes the potential N immobilization estimated by the tentative decomposition procedure; $f_{cm,i}$ denotes the cumulative effect of tillage at day i ; EF_{mix} denotes the mixing efficiency; θ and θ_{sat} denote the actual and saturated soil moisture contents of a given soil layer at day i . The decomposition rate is calculated separately in each soil layer, and f_{till} is only considered in those soil layers affected by tillage practice.

2.2.3 Vertical discretization of soil profile and soil biogeochemical processes

Soil carbon represents the largest terrestrial carbon pool, and understanding its dynamics is critical for both predicting future climate change and assessing climate change impacts (Jobbágy and Jackson 2000; Todd-Brown et al. 2014). Deep soil carbon, which constitutes more than half of the global SOC stocks, has been stabilized for long periods (Jobbágy and Jackson 2000; Koarashi et al. 2012). However, recent studies suggest that various environmental changes could potentially destabilize deep soil carbon (Fontaine et al. 2007; Harrison et al. 2011; Henneron et al. 2022; Mathieu et al. 2015). For example, accelerated decomposition of deep SOC may occur when readily decomposable organic matter is supplied to microbial communities (Fontaine et al. 2007), rendering the deep soil carbon particularly susceptible to alterations in root profiles caused by land use and land cover changes as well as soil management practices. Despite the critical role of deep soil carbon, only a limited number of TBMs (e.g., CLM and ORCHIDEE-SOM) have integrated the vertical discretization of SOC distribution and calculated related soil biogeochemical processes at different soil depths (Camino-Serrano et al. 2018; Koven et al. 2013). This oversight could potentially compromise accurate predictions of soil feedbacks in response to global warming,

considering that most existing TBMs operate under the assumption that deep SOC remains inactive in the terrestrial carbon cycle. Thus, improving model representations of vertical SOC distribution, as well as the corresponding soil biogeochemical processes throughout the soil profile, is essential for more accurate simulations and projections of soil carbon dynamics.

2.2.3.1 Vertical discretization scheme

In the improved soil module, the vertical soil profile is described by a ten-layer discretization of a 3.5 m soil profile, and the layer thickness increases geometrically from top to bottom with values of 0.05 m, 0.05 m, 0.1 m, 0.2 m, 0.2 m, 0.3 m, 0.3 m, 0.5 m, 0.8 m, and 1 m, respectively. The SOC is distributed belowground following an exponential function characterizing the specific root density profile for each plant functional type (PFT) (Camino-Serrano et al. 2018; Jobbágy and Jackson 2000):

$$cp = vd_{par1} * \exp(vd_{par2} * depth) + vd_{par3} \quad (41)$$

where cp represents the cumulative percentage of SOC along the soil profile, $depth$ represents soil depth (in meters), and vd_{par1} , vd_{par2} , and vd_{par3} are the PFT-specific parameters used for characterizing specific vertical root density profiles. These PFT-specific parameters are parameterized according to Jobbágy and Jackson (2000).

After discretizing SOC along the vertical soil profile, we first calculated the relevant soil biogeochemical processes for each soil layer subject to layer-specific environmental controls (e.g., soil moisture and soil temperature), and we then integrated these layer-specific results to produce a comprehensive estimate for the entire soil profile.

2.2.3.2 Simulation of soil decomposition processes

To simulate the soil decomposition process, DLEM set various pools, including one Dissolved Organic Matter (*DOM*) pool, two woody debris pools—Aboveground Woody Debris (*CWD_{ag}*) pool and Belowground Woody Debris (*CWD_{bg}*) pool, and four litter pools, namely Aboveground Added Organic Matter 1 (*AOM1_{ag}*) pool, Belowground Added Organic Matter 1 (*AOM1_{bg}*) pool, Aboveground Added Organic Matter 2 (*AOM2_{ag}*) pool, and Belowground Added Organic Matter 2 (*AOM2_{bg}*) pool. Additionally, the DLEM incorporates three microbial pools: Soil Microbial 1 (*SMB1*) pool, Soil Microbial 2 (*SMB2*) pool, and Soil Microbial Residues (*SMR*) pool, as well as two slow soil organic matter pools, specifically Native Organic Matter (*NOM*) pool and Passive Soil Organic Matter (*PSOM*) pool. Among these pools, *AOM1* represents the litter pool resistant to decomposition and is characterized by a longer turnover period, whereas *AOM2* is more readily decomposable. In terms of microbial pools, *SMB1* consists of autochthonous microbes, while *SMB2* contains zymogenous microbes.

The sizes of soil carbon pools and the carbon fluxes that transfer between these pools dictate both the sources and losses of soil organic and inorganic carbon. All forms of organic carbon input—whether derived from tissue turnover, manure, or crop residue—are allocated to specific litter pools based on their carbon/N ratios. Subsequently, carbon fluxes are transferred between these pools through various mechanisms, including biological decomposition, physical adsorption, desorption, surface runoff, and leaching. The decomposition rate of each pool is calculated using a first-order decay algorithm (Liu et al. 2005; Parton et al. 1993; Petersen et al. 2005) that is influenced by soil temperature, soil water content, nutrient availability, soil texture, and management practices, as outlined in Equations (32)-(40). Further details regarding these processes can be found in previous studies (Banger et al. 2015; Ren et al. 2020; Tian et al. 2015c).

2.2.3.3 Simulation of N₂O dynamics

In DLEM, major N cycling processes include atmospheric N input via N deposition and biological N fixation, N fertilizer application (i.e., synthetic N fertilizer and manure), N immobilization/mineralization, plant N uptake, nitrification/denitrification, adsorption/desorption, N leaching, and unspecified N losses due to fire or other disturbances. Notably, N₂O emissions are primarily from soil N transformation processes (i.e., nitrification and denitrification). Further details of the N₂O module in DLEM can refer to Lu et al. (2021); Tian et al. (2010b); Xu et al. (2012).

(1) Nitrification

Nitrification—a biochemical process that transforms ammonium into nitrate—is simulated as a function of soil temperature, soil moisture, soil pH, and ammonium content:

$$N_{nit} = k_{nit}f(T_{soil})f(w)f(pH)av_{NH_4} \quad (42)$$

where N_{nit} represents the nitrification rate (g N/m²/d), k_{nit} represents the daily maximum fraction of ammonia converted into nitrate and N gases, and it varies with different PFTs with a range of 0.04 to 0.15 d⁻¹; av_{NH_4} represents the soil NH₄⁺ content.

The impact of soil temperature on nitrification, $f(T_{soil})$, is calculated as:

$$f(T_{soil}) = 7.24 \times e^{-3.432+0.168 \times T \times (1-0.5 \times T/36.9)} \quad (43)$$

Likewise, the impact of soil moisture on nitrification, $f(w)$, is calculated as:

$$f(w) = -12.904 \times wfp^4 + 17.651 \times wfp^3 + 5.5368 \times wfp^2 + 0.9975 \times wfp - 0.0243 \quad (44)$$

where wfp represents the percentage of soil porosity filled with water and is defined as:

$$wfp = \frac{\theta}{\theta_{sat}} \quad (45)$$

where θ and θ_{sat} represent the actual and saturated soil moisture contents, respectively.

The impact of soil pH on nitrification, $f(pH)$, is calculated as:

$$f(pH) = -0.0604 \times pH \times pH + 0.7347 * pH - 1.2314 \quad (46)$$

(2) Denitrification

Denitrification is a biochemical process that transforms nitrate (NO_3^-) into three types of N gases: nitric oxide (NO), nitrous oxide (N_2O), and dinitrogen (N_2). The rate of denitrification, N_{denit} , is calculated as:

$$N_{denit} = N_{pot,denit} f(T_{soil}) f(w) f(c_{avNO_3}) \quad (47)$$

In this equation, $N_{pot,denit}$ represents the potential denitrification rate and is calculated as:

$$N_{pot,denit} = (0.151 + 0.015 \times P_{clay}) \times Rh \times kden \quad (48)$$

where P_{clay} represents the percentage of clay content in the soil, Rh is the soil respiration rate, and $kden$ is a parameter that varies by PFTs to fine-tune the potential denitrification rate.

$f(T_{soil})$ represents the influence of soil temperature on denitrification, and is the same as that used in the nitrification process. $f(w)$ represents the impact of soil moisture on denitrification and is defined as:

$$f(w) = 0.0116 + 1.36 / (1 + e^{\frac{wfp - 0.815}{0.0896}}) \quad (49)$$

In addition, $f(c_{avNO_3})$ represents the effect of nitrate concentration on denitrification and is computed as:

$$f(c_{avNO_3}) = 1.17 c_{avNO_3} / (32.7 c_{avNO_3}) \quad (50)$$

$$c_{avNO_3} = av_{NO_3} / BD_{soil} \quad (51)$$

where av_{NO_3} represents the soil NO_3^- content and BD_{soil} represents the soil bulk density.

(3) N₂O emissions

In DLEM, soil N₂O emission is generated through nitrification and denitrification processes:

$$N_2O = (N_{gas_{nit}} + N_{gas_{denit}})f(T)(1 - f(w))f(clay) \quad (52)$$

For the nitrification process, the emission of nitrogenous gases, denoted by $N_{gas_{nit}}$, is calculated as:

$$N_{gas_{nit}} = k_{np}f(T_n)wfp N_{nit} \quad (53)$$

where N_{nit} is the nitrification rate as determined by Equation (42), wfp is the percentage of soil porosity filled with water as calculated by Equation (45), k_{np} is the proportion of N intermediates that contribute to N₂O emissions, and $f(T_n)$ is the effect of temperature on $N_{gas_{nit}}$:

$$f(T) = e^{-0.5((T-34.2)/17.1)^2} \quad (54)$$

For the denitrification process, the quantity of gas emission, denoted by $N_{gas_{denit}}$, is equal to the denitrification rate N_{denit} itself:

$$N_{gas_{denit}} = N_{denit} \quad (55)$$

$f(T)$ in Equation (52) represents the temperature effect:

$$f(T) = \frac{1}{1 + e^{-0.64+0.08T}} \quad (56)$$

$f(w)$ in Equation (52) represents the soil water effect:

$$f(w) = 0.0116 + 1.36/(1 + e^{-\frac{wfp-0.815}{0.0896}}) \quad (57)$$

$f(clay)$ in Equation (52) represents the soil texture effect:

$$f(clay) = 1.26e^{-0.0116P_{clay}} - 0.249 \quad (58)$$

2.2.3.4 Simulation of CH₄ dynamics

The CH₄ flux module within the DLEM has been comprehensively described in our previous studies (Tian et al. 2010b; Tian et al. 2011). Specifically, DLEM simulates the production, consumption, and transport of CH₄. Given the negligible contribution of other substrates to CH₄

production (Le Mer and Roger 2001), DLEM only considers CH₄ production from dissolved organic carbon (DOC), which is indirectly controlled by environmental factors such as soil pH, soil temperature, and soil moisture content. The DOC is produced through three main pathways: gross primary production allocation, and decomposition byproducts from soil organic matter and litterfall. CH₄ oxidation processes, including the oxidation during CH₄ transport to the atmosphere, CH₄ oxidation in the soil/water, and atmospheric CH₄ oxidation on the soil surface, are determined by CH₄ concentrations in the air or soil/water, as well as by soil moisture, soil pH, and soil temperature conditions. Most CH₄-related biogeochemical reactions in DLEM are modeled using the Michaelis-Menten equation, characterized by two coefficients: the maximum reaction rate and the half-saturated coefficient. The model considers three pathways for the transport of CH₄ from the soil to the atmosphere: ebullition, diffusion, and plant-mediated transport. The net CH₄ flux between the atmosphere and the soil is determined by the following equation:

$$F_{CH_4} = F_P + F_D + F_E - F_{air,oxid} - F_{trans,oxid} \quad (59)$$

where F_{CH_4} is the net flux of CH₄ between the soil and the atmosphere (g C/m²/d); F_P is plant-mediated transport from the soil pore water to the atmosphere (g C/m²/d); F_D is the diffusive flux of CH₄ from the water surface to the atmosphere (g C/m²/d); F_E is the ebullitive CH₄ emission to the atmosphere; $F_{air,oxid}$ is the rate of atmospheric CH₄ oxidation (g C/m²/d); and $F_{trans,oxid}$ is the oxidized CH₄ during plant-mediated transport (g C/m²/d).

2.3 Model forcing data

Four long-term datasets distributed over the U.S. at 5×5 arc-min spatial resolution were developed to provide forcing conditions for DLEM v4.0:

- (1) Agricultural management practices (N fertilizer use rate, crop rotation, tillage, irrigation, and manure application): The annual crop-specific N fertilizer use rate dataset from 1910

to 2018 was reconstructed using the state-level N fertilizer use rates from USDA-NASS and the national-level commercial N fertilizer consumption data from (Mehring et al. 1957) and (USDA-ERS 2019) following Cao et al. (2018). The annual crop rotation dataset from 1910 to 2018 was developed by combining the USDA Cropland Data Layer (CDL) product and National Agricultural Statistics Service (NASS) survey of county-level crop planting areas using the spatialization method of Yu et al. (2018). The annual tillage intensity map from 1960 to 2018 was reconstructed from the county-level tillage practices survey data obtained from the National Crop Residue Management Survey (CRM) of the Conservation Technology Information Center (<https://www.ctic.org/CRM>) following (You et al. 2022). Tillage maps for missing years were kept the same as the nearest years with available data. The original five tillage practices in the CRM dataset were reorganized into four types by combining ridge and mulch tillage types to conservation tillage. The county-level CRM dataset was combined with the CDL-derived crop rotation map and the USDA-NASS crop planting area to estimate historical spatial distributions of tillage practices. The annual crop-specific irrigation dataset from 1950 to 2018 was downscaled from the county-level irrigation reanalysis (McManamay et al. 2021) and NASS irrigated cropland area survey, using the MODIS Irrigated Agriculture Dataset (Brown and Pervez 2014; Pervez and Brown 2010) as a base map. The annual manure N application dataset from 1860 to 2018 was acquired from Bian et al. (2021). The state-level earliest and latest crop planting dates were obtained from the NASS survey report (NASS 2010), which provides planting and harvesting windows in most historical years.

- (2) Land use and land cover change (LULC): We developed a spatially explicit annual LULC dataset at a spatial resolution of 1×1 km over the contiguous U.S. during 1630–2020 using

machine learning and geospatial modeling approaches (Li et al. 2023). Multi-source datasets such as satellite-derived land cover maps, national inventories, topographical data, and model-based land use change data were used for the reconstruction.

(3) Natural environmental changes (climate conditions, atmospheric CO₂, and N deposition):

The historical daily climate dataset (including precipitation, solar radiation, maximum, minimum and mean temperatures) from 1860 to 2018 was reconstructed from the North American Land Data Assimilation System product (Mitchell et al. 2004; Xia et al. 2012), the Climate Research Unit-National Centers for Environmental Prediction dataset (Mitchell and Jones 2005), and the IPSL Climate Model dataset (Boucher et al. 2020) using the delta downscaling method (Liu et al. 2013). Monthly atmospheric CO₂ concentration variations during 1860-2018 were from the NOAA GLOBALVIEW-CO₂ dataset derived from atmospheric and ice core measurements (www.esrl.noaa.gov). Monthly atmospheric N deposition variations during 1860-2018 were acquired from the International Global Atmospheric Chemistry (IGAC)/Stratospheric Processes and Their Role in Climate (SPARC) Chemistry–Climate Model Initiative (CCMI) (Eyring et al. 2013).

(4) Soil properties and other auxiliary information: Soil physical and chemical properties were

obtained from the ISRIC-WISE Harmonized Global Soil Profile dataset (Batjes 2008). Other auxiliary information such as topography and river network was obtained from our previous studies (Tian et al. 2010a; Tian et al. 2020b).

2.4 Summary

In this study, a new agricultural module was developed within the framework of DLEM v4.0 to better simulate crop yield, SOC, and GHG emissions driven by multiple environmental changes

and agricultural management practices. Specifically, the new agricultural module has incorporated explicit and mechanistic representations of dynamic crop growth processes and agricultural management practices, including but not limited to crop-specific phenological development, carbon allocation, yield formation, and biological N fixation processes, as well as management practices such as N fertilization, irrigation, rotation, manure application, tillage, cover cropping, and crop genetic improvements. Moreover, the module has also improved the vertical discretization of the soil profile and calculated the relevant soil biogeochemical processes for each soil layer in accordance with its unique environmental conditions. These layer-specific calculations were then integrated to produce a comprehensive estimate for the entire soil profile. This unified agricultural module can be applied to evaluate the impacts of historical climate change and anthropogenic activities on crop yields and GHG emissions, predict future crop yields and GHG emissions, as well as assess the efficacy of potential agricultural climate change adaptation and mitigation strategies.

References

- Aluko, G.K., & Fischer, K.S. (1988). The effect of changes of assimilate supply around flowering on grain sink size and yield of maize (*Zea mays* L.) cultivars of tropical and temperate adaptation. *Australian Journal of Agricultural Research*, *39*, 153-161
- Andrade, F.H., Vega, C., Uhart, S., Cirilo, A., Cantarero, M., & Valentinuz, O. (1999). Kernel number determination in maize. *Crop Science*, *39*, 453-459
- Banger, K., Tian, H., Tao, B., Lu, C., Ren, W., & Yang, J. (2015). Magnitude, Spatiotemporal Patterns, and Controls for Soil Organic Carbon Stocks in India during 1901–2010. *Soil Science Society of America Journal*, *79*, 864-875
- Batjes, N.H. (2008). ISRIC-WISE Harmonized Global Soil Profile Dataset. *ISRIC-World Soil Information, Wageningen*
- Bian, Z., Tian, H., Yang, Q., Xu, R., Pan, S., & Zhang, B. (2021). Production and application of manure nitrogen and phosphorus in the United States since 1860. *Earth System Science Data*, *13*, 515-527
- Bindraban, P.S., Sayre, K.D., & Solis-Moya, E. (1998). Identifying factors that determine kernel number in wheat. *Field Crops Research*, *58*, 223-234
- Board, J.E., & Tan, Q. (1995). Assimilatory capacity effects on soybean yield components and pod number. *Crop Science*, *35*, 846-851

- Boucher, O., Servonnat, J., Albright, A.L., Aumont, O., Balkanski, Y., Bastrikov, V., Bekki, S., Bonnet, R., Bony, S., & Bopp, L. (2020). Presentation and evaluation of the IPSL-CM6A-LR climate model. *Journal of Advances in Modeling Earth Systems*, *12*, e2019MS002010
- Brown, J.F., & Pervez, M.S. (2014). Merging remote sensing data and national agricultural statistics to model change in irrigated agriculture. *Agricultural systems*, *127*, 28-40
- Cabelguenne, M., Debaeke, P., & Bouniols, A. (1999). EPICphase, a version of the EPIC model simulating the effects of water and nitrogen stress on biomass and yield, taking account of developmental stages: validation on maize, sunflower, sorghum, soybean and winter wheat. *Agricultural systems*, *60*, 175-196
- Camino-Serrano, M., Guenet, B., Luyssaert, S., Ciais, P., Bastrikov, V., De Vos, B., Gielen, B., Gleixner, G., Jorner-Puig, A., Kaiser, K., Kothawala, D., Lauerwald, R., Peñuelas, J., Schrumpf, M., Vicca, S., Vuichard, N., Walmsley, D., & Janssens, I.A. (2018). ORCHIDEE-SOM: modeling soil organic carbon (SOC) and dissolved organic carbon (DOC) dynamics along vertical soil profiles in Europe. *Geosci. Model Dev.*, *11*, 937-957
- Cao, P., Lu, C., & Yu, Z. (2018). Historical nitrogen fertilizer use in agricultural ecosystems of the contiguous United States during 1850–2015: application rate, timing, and fertilizer types. *Earth System Science Data*, *10*, 969-984
- Chen, M., Griffis, T.J., Baker, J., Wood, J.D., & Xiao, K. (2015). Simulating crop phenology in the Community Land Model and its impact on energy and carbon fluxes. *Journal of Geophysical Research: Biogeosciences*, *120*, 310-325
- Chen, M., Griffis, T.J., Baker, J.M., Wood, J.D., Meyers, T., & Suyker, A. (2018). Comparing crop growth and carbon budgets simulated across AmeriFlux agricultural sites using the Community Land Model (CLM). *Agricultural and Forest Meteorology*, *256-257*, 315-333
- Dadoun, F.A. (1993). Modelling tillage effects on soil physical properties and maize (*Zea mays*, L.) development and growth
- Di Vittorio, A.V., Anderson, R.S., White, J.D., Miller, N.L., & Running, S.W. (2010). Development and optimization of an Agro-BGC ecosystem model for C4 perennial grasses. *Ecological Modelling*, *221*, 2038-2053
- Duvick, D.N. (1984). Genetic contributions to yield gains of US hybrid maize, 1930 to 1980. *Genetic contributions to yield gains of five major crop plants*, *7*, 15-47
- Duvick, D.N. (2005). The contribution of breeding to yield advances in maize (*Zea mays* L.). *Advances in agronomy*, *86*, 83-145
- Early, E.B., McIlrath, W.O., Seif, R.D., & Hageman, R.H. (1967). Effects of Shade Applied at Different Stages of Plant Development on Corn (*Zea mays* L.) Production 1. *Crop Science*, *7*, 151-156
- Egli, D.B. (1998). *Seed biology and the yield of grain crops*. CAB international
- Enrique, G.-s., Braud, I., Jean-Louis, T., Michel, V., Pierre, B., & Jean-Christophe, C. (1999). Modelling heat and water exchanges of fallow land covered with plant-residue mulch. *Agricultural and Forest Meteorology*, *97*, 151-169
- Eyring, V., Lamarque, J.-F., Hess, P., Arfeuille, F., Bowman, K., Chipperfield, M.P., Duncan, B., Fiore, A., Gettelman, A., & Giorgetta, M.A. (2013). Overview of IGAC/SPARC Chemistry-Climate Model Initiative (CCMI) community simulations in support of upcoming ozone and climate assessments. *SPARC newsletter*, *40*, 48-66
- Fischer, R.A. (1985). Number of kernels in wheat crops and the influence of solar radiation and temperature
- Fontaine, S., Barot, S., Barré, P., Bdioui, N., Mary, B., & Rumpel, C. (2007). Stability of organic carbon in deep soil layers controlled by fresh carbon supply. *Nature*, *450*, 277-280
- Friedlingstein, P., O'Sullivan, M., Jones, M.W., Andrew, R.M., Hauck, J., Olsen, A., Peters, G.P., Peters, W., Pongratz, J., Sitch, S., Le Quéré, C., Canadell, J.G., Ciais, P., Jackson, R.B., Alin, S., Aragão, L.E.O.C., Arneeth, A., Arora, V., Bates, N.R., Becker, M., Benoit-Cattin, A., Bittig, H.C., Bopp, L., Bultan, S., Chandra, N., Chevallier, F., Chini, L.P., Evans, W., Florentie, L., Forster, P.M., Gasser, T., Gehlen, M., Gilfillan, D., Gkritzalis, T., Gregor, L., Gruber, N., Harris, I., Hartung, K., Haverd, V., Houghton, R.A., Ilyina, T., Jain, A.K., Joetzjer, E., Kadono, K., Kato, E., Kitidis, V., Korsbakken, J.I., Landschützer, P., Lefèvre, N., Lenton, A., Lienert, S., Liu, Z., Lombardozzi, D., Marland, G., Metzl, N., Munro, D.R., Nabel, J.E.M.S., Nakaoka, S.I., Niwa, Y., O'Brien, K., Ono, T., Palmer, P.I., Pierrot, D., Poulter, B., Resplandy, L., Robertson, E., Rödenbeck, C., Schwinger, J., Séférian, R., Skjelvan, I., Smith, A.J.P., Sutton, A.J., Tanhua, T., Tans, P.P., Tian, H., Tilbrook, B., van der Werf, G., Vuichard, N., Walker, A.P., Wanninkhof, R., Watson, A.J., Willis, D., Wiltshire, A.J., Yuan, W., Yue, X., & Zaehle, S. (2020). Global Carbon Budget 2020. *Earth Syst. Sci. Data*, *12*, 3269-3340

- Gaspar, A.P., Laboski, C.A.M., Naeve, S.L., & Conley, S.P. (2017). Dry Matter and Nitrogen Uptake, Partitioning, and Removal across a Wide Range of Soybean Seed Yield Levels. *Crop Science*, 57, 2170-2182
- Gregory, J.M. (1982). Soil cover prediction with various amounts and types of crop residue. *Transactions of the ASAE*, 25, 1333-1337
- Gregory, P.J., & Atwell, B.J. (1991). The fate of carbon in pulse-labelled crops of barley and wheat. *Plant and Soil*, 136, 205-213
- Gregory, P.J., Palta, J.A., & Batts, G.R. (1995). Root systems and root: mass ratio-carbon allocation under current and projected atmospheric conditions in arable crops. *Plant and Soil*, 187, 221-228
- Guérif, J., Richard, G., Dürr, C., Machet, J.M., Recous, S., & Roger-Estrade, J. (2001). A review of tillage effects on crop residue management, seedbed conditions and seedling establishment. *Soil and Tillage Research*, 61, 13-32
- Gungula, D.T., Kling, J.G., & Togun, A.O. (2003). CERES-Maize Predictions of Maize Phenology under Nitrogen-Stressed Conditions in Nigeria. *Agronomy journal*, 95, 892-899
- Hammer, G.L., Dong, Z., McLean, G., Doherty, A., Messina, C., Schussler, J., Zinselmeier, C., Paszkiewicz, S., & Cooper, M. (2009). Can changes in canopy and/or root system architecture explain historical maize yield trends in the US corn belt? *Crop Science*, 49, 299-312
- Harrison, R.B., Footen, P.W., & Strahm, B.D. (2011). Deep Soil Horizons: Contribution and Importance to Soil Carbon Pools and in Assessing Whole-Ecosystem Response to Management and Global Change. *Forest Science*, 57, 67-76
- Hay, R.K.M. (1995). Harvest index: a review of its use in plant breeding and crop physiology. *Annals of applied biology*, 126, 197-216
- Henneron, L., Balesdent, J., Alvarez, G., Barré, P., Baudin, F., Basile-Doelsch, I., Cécillon, L., Fernandez-Martinez, A., Hatté, C., & Fontaine, S. (2022). Bioenergetic control of soil carbon dynamics across depth. *Nature Communications*, 13, 7676
- Huang, Y., Ren, W., Grove, J., Poffenbarger, H., Jacobsen, K., Tao, B., Zhu, X., & McNear, D. (2020). Assessing synergistic effects of no-tillage and cover crops on soil carbon dynamics in a long-term maize cropping system under climate change. *Agricultural and Forest Meteorology*, 291, 108090
- Jiang, H., & Egli, D.B. (1995). Soybean seed number and crop growth rate during flowering. *Agronomy journal*, 87, 264-267
- Jobbágy, E.G., & Jackson, R.B. (2000). THE VERTICAL DISTRIBUTION OF SOIL ORGANIC CARBON AND ITS RELATION TO CLIMATE AND VEGETATION. *Ecological Applications*, 10, 423-436
- Jones, J.W., Hoogenboom, G., Porter, C.H., Boote, K.J., Batchelor, W.D., Hunt, L.A., Wilkens, P.W., Singh, U., Gijsman, A.J., & Ritchie, J.T. (2003). The DSSAT cropping system model. *European Journal of Agronomy*, 18, 235-265
- Keating, B.A., Carberry, P.S., Hammer, G.L., Probert, M.E., Robertson, M.J., Holzworth, D., Huth, N.I., Hargreaves, J.N.G., Meinke, H., Hochman, Z., McLean, G., Verburg, K., Snow, V., Dimes, J.P., Silburn, M., Wang, E., Brown, S., Bristow, K.L., Asseng, S., Chapman, S., McCown, R.L., Freebairn, D.M., & Smith, C.J. (2003). An overview of APSIM, a model designed for farming systems simulation. *European Journal of Agronomy*, 18, 267-288
- Koarashi, J., Hockaday, W.C., Masiello, C.A., & Trumbore, S.E. (2012). Dynamics of decadal cycling carbon in subsurface soils. *Journal of Geophysical Research: Biogeosciences*, 117
- Koven, C.D., Riley, W.J., Subin, Z.M., Tang, J.Y., Torn, M.S., Collins, W.D., Bonan, G.B., Lawrence, D.M., & Swenson, S.C. (2013). The effect of vertically resolved soil biogeochemistry and alternate soil C and N models on C dynamics of CLM4. *Biogeosciences*, 10, 7109-7131
- Kucharik, C.J. (2006). A multidecadal trend of earlier corn planting in the central USA. *Agronomy journal*, 98, 1544-1550
- Laux, P., Jäckel, G., Tingem, R.M., & Kunstmann, H. (2010). Impact of climate change on agricultural productivity under rainfed conditions in Cameroon—A method to improve attainable crop yields by planting date adaptations. *Agricultural and Forest Meteorology*, 150, 1258-1271
- Le Mer, J., & Roger, P. (2001). Production, oxidation, emission and consumption of methane by soils: A review. *European Journal of Soil Biology*, 37, 25-50
- Lei, H., Yang, D., Lokupitiya, E., & Shen, Y. (2010). Coupling land surface and crop growth models for predicting evapotranspiration and carbon exchange in wheat-maize rotation croplands. *Biogeosciences*, 7, 3363-3375
- Levis, S., Bonan, G.B., Kluzek, E., Thornton, P.E., Jones, A., Sacks, W.J., & Kucharik, C.J. (2012). Interactive crop management in the Community Earth System Model (CESM1): Seasonal influences on land-atmosphere fluxes. *Journal of Climate*, 25, 4839-4859

- Li, X., Tian, H., Lu, C., & Pan, S. (2023). Four-century history of land transformation by humans in the United States (1630–2020): annual and 1 km grid data for the HIStory of LAND changes (HISLAND-US). *Earth System Science Data*, 2023, 1005-1035
- Liu, J., Price, D.T., & Chen, J.M. (2005). Nitrogen controls on ecosystem carbon sequestration: a model implementation and application to Saskatchewan, Canada. *Ecological Modelling*, 186, 178-195
- Liu, M., Tian, H., Yang, Q., Yang, J., Song, X., Lohrenz, S.E., & Cai, W.-J. (2013). Long-term trends in evapotranspiration and runoff over the drainage basins of the Gulf of Mexico during 1901–2008. *Water Resources Research*, 49, 1988-2012
- Liu, Y., Wu, L., Baddeley, J.A., & Watson, C.A. (2011). Models of biological nitrogen fixation of legumes. *Sustainable Agriculture Volume 2*, 883-905
- Lokupitiya, E., Denning, S., Paustian, K., Baker, I., Schaefer, K., Verma, S.B., Meyers, T., Bernacchi, C.J., Suyker, A.E., & Fischer, M.L. (2009). Incorporation of crop phenology in Simple Biosphere Model (SiBcrop) to improve land-atmosphere carbon exchanges from croplands
- Long, Stephen P., Marshall-Colon, A., & Zhu, X.-G. (2015). Meeting the Global Food Demand of the Future by Engineering Crop Photosynthesis and Yield Potential. *Cell*, 161, 56-66
- Lu, C., Yu, Z., Tian, H., Hennessy, D.A., Feng, H., Al-Kaisi, M., Zhou, Y., Sauer, T., & Arritt, R. (2018). Increasing carbon footprint of grain crop production in the US Western Corn Belt. *Environmental Research Letters*, 13, 124007
- Lu, C., Yu, Z., Zhang, J., Cao, P., Tian, H., & Nevison, C. (2021). Century-long changes and drivers of soil nitrous oxide (N₂O) emissions across the contiguous United States. *Global Change Biology*, 28, 2505– 2524
- Lutz, F., Herzfeld, T., Heinke, J., Rolinski, S., Schaphoff, S., von Bloh, W., Stoorvogel, J.J., & Müller, C. (2019). Simulating the effect of tillage practices with the global ecosystem model LPJmL (version 5.0-tillage). *Geosci. Model Dev.*, 12, 2419-2440
- Maharjan, G.R., Prescher, A.-K., Nendel, C., Ewert, F., Mboh, C.M., Gaiser, T., & Seidel, S.J. (2018). Approaches to model the impact of tillage implements on soil physical and nutrient properties in different agro-ecosystem models. *Soil and Tillage Research*, 180, 210-221
- Mathieu, J.A., Hatté, C., Balesdent, J., & Parent, É. (2015). Deep soil carbon dynamics are driven more by soil type than by climate: a worldwide meta-analysis of radiocarbon profiles. *Global Change Biology*, 21, 4278-4292
- McManamay, R.A., Kc, B., Allen-Dumas, M.R., Kao, S.-C., Brelsford, C.M., Ruddell, B.L., Sanyal, J., Stewart, R.N., & Bhaduri, B.L. (2021). Reanalysis of Water Withdrawal for Irrigation, Electric Power, and Public Supply Sectors in the Conterminous United States, 1950–2016. *Water Resources Research*, 57, e2020WR027751
- Mehring, A.L., Adams, J.R., & Jacob, K.D. (1957). *Statistics on fertilizers and liming materials in the United States*. Soil and Water Conservation Research Branch, Agricultural Research Service ...
- Mitchell, K.E., Lohmann, D., Houser, P.R., Wood, E.F., Schaake, J.C., Robock, A., Cosgrove, B.A., Sheffield, J., Duan, Q., Luo, L., Higgins, R.W., Pinker, R.T., Tarpley, J.D., Lettenmaier, D.P., Marshall, C.H., Entin, J.K., Pan, M., Shi, W., Koren, V., Meng, J., Ramsay, B.H., & Bailey, A.A. (2004). The multi-institution North American Land Data Assimilation System (NLDAS): Utilizing multiple GCIP products and partners in a continental distributed hydrological modeling system. *Journal of Geophysical Research: Atmospheres*, 109
- Mitchell, T.D., & Jones, P.D. (2005). An improved method of constructing a database of monthly climate observations and associated high-resolution grids. *International Journal of Climatology*, 25, 693-712
- NASS, U. (2010). Field crops: Usual planting and harvesting dates. *USDA National Agricultural Statistics Service, Agricultural Handbook*, 628
- Pan, S., Bian, Z., Tian, H., Yao, Y., Najjar, R.G., Friedrichs, M.A.M., Hofmann, E.E., Xu, R., & Zhang, B. (2021). Impacts of Multiple Environmental Changes on Long-term Nitrogen Loading from the Chesapeake Bay Watershed. *Journal of Geophysical Research: Biogeosciences*, 126, e2020JG005826
- Pan, S., Pan, N., Tian, H., Friedlingstein, P., Sitch, S., Shi, H., Arora, V.K., Haverd, V., Jain, A.K., Kato, E., Lienert, S., Lombardozzi, D., Nabel, J.E.M.S., Ottlé, C., Poulter, B., Zaehle, S., & Running, S.W. (2020). Evaluation of global terrestrial evapotranspiration using state-of-the-art approaches in remote sensing, machine learning and land surface modeling. *Hydrol. Earth Syst. Sci.*, 24, 1485-1509
- Pan, S., Tian, H., Dangal, S.R.S., Yang, Q., Yang, J., Lu, C., Tao, B., Ren, W., & Ouyang, Z. (2015). Responses of global terrestrial evapotranspiration to climate change and increasing atmospheric CO₂ in the 21st century. *Earth's Future*, 3, 15-35
- Parry, M.A.J., Reynolds, M., Salvucci, M.E., Raines, C., Andralojc, P.J., Zhu, X.-G., Price, G.D., Condon, A.G., & Furbank, R.T. (2011). Raising yield potential of wheat. II. Increasing photosynthetic capacity and efficiency. *Journal of Experimental Botany*, 62, 453-467

- Parton, W.J., Scurlock, J.M.O., Ojima, D.S., Gilmanov, T.G., Scholes, R.J., Schimel, D.S., Kirchner, T., Menaut, J.C., Seastedt, T., Garcia Moya, E., Kamnalrut, A., & Kinyamario, J.I. (1993). Observations and modeling of biomass and soil organic matter dynamics for the grassland biome worldwide. *Global Biogeochemical Cycles*, 7, 785-809
- Peart, R.M., & Shoup, W.D. (2018). *Agricultural systems modeling and simulation*. CRC press
- Peng, B., Guan, K., Chen, M., Lawrence, D.M., Pokhrel, Y., Suyker, A., Arkebauer, T., & Lu, Y. (2018). Improving maize growth processes in the community land model: Implementation and evaluation. *Agricultural and Forest Meteorology*, 250, 64-89
- Pervez, M.S., & Brown, J.F. (2010). Mapping irrigated lands at 250-m scale by merging MODIS data and national agricultural statistics. *Remote Sensing*, 2, 2388-2412
- Petersen, B.M., Berntsen, J., Hansen, S., & Jensen, L.S. (2005). CN-SIM—a model for the turnover of soil organic matter. I. Long-term carbon and radiocarbon development. *Soil Biology and Biochemistry*, 37, 359-374
- Pingali, P.L. (2012). Green revolution: impacts, limits, and the path ahead. *Proceedings of the National Academy of Sciences*, 109, 12302-12308
- Porker, K., Straight, M., & Hunt, J.R. (2020). Evaluation of G× E× M Interactions to Increase Harvest Index and Yield of Early Sown Wheat. *Frontiers in plant science*, 11, 994
- Porwollik, V., Rolinski, S., Heinke, J., & Müller, C. (2019). Generating a rule-based global gridded tillage dataset. *Earth Syst. Sci. Data*, 11, 823-843
- Ren, W., Banger, K., Tao, B., Yang, J., Huang, Y., & Tian, H. (2020). Global pattern and change of cropland soil organic carbon during 1901-2010: Roles of climate, atmospheric chemistry, land use and management. *Geography and Sustainability*, 1, 59-69
- Ren, W., Tian, H., Tao, B., Huang, Y., & Pan, S. (2012). China's crop productivity and soil carbon storage as influenced by multifactor global change. *Global Change Biology*, 18, 2945-2957
- Ren, W., Tian, H., Xu, X., Liu, M., Lu, C., Chen, G., Melillo, J., Reilly, J., & Liu, J. (2011). Spatial and temporal patterns of CO₂ and CH₄ fluxes in China's croplands in response to multifactor environmental changes. *Tellus B: Chemical and Physical Meteorology*, 63, 222-240
- Ritchie, J.T. (1991). Wheat phasic development. *Modeling plant and soil systems*, 31, 31-54
- Saunois, M., Stavert, A.R., Poulter, B., Bousquet, P., Canadell, J.G., Jackson, R.B., Raymond, P.A., Dlugokencky, E.J., Houweling, S., Patra, P.K., Ciais, P., Arora, V.K., Bastviken, D., Bergamaschi, P., Blake, D.R., Brailsford, G., Bruhwiler, L., Carlson, K.M., Carrol, M., Castaldi, S., Chandra, N., Crevoisier, C., Crill, P.M., Covey, K., Curry, C.L., Etiope, G., Frankenberg, C., Gedney, N., Hegglin, M.I., Höglund-Isaksson, L., Hugelius, G., Ishizawa, M., Ito, A., Janssens-Maenhout, G., Jensen, K.M., Joos, F., Kleinen, T., Krummel, P.B., Langenfelds, R.L., Laruelle, G.G., Liu, L., Machida, T., Maksyutov, S., McDonald, K.C., McNorton, J., Miller, P.A., Melton, J.R., Morino, I., Müller, J., Murguía-Flores, F., Naik, V., Niwa, Y., Noce, S., O'Doherty, S., Parker, R.J., Peng, C., Peng, S., Peters, G.P., Prigent, C., Prinn, R., Ramonet, M., Regnier, P., Riley, W.J., Rosentretter, J.A., Segers, A., Simpson, I.J., Shi, H., Smith, S.J., Steele, L.P., Thornton, B.F., Tian, H., Tohjima, Y., Tubiello, F.N., Tsuruta, A., Viovy, N., Voulgarakis, A., Weber, T.S., van Weele, M., van der Werf, G.R., Weiss, R.F., Worthy, D., Wunch, D., Yin, Y., Yoshida, Y., Zhang, W., Zhang, Z., Zhao, Y., Zheng, B., Zhu, Q., Zhu, Q., & Zhuang, Q. (2020). The Global Methane Budget 2000–2017. *Earth Syst. Sci. Data*, 12, 1561-1623
- Sinclair, T.R. (1998). Historical Changes in Harvest Index and Crop Nitrogen Accumulation. *Crop Science*, 38, cropscl1998.0011183X003800030002x
- Soltani, A., & Sinclair, T.R. (2012). *Modeling physiology of crop development, growth and yield*. Wallingford: CABI
- Song, Y., Jain, A.K., & McIsaac, G.F. (2013). Implementation of dynamic crop growth processes into a land surface model: evaluation of energy, water and carbon fluxes under corn and soybean rotation. *Biogeosciences*, 10, 8039-8066
- Srivastava, A.C., Tikku, A.K., & Pal, M. (2006). Nitrogen and carbon partitioning in soybean under variable nitrogen supplies and acclimation to the prolonged action of elevated CO₂. *Acta Physiologiae Plantarum*, 28, 181-188
- Taylor, H.M., Mason, W.K., Bennie, A.T.P., & Rowse, H.R. (1982). Responses of soybeans to two row spacings and two soil water levels. I. An analysis of biomass accumulation, canopy development, solar radiation interception and components of seed yield. *Field Crops Research*, 5, 1-14
- Tian, H., Chen, G., Liu, M., Zhang, C., Sun, G., Lu, C., Xu, X., Ren, W., Pan, S., & Chappelka, A. (2010a). Model estimates of net primary productivity, evapotranspiration, and water use efficiency in the terrestrial ecosystems of the southern United States during 1895–2007. *Forest Ecology and Management*, 259, 1311-1327

- Tian, H., Chen, G., Lu, C., Xu, X., Hayes, D.J., Ren, W., Pan, S., Huntzinger, D.N., & Wofsy, S.C. (2015a). North American terrestrial CO₂ uptake largely offset by CH₄ and N₂O emissions: toward a full accounting of the greenhouse gas budget. *Climatic Change*, *129*, 413-426
- Tian, H., Chen, G., Zhang, C., Liu, M., Sun, G., Chappelka, A., Ren, W., Xu, X., Lu, C., Pan, S., Chen, H., Hui, D., McNulty, S., Lockaby, G., & Vance, E. (2012a). Century-Scale Responses of Ecosystem Carbon Storage and Flux to Multiple Environmental Changes in the Southern United States. *Ecosystems*, *15*, 674-694
- Tian, H., Lu, C., Melillo, J., Ren, W., Huang, Y., Xu, X., Liu, M., Zhang, C., Chen, G., Pan, S., Liu, J., & Reilly, J. (2012b). Food benefit and climate warming potential of nitrogen fertilizer uses in China. *Environmental Research Letters*, *7*, 044020
- Tian, H., Lu, C., Yang, J., Banger, K., Huntzinger, D.N., Schwalm, C.R., Michalak, A.M., Cook, R., Ciais, P., Hayes, D., Huang, M., Ito, A., Jain, A.K., Lei, H., Mao, J., Pan, S., Post, W.M., Peng, S., Poulter, B., Ren, W., Ricciuto, D., Schaefer, K., Shi, X., Tao, B., Wang, W., Wei, Y., Yang, Q., Zhang, B., & Zeng, N. (2015b). Global patterns and controls of soil organic carbon dynamics as simulated by multiple terrestrial biosphere models: Current status and future directions. *Global Biogeochemical Cycles*, *29*, 775-792
- Tian, H., Xu, R., Canadell, J.G., Thompson, R.L., Winiwarter, W., Suntharalingam, P., Davidson, E.A., Ciais, P., Jackson, R.B., Janssens-Maenhout, G., Prather, M.J., Regnier, P., Pan, N., Pan, S., Peters, G.P., Shi, H., Tubiello, F.N., Zaehle, S., Zhou, F., Arneeth, A., Battaglia, G., Berthet, S., Bopp, L., Bouwman, A.F., Buitenhuis, E.T., Chang, J., Chipperfield, M.P., Dangal, S.R.S., Dlugokencky, E., Elkins, J.W., Eyre, B.D., Fu, B., Hall, B., Ito, A., Joos, F., Krummel, P.B., Landolfi, A., Laruelle, G.G., Lauerwald, R., Li, W., Lienert, S., Maavara, T., MacLeod, M., Millet, D.B., Olin, S., Patra, P.K., Prinn, R.G., Raymond, P.A., Ruiz, D.J., van der Werf, G.R., Vuichard, N., Wang, J., Weiss, R.F., Wells, K.C., Wilson, C., Yang, J., & Yao, Y. (2020a). A comprehensive quantification of global nitrous oxide sources and sinks. *Nature*, *586*, 248-256
- Tian, H., Xu, R., Pan, S., Yao, Y., Bian, Z., Cai, W.-J., Hopkinson, C.S., Justic, D., Lohrenz, S., Lu, C., Ren, W., & Yang, J. (2020b). Long-Term Trajectory of Nitrogen Loading and Delivery From Mississippi River Basin to the Gulf of Mexico. *Global Biogeochemical Cycles*, *34*, e2019GB006475
- Tian, H., Xu, X., Liu, M., Ren, W., Zhang, C., Chen, G., & Lu, C. (2010b). Spatial and temporal patterns of CH₄ and N₂O fluxes in terrestrial ecosystems of North America during 1979–2008: application of a global biogeochemistry model. *Biogeosciences*, *7*, 2673-2694
- Tian, H., Xu, X., Lu, C., Liu, M., Ren, W., Chen, G., Melillo, J., & Liu, J. (2011). Net exchanges of CO₂, CH₄, and N₂O between China's terrestrial ecosystems and the atmosphere and their contributions to global climate warming. *Journal of Geophysical Research: Biogeosciences*, *116*
- Todd-Brown, K.E.O., Randerson, J.T., Hopkins, F., Arora, V., Hajima, T., Jones, C., Shevliakova, E., Tjiputra, J., Volodin, E., Wu, T., Zhang, Q., & Allison, S.D. (2014). Changes in soil organic carbon storage predicted by Earth system models during the 21st century. *Biogeosciences*, *11*, 2341-2356
- Uhart, S.A., & Andrade, F.H. (1995). Nitrogen Deficiency in Maize: I. Effects on Crop Growth, Development, Dry Matter Partitioning, and Kernel Set. *Crop Science*, *35*, cropscl1995.0011183X003500050020x
- USDA-ERS (2019). U.S. Department of Agriculture-Economic Research Service: Fertilizer Use and Price
- Vega, C.R.C., Andrade, F.H., Sadras, V.O., Uhart, S.A., & Valentinuz, O.R. (2001). Seed Number as a Function of Growth. A Comparative Study in Soybean, Sunflower, and Maize. *Crop Science*, *41*, 748-754
- Villalobos, F.J., Hall, A.J., Ritchie, J.T., & Orgaz, F. (1996). OILCROP-SUN: A development, growth, and yield model of the sunflower crop. *Agronomy journal*, *88*, 403-415
- Wilhelm, W.W. (1998). Dry-matter partitioning and leaf area of winter wheat grown in a long-term fallow tillage comparisons in the US Central Great Plains. *Soil and Tillage Research*, *49*, 49-56
- Wilhelm, W.W., McMaster, G.S., Rickman, R.W., & Klepper, B. (1993). Above-ground vegetative development and growth of winter wheat as influenced by nitrogen and water availability. *Ecological Modelling*, *68*, 183-203
- Williams, J.R., Izaurrealde, R.C., & Steglich, E.M. (2008). Agricultural policy/environmental extender model. *Theoretical Documentation, Version*, *604*, 2008-2017
- Wu, A., Hammer, G.L., Doherty, A., von Caemmerer, S., & Farquhar, G.D. (2019). Quantifying impacts of enhancing photosynthesis on crop yield. *Nature Plants*, *5*, 380-388
- Xia, Y., Mitchell, K., Ek, M., Sheffield, J., Cosgrove, B., Wood, E., Luo, L., Alonge, C., Wei, H., Meng, J., Livneh, B., Lettenmaier, D., Koren, V., Duan, Q., Mo, K., Fan, Y., & Mocko, D. (2012). Continental-scale water and energy flux analysis and validation for the North American Land Data Assimilation System project phase 2 (NLDAS-2): 1. Intercomparison and application of model products. *Journal of Geophysical Research: Atmospheres*, *117*
- Xu, X.F., Tian, H.Q., Chen, G.S., Liu, M.L., Ren, W., Lu, C.Q., & Zhang, C. (2012). Multifactor controls on terrestrial N₂O flux over North America from 1979 through 2010. *Biogeosciences*, *9*, 1351-1366

- Xu, X.F., Tian, H.Q., Zhang, C., Liu, M.L., Ren, W., Chen, G.S., Lu, C.Q., & Bruhwiler, L. (2010). Attribution of spatial and temporal variations in terrestrial methane flux over North America. *Biogeosciences*, 7, 3637-3655
- Yamagata, M., Kouchi, H., & Yoneyama, T. (1987). Partitioning and utilization of photosynthate produced at different growth stages after anthesis in soybean (*Glycine max* L. Merr.): Analysis by long-term ¹³C-labelling experiments. *Journal of Experimental Botany*, 38, 1247-1259
- Yang, Y., Ren, W., Tao, B., Ji, L., Liang, L., Ruane, A.C., Fisher, J.B., Liu, J., Sama, M., Li, Z., & Tian, Q. (2020). Characterizing spatiotemporal patterns of crop phenology across North America during 2000–2016 using satellite imagery and agricultural survey data. *ISPRS Journal of Photogrammetry and Remote Sensing*, 170, 156-173
- Yao, Y., Tian, H., Shi, H., Pan, S., Xu, R., Pan, N., & Canadell, J.G. (2020). Increased global nitrous oxide emissions from streams and rivers in the Anthropocene. *Nature Climate Change*, 10, 138-142
- You, Y., Tian, H., Pan, S., Shi, H., Bian, Z., Gurgel, A., Huang, Y., Kicklighter, D., Liang, X.-Z., Lu, C., Melillo, J., Miao, R., Pan, N., Reilly, J., Ren, W., Xu, R., Yang, J., Yu, Q., & Zhang, J. (2022). Incorporating dynamic crop growth processes and management practices into a terrestrial biosphere model for simulating crop production in the United States: Toward a unified modeling framework. *Agricultural and Forest Meteorology*, 325, 109144
- Yu, Z., Lu, C., Cao, P., & Tian, H. (2018). Long-term terrestrial carbon dynamics in the Midwestern United States during 1850–2015: Roles of land use and cover change and agricultural management. *Global Change Biology*, 24, 2673-2690
- Zhang, C., Tian, H., Chen, G., Chappelka, A., Xu, X., Ren, W., Hui, D., Liu, M., Lu, C., & Pan, S. (2012). Impacts of urbanization on carbon balance in terrestrial ecosystems of the Southern United States. *Environmental Pollution*, 164, 89-101
- Zhang, J., Tian, H., Yang, J., & Pan, S. (2018). Improving representation of crop growth and yield in the Dynamic Land Ecosystem Model and its application to China. *Journal of Advances in Modeling Earth Systems*, 10, 1680-1707
- Zheng, B., Chenu, K., Doherty, A., & Chapman, S. (2014). The APSIM-wheat module (7.5 R3008). *Agricultural Production Systems Simulator (APSIM) Initiative*

Chapter 3. Multi-scale crop yield simulation in the United States using a data-driven systems approach: Parameterization, evaluation, and application

Abstract

Agricultural decision-making by different interest groups (e.g., farmers, development agents and policy makers) usually takes place on different scales (e.g., plot, landscape and country). Currently, tools to assist decision-making are either dedicated to small-scale management guidance or large-scale assessment, which ignore the cross-scale linkages and interactions and thus may not provide robust and consistent guidance and assessment. Here, we developed an advanced agricultural modeling framework by integrating the strengths of conventional crop models in representing crop growth processes and management practices into a terrestrial biosphere model (TBM), the Dynamic Land Ecosystem Model (DLEM), to meet the cross-scale application needs (e.g., adaptation and mitigation). Specifically, dynamic crop growth processes, including crop-specific phenological development, carbon allocation, yield formation, biological nitrogen fixation processes, and management practices such as tillage, cover cropping and genetic improvements, were explicitly represented in DLEM. The new model was evaluated against site-scale observations and the results showed that the model performed generally well, with an average normalized root mean square error of 19.91% for leaf area index and 17.46% for aboveground biomass at the seasonal scale and 14.42% for annual yield. Then the model was applied to simulate corn, soybean, and winter wheat productions in the conterminous United States from 1960 to 2018. The spatial patterns of simulated crop productions were consistent with ground survey data. Our model also captured both the long-term trends and interannual variations of the total national productions of the three crops. This study demonstrates the significance of fusing conventional

crop modeling techniques into TBMs to establish a unified modeling framework, which holds the potential to address climate impacts, adaptation and mitigation across varied spatiotemporal scales.

3.1 Introduction

Ensuring global food security while achieving sustainable agricultural development is a grand challenge for human society (Davis et al. 2016; Rosenzweig et al. 2014). During the past several decades, climate change and associated environmental stressors (e.g., water scarcity, pest prevalence, and soil degradation) have significantly impacted crop growth and production and are likely to reduce the resilience of global food systems (Bezner Kerr et al. 2022; Lesk et al. 2016; Wheeler and von Braun 2013b). Agricultural activities (e.g., fertilization, irrigation, and cropland expansion) have, in turn, exacerbated climatic and environmental changes through pathways such as greenhouse gas (GHG) emissions, groundwater extraction, and nutrient pollution (Giordano and Villholth 2007; Tian et al. 2016; Tian et al. 2020a). In view of the increasing uncertainty in the agriculture-climate-environment system caused by complex cross-sector interactions, effective climate change mitigation and adaptation strategies in the agricultural sector are needed to limit further changes in the climate system and reduce the negative impacts of climate change on food production (Howden et al. 2007; Vermeulen et al. 2012). Such mitigation and adaptation actions occur on multiple scales and are intertwined in intricate ways (Beveridge et al. 2018; Klein et al. 2007; Tol 2005). Specifically, stakeholders' adaptation decisions to sustain food production are usually carried out on a small scale (e.g., field-farm-landscape scales) and benefit local communities, as the influences of climate change on crop growth and production are largely mediated by local environments and local-specific adaptation strategies would be more effective (Hammer et al. 2014; Ofgeha and Abshare 2021). In contrast, agricultural mitigation measures (e.g., soil organic carbon sequestration and GHG mitigation) and their potential feedbacks to the

environment and climate are often implemented and assessed on a broader scale (e.g., regional-national-global scales), because effective mitigation requires the participation of major GHG emitters globally and is primarily driven by international agreements and ensuing national public policies (Hansen and Jones 2000; Klein et al. 2007; Locatelli 2011). Therefore, a unified tool that is capable of addressing cross-scale agricultural application demands is needed (Beveridge et al. 2018; Peng et al. 2020). Such a tool would enable a more consistent and robust prediction and assessment of crop production and the concomitant environmental and climatic tradeoffs.

Process-based crop models are commonly used to inform small-scale farm adaptation decisions to sustain food production (Chenu et al. 2017; Jones et al. 2017). A number of crop models that simulate crop growth and yields as influenced by weather, soil, cultivar, and management strategies have been developed, such as DSSAT (Decision Support System for Agrotechnology Transfer) (Jones et al. 2003), APSIM (Agricultural Production Systems sIMulator) (Holzworth et al. 2014; Keating et al. 2003), EPIC (Erosion Productivity Impact Calculator) (Williams et al. 1989), and CROPSYST (Cropping Systems Simulation Model) (Stöckle et al. 2003; Stöckle et al. 2014). Physiological mechanisms of crop development, growth, and yield formation processes under biotic and abiotic stresses, and farming management practices such as tillage and irrigation, are well-represented in these models. However, since crop models are originally designed for farmer's decision support, they generally focus on field-scale yield simulation over homogeneous plot conditions. Meanwhile, they typically have a reduced-form representation of hydrologic, energy and biogeochemical cycles. These properties limit their ability to simulate regional crop production, assess mitigation potential in the agriculture sector, and evaluate the environmental impacts of agricultural management activities.

Terrestrial biosphere models (TBMs) with agricultural components provide new insights for agricultural climate change mitigation and adaptation on a broader scale (Bondeau et al. 2007; Lombardozzi et al. 2020; McDermid et al. 2017). Most TBMs have included detailed hydrological, biophysical, and biogeochemical processes and can be further integrated with general circulation models for future climate change impact projections (Alo and Wang 2008; Fisher et al. 2014; Schaphoff et al. 2006). Therefore, they can potentially be used to simulate regional crop production under historical and future climate scenarios, assess the mitigation potential of agricultural management options, and quantify the exchange of carbon, water, nutrient and energy fluxes within the agriculture-climate-environment system. However, the representation of agriculture in most TBMs is relatively simple (e.g., lacking or simplifying dynamic crop growth processes and management practices), with some TBMs even treating crops as natural grasses though using different eco-physiological parameters as a distinction (Betts 2005; McDermid et al. 2017). Since crops have rather different phenological development processes compared with natural vegetation and often involve implementation of management practices (e.g., irrigation and fertilization), such simplified schemes are unlikely to be able to closely replicate observed yields under varying climatic and environmental conditions across different spatiotemporal scales, which limit their use for agricultural adaptation and mitigation assessments.

In view of the strengths and weaknesses of process-based crop models and TBMs, it is highly desirable to integrate these two types of models into a unified framework to complement each other (Peng et al. 2020). Such a framework is capable of meeting cross-scale agricultural application needs and providing more robust and consistent predictions and assessments. Some recent developments of TBMs have attempted to move in this direction, such as the Joint UK Land Environment Simulator (JULES) (Van den Hoof et al. 2011), the Organizing Carbon and

Hydrology in Dynamic Ecosystems Model (ORCHIDEE) (Wu et al. 2016), the Lund Potsdam Jena managed Land model (LPJmL5) (Lutz et al. 2019a), and the Community Land Model (CLM) (Boas et al. 2021; Lombardozzi et al. 2020; Peng et al. 2018). These augmented models are not only conducive to yield simulation, but also improve the estimation of regional-scale carbon, water and energy exchanges within the agriculture-climate-environment system (Boas et al. 2021; Lokupitiya et al. 2009; Song et al. 2013). However, despite these recent progresses, most TBMs still lack a sound representation of crop-specific physiology and/or agricultural land-use changes and management practices (e.g., tillage, cover cropping, and genetic improvement). Moreover, some TBMs still fail to adequately represent the effects of multiple environmental changes (e.g., CO₂ fertilization, nitrogen (N) deposition, and ozone pollution) on crop growth and development. Improvements in our knowledge of the environmental and management factors influencing crop growth and yield will further deepen our understanding of the food-energy-water nexus and lead toward sustainable agricultural systems.

In this study, we implemented such a unified framework in the platform of the Dynamic Land Ecosystem Model v4.0 (hereinafter referred to as the agricultural module of DLEM v4.0), which is well-recognized for simulating coupled carbon-water-nutrient cycles (Pan et al. 2021; Tian et al. 2010a; Tian et al. 2020b; Yao et al. 2020). Specifically, leveraging the strengths of DLEM v4.0 in representing hydrological, biophysical and biogeochemical processes under multiple environmental changes, we incorporated explicit and mechanistic representations of dynamic crop growth processes and agricultural management practices into it, including but not limited to crop-specific phenological development, carbon allocation, yield formation, and biological N fixation processes, as well as management practices such as tillage, cover cropping, and crop genetic improvements. The performance of the new agricultural module in reproducing the seasonal

variations and magnitudes of leaf area index (LAI), aboveground biomass, and yield was evaluated against field observations. Using this model, we also simulated corn, soybean, and winter wheat production in the conterminous United States (U.S.) over 1960-2018 and examined how they varied spatially and temporally.

3.2 Materials and methods

3.2.1 Model descriptions

DLEM v4.0 is a highly integrated TBM that is capable of quantifying daily, spatially explicit carbon, water, and nutrient stocks and fluxes in terrestrial ecosystems and inland water systems across site, regional, and global scales (Pan et al. 2021; Tian et al. 2010a; Tian et al. 2020b; Yao et al. 2020). It contains five key components, including biophysics, plant physiology, dynamic vegetation, soil biogeochemistry, and natural and anthropogenic disturbances. DLEM has been extensively used to investigate the responses of terrestrial carbon, nitrogen, and water cycles to multiple natural and anthropogenic forcings. The agricultural module in DLEM v4.0 is developed by incorporating explicit and mechanistic representations of dynamic crop growth processes and agricultural management practices, including but not limited to crop-specific phenological development, carbon allocation, yield formation, and biological N fixation processes, as well as management practices such as nitrogen fertilization, irrigation, rotation, manure application, tillage, cover cropping, and crop genetic improvements (You et al. 2022). By integrating detailed biogeochemical, biophysical, and hydrological processes, the agricultural module is capable of simulating and predicting the exchange of carbon (including crop yield), water, nutrient and energy fluxes within the agriculture-climate-environment system. The detailed processes and descriptions of the agricultural model in DLEM v4.0 have been presented in Chapter 2.

3.2.2 Input data

To drive DLEM v4.0, long-term spatial datasets at a resolution of 5×5 arc-min were developed, including climate, atmospheric CO₂ concentration, N deposition, soil properties, crop rotation, N fertilizer use rates, manure N application rates, irrigation, tillage intensity, and the earliest and latest crop planting dates (Table 3-1). More details about these datasets are presented in Section 2.3 in Chapter 2. In addition, to better represent crop growth characteristics across a wide range of temperature and precipitation regimes, we divided corn, soybean and winter wheat varieties in the U.S. into seven, seven, and three groups, respectively (Figure 3-1), based on the classification of relative maturity groups (Zhang et al. 2007; Zhang et al. 2020b). The spatial distribution of crop maturity groups remains relatively stable over time but differed in several genetic characteristics, including the total CBD required for maturity, the timing and duration of different phenological stages, and photoperiod-related parameters (Table 3-2). The spatial distribution of corn variety groups was adapted from the corn maturity zones provided by the Elkmound Seed Company (<https://www.elkmoundseed.com/seed-corn/seed-corn-resources/>), and we merged the zone with maturity between 91 and 95 days and the zone with maturity between 95 and 100 days into one. The distribution of soybean variety groups was derived from the revised optimum adaptation zones for soybean maturity groups (Zhang et al. 2007). The distribution of winter wheat variety groups was determined based on the wheat production map by the National Association of Wheat Growers (<https://www.wheatworld.org/wheat-101/wheat-production-map/>), and we divided the U.S. winter wheat varieties into three groups, i.e., soft white winter wheat, hard red winter wheat, and soft red winter wheat.

Table 3-1. Input datasets to drive DLEM v4.0.

Dataset name	Period	Spatial resolution	Temporal resolution	Methods and data sources
Climate (precipitation, solar radiation, maximum, minimum and mean temperatures)	1860-2018	5 arc-min	Daily	Reconstructed from the North American Land Data Assimilation System product (Mitchell et al., 2004; Xia et al., 2012), the Climate Research Unit-National Centers for Environmental Prediction dataset (Mitchell and Jones, 2005), and the IPSL Climate Model dataset (Boucher et al., 2020), using a revised delta downscaling method (Liu et al., 2013)
CO ₂ concentration	1860-2018	5 arc-min	Monthly	Obtained from the NOAA GLOBALVIEW-CO ₂ data set (www.esrl.noaa.gov)
Nitrogen deposition	1860-2018	5 arc-min	Yearly	Acquired from the International Global Atmospheric Chemistry (IGAC)/Stratospheric Processes and Their Role in Climate (SPARC) Chemistry–Climate Model Initiative (CCMI) (Eyring et al. 2013)
Soil physical and chemical properties (e.g., texture and pH)	One time	5 arc-min	One time	Obtained from the ISRIC-WISE Harmonized Global Soil Profile dataset (Batjes 2008)
Crop rotation maps	1910-2018	5 arc-min	Yearly	Developed by combining the United States Department of Agriculture (USDA) Cropland Data Layer (CDL) product, the USDA-National Agricultural Statistics Service (NASS) survey data of county-scale crop planting area, and the Google Earth Engine cloud computing platform, using the spatialization method implemented in Yu et al. (2018)
Crop-specific nitrogen fertilizer use rate	1910-2018	State-level	Yearly	Reconstructed using the state-level N fertilizer use rates from USDA-NASS and the national-level commercial N fertilizer consumption data from Mehring et al. (1957) and USDA-ERS (2019), following a method similar to that used in Cao et al. (2018b)
Manure nitrogen application	1860-2018	5 arc-min	Yearly	Acquired from Bian et al. (2021b)
Crop-specific irrigation map	1950-2018	5 arc-min	Yearly	Using the MODIS Irrigated Agriculture Dataset (MIrAD) (Brown and Pervez, 2014; Pervez and Brown, 2010) as a base map, and then combining the county-scale irrigation reanalysis dataset derived from the United States Geological Survey (USGS) (McManamay et al., 2021) and the USDA-NASS county-scale irrigated cropland area to extrapolate the spatially explicit irrigation map in historical years
Tillage map	1960-2018	5 arc-min	Yearly	Reconstructed from the county-scale tillage practices survey data obtained from the National Crop Residue Management Survey (CRM) of the Conservation Technology Information Center (https://www.ctic.org/CRM), where tillage maps for missing years were kept consistent with the nearest years for which data were available
The earliest and latest crop planting dates	One time	State-level	One time	Obtained from the USDA-NASS survey report (NASS, 2010)
Auxiliary data (e.g., topography and river network)	One time	5 arc-min	One time	Obtained from previous DLEM studies (Tian et al. 2010a; Tian et al. 2012c; Tian et al. 2020b; Xu et al. 2019)

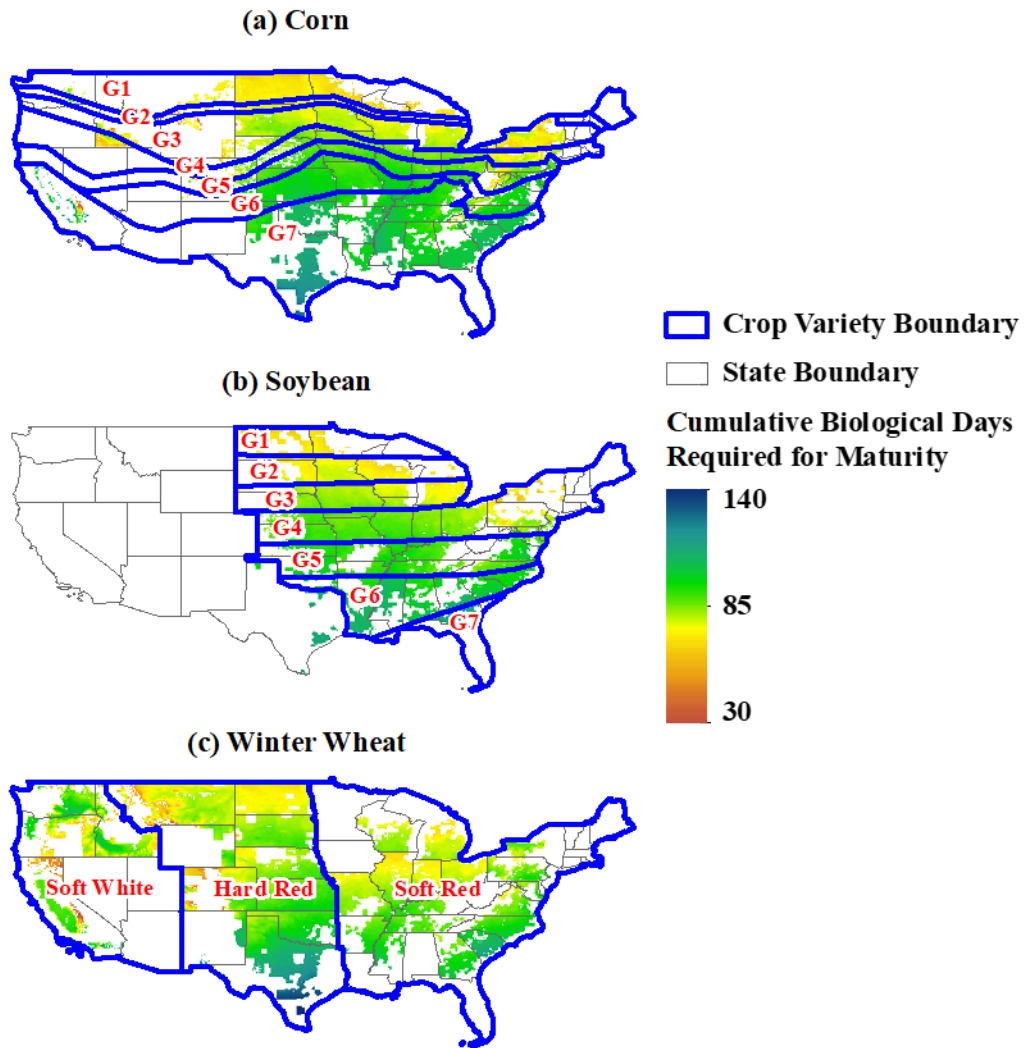


Figure 3-1. Boundaries of crop variety groups in the conterminous United States and the spatial distribution of cumulative biological days required for maturity for corn (a), soybean (b), and winter wheat (c). The blue lines are the boundaries of crop variety groups, and the labels denote the crop variety groups presented in Table 3-2.

Table 3-2. Major parameter values of the crop variety groups used in this study.

Variety Group	Corn							Soybean							Winter Wheat		
	G1	G2	G3	G4	G5	G6	G7	G1	G2	G3	G4	G5	G6	G7	Soft White	Hard Red	Soft Red
Relative Maturity	≤85	86-90	91-100	101-105	106-110	111-115	>116	MG_0	MG_I	MG_II	MG_III	MG_IV	MG_V	MG_VI	NA		
Average CBD	60	65	69	76	86	97	109	51	58	65	71	83	94	105	93	91	87
<i>CPP</i> (h)	NA							14.4	14.1	13.8	13.6	13.4	13.1	12.8	16		
<i>ppsen</i>	NA							0.148	0.171	0.203	0.249	0.285	0.294	0.303	0.11	0.10	0.09
V_{cmax} ($\mu\text{mol CO}_2 \text{ m}^{-2} \text{ s}^{-1}$)	80	80	90	90	90	85	80	65	70	80	80	70	60	60	90	80	80
<i>f_s1</i>	0.050	0.045	0.041	0.039	0.038	0.036	0.035	0.054	0.053	0.052	0.050	0.047	0.045	0.044	0.026	0.027	0.027
<i>f_s2</i>	0.254	0.252	0.250	0.255	0.254	0.253	0.258	0.145	0.142	0.139	0.133	0.126	0.120	0.117	0.199	0.265	0.208
<i>f_s3</i>	0.254	0.252	0.250	0.255	0.254	0.253	0.258	0.236	0.231	0.225	0.215	0.205	0.195	0.190	0.395	0.472	0.413
<i>f_s4</i>	0.311	0.303	0.297	0.300	0.297	0.294	0.297	0.337	0.338	0.337	0.348	0.355	0.368	0.372	0.447	0.527	0.467
<i>f_s5</i>	0.479	0.455	0.434	0.430	0.422	0.414	0.412	0.550	0.551	0.550	0.558	0.562	0.572	0.574	0.749	0.735	0.738
<i>f_s6</i>	0.966	0.965	0.965	0.965	0.965	0.965	0.965	0.982	0.982	0.983	0.983	0.984	0.985	0.985	0.978	0.977	0.977
<i>f_s7</i>	1.000	1.000	1.000	1.000	1.000	1.000	1.000	1.000	1.000	1.000	1.000	1.000	1.000	1.000	1.000	1.000	1.000

Note: CBD denotes the cumulative biological days required for maturity; *CPP* denotes the critical daylength at which the rate of phenological development began to be restricted by daylength; *ppsen* is the photoperiod sensitivity coefficient; *f_s1*, *f_s2*, *f_s3*, *f_s4*, *f_s5*, *f_s6* and *f_s7* for corn denote the fraction of accumulated biological days required to trigger the initiation of emergence, end juvenile, tassel initiation, silking, begin grain filling, end grain filling, and maturity, respectively; *f_s1*, *f_s2*, *f_s3*, *f_s4*, *f_s5*, *f_s6* and *f_s7* for soybean denote the fraction of accumulated biological days required to trigger the initiation of emergence, flowering (R1), begin pod growth (R3), begin grain filling (R5), end pod growth, end grain filling, and maturity, respectively; *f_s1*, *f_s2*, *f_s3*, *f_s4*, *f_s5*, *f_s6* and *f_s7* for winter wheat denote the fraction of accumulated biological days required to trigger the initiation of emergence, terminal spikelet, end leaf growth, end ear growth, begin grain filling, end grain filling, and maturity, respectively.

3.2.3 Model calibration and validation

We calibrated and validated the new model using data collected from multiple sources, including the AmeriFlux Network, the Greenhouse Gas Reduction through Agricultural Carbon Enhancement Network, the Resilient Economic Agricultural Practices Project, the USDA-NASS, and relevant literature. The values of the crop variety group parameters (Table 3-2) and the general model parameters related to crop growth processes (Table 3-3) were determined through model calibration within a reasonable range of reported values in literature. Specifically, we first used the default parameters to run the model, and then we adjusted the parameters (within a $\pm 20\%$ range of default values) to obtain a close match between the observed and predicted values for LAI, aboveground biomass, and grain yield. The parameter set obtaining the minimal bias between the simulated and measured values across all sites was adopted. In addition, we calibrated parameters related to crop genetic improvements (Table 3-4), including N uptake capability (N_{upmax}) and the maximum carboxylation rate (V_{cmax}). Specifically, we first calibrated the temporal changes of N_{upmax} using the time series of N_{upmax} obtained from Lu et al. (2018), in which a logistic equation was used to model the impacts of crop genetic improvements in enhancing N_{upmax} . Then, a linear regression model was used to estimate the temporal changes in increasing rate of V_{cmax} to obtain the best match between the simulated time series of national crop yields and the USDA-NASS records.

Table 3-3. General model parameters related to crop growth, development, and yield formation processes in the Dynamic Land Ecosystem Model.

Symbol	Definition	Corn	Soybean	Winter Wheat	Source
T_{avg}^p	Threshold of 10-day running average temperature for sowing (K)	283.15	286.15	294.15	Levis et al. (2012)
T_{min}^p	Threshold of 10-day running minimum temperature for sowing (K)	279.15	279.15	283.15	Levis et al. (2012)
ATT_{min}	Threshold of minimum thermal time since the earliest day in planting window for sowing	200	50	200	This study
$Card_{min}$	The minimum cardinal temperature required for photosynthesis (°C)	8	8	0	Soltani and Sinclair (2012)
$Card_{opt1}$	The lower optimal cardinal temperature required for photosynthesis (°C)	30	30	24	Soltani and Sinclair (2012)
$Card_{opt2}$	The upper optimal cardinal temperature required for photosynthesis (°C)	37	35	28	Soltani and Sinclair (2012)
$Card_{max}$	The maximum cardinal temperature required for photosynthesis (°C)	45	40	37	Soltani and Sinclair (2012)
CPP	Critical photoperiod at which the rate of phenological development began to be restricted by daylength	/	Table 3-2	Table 3-2	Soltani and Sinclair (2012)
$ppsen$	Photoperiod sensitivity coefficient	/	Table 3-2	Table 3-2	Soltani and Sinclair (2012)
$VDSAT$	The number of vernalization days needed to saturate the vernalization response	/	/	50	Soltani and Sinclair (2012)
$vsen$	Vernalization sensitivity coefficient	/	/	0.033	Soltani and Sinclair (2012)
Ver_{min}	The minimum temperature required for vernalization (°C)	/	/	-1	Soltani and Sinclair (2012)
Ver_{opt1}	The lower optimal temperature required for vernalization (°C)	/	/	0	Soltani and Sinclair (2012)
Ver_{opt2}	The upper optimal temperature required for vernalization (°C)	/	/	8	Soltani and Sinclair (2012)
Ver_{max}	The maximum temperature required for vernalization (°C)	/	/	12	Soltani and Sinclair (2012)
$P_{density}$	Planting density (plant/m ²)	6	30	150	Grichar (2007), Liu et al. (2017), and Cox (1996)
pKW	Potential kernel weight (g/grain)	0.3	0.3	0.06	Keating et al. (2003) and Borrás et al. (2004)
GN_{max}	Maximum grain number per plant	800	500	110	Andrade et al. (1999) and Vega et al. (2001)
GNg_{stem}	Number of kernels per gram stem	/	/	25	Zheng et al. (2014)
$HeatTemp_{min}$	Lower cardinal temperature for heat stress to reduce grain number (°C)	37	35	28	Soltani and Sinclair (2012)
$HeatTemp_{max}$	Upper cardinal temperature for heat stress to reduce grain number (°C)	45	40	37	Soltani and Sinclair (2012)
SLA	Specific leaf area (m ² /g)	0.03	0.025	0.022	This study
LAI_{max}	Maximum leaf area index	8	7	6	This study
$H_{canopy,max}$	Maximum canopy height (m)	2.5	0.6	1.2	This study
EF_{mix}	Mixing efficiency	Table 2-3	Table 2-3	Table 2-3	Porwollik et al. (2019)

Table 3-4. Temporal changes in photosynthesis rate and nitrogen uptake capability due to crop genetic improvement.

Crop type	Improvement in V_{cmax}	Improvement in nitrogen uptake capability	Source
Corn	$1.064 + 0.034 \times (\text{Year} - 1960)$	$0.075 + 0.05/(1 + \exp(-0.060 \times (\text{Year} - 1970)))$	
Soybean	$0.899 + 0.019 \times (\text{Year} - 1960)$	$0.040 + 0.03/(1 + \exp(-0.140 \times (\text{Year} - 1955)))$	Lu et al. (2018)
Winter Wheat	$0.929 + 0.014 \times (\text{Year} - 1960)$	$0.035 + 0.015/(1 + \exp(-0.07 \times (\text{Year} - 1970)))$	

After model calibration, field observed LAI, aboveground biomass, and yield data (excluding the data for model calibration), as well as the regional-scale crop production survey data were used to evaluate the new model performance. The distribution of these field sites are presented in Figure 3-2. Further details of the descriptions of these sites can be found in You et al. (2022). Several metrics were used to quantitatively evaluate the model performance, including the coefficient of determination (R^2), the root mean square error (RMSE), and the normalized root mean square error (NRMSE).

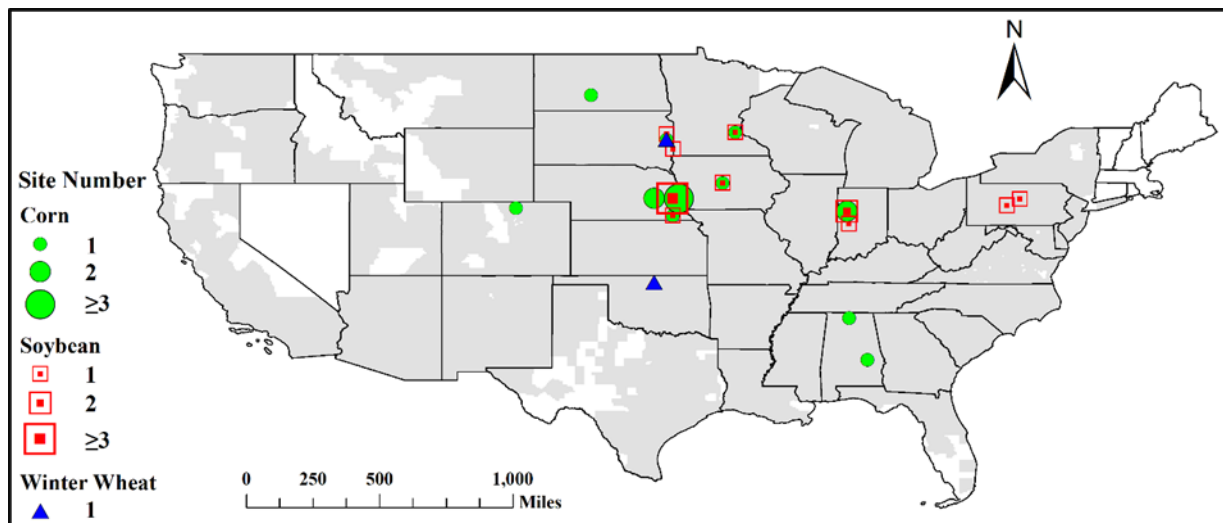


Figure 3-2. Spatial distribution of field sites. The green, red and blue colors represent the sites of corn, soybean and winter wheat, respectively, and the size of symbols indicates the number of sites.

3.2.4 Model implementation

The implementation of the agricultural module of DLEM v4.0 includes three major steps: an equilibrium run, a spin-up run, and a transient run. The equilibrium run was driven by the average climate data during the 1860s and other environmental factors in 1860. The equilibrium state was assumed to be reached when the changes in carbon, N, and water pools between two consecutive 20 years period were less than $0.5 \text{ g C m}^{-2} \text{ year}^{-1}$, $0.5 \text{ g N m}^{-2} \text{ year}^{-1}$, and 0.5 mm year^{-1} , respectively. The spin-up run was driven by the detrended climate data during the 1860s to eliminate model fluctuations due to the mode transition from equilibrium run to transient run. Finally, the transient run was driven by the historical data from 1860 to 2018.

3.2.5 Parameter sensitivity analysis

The Sobol's method, a variance-based global sensitivity analysis method, was used to measure the sensitivity of simulated crop yield to key model parameters. The Sobol' method decomposes model output variance into the contribution of each input parameter and their interactions to calculate sensitivity index (Sobol 1993a):

$$V_Y = \sum_i V_i + \sum_i \sum_{j>i} V_{ij} + \sum_i \sum_{j>i} \sum_{k>j} V_{ijk} + \dots + V_{1,2,\dots,n} \quad (1)$$

where V_Y represents the total variance of model output, V_i represents the variance explained by the i th input parameter, V_{ij} represents the variance explained by the interactions between the i th and j th input parameters, and n represents the number of input parameters. The first-order sensitivity index is defined as $S_i = V_i/V_Y$, the higher-order sensitivity indices are defined as $S_{ij} = V_{ij}/V_Y$, $S_{ijk} = V_{ijk}/V_Y, \dots$, $S_{1,2,\dots,i,\dots,n} = V_{1,2,\dots,i,\dots,n}/V_Y$, respectively, and the total-order sensitivity index S_{Ti} of the i th parameter is defined as the sum of its first-order sensitivity index and all the

higher-order sensitivity indices involving it. Among them, S_i measures the direct impact of each input parameter on the output variance and S_{Ti} measures the total impacts (i.e., the sum of direct and indirect impacts). A large difference between S_i and S_{Ti} indicates that the parameter mainly affects output through interactions. The Sobol' method uses the Monte Carlo sampling scheme to generate random parameter samples. To calculate sensitivity indices, it requires a parameter set with a sample size of $M \times (2n + 2)$, where M represents the number of base samples and n represents the number of input parameters. Here, M is set to 512 (You et al. 2019).

3.3 Results

3.3.1 Site-scale model performance

3.3.1.1 Evaluation of the simulated leaf area index

The performance of the LAI simulation was evaluated against 15 site-years of field observations for corn, 6 site-years for soybean, and 10 site-years for winter wheat. Generally, the simulated LAI was consistent with the observed LAI (Figure 3-3), with RMSE (NRMSE) values for corn, soybean, and winter wheat being 1.26 m²/m² (20%), 0.87 m²/m² (19%), and 0.66 m²/m² (21%), respectively, and R² values being 0.68, 0.66, and 0.57, respectively. The model also captured the seasonal dynamics of LAI, for example, in the US-Ne3 corn-soybean rotation site, where the model reproduced well the timing of LAI increase and decrease as well as its amplitude (Figure 3-4). However, some discrepancies still existed between the simulated LAI and the observations. Specifically, the simulated LAI underestimated the observed LAI at its low end, suggesting that the simulated leaf onset slightly lags behind the actual leaf onset, which may be due to the simulated planting date being later than the actual planting date. For instance, our simulated planting date of corn in 2001 at the US-Ne3 site is May 22, while the actual planting

date was May 14. In addition, at the US-Ne3 site, the simulated LAI of corn was slightly overestimated during the late growing season compared with the observations, and the peak LAI of soybean was underestimated in the year 2002 and 2006 (Figure 3-4).

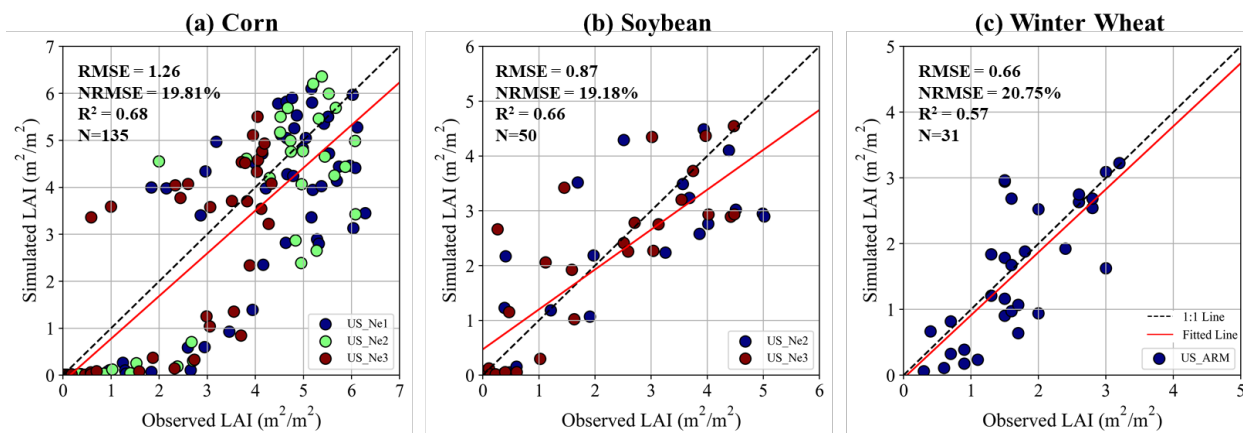


Figure 3-3. Site-scale comparisons between the simulated leaf area index (LAI) and field observations for corn (a), soybean (b), and winter wheat (c). Different colors indicate different crop sites.

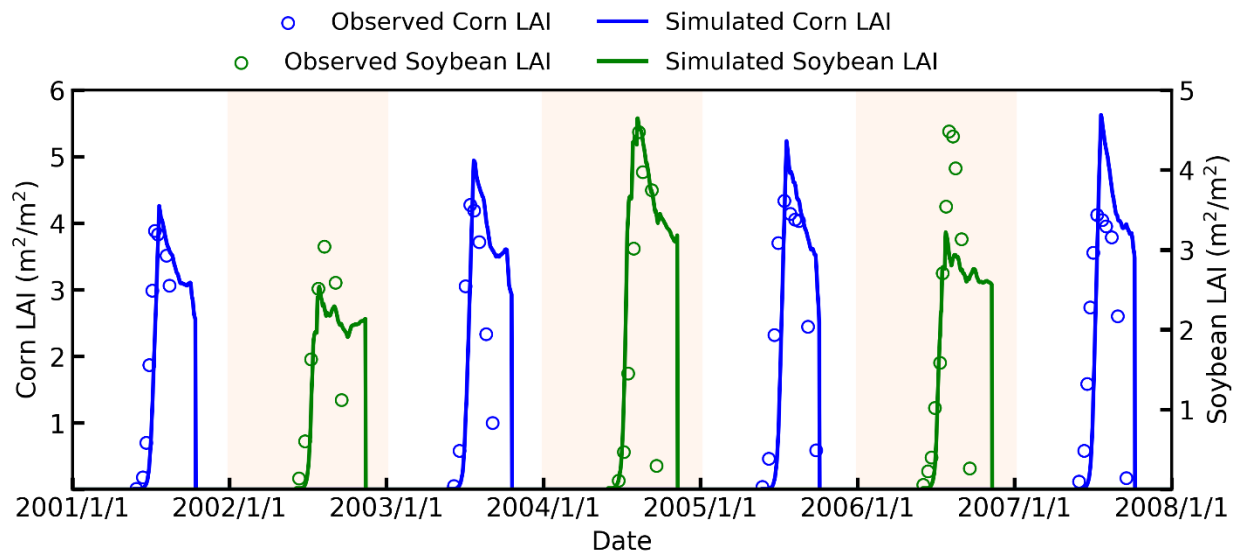


Figure 3-4. The seasonal evolution of observed and simulated leaf area index (LAI) in a corn-soybean rotation rainfed site, US-Ne3, where corn is planted in odd years (2001, 2003, 2005, and 2007) and soybean is planted in even years (2002, 2004, 2006).

3.3.1.2 Evaluation of the simulated aboveground biomass

Generally, the simulated aboveground biomass was in line with the observed data (Figure 3-5), where the RMSE (NRMSE) values between them for corn, soybean, and winter wheat were 2912 kg/ha (12%), 658 kg/ha (14%), and 278 kg/ha (27%), respectively, and the R^2 between them were 0.82, 0.79, and 0.45, respectively. Meanwhile, similar to LAI, the modeled seasonal variations in aboveground biomass was well consistent with the observations (Figure 3-6).

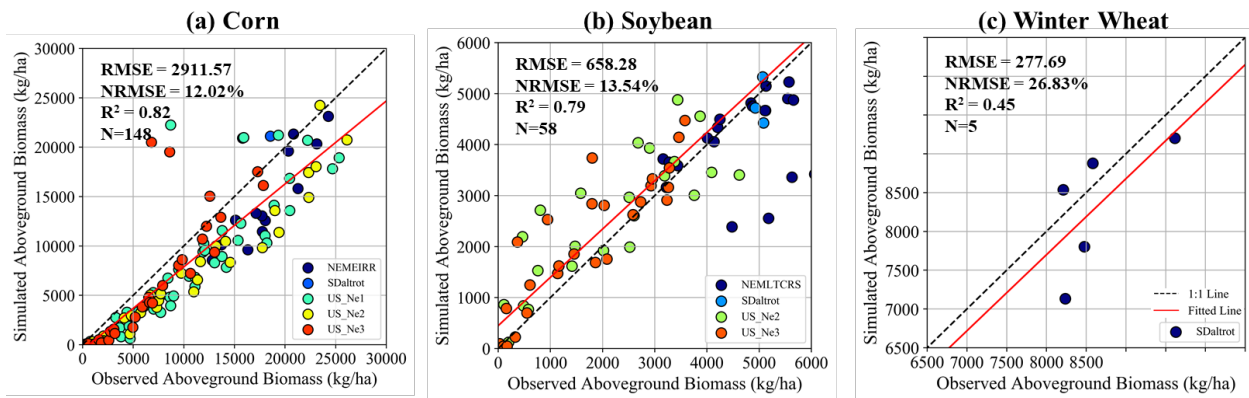


Figure 3-5. Site-scale comparisons between the simulated aboveground biomass and field observations for corn (a), soybean (b), and winter wheat (c). Different colors indicate different crop sites.

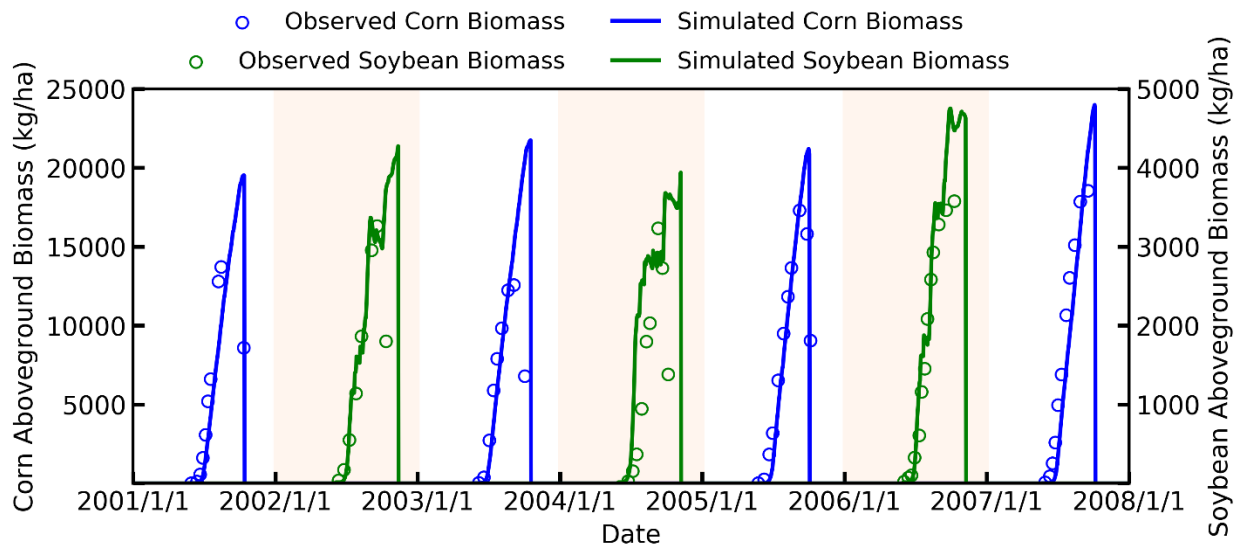


Figure 3-6. The seasonal evolution of observed and simulated aboveground biomass in a corn-soybean rotation rainfed site, US-Ne3, where corn is planted in odd years (2001, 2003, 2005, and 2007) and soybean is planted in even years (2002, 2004, 2006).

3.3.1.3 Evaluation of the simulated crop yield

The simulated yields agreed well with the observations of 94 site-years for corn, of 87 site-years for soybean, and of 12 site-years for winter wheat (Figure 3-7), with the RMSE values for corn, soybean, and winter wheat ranging from 351 kg/ha to 1080 kg/ha, and the NRMSE values ranging from 11% to 20%. Meanwhile, the R^2 values for all crops were greater than 0.4. Compared to corn and soybean, the simulation accuracy for winter wheat yield was lower, maybe partly due to the smaller number of observations in correlation analysis.

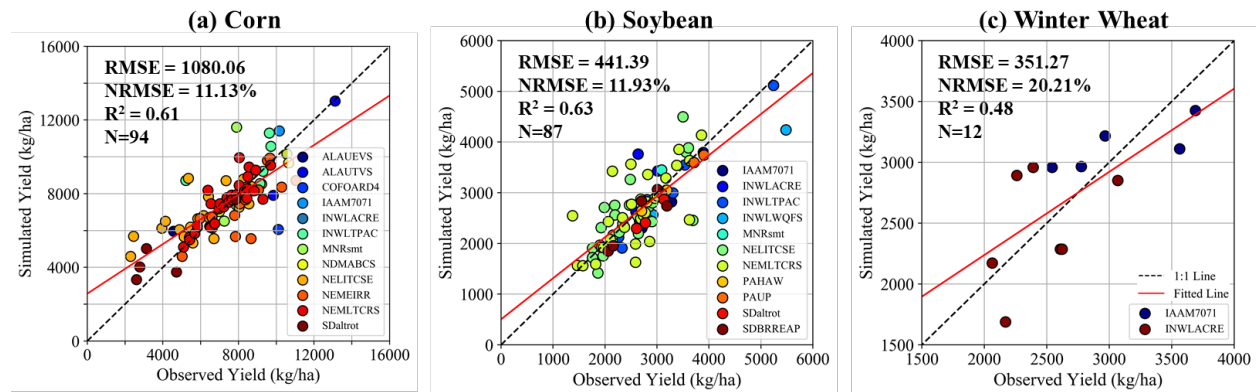


Figure 3-7. Site-scale comparisons between the simulated yield and field observations for corn (a), soybean (b) and winter wheat (c). Different colors indicate different crop sites.

3.3.2 Spatial patterns of simulated crop production

We used the calibrated model to simulate the production of corn, soybean, and winter wheat in the conterminous U.S. from 1960 to 2018. The simulation results show that corn and soybean had relatively high production in the Midwest region but low production in the southern region, while winter wheat had relatively high production in the Southern Plains and northwestern regions

(Figure 3-8). Overall, the spatial pattern of simulated mean annual crop production during 1960-2018 simulated by our model was consistent with the USDA-NASS survey data, which suggest that our model is capable of reproducing the spatial pattern of crop production across a wide range of temperature and precipitation regimes. At the grid level, the simulated crop production was mostly significantly correlated (P value < 0.05) with the USDA-NASS survey data (Figure 3-9). The areas with $R^2 > 0.7$ accounted for 88.91%, 97.51% and 64.62% of the total planting areas of corn, soybean and winter wheat, respectively.

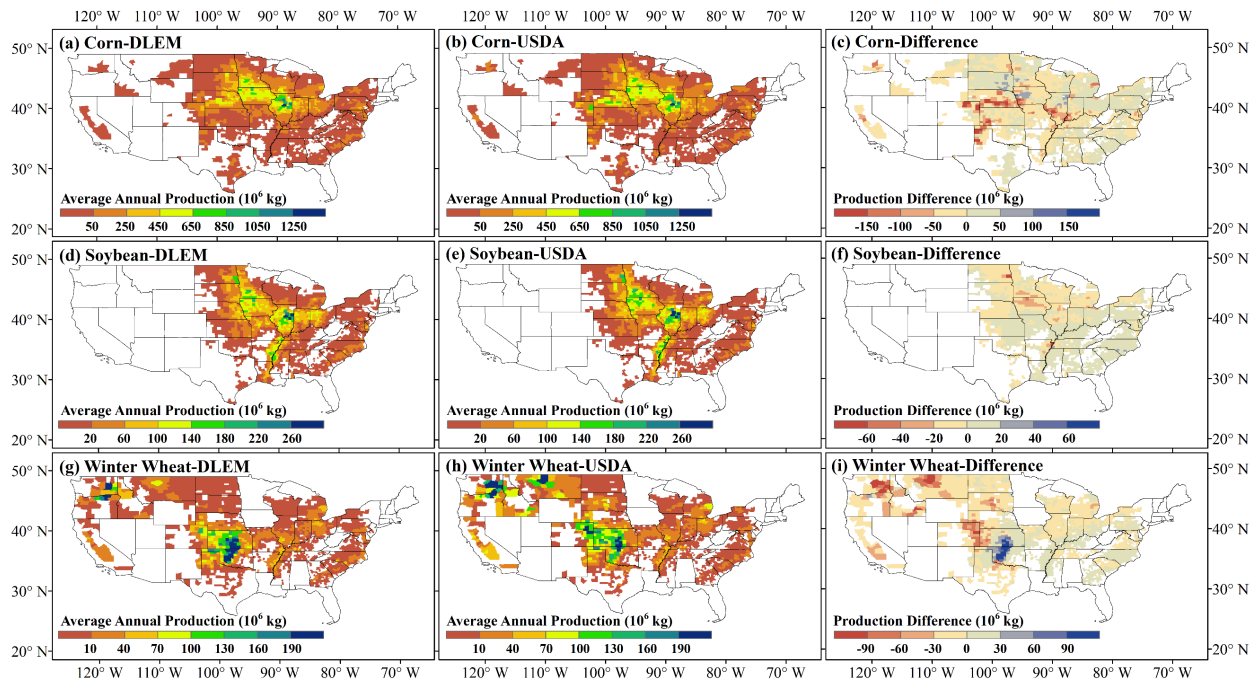


Figure 3-8. Comparisons between the spatial patterns of average annual crop production simulated by the Dynamic Land Ecosystem Model (DLEM) and derived from the United States Department of Agriculture-National Agricultural Statistics Service (USDA-NASS) during 1960-2018, as well as the differences between them. (a-c) Corn production obtained from the DLEM and the USDA-NASS and their difference; (d-f) Soybean production obtained from the DLEM and the USDA-NASS and their difference; (g-i) Winter wheat production obtained from the DLEM and the USDA-NASS and their difference. A negative value in the difference of production indicates an underestimation of production by the DLEM, and a positive value indicates an overestimation of production by the DLEM.

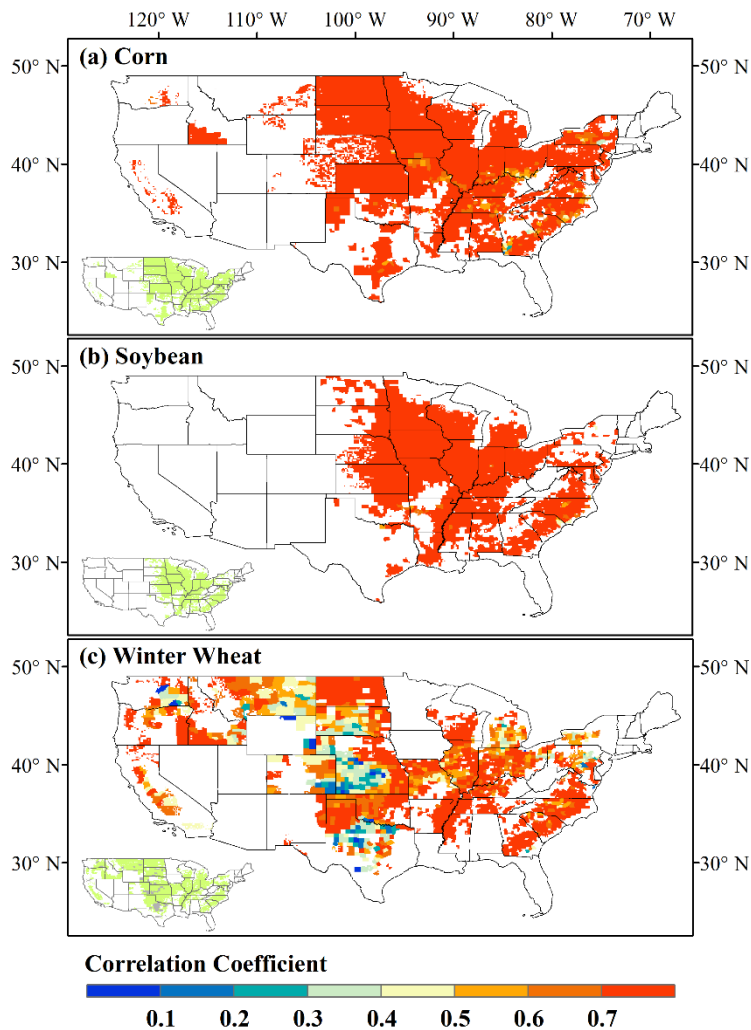


Figure 3-9. Correlation coefficient between the simulated and observed crop productions in each county during 1960-2018 for corn (a), soybean (b) and winter wheat (c). The inset shows the spatial distribution of the corresponding P value, in which green color denotes significant correlation (P value < 0.05), and gray color denotes non-significant correlation (P value > 0.05).

In addition, we also used NRMSE and R^2 to quantitatively evaluate the simulation accuracy of crop production at county scale (Figure 3-10). The NRMSE values between the DLEM-simulated crop production and the USDA-NASS survey data for corn, soybean, and winter wheat were all smaller than 5%, and the corresponding R^2 values were 0.93, 0.94, and 0.67, respectively. However, despite the overall good performance, it should be noted that there were still some

discrepancies between the simulated production of winter wheat and the survey data (e.g., the underestimated winter wheat production in the northwestern U.S.).

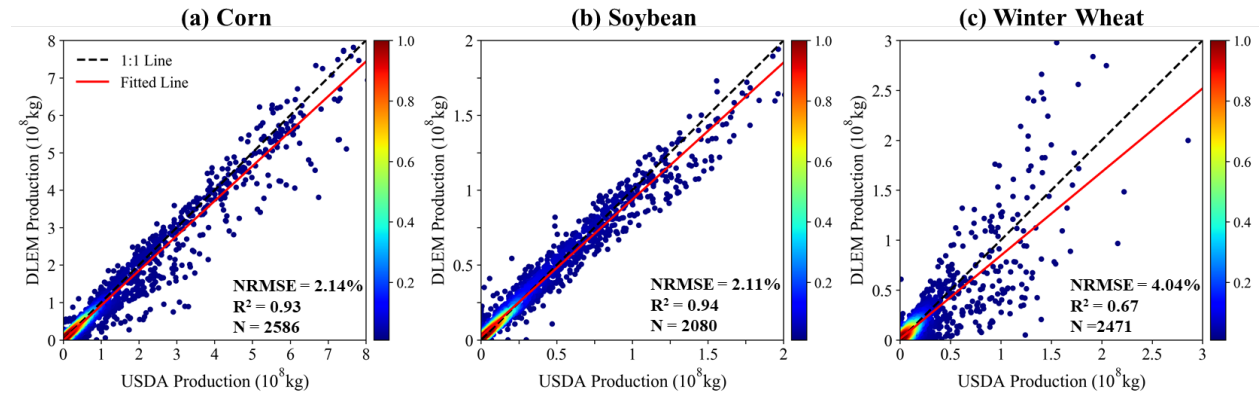


Figure 3-10. Quantitative comparisons between the average annual crop production during 1960-2018 simulated by the Dynamic Land Ecosystem Model (DLEM) and obtained from the United States Department of Agriculture-National Agricultural Statistics Service (USDA-NASS) survey data at county-scale for corn (a), soybean (b) and winter wheat (c), respectively. The number next to the color bar represents the normalized point density.

3.3.3 Temporal variations of simulated crop production

Temporal variations in simulated crop production at the national scale was also examined (Figure 3-11). From the 1960s to the 2010s, the national corn production almost tripled and the soybean production almost quadrupled. Winter wheat production showed large interannual variations, increasing at first and then decreasing. Generally, the temporal variations of national crop production simulated by DLEM agreed well with the USDA-NASS survey data. The NRMSE values between them for corn, soybean, and winter wheat ranged from 6.89% to 10.92%, and the R² values between them are all greater than 0.7. Meanwhile, the results indicate that the new model was capable of capturing the reductions in crop production caused by extreme weather disasters. For example, the extreme drought event that occurred in 2012 swept most of the contiguous U.S. (Mallya et al. 2013), leading to a significant reduction in crop production, and our simulated results

also showed a large reduction. However, it should be noted that the simulated production responded more severely to extreme weather events than the observations. For instance, the corn production loss in 2012 estimated by DLEM was about twice the actual loss relative to the average corn production in 2011 and 2013.

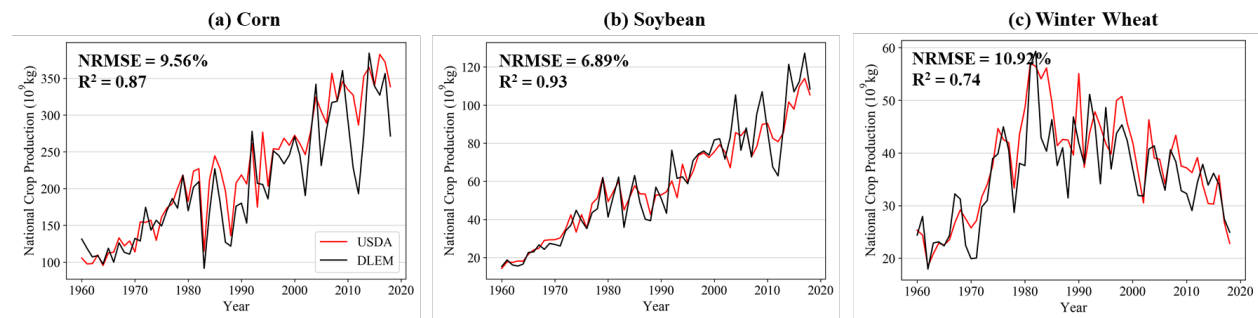


Figure 3-11. Historical trends of national crop production simulated by the Dynamic Land Ecosystem Model (DLEM) and obtained from the United States Department of Agriculture-National Agricultural Statistics Service (USDA-NASS) for corn (a), soybean (b) and winter wheat (c), respectively.

3.4 Discussion

3.4.1 General performance of the agricultural module of DLEM

The site-scale validation results indicate that the DLEM-simulated LAI, aboveground biomass, and yield were generally consistent with the observations, although part of the modeled LAI during the late growing season was still overestimated and the peak LAI in some years was underestimated. The deviations in the simulated LAI may be partly due to the constant SLA used in our model. Specifically, daily LAI in DLEM is calculated based on the leaf carbon and the constant SLA, while SLA actually varies with the crop growth stage and is simultaneously regulated by environmental conditions (Danalatos et al. 1994; Tardieu et al. 1999). However, the mechanism of how SLA responds to changes in climate and environmental factors throughout the growing season is still unclear (Drewniak et al. 2013), making it difficult to include dynamic SLA

in the model at this time. Another possible explanation for the deviations in the simulated LAI might be bias in the modeled planting date and growing season length. Specifically, our model tended to estimate later planting dates and longer growing seasons than observations (Figure 3-4), which cause the simulated LAI to maintain a high value for a longer period than the actual duration and in turn overestimates LAI during the late growing season. The accurate simulation of plant phenology (e.g., planting date and growing season length) has been shown to be critical for modeling productivity (Anapalli et al. 2005; Wallach et al. 2021; You et al. 2020). In our model, to reduce model complexity and its associated uncertainty, only temperature-derived metrics are used to determine planting date (Levis et al. 2012). Given that planting date depends not only on temperature but on other factors as well, for example, soil moisture, terrain condition and factors that may affect farmers' decisions such as labor and equipment availability (Kucharik 2006; Sacks et al. 2010), it is not surprising that there are some discrepancies in the modeled phenology. Consideration of these additional factors on planting date may help to improve the simulation of crop phenology in the future.

The spatial pattern of crop production simulated by our model was also comparable to survey data (Figure 3-8), although some discrepancies still exist. The underestimated winter wheat production in the northwestern U.S. may be partly due to the deficiency of our model in simulating available soil water. A similar problem has also been reported in the spatial pattern of winter wheat yield simulated by CLM 4.5 (Lu et al. 2017b). In DLEM, we use a water regulation factor, β , to represent the limitation of soil water on photosynthesis and other water-related processes (Pan et al. 2015; Tian et al. 2010a). A β value of 0 denotes complete water restriction, whereas a β value of 1 denotes no water stress. The spatial pattern of DLEM-modeled β during the growing season of winter wheat indicates that the modeled β in the northwestern U.S. is very low (Figure 3-12),

with an average value less than 0.5, suggesting that soil water availability severely limits photosynthesis in this region and thus leads to the underestimated production. If we applied full irrigation over this region, the simulated pattern of winter wheat production better captures the USDA’s spatial pattern (Figure 3-13). This result suggests that there is less water stress on winter wheat growth in the region than indicated by the model. Crop water supply may be enhanced by an abundant groundwater resource and snowmelt water in this region. However, these hydrological processes are under-represented in our model. In addition to water stress issues, the discrepancy in crop production patterns may also stem from the deficiencies of our model in representing the growth characteristics of winter wheat (e.g., frost tolerance and damage) and relevant farming practices (e.g., irrigation and fertilization).

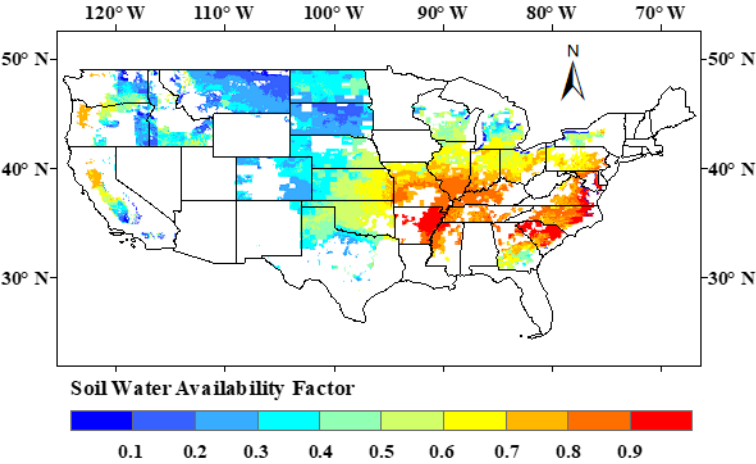


Figure 3-12. The spatial distribution of the simulated average annual β (i.e., soil water availability) during the growing season of winter wheat from 1960 to 2018.

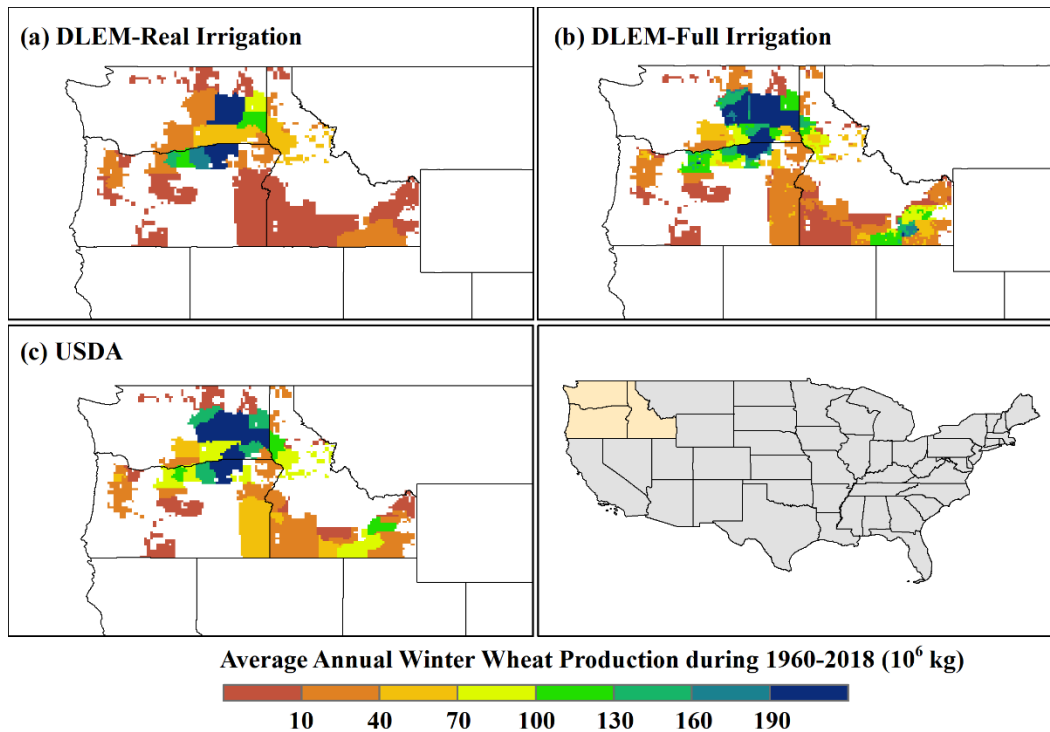


Figure 3-13. Comparisons between the winter wheat production simulated by the Dynamic Land Ecosystem Model (DLEM) under real irrigation (a) and full irrigation (b), and obtained from the United States Department of Agriculture-National Agricultural Statistics Service (USDA-NASS) (c).

With respect to the simulation accuracy of different crops, we found that the accuracy of winter wheat production is lower than that of corn and soybean (Figures 3-8 and 3-10). Winter wheat has a unique growth cycle (i.e., planted in fall and harvested in summer) compared with summer crops. Therefore, it may also have different response mechanisms to environmental stresses due to its frequent exposure to frost damage (Lu et al. 2017b; Vico et al. 2014). Frost damage and its related processes are not considered in our model. Another possible reason for the lower accuracy of winter wheat production may be that we limited winter wheat to only three varieties. The varieties of winter wheat span a large range of latitudes, so there exists large spatial heterogeneity in the temperature and precipitation regimes in which they grow that we have not

fully captured (Zhang et al. 2020b). The consideration of frost damage effects and a further subdivision of varieties may improve the estimation of winter wheat production in the future.

The advances in crop genetic and breeding technologies, agricultural expansion and intensive management practices have led to a one to four-fold increase in crop production in the U.S. during the past several decades (USDA 2018). Our model captured this trend (Figure 3-11). Nevertheless, despite the overall good performance, the model probably has not captured some effects of improvements in genetic and breeding technologies on crop resistance to pests and diseases as well as adaptation to environmental stress (Bailey-Serres et al. 2019; Hammer et al. 2002). This deficiency may partly explain the high sensitivity of our model to extreme weather disasters. In addition, the high sensitivity may be attributed to human adaptive behaviors such as farmers' preparedness and response strategies to extreme weather (Annan and Schlenker 2015), which are not considered in the model.

In addition, we also compared the performance of the new model in simulating national crop production with a previous DLEM version, namely the DLEM-Ag2 (Figure 3-14). Generally, our new model achieved higher simulation accuracy than the DLEM-Ag2, in which the NRMSE values reduced by 6.24%, 1.21%, and 2.18% for corn, soybean and winter wheat, respectively, and the R^2 values increased by 0.13, 0.04, and 0.11, respectively. Meanwhile, the new model better captured the interannual variations and trends of national crop production as compared with the DLEM-Ag2. For example, the DLEM-Ag2 overestimated national corn production in the 1960s and 1970s and substantially underestimated corn production after the 2000s, however, the new model simulated the production changes well over the entire period. The improved performance of the new model also demonstrated the effectiveness of the newly incorporated crop growth processes and agricultural management practices.

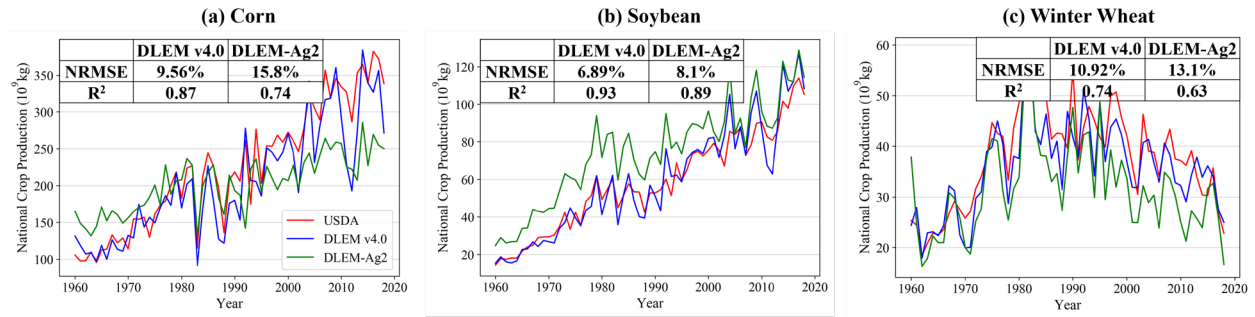


Figure 3-14. Comparisons between the historical trends of national crop production simulated by the Dynamic Land Ecosystem Model v4.0 (DLEM v4.0) and DLEM-Ag2, as well as obtained from the United States Department of Agriculture-National Agricultural Statistics Service (USDA-NASS) for corn (a), soybean (b) and winter wheat (c), respectively.

3.4.2 Parameter sensitivity analysis

Since the new model involves a lot of parameters (Tables 3-2 and 3-3), we conducted global sensitivity analysis to quantify the relative importance of each model parameter to crop yield simulation using the Sobol' method. The Sobol' sensitivity analysis was implemented by evaluating the changes in simulated yield in response to variations in parameter values over a large amount of random parameter samples, which were generated using the Monte Carlo sampling scheme by assuming a uniform distribution for each parameter and randomly varying its value within 20% of the calibrated value (Tian et al. 2011). The number of parameters included in the analysis was 17, 19, and 26 for corn, soybean, and winter wheat, respectively, and after sampling, a total of 18432, 20480, and 27648 parameter samples were generated, respectively. In addition, we performed a resampling analysis over the generated parameter sample space to estimate the variability of the derived first-order (S_i) and total-order (S_{Ti}) sensitivity indices, and the resulting standard deviations of these indices are displayed as error bars in Figures 3-15, 3-16, and 3-17.

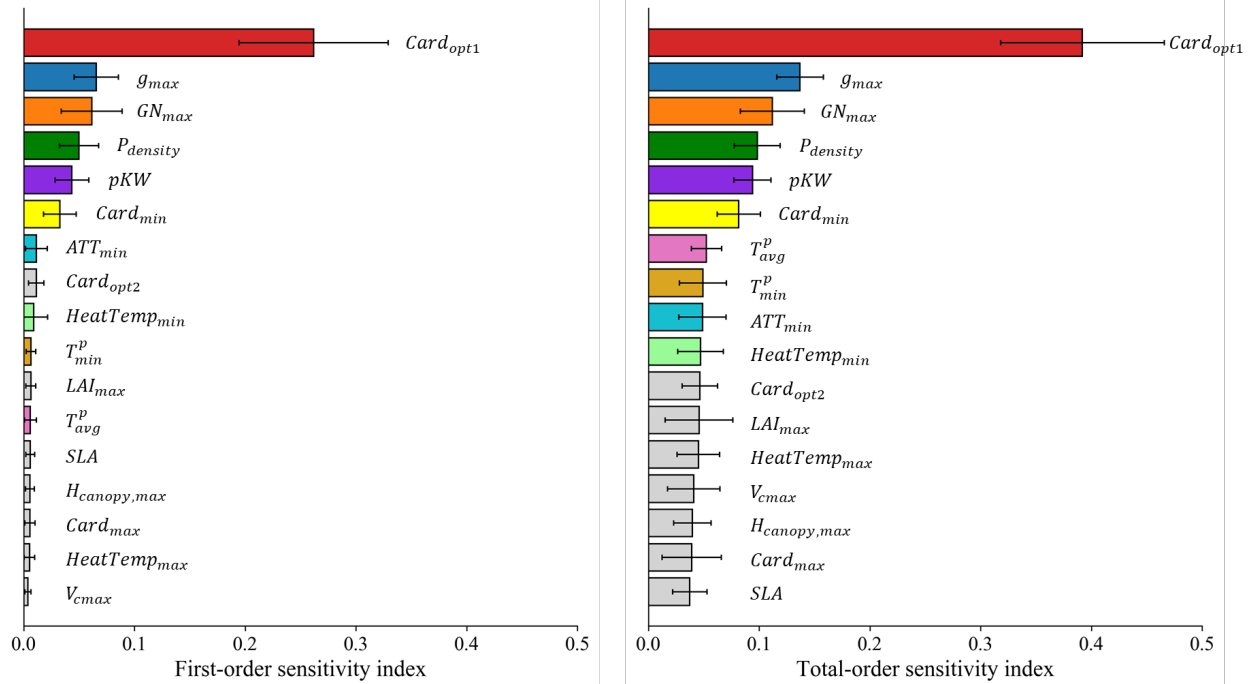


Figure 3-15. The first-order and total-order sensitivity indices of corn-related parameters calculated by the Sobol' global sensitivity analysis method, in which the error bars indicate the corresponding standard deviations derived from the resampling analysis.

We used S_i and S_{Ti} to measure the relative contribution of each parameter to the variance of simulated yield. For corn, the top three most influential parameters revealed by both S_i and S_{Ti} are the lower optimal cardinal temperature required for photosynthesis ($Card_{opt1}$), maximum stomatal conductance (g_{max}), and maximum grain number per plant (GN_{max}) (Figure 3-15). For soybean, there are slight differences in the ranking of influential parameters revealed by S_i and S_{Ti} (Figure 3-16), but in general, the lower and upper optimal cardinal temperatures required for photosynthesis ($Card_{opt1}$ and $Card_{opt2}$) still play a dominant role, and g_{max} as well as the threshold of 10-day running average temperature for sowing (T_{avg}^p) also have a significant impact. For winter wheat, the lower cardinal temperature for heat stress to reduce grain number ($HeatTemp_{min}$) and T_{avg}^p are identified as influential parameters by both S_i and S_{Ti} , whereas

$Card_{opt1}$ is identified as a dominant parameter by S_{Ti} but not by S_i , suggesting that this parameter mainly affects output through interactions with other parameters. Overall, $Card_{opt1}$ was identified as the most influential parameter affecting yield simulation for all the three crops, as this parameter determines the critical point of temperature at which photosynthesis rate reaches the optimum.

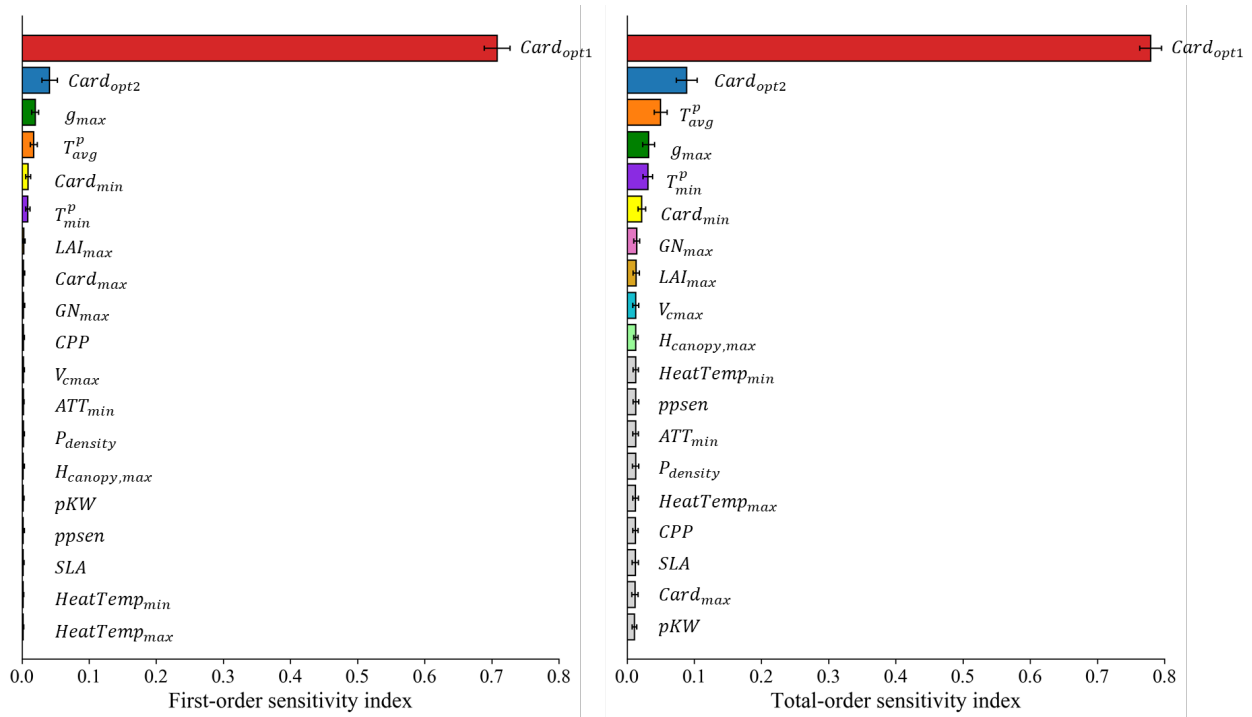


Figure 3-16. The first-order and total-order sensitivity indices of soybean-related parameters calculated by the Sobol' global sensitivity analysis method, in which the error bars indicate the corresponding standard deviations derived from the resampling analysis.

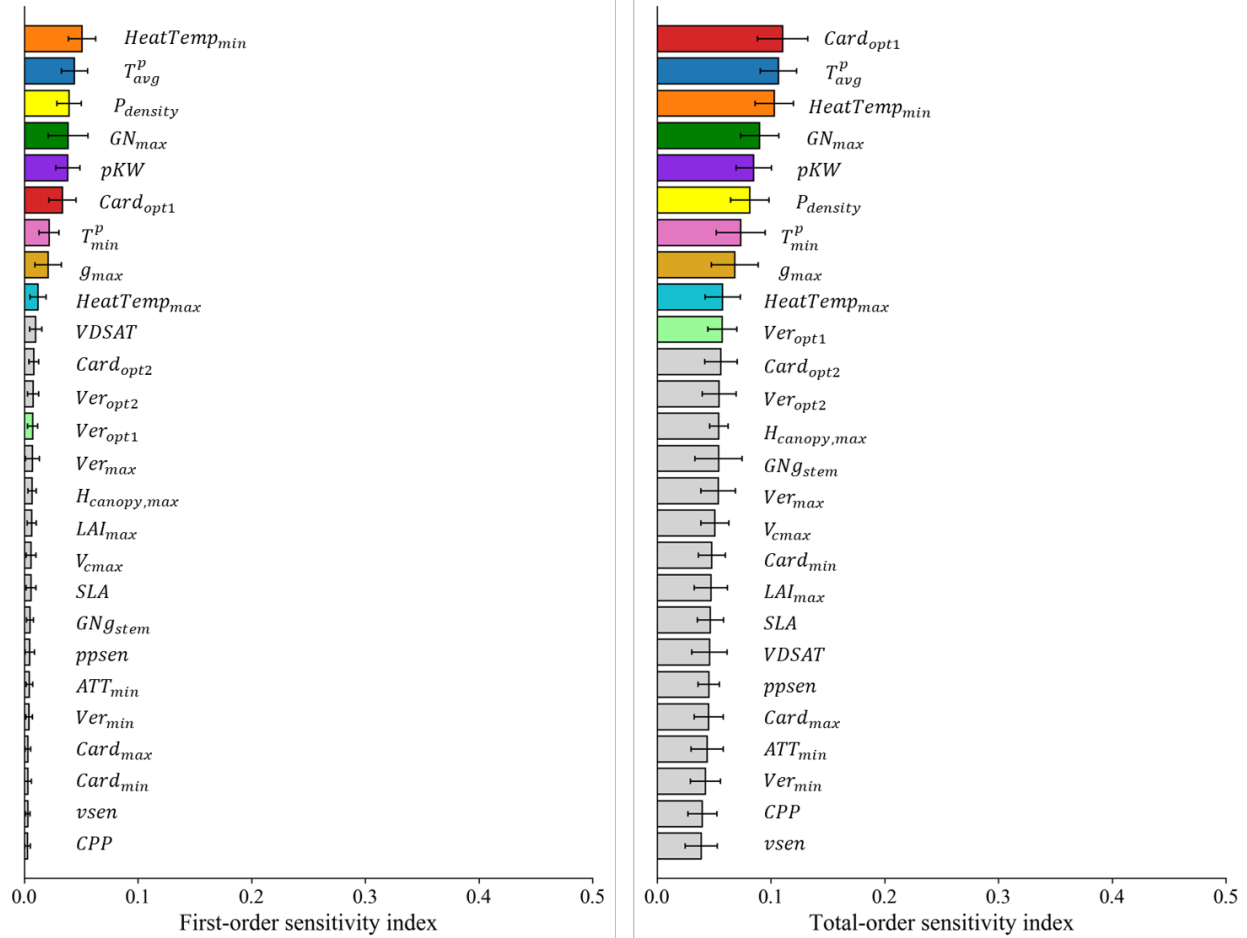


Figure 3-17. The first-order and total-order sensitivity indices of winter wheat-related parameters calculated by the Sobol’ global sensitivity analysis method, in which the error bars indicate the corresponding standard deviations derived from the resampling analysis.

3.4.3 Uncertainties

Despite the overall sound performance of our model, some limitations remain in this study. First, the representation of groundwater and irrigation practice (i.e., without considering the irrigation amount and frequency) in our model is relatively simple, which biased the simulated soil moisture and then crop production. Considering that some satellite-derived soil moisture products are available (e.g., SMAP and ESA-CCI datasets) (Dorigo et al. 2017; Entekhabi et al. 2010), we may solve this problem by assimilating soil moisture products into our model. Second, input data

used to drive DLEM may introduce bias. For example, the crop-specific N fertilizer use rate was obtained from the state-level surveys, which cannot reflect the actual variations of fertilizer use in both magnitude and timing. Previous studies have developed some optimized fertilization schemes to better represent fertilization practice in the model (Fu et al. 2020; Leng et al. 2016), which could be incorporated into our model in the future. Third, cover cropping practices were not included in our regional-scale simulation due to the lack of an available spatialized dataset, which may also introduce biases in our results. Finally, as discussed in Section 4.2, crop yield simulations are sensitive to some parameters (e.g., $Card_{opt1}$ and g_{max}) so uncertainty in model parameters also constitutes a possible source of deviation in our results. In the long term, our goal is to develop a crop module applicable to all crop growing regions worldwide. Here, the parameterization and calibration schemes mainly focused on the three major crops grown in the U.S. Extending this parameterization effort to additional crops and varieties from other regions will likely be needed to make the model more broadly applicable. Addressing these limitations is critical to further improve the simulation performance of the new model at regional and global scales.

3.4.4 Future research opportunities

This study focused on how a better mechanistic representation of the effects of environmental factors and management practices on crop growth processes improved model estimates of crop production and yield at both the site and regional scales. Applying this knowledge to future climate scenarios should improve our understanding of how climate change may impact crop production at the site scale and food security at the regional scale in the future. In addition, the model improvements described in this study provide new ways to evaluate the effectiveness of potential climate mitigation and adaptation policies to sustain crop production and help protect food security. For example, climate-smart practices such as no-tillage and using cover crops have been

widely advocated to promote soil carbon sequestration and GHG mitigation while sustaining or boosting crop production (FAO 2010). The incorporation of different tillage and cover cropping effects on soil characteristics and crop growth into DLEM 4.0 allows the model to quantify the potential benefits of such climate-smart practices on GHG mitigation and crop production under future climate scenarios. Diversified crop rotations have also been advocated to reduce adverse environmental and climatic effects on crop production (Bowles et al. 2020), and when rotated with legumes, they can also contribute to climate change mitigation by reducing N fertilizer use (Ma et al. 2018). The inclusion of the dynamic crop rotation scheme in the new model allows us to explore the benefits of diversified crop rotations on crop production and climate. Besides quantifying the benefits of climate mitigation and adaptation policies, the new model can help identify unintended consequences of other management policies, such as changes in nutrient loading from agroecosystems to river networks (Pan et al. 2021; Yao et al. 2020).

3.5 Conclusion

To meet the multiscale agricultural application demands (e.g., farm-scale decision support and regional-scale climate change mitigation), we developed an advanced agricultural modeling framework on the platform of DLEM v4.0 through incorporating a more detailed representation of crop growth processes and management practices, including but not limited to crop-specific phenological development, dynamic carbon allocation, yield formation, biological N fixation, and the implementation of tillage, cover cropping, and crop genetic improvement practices. Comprehensive evaluations against site-scale observations generally show good performance of the new agricultural module in simulating the seasonal variations and magnitudes of LAI and aboveground biomass and annual yield. Regarding the regional-scale performance, the simulated spatial pattern of crop production is also consistent with ground survey data. Meanwhile, the

national average crop production estimated by our model has increased by 1–4 times from the 1960s to the 2010s, which is consistent with the observed trend. Our new agricultural module holds the potential to better predict future crop production to deploy early-warning measures, and to assess the efficacy of potential agricultural climate change adaptation and mitigation strategies.

References

- Alo, C.A., & Wang, G. (2008). Potential future changes of the terrestrial ecosystem based on climate projections by eight general circulation models. *Journal of Geophysical Research: Biogeosciences*, 113
- Anapalli, S.S., Ma, L., Nielsen, D.C., Vigil, M.F., & Ahuja, L.R. (2005). Simulating planting date effects on corn production using RZWQM and CERES-Maize models. *Agronomy journal*, 97, 58-71
- Andrade, F.H., Vega, C., Uhart, S., Cirilo, A., Cantarero, M., & Valentinuz, O. (1999). Kernel number determination in maize. *Crop Science*, 39, 453-459
- Annan, F., & Schlenker, W. (2015). Federal crop insurance and the disincentive to adapt to extreme heat. *American Economic Review*, 105, 262-266
- Bailey-Serres, J., Parker, J.E., Ainsworth, E.A., Oldroyd, G.E.D., & Schroeder, J.I. (2019). Genetic strategies for improving crop yields. *Nature*, 575, 109-118
- Batjes, N.H. (2008). ISRIC-WISE Harmonized Global Soil Profile Dataset. *ISRIC-World Soil Information, Wageningen*
- Betts, R.A. (2005). Integrated approaches to climate-crop modelling: needs and challenges. *Philosophical transactions of the Royal Society of London. Series B, Biological sciences*, 360, 2049-2065
- Beveridge, L., Whitfield, S., & Challinor, A. (2018). Crop modelling: towards locally relevant and climate-informed adaptation. *Climatic Change*, 147, 475-489
- Bezner Kerr, R., Hasegawa, T., Lasco, R., Bhatt, I., Deryng, D., Farrell, A., Gurney-Smith, H., Ju, H., Lluch-Cota, S., Meza, F., Nelson, G., Neufeldt, H., & Thornton, P. (2022). *Food, Fibre, and Other Ecosystem Products. In: Climate Change 2022: Impacts, Adaptation, and Vulnerability. Contribution of Working Group II to the Sixth Assessment Report of the Intergovernmental Panel on Climate Change [H.-O. Pörtner, D.C. Roberts, M. Tignor, E.S. Poloczanska, K. Mintenbeck, A. Alegria, M. Craig, S. Langsdorf, S. Löschke, V. Möller, A. Okem, B. Rama (eds.)]. Cambridge University Press. In Press.*
- Bian, Z., Tian, H., Yang, Q., Xu, R., Pan, S., & Zhang, B. (2021). Production and application of manure nitrogen and phosphorus in the United States since 1860. *Earth Syst. Sci. Data*, 13, 515-527
- Boas, T., Bogena, H., Grünwald, T., Heinesch, B., Ryu, D., Schmidt, M., Vereecken, H., Western, A., & Hendricks Franssen, H.J. (2021). Improving the representation of cropland sites in the Community Land Model (CLM) version 5.0. *Geosci. Model Dev.*, 14, 573-601
- Bondeau, A., Smith, P.C., Zaehle, S., Schaphoff, S., Lucht, W., Cramer, W., Gerten, D., Lotze-Campen, H., Müller, C., & Reichstein, M. (2007). Modelling the role of agriculture for the 20th century global terrestrial carbon balance. *Global Change Biology*, 13, 679-706
- Borrás, L., Slafer, G.A., & Otegui, M.a.E. (2004). Seed dry weight response to source–sink manipulations in wheat, maize and soybean: a quantitative reappraisal. *Field Crops Research*, 86, 131-146
- Bowles, T.M., Mooshammer, M., Socolar, Y., Calderón, F., Cavigelli, M.A., Culman, S.W., Deen, W., Drury, C.F., Garcia y Garcia, A., Gaudin, A.C.M., Harkcom, W.S., Lehman, R.M., Osborne, S.L., Robertson, G.P., Salerno, J., Schmer, M.R., Strock, J., & Grandy, A.S. (2020). Long-Term Evidence Shows that Crop-Rotation Diversification Increases Agricultural Resilience to Adverse Growing Conditions in North America. *One Earth*, 2, 284-293
- Cao, P., Lu, C., & Yu, Z. (2018). Historical nitrogen fertilizer use in agricultural ecosystems of the contiguous United States during 1850–2015: application rate, timing, and fertilizer types. *Earth Syst. Sci. Data*, 10, 969-984
- Chenu, K., Porter, J.R., Martre, P., Basso, B., Chapman, S.C., Ewert, F., Bindi, M., & Asseng, S. (2017). Contribution of Crop Models to Adaptation in Wheat. *Trends in Plant Science*, 22, 472-490

- Cox, W.J. (1996). Whole-plant physiological and yield responses of maize to plant density. *Agronomy journal*, 88, 489-496
- Danalatos, N.G., Kosmas, C.S., Driessen, P.M., & Yassoglou, N. (1994). The change in the specific leaf area of maize grown under Mediterranean conditions. *Agronomie*, 14, 433-443
- Davis, K.F., Gephart, J.A., Emery, K.A., Leach, A.M., Galloway, J.N., & D'Odorico, P. (2016). Meeting future food demand with current agricultural resources. *Global Environmental Change*, 39, 125-132
- Dorigo, W., Wagner, W., Albergel, C., Albrecht, F., Balsamo, G., Brocca, L., Chung, D., Ertl, M., Forkel, M., Gruber, A., Haas, E., Hamer, P.D., Hirschi, M., Ikonen, J., de Jeu, R., Kidd, R., Lahoz, W., Liu, Y.Y., Miralles, D., Mistelbauer, T., Nicolai-Shaw, N., Parinussa, R., Pratola, C., Reimer, C., van der Schalie, R., Seneviratne, S.I., Smolander, T., & Lecomte, P. (2017). ESA CCI Soil Moisture for improved Earth system understanding: State-of-the art and future directions. *Remote Sensing of Environment*, 203, 185-215
- Drewniak, B., Song, J., Prell, J., Kotamarthi, V.R., & Jacob, R. (2013). Modeling agriculture in the Community Land Model. *Geosci. Model Dev.*, 6, 495-515
- Entekhabi, D., Njoku, E.G., O'Neill, P.E., Kellogg, K.H., Crow, W.T., Edelstein, W.N., Entin, J.K., Goodman, S.D., Jackson, T.J., & Johnson, J. (2010). The soil moisture active passive (SMAP) mission. *Proceedings of the IEEE*, 98, 704-716
- Eyring, V., Lamarque, J.-F., Hess, P., Arfeuille, F., Bowman, K., Chipperfield, M.P., Duncan, B., Fiore, A., Gettelman, A., & Giorgetta, M.A. (2013). Overview of IGAC/SPARC Chemistry-Climate Model Initiative (CCMI) community simulations in support of upcoming ozone and climate assessments. *SPARC newsletter*, 40, 48-66
- FAO (2010). *"Climate-Smart" Agriculture: Policies, Practices and Financing for Food Security, Adaptation and Mitigation*. Rome, Italy: Food and Agriculture Organization of the United Nations (FAO)
- Fisher, J.B., Huntzinger, D.N., Schwalm, C.R., & Sitch, S. (2014). Modeling the terrestrial biosphere. *Annual review of environment and resources*, 39, 91-123
- Fu, C., Wang, J., Gong, S., Zhang, Y., Wang, C., & Mo, Y. (2020). Optimization of irrigation and fertilization of drip-irrigated corn in the chernozem area of north-east China based on the CERES-Maize model. *Irrigation and Drainage*, 69, 714-731
- Giordano, M., & Villholth, K.G. (2007). *The agricultural groundwater revolution: opportunities and threats to development*. CABI
- Grichar, W.J. (2007). Row Spacing, Plant Populations, and Cultivar Effects on Soybean Production Along the Texas Gulf Coast. *Crop Management*, 6, 1-6
- Hammer, G.L., Kropff, M.J., Sinclair, T.R., & Porter, J.R. (2002). Future contributions of crop modelling—from heuristics and supporting decision making to understanding genetic regulation and aiding crop improvement. *European Journal of Agronomy*, 18, 15-31
- Hammer, G.L., McLean, G., Chapman, S., Zheng, B., Doherty, A., Harrison, M.T., van Oosterom, E., & Jordan, D. (2014). Crop design for specific adaptation in variable dryland production environments. *Crop and Pasture Science*, 65, 614-626
- Hansen, J.W., & Jones, J.W. (2000). Scaling-up crop models for climate variability applications. *Agricultural systems*, 65, 43-72
- Holzworth, D.P., Huth, N.I., deVoil, P.G., Zurcher, E.J., Herrmann, N.I., McLean, G., Chenu, K., van Oosterom, E.J., Snow, V., & Murphy, C. (2014). APSIM—evolution towards a new generation of agricultural systems simulation. *Environmental Modelling & Software*, 62, 327-350
- Howden, S.M., Soussana, J.-F., Tubiello, F.N., Chhetri, N., Dunlop, M., & Meinke, H. (2007). Adapting agriculture to climate change. *Proceedings of the National Academy of Sciences*, 104, 19691
- Jones, J.W., Antle, J.M., Basso, B., Boote, K.J., Conant, R.T., Foster, I., Godfray, H.C.J., Herrero, M., Howitt, R.E., & Janssen, S. (2017). Toward a new generation of agricultural system data, models, and knowledge products: State of agricultural systems science. *Agricultural systems*, 155, 269-288
- Jones, J.W., Hoogenboom, G., Porter, C.H., Boote, K.J., Batchelor, W.D., Hunt, L.A., Wilkens, P.W., Singh, U., Gijsman, A.J., & Ritchie, J.T. (2003). The DSSAT cropping system model. *European Journal of Agronomy*, 18, 235-265
- Keating, B.A., Carberry, P.S., Hammer, G.L., Probert, M.E., Robertson, M.J., Holzworth, D., Huth, N.I., Hargreaves, J.N.G., Meinke, H., Hochman, Z., McLean, G., Verburg, K., Snow, V., Dimes, J.P., Silburn, M., Wang, E., Brown, S., Bristow, K.L., Asseng, S., Chapman, S., McCown, R.L., Freebairn, D.M., & Smith, C.J. (2003). An overview of APSIM, a model designed for farming systems simulation. *European Journal of Agronomy*, 18, 267-288

- Klein, R.J.T., Huq, S., Denton, F., Downing, T.E., Richels, R.G., Robinson, J.B., & Toth, F.L. (2007). Interrelationships between adaptation and mitigation. *Climate Change 2007: impacts, adaptation and vulnerability*. In: Parry ML, Canziani OF, Palutikof JP, van der Linden PJ, Hanson CE (eds) Contribution of working group II to the fourth assessment report of the intergovernmental panel on climate change. Cambridge, UK: Cambridge University Press, Cambridge
- Kucharik, C.J. (2006). A multidecadal trend of earlier corn planting in the central USA. *Agronomy journal*, 98, 1544-1550
- Leng, G., Zhang, X., Huang, M., Yang, Q., Rafique, R., Asrar, G.R., & Ruby Leung, L. (2016). Simulating county-level crop yields in the Conterminous United States using the Community Land Model: The effects of optimizing irrigation and fertilization. *Journal of Advances in Modeling Earth Systems*, 8, 1912-1931
- Lesk, C., Rowhani, P., & Ramankutty, N. (2016). Influence of extreme weather disasters on global crop production. *Nature*, 529, 84-87
- Levis, S., Bonan, G.B., Kluzek, E., Thornton, P.E., Jones, A., Sacks, W.J., & Kucharik, C.J. (2012). Interactive crop management in the Community Earth System Model (CESM1): Seasonal influences on land-atmosphere fluxes. *Journal of Climate*, 25, 4839-4859
- Liu, S., Baret, F., Andrieu, B., Burger, P., & Hemmerle, M. (2017). Estimation of wheat plant density at early stages using high resolution imagery. *Frontiers in plant science*, 8, 739
- Locatelli, B. (2011). *Synergies between adaptation and mitigation in a nutshell*. CIFOR
- Lokupitiya, E., Denning, S., Paustian, K., Baker, I., Schaefer, K., Verma, S.B., Meyers, T., Bernacchi, C.J., Suyker, A.E., & Fischer, M.L. (2009). Incorporation of crop phenology in Simple Biosphere Model (SiBcrop) to improve land-atmosphere carbon exchanges from croplands
- Lombardozi, D.L., Lu, Y., Lawrence, P.J., Lawrence, D.M., Swenson, S., Oleson, K.W., Wieder, W.R., & Ainsworth, E.A. (2020). Simulating Agriculture in the Community Land Model Version 5. *Journal of Geophysical Research: Biogeosciences*, 125, e2019JG005529
- Lu, C., Yu, Z., Tian, H., Hennessy, D.A., Feng, H., Al-Kaisi, M., Zhou, Y., Sauer, T., & Arritt, R. (2018). Increasing carbon footprint of grain crop production in the US Western Corn Belt. *Environmental Research Letters*, 13, 124007
- Lu, Y., Williams, I.N., Bagley, J.E., Torn, M.S., & Kueppers, L.M. (2017). Representing winter wheat in the Community Land Model (version 4.5). *Geosci. Model Dev.*, 10, 1873-1888
- Lutz, F., Herzfeld, T., Heinke, J., Rolinski, S., Schaphoff, S., von Bloh, W., Stoorvogel, J.J., & Müller, C. (2019). Simulating the effect of tillage practices with the global ecosystem model LPJmL (version 5.0-tillage). *Geosci. Model Dev.*, 12, 2419-2440
- Ma, Y., Schwenke, G., Sun, L., Liu, D.L., Wang, B., & Yang, B. (2018). Modeling the impact of crop rotation with legume on nitrous oxide emissions from rain-fed agricultural systems in Australia under alternative future climate scenarios. *Science of the Total Environment*, 630, 1544-1552
- Mallya, G., Zhao, L., Song, X.C., Niyogi, D., & Govindaraju, R.S. (2013). 2012 Midwest drought in the United States. *Journal of Hydrologic Engineering*, 18, 737-745
- McDermid, S.S., Mearns, L.O., & Ruane, A.C. (2017). Representing agriculture in Earth System Models: Approaches and priorities for development. *Journal of Advances in Modeling Earth Systems*, 9, 2230-2265
- Mehring, A.L., Adams, J.R., & Jacob, K.D. (1957). *Statistics on fertilizers and liming materials in the United States*. Soil and Water Conservation Research Branch, Agricultural Research Service ...
- Ofgeha, G.Y., & Abshare, M.W. (2021). Local adaptation and coping strategies to global environmental changes: Portraying agroecology beyond production functions in southwestern Ethiopia. *Plos One*, 16, e0255813
- Pan, S., Bian, Z., Tian, H., Yao, Y., Najjar, R.G., Friedrichs, M.A.M., Hofmann, E.E., Xu, R., & Zhang, B. (2021). Impacts of Multiple Environmental Changes on Long-term Nitrogen Loading from the Chesapeake Bay Watershed. *Journal of Geophysical Research: Biogeosciences*, 126, e2020JG005826
- Pan, S., Tian, H., Dangal, S.R.S., Yang, Q., Yang, J., Lu, C., Tao, B., Ren, W., & Ouyang, Z. (2015). Responses of global terrestrial evapotranspiration to climate change and increasing atmospheric CO₂ in the 21st century. *Earth's Future*, 3, 15-35
- Peng, B., Guan, K., Chen, M., Lawrence, D.M., Pokhrel, Y., Suyker, A., Arkebauer, T., & Lu, Y. (2018). Improving maize growth processes in the community land model: Implementation and evaluation. *Agricultural and Forest Meteorology*, 250, 64-89
- Peng, B., Guan, K., Tang, J., Ainsworth, E.A., Asseng, S., Bernacchi, C.J., Cooper, M., Delucia, E.H., Elliott, J.W., Ewert, F., Grant, R.F., Gustafson, D.I., Hammer, G.L., Jin, Z., Jones, J.W., Kimm, H., Lawrence, D.M., Li, Y., Lombardozi, D.L., Marshall-Colon, A., Messina, C.D., Ort, D.R., Schnable, J.C., Vallejos, C.E., Wu,

- A., Yin, X., & Zhou, W. (2020). Towards a multiscale crop modelling framework for climate change adaptation assessment. *Nature Plants*, 6, 338-348
- Porwollik, V., Rolinski, S., Heinke, J., & Müller, C. (2019). Generating a rule-based global gridded tillage dataset. *Earth Syst. Sci. Data*, 11, 823-843
- Rosenzweig, C., Elliott, J., Deryng, D., Ruane, A.C., Müller, C., Arneth, A., Boote, K.J., Folberth, C., Glotter, M., & Khabarov, N. (2014). Assessing agricultural risks of climate change in the 21st century in a global gridded crop model intercomparison. *Proceedings of the National Academy of Sciences*, 111, 3268-3273
- Sacks, W.J., Deryng, D., Foley, J.A., & Ramankutty, N. (2010). Crop planting dates: an analysis of global patterns. *Global Ecology and Biogeography*, 19, 607-620
- Schaphoff, S., Lucht, W., Gerten, D., Sitch, S., Cramer, W., & Prentice, I.C. (2006). Terrestrial biosphere carbon storage under alternative climate projections. *Climatic Change*, 74, 97-122
- Sobol, I.M. (1993). Sensitivity estimates for nonlinear mathematical models. *Mathematical modelling and computational experiments*, 1, 407-414
- Soltani, A., & Sinclair, T.R. (2012). *Modeling physiology of crop development, growth and yield*. Wallingford: CABI
- Song, Y., Jain, A.K., & McIsaac, G.F. (2013). Implementation of dynamic crop growth processes into a land surface model: evaluation of energy, water and carbon fluxes under corn and soybean rotation. *Biogeosciences*, 10, 8039-8066
- Stöckle, C.O., Donatelli, M., & Nelson, R. (2003). CropSyst, a cropping systems simulation model. *European Journal of Agronomy*, 18, 289-307
- Stöckle, C.O., Kemanian, A.R., Nelson, R.L., Adam, J.C., Sommer, R., & Carlson, B. (2014). CropSyst model evolution: From field to regional to global scales and from research to decision support systems. *Environmental Modelling & Software*, 62, 361-369
- Tardieu, F., Granier, C., & Muller, B. (1999). Modelling leaf expansion in a fluctuating environment: are changes in specific leaf area a consequence of changes in expansion rate? *New Phytologist*, 143, 33-43
- Tian, H., Chen, G., Liu, M., Zhang, C., Sun, G., Lu, C., Xu, X., Ren, W., Pan, S., & Chappelka, A. (2010). Model estimates of net primary productivity, evapotranspiration, and water use efficiency in the terrestrial ecosystems of the southern United States during 1895–2007. *Forest Ecology and Management*, 259, 1311-1327
- Tian, H., Lu, C., Ciais, P., Michalak, A.M., Canadell, J.G., Saikawa, E., Huntzinger, D.N., Gurney, K.R., Sitch, S., Zhang, B., Yang, J., Bousquet, P., Bruhwiler, L., Chen, G., Dlugokencky, E., Friedlingstein, P., Melillo, J., Pan, S., Poulter, B., Prinn, R., Saunio, M., Schwalm, C.R., & Wofsy, S.C. (2016). The terrestrial biosphere as a net source of greenhouse gases to the atmosphere. *Nature*, 531, 225-228
- Tian, H., Lu, C., Melillo, J., Ren, W., Huang, Y., Xu, X., Liu, M., Zhang, C., Chen, G., Pan, S., Liu, J., & Reilly, J. (2012). Food benefit and climate warming potential of nitrogen fertilizer uses in China. *Environmental Research Letters*, 7, 044020
- Tian, H., Xu, R., Canadell, J.G., Thompson, R.L., Winiwarter, W., Suntharalingam, P., Davidson, E.A., Ciais, P., Jackson, R.B., Janssens-Maenhout, G., Prather, M.J., Regnier, P., Pan, N., Pan, S., Peters, G.P., Shi, H., Tubiello, F.N., Zaehle, S., Zhou, F., Arneth, A., Battaglia, G., Berthet, S., Bopp, L., Bouwman, A.F., Buitenhuis, E.T., Chang, J., Chipperfield, M.P., Dangal, S.R.S., Dlugokencky, E., Elkins, J.W., Eyre, B.D., Fu, B., Hall, B., Ito, A., Joos, F., Krummel, P.B., Landolfi, A., Laruelle, G.G., Lauerwald, R., Li, W., Lienert, S., Maavara, T., MacLeod, M., Millet, D.B., Olin, S., Patra, P.K., Prinn, R.G., Raymond, P.A., Ruiz, D.J., van der Werf, G.R., Vuichard, N., Wang, J., Weiss, R.F., Wells, K.C., Wilson, C., Yang, J., & Yao, Y. (2020a). A comprehensive quantification of global nitrous oxide sources and sinks. *Nature*, 586, 248-256
- Tian, H., Xu, R., Pan, S., Yao, Y., Bian, Z., Cai, W.-J., Hopkinson, C.S., Justic, D., Lohrenz, S., Lu, C., Ren, W., & Yang, J. (2020b). Long-Term Trajectory of Nitrogen Loading and Delivery From Mississippi River Basin to the Gulf of Mexico. *Global Biogeochemical Cycles*, 34, e2019GB006475
- Tian, H., Xu, X., Lu, C., Liu, M., Ren, W., Chen, G., Melillo, J., & Liu, J. (2011). Net exchanges of CO₂, CH₄, and N₂O between China's terrestrial ecosystems and the atmosphere and their contributions to global climate warming. *Journal of Geophysical Research: Biogeosciences*, 116
- Tol, R.S.J. (2005). Adaptation and mitigation: trade-offs in substance and methods. *Environmental Science & Policy*, 8, 572-578
- USDA-ERS (2019). U.S. Department of Agriculture-Economic Research Service: Fertilizer Use and Price
- USDA, N. (2018). Crop production historical track records. In: United States Department of Agriculture, National Agricultural Statistics ...

- Van den Hoof, C., Hanert, E., & Vidale, P.L. (2011). Simulating dynamic crop growth with an adapted land surface model—JULES-SUCROS: Model development and validation. *Agricultural and Forest Meteorology*, *151*, 137-153
- Vega, C.R.C., Andrade, F.H., Sadras, V.O., Uhart, S.A., & Valentinuz, O.R. (2001). Seed Number as a Function of Growth. A Comparative Study in Soybean, Sunflower, and Maize. *Crop Science*, *41*, 748-754
- Vermeulen, S.J., Campbell, B.M., & Ingram, J.S.I. (2012). Climate change and food systems. *Annual review of environment and resources*, *37*, 195-222
- Vico, G., Hurry, V., & Weih, M. (2014). Snowed in for survival: Quantifying the risk of winter damage to overwintering field crops in northern temperate latitudes. *Agricultural and Forest Meteorology*, *197*, 65-75
- Wallach, D., Palosuo, T., Thorburn, P., Gourdain, E., Asseng, S., Basso, B., Buis, S., Crout, N., Dibari, C., Dumont, B., Ferrise, R., Gaiser, T., Garcia, C., Gayler, S., Ghahramani, A., Hochman, Z., Hoek, S., Hoogenboom, G., Horan, H., Huang, M., Jabloun, M., Jing, Q., Justes, E., Kersebaum, K.C., Klosterhalfen, A., Launay, M., Luo, Q., Maestrini, B., Mielenz, H., Moriondo, M., Nariman Zadeh, H., Olesen, J.E., Poyda, A., Priesack, E., Pullens, J.W.M., Qian, B., Schütze, N., Shelia, V., Souissi, A., Specka, X., Srivastava, A.K., Stella, T., Streck, T., Trombi, G., Wallor, E., Wang, J., Weber, T.K.D., Weihermüller, L., de Wit, A., Wöhling, T., Xiao, L., Zhao, C., Zhu, Y., & Seidel, S.J. (2021). How well do crop modeling groups predict wheat phenology, given calibration data from the target population? *European Journal of Agronomy*, *124*, 126195
- Wheeler, T., & von Braun, J. (2013). Climate Change Impacts on Global Food Security. *Science*, *341*, 508
- Williams, J.R., Jones, C.A., Kiniry, J.R., & Spanel, D.A. (1989). The EPIC crop growth model. *Transactions of the ASAE*, *32*, 497-0511
- Wu, X., Vuichard, N., Ciais, P., Viovy, N., Noblet-Ducoudré, N.d., Wang, X., Magliulo, V., Wattenbach, M., Vitale, L., & Tommasi, P.D. (2016). ORCHIDEE-CROP (v0), a new process-based agro-land surface model: model description and evaluation over Europe. *Geoscientific Model Development*, *9*, 857-873
- Xu, R., Tian, H., Pan, S., Prior, S.A., Feng, Y., Batchelor, W.D., Chen, J., & Yang, J. (2019). Global ammonia emissions from synthetic nitrogen fertilizer applications in agricultural systems: Empirical and process-based estimates and uncertainty. *Global Change Biology*, *25*, 314-326
- Yao, Y., Tian, H., Shi, H., Pan, S., Xu, R., Pan, N., & Canadell, J.G. (2020). Increased global nitrous oxide emissions from streams and rivers in the Anthropocene. *Nature Climate Change*, *10*, 138-142
- You, Y., Tian, H., Pan, S., Shi, H., Bian, Z., Gurgel, A., Huang, Y., Kicklighter, D., Liang, X.-Z., Lu, C., Melillo, J., Miao, R., Pan, N., Reilly, J., Ren, W., Xu, R., Yang, J., Yu, Q., & Zhang, J. (2022). Incorporating dynamic crop growth processes and management practices into a terrestrial biosphere model for simulating crop production in the United States: Toward a unified modeling framework. *Agricultural and Forest Meteorology*, *325*, 109144
- You, Y., Wang, S., Ma, Y., Wang, X., & Liu, W. (2019). Improved modeling of gross primary productivity of Alpine Grasslands on the Tibetan Plateau using the biome-BGC model. *Remote Sensing*, *11*, 1287
- You, Y., Wang, S., Pan, N., Ma, Y., & Liu, W. (2020). Growth stage-dependent responses of carbon fixation process of alpine grasslands to climate change over the Tibetan Plateau, China. *Agricultural and Forest Meteorology*, *291*, 108085
- Yu, Z., Lu, C., Cao, P., & Tian, H. (2018). Long-term terrestrial carbon dynamics in the Midwestern United States during 1850–2015: Roles of land use and cover change and agricultural management. *Global Change Biology*, *24*, 2673-2690
- Zhang, L.X., Kyei-Boahen, S., Zhang, J., Zhang, M.H., Freeland, T.B., Watson Jr, C.E., & Liu, X. (2007). Modifications of Optimum Adaptation Zones for Soybean Maturity Groups in the USA. *Crop Management*, *6*, 1-11
- Zhang, Y., Gurung, R., Marx, E., Williams, S., Ogle, S.M., & Paustian, K. (2020). DayCent Model Predictions of NPP and Grain Yields for Agricultural Lands in the Contiguous U.S. *Journal of Geophysical Research: Biogeosciences*, *125*, e2020JG005750
- Zheng, B., Chenu, K., Doherty, A., & Chapman, S. (2014). The APSIM-wheat module (7.5 R3008). *Agricultural Production Systems Simulator (APSIM) Initiative*

Chapter 4. Decreased sensitivity of corn and soybean yields to the concurrent droughts and heatwaves in the United States

Abstract

Due to the increased frequency and severity of extreme weather events accompanying climate change, enhancing the resilience of agricultural systems to minimize disaster risks and sustain food security has become essential. A pivotal indicator for assessing resilience is whether agricultural systems have become less sensitive to climate change over time. While detailed accounts of the impacts of single climate extremes on crop yields exist, crop vulnerabilities to compound climate events (e.g., concurrent droughts and heatwaves) remain largely explored. Here, we evaluated yield losses for U.S. corn and soybean resulting from compound extreme drought and heatwave events, and we also examined time trends in yield sensitivity to these compound extreme events, using both ground survey data and simulations derived from a process-based terrestrial biosphere model, Dynamic Land Ecosystem Model (DLEM) v4.0. Our results show that corn and soybean yields are most vulnerable to heatwaves and short-term (1-2 months) droughts occurring during critical reproductive stages from July to September. Yield losses caused by concurrent droughts and heatwaves are more severe than those caused by individual events, resulting in yield losses of 29.6% for corn and 25.4% for soybean. Additionally, our study indicates a decreased sensitivity in corn and soybean yields to concurrent droughts and heatwaves from 1964 to 2018. Our study underscores the significance of accounting for compound extreme climate events when assessing the resilience of agricultural systems and advocates for the implementation of adaptive strategies to mitigate such devastating impacts.

4.1 Introduction

Ensuring global food security in the context of climate change and rapid population growth is a huge challenge facing human society (Drewniak et al. 2013; Rosenzweig et al. 2014). The United States (U.S.) stands as a pivotal player in the world's agricultural system, contributing about 41% and 38% of the global trade in corn and soybean, respectively (USDA 2015). Considering that corn and soybean are among the four largest sources of caloric energy globally, U.S. production of these crops is thus critical for sustaining the world's food supply (Schlenker and Roberts 2009a). Notably, however, approximately 90% of U.S. corn and soybean productions are rainfed (NASS 2013), rendering them particularly vulnerable to extreme climate events such as droughts and heatwaves (Jin et al. 2017). Over recent decades, the frequency and intensity of these adverse weather conditions have increased in the U.S. (Janssen et al. 2014; Mazdiyasi and AghaKouchak 2015), resulting in considerable damage to the agricultural system (Lobell et al. 2013; Lobell et al. 2014; Troy et al. 2015; Zipper et al. 2016). In light of the increasing climate-related risks and the U.S.'s pivotal role in the global supply of corn and soybean, a comprehensive analysis of how extreme climate events (e.g., drought and heatwave) have affected these critical crops in the U.S. becomes indispensable for safeguarding global food security.

Extreme drought and heatwave disasters pose huge threats to food security (IPCC 2014b; Lesk et al. 2016; Lobell et al. 2013), compromising crop yields through a variety of mechanisms, including but not limited to declines in net photosynthesis rates (Eyshi Rezaei et al. 2015), heightened sensitivity of the anthesis-silking period to high temperatures (Bolaños and Edmeades 1996), accelerated leaf senescence (Parent and Tardieu 2012), and inadequate water availability for optimal crop growth (Prasad et al. 2008; Schlenker and Roberts 2009a). As these extreme climate disasters are anticipated to become more frequent in the future (Allen et al. 2012; Battisti

and Naylor 2009; Meehl and Tebaldi 2004), there is a pressing need for actionable, science-based information that can inform disaster risk management and adaptation strategies for farmers, stakeholders, and policymakers (Anderson et al. 2020; Howden et al. 2007). Central to these discussions is an overarching question regarding the resilience and adaptability of agricultural systems: Have these systems evolved to become less sensitive to extreme climatic events? Effective adaptation strategies should aim not only to mitigate the immediate impacts of climate change but also to reduce the agricultural system's inherent sensitivity to increasing climate risks (Lobell 2014; Lobell et al. 2020). However, despite the importance of this question, relatively few studies have analyzed whether the sensitivity of agricultural systems to climate change has evolved during past decades (Lobell et al. 2020).

Further complicating this issue is the emerging threat of compound extreme climate events (e.g., simultaneous occurrences of droughts and heatwaves) (Ridder et al. 2022), which could potentially produce synergistic impacts on crop yields, exacerbating losses beyond what might be expected from any single event (Cohen et al. 2021; Haqiqi et al. 2021; Lesk et al. 2022). Existing studies analyzing the sensitivity of crop yields to extreme climate disasters usually focus on single events, such as drought (Lobell et al. 2020); relatively few studies have focused compound extreme climate events (e.g., concurrent droughts and heatwaves), even though the concurrence of droughts and heatwaves has shown a significant increase in the U.S. during the past decades (Mazdiyasn and AghaKouchak 2015). Given this context, there remains an urgent need to understand changes in the sensitivity of U.S. corn and soybean yields to these concurrent events, which is critical for the development of adaptive strategies and policies that are commensurate with the evolving threats to global food security and agricultural sustainability.

Process-based crop models that incorporate detailed crop physiological, development, growth, and yield processes provide useful tools for assessing the impacts of climate change on crop yields and investigating the complex interactions between yields and various environmental stressors (e.g., heat and drought) (Bassu et al. 2014; Rosenzweig et al. 2013; You et al. 2022). By assimilating high-resolution, real-time weather, management, and environmental data, these models can increasingly assist stakeholders in predicting crop production and making informed decisions (Peng et al. 2020). However, the majority of existing terrestrial biosphere models (TBMs) with specific crop modules have been primarily developed to simulate average conditions based on long-term climatology (Reichstein et al. 2013). The algorithms within them, designed to simulate specific processes constrained by multiple stresses, are often inadequately parameterized, possibly due to the lack of data on how crops respond to extreme climate conditions like high temperatures and severe droughts with which to constrain model simulations (Bassu et al. 2014). Given these limitations, there exists a need to evaluate the models' effectiveness in capturing the impacts of extreme climate events on crop yields, as well as their sensitivity to these events. Such a comprehensive assessment could significantly improve the operational utility of existing TBMs for agricultural applications, while providing insights into their capabilities and uncertainties.

In this study, we analyzed the impact of extreme drought and heatwave events, as well as their combinations, on U.S. corn and soybean yields, using yield data from model simulations and from United States Department of Agriculture (USDA) surveys. We also investigated changes in their sensitivity to concurrent droughts and heatwaves. Our work was conducted around four key objectives: (1) to analyze the sensitivity of U.S. corn and soybean yields to the timing and duration of droughts and heatwaves; (2) to estimate crop yield loss caused by extreme drought and heatwave disasters and their concurrent events; (3) to evaluate whether the sensitivity of U.S. corn and

soybean yields to extreme drought, heatwave, and their combinations has changed over the past six decades (i.e., from 1964 to 2018); and (4) to assess the performance of a TBM, Dynamic Land Ecosystem Model (DLEM) v4.0, in reproducing the observed yield loss caused by extreme drought and heatwave disasters, as well as its ability in reproducing the time trend of the sensitivity of crop yields to extreme climate events. By systematically addressing these objectives, our research aims to provide an improved understanding of the synergistic effects of compound climate events on crop yields, thereby facilitating the development of a more resilient agricultural system capable of withstanding the challenges posed by a rapidly changing climate.

4.2 Materials and methods

4.2.1 Model descriptions

DLEM v4.0 is a highly integrated TBM that is capable of quantifying daily, spatially explicit carbon, water, and nutrient stocks and fluxes in terrestrial ecosystems and inland water systems across site, regional, and global scales (Pan et al. 2021; Tian et al. 2010a; Tian et al. 2020b; Yao et al. 2020). It includes five core components: biophysics, plant physiology, dynamic vegetation, soil biogeochemistry, and natural and anthropogenic disturbances. To meet cross-scale agricultural application needs (e.g., management guidance, agricultural climate change mitigation and adaptation), DLEM v4.0 has incorporated explicit and mechanistic representations of dynamic crop growth processes and multiple agricultural management practices. These include but are not limited to crop-specific phenological development, carbon allocation, yield formation, and biological N fixation processes, as well as management practices such as N fertilization, irrigation, rotation, manure application, tillage, cover cropping, and crop genetic improvements (You et al. 2022). By fully coupling these agricultural processes with biogeochemical, biophysical, and hydrological processes, DLEM v4.0 is capable of simulating and predicting the exchange of carbon

(including crop yield), water, nutrient and energy fluxes within the agriculture-climate-environment system. A thorough description of the processes incorporated into the agricultural module of DLEM v4.0 is presented in Chapter 2.

In this study, we used the DLEM v4.0 to simulate U.S. corn and soybean yields during the 1964-2018 period. We further examined the effectiveness of DLEM v4.0 in capturing the impacts of extreme climate events on crop yields, as well as changes in their sensitivity to these events.

4.2.2 Model forcing data and yield survey data

4.2.2.1 Model forcing data

To drive DLEM v4.0, four types of long-term datasets at 5×5 arc-min spatial resolution were developed. These datasets include agricultural management practices (e.g., N fertilizer use rate, crop rotation, tillage, irrigation, and manure application), land use and land cover change (LULC), natural environmental changes (e.g., climate conditions, atmospheric CO₂ concentration, and N deposition), and other auxiliary data (e.g., soil properties and topography). More details about these forcing datasets are presented in Section 2.3 in Chapter 2.

4.2.2.2 Yield survey data

We obtained corn and soybean yield survey datasets from the USDA-National Agriculture Statistics Service during 1964-2018, retrieving from <https://quickstats.nass.usda.gov/#AF9A0104-19EF-3BFE-90D2-C67700892F3E>. This website provides crop yield statistics at the county level.

4.2.3 Calculation of yield anomaly, SPEI, and HWMId

4.2.3.1 Yield anomaly calculation

Crop yields are influenced by a variety of factors, such as management practices (e.g., nitrogen fertilization and irrigation), genetic improvement, and climate conditions (Egli 2008). Typically, long-term increasing trends in crop yield are predominantly attributed to improvements in management practices and genetic technologies, while high-frequency fluctuations are largely driven by climatic conditions (Lu et al. 2017a). To more accurately delineate the relationship between climate variation and crop yields, it is essential to detrend the annual crop yield series to mitigate the long-term influences, focusing on yield anomalies for analysis. In addition, given the inherently nonlinear and non-stationary nature of long-term crop yield data, traditional detrending approaches like linear regression models are not suitable. To this end, this study used a locally weighted regression model in conjunction with a multiplicative decomposition model for detrending and calculating crop yield anomalies. This methodology has been demonstrated to be the most suitable method for detrending crop yield series (Lu et al. 2017a).

4.2.3.2 Standardized Precipitation-Evapotranspiration Index (SPEI) calculation

The Standardized Precipitation-Evapotranspiration Index (SPEI) is a widely used drought index (Vicente-Serrano et al. 2010), defined as the difference between precipitation and potential evapotranspiration. Compared with other drought indices that rely solely on precipitation, the SPEI allows for better identification of the impact of extreme warm air temperatures and heatwaves on drought severity (Beguería et al. 2014). Using the daily precipitation and maximum and minimum air temperature series corresponding to each county from Section 4.2.2.1, we calculated the daily SPEI and subsequently aggregated it into monthly values for analysis. The Penman–Monteith equation was used to calculate potential evapotranspiration in SPEI. Additionally, to investigate the sensitivity of crop yields to the timing and duration of drought events, we calculate SPEI at 1-, 12, 18, and 24 month timescales for the 1964-2018 period.

4.2.3.3 Heatwave Magnitude Index daily (HWMId) calculation

Heatwave Magnitude Index daily (HWMId) is heatwave index defined as the maximum magnitude of a heatwave within a given year, where a heatwave is defined as a period with maximum air temperature (T_{max}) above a daily threshold for three or more consecutive days (Russo et al. 2014; Russo et al. 2015). In this study, we have revised the HWMId to diagnose heat stress and temperature anomalies for each month during the crop growing season, which allows us to investigate the impact of the timing of heatwaves on crop yields. Specifically, a heatwave in the revised HWMId is defined as a period of three or more consecutive days where T_{max} is above the daily threshold for the reference period. The threshold is set at the 90th percentile of daily maxima temperature, centered on a 31-day window. The HWMId is further calculated as the sum of the magnitudes of the consecutive days composing a heatwave, where the daily magnitude is defined as:

$$M_d(T_d) = \begin{cases} \frac{T_d - T_{30y25p}}{T_{30y75p} - T_{30y25p}} & \text{if } T_d > T_{30y25p} \\ 0 & \text{if } T_d \leq T_{30y25p} \end{cases} \quad (1)$$

Here, T_d denotes the maximum daily temperature on day d of the heatwave, T_{30y25p} and T_{30y75p} are the 25th and 75th percentile values, respectively, of the time series composed of 55-year annual T_{max} values within the reference period 1964-2018.

4.2.4 Impact of timing of drought and heatwave on crop yields

A factorial approach was used to analyze the sensitivity of corn and soybean yields to the timing and duration of drought events (Zipper et al. 2016). Specifically, for each county and each crop, we fitted 168 separate linear relationships between crop yield anomalies and the SPEI, based on 12 different months (from January to December) and 14 different timescales (i.e., 1-12, 18, and

24 months). For each relationship, we extracted the R^2 value and the P-value of the relationship based on the two-tailed t-test. The best relationship in each county was identified as the timing and timescale combination with the highest R^2 . We considered this timing and timescale (i.e., duration) as the stage at which crop yield anomalies are most sensitive to drought events.

Similarly, for heatwaves, we also used a factorial approach to analyze the sensitivity of crop yields to the timing of such events. Specifically, for each county and each crop, we fitted 6 separate linear relationships between crop yield anomalies and the HWMId, based on 6 different months (from April to September) covering the main growing seasons of corn and soybean. For each relationship, we extracted the R^2 and P-value based on the two-tailed t-test. The best relationship in each county was defined as the timing with the highest R^2 , and we regarded this timing as the stage at which crop yield anomalies are most sensitive to heatwave events.

4.2.5 Quantifying crop yield loss caused by extreme drought and heatwave events

4.2.5.1 Identifying the occurrence of extreme drought and heatwave events

According to Shi et al. (2021), an extreme drought disaster is defined as an event where the ratio of the covered area is greater than 25% and the ratio of the affected area is greater than 12.5%. In this study, we defined an extreme drought disaster as occurring when the SPEI for more than 20% of the crop planting area in a county is less than -1.5 (corresponding to the ‘extreme drought’ category in Table 4-1). Similarly, we define an extreme heatwave event as occurring when the HWMId for more than 20% of the crop planting area in a county is larger than 4 (corresponding to the ‘extreme heatwave’ category in Table 4-2).

Table 4-1. Classification of droughts following the U.S. Drought Monitor
(<http://droughtmonitor.unl.edu/>).

Category	Range of SPEI
Moderate drought	$-1.2 \leq \text{SPEI} < -0.8$
Severe drought	$-1.5 \leq \text{SPEI} < -1.2$
Extreme drought	$-2.0 \leq \text{SPEI} < -1.5$
Exceptional drought	$\text{SPEI} < -2.0$

Table 4-2. Classification of heatwaves adapted from Ceccherini et al. (2017).

Category	Range of HWMId
Normal	$1 \leq \text{HWMId} < 2$
Moderate	$2 \leq \text{HWMId} < 3$
Severe	$3 \leq \text{HWMId} < 4$
Extreme	$4 \leq \text{HWMId} < 8$
Very extreme	$8 \leq \text{HWMId} < 16$
Super extreme	$16 \leq \text{HWMId} < 32$
Ultra extreme	$32 \leq \text{HWMId}$

4.2.5.2 Composite analysis

We used composite analysis to quantify crop yield losses attributable to drought and heatwave events, following the method described in previous studies (Jägermeyr and Frieler 2018; Lesk et al. 2016). This method was conducted by extracting a 7-year time window from historical annual yield time series, with the extreme event year situated at the center. For multiyear extreme events, we averaged consecutive extreme years to represent them as a single disaster event, ensuring that the time window consistently contained seven entries. We then normalized the extracted 7-year time series by dividing it by the average yield of the three years preceding and three years following the extreme event.

4.2.6 Time trends in yield sensitivity to droughts and heatwaves and their combinations

We used a panel model with year interaction terms to evaluate changes in the sensitivity of crop yields to concurrent droughts and heatwaves, following the methodology of Lobell et al. (2020). To capture time-invariant unobserved heterogeneity, we introduced fixed effects into the model. As an additional control to obtain unbiased estimates, we also included state-by-year terms in the model to remove any signal related to linear time trends. The final panel model can be represented as:

$$Y_{i,t} = \sum_{k=1}^d \beta_k X_{i,t,k} + c_i + s_i \times t + \varepsilon_{i,t} \quad (2)$$

where $Y_{i,t}$ represents yield anomalies at location i and time t ; X includes variables of $SPEI$, $HWMId$, and their combinations ($SPEI \times HWMId$), as well as linear interactions between them and the year (i.e., $SPEI \times Year$, $HWMId \times Year$, and $SPEI \times HWMId \times Year$) to test whether the sensitivity of crop yields to droughts, heatwaves and their combinations is changing over time; c_i represents fixed effects at location i ; s_i represents the state for county i ; and $\varepsilon_{i,t}$ is the error term.

We applied the above panel model to county-level yield data for the 1964-2018 period, and coefficient uncertainties were quantified by performing 200 block-bootstrap estimates of the model, with blocking done at the year level to account for spatial correlation in model residuals.

4.3 Results

4.3.1 Impact of timing and duration of droughts and heatwaves on crop yields

The correlations between corn and soybean yield anomalies and the SPEI revealed that both crops are highly susceptible to short-term droughts lasting 1-3 months, occurring during the critical

reproductive stages of crop development that typically span from July to September (Figure 4-1). Overall, we found that 84% of counties (1396 counties) exhibit the strongest yield correlations with droughts spanning 1-3 months for corn, and 78% (945 counties) for soybeans. Specifically, corn is most sensitive to 1-month droughts occurring in July, a period that coincides with its silking and reproductive stages. In contrast, soybean, usually sown later than corn, is most sensitive to 2-month droughts occurring in August. Therefore, to more accurately reveal the relationship between yield anomalies and droughts, we have selected the 1-month SPEI during July-August for corn analysis and the 2-month SPEI during August-September for soybean analysis.

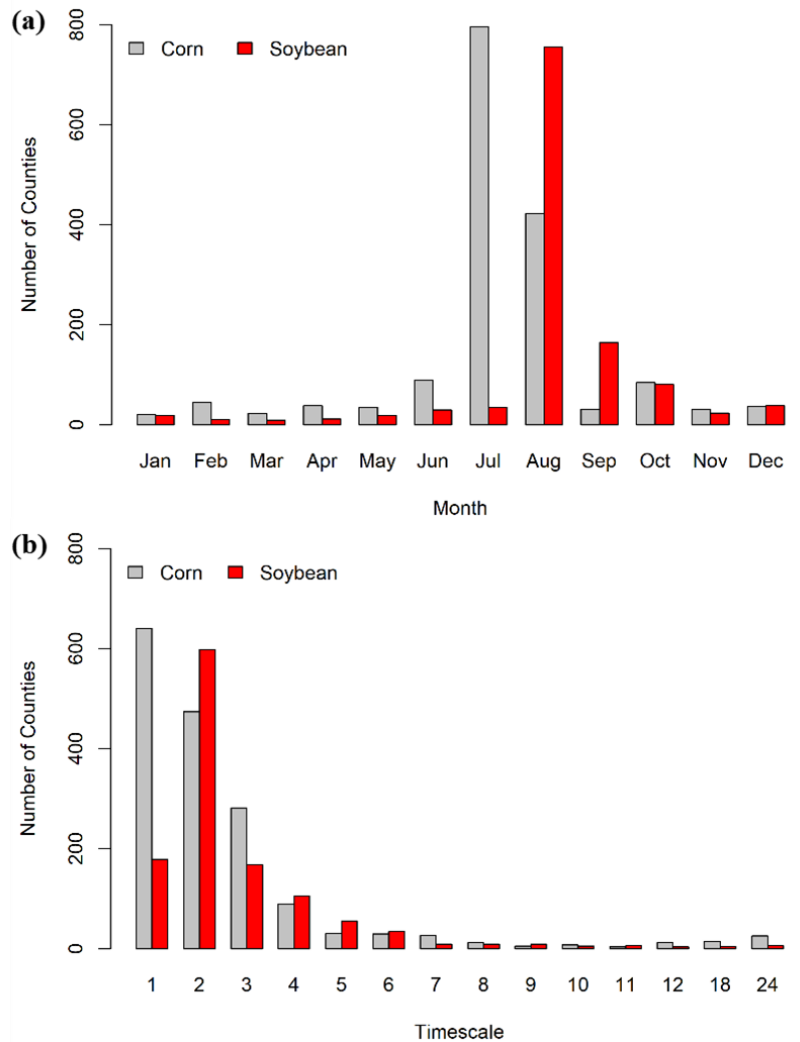


Figure 4-1. Histograms showing the timing (a) and duration (timescale) (b) of droughts with the strongest correlation for the relationship between crop yield anomalies and the Standardized Precipitation-Evapotranspiration Index (SPEI) across U.S. counties.

Similar to drought analysis, we found that both corn and soybean are highly susceptible to heatwaves occurring during July-August (Figure 4-2). Overall, 67% of counties exhibit the most significant yield relationships with heatwaves during this period for corn, and 59% do so for soybean. Consequently, to further explore the impact of heatwaves on crop yields, we have selected the HWMId during July-August for subsequent analysis.

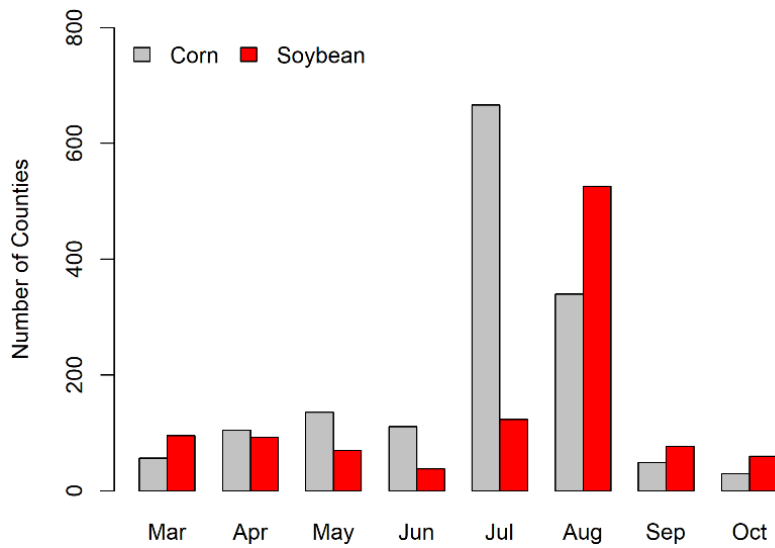


Figure 4-2. Histogram showing the timing of heatwaves with the strongest correlation for the relationship between crop yield anomalies and the Heatwave Magnitude Index daily (HWMId) across U.S. counties.

4.3.2 Influence of extreme droughts and heatwaves on crop yield losses

We analyzed the proportion of counties that experienced concurrent droughts and heatwaves in U.S. corn and soybean planting regions from 1964 to 2018 (Figure 4-3). Result generally shows an increasing trend, suggesting that the likelihood of facing concurrent droughts and heatwaves in U.S. corn and soybean growing regions has significantly increased over recent decades. This

heightened risk underscores the imperative to quantify its impact on crop yields and to formulate climate change adaptation strategies accordingly.

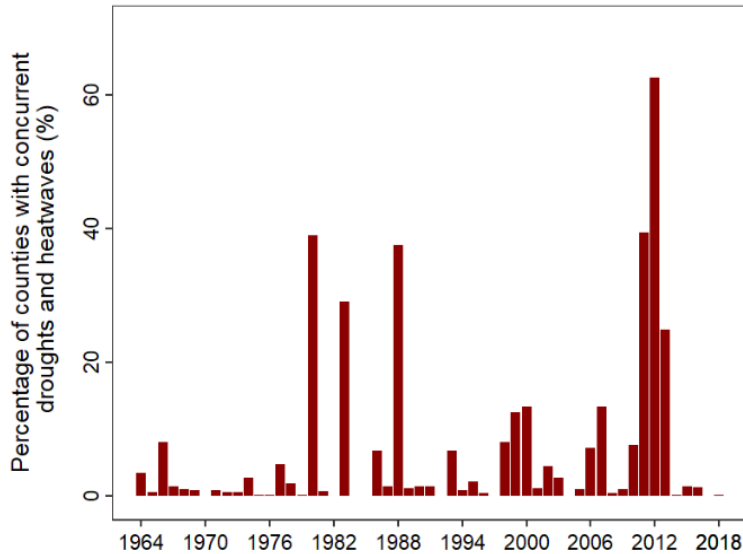


Figure 4-3. The percentage of counties experiencing concurrent droughts and heatwaves in corn and soybean planting regions during 1964-2018.

Based on the constructed SPEI and HWMId datasets during the sensitive stages of crop growth (Sections 4.3.1 and 4.3.2), we used the composite analysis method to quantify crop yield losses attributable to extreme drought and heatwave disasters (Figure 4-4). Our analysis revealed that both types of extreme climate events have significantly impacted corn and soybean yields. Specifically, between 1964 and 2018, extreme drought events resulted in an average yield reduction of 17.4% for corn and 17.0% for soybean, relative to the mean yield in the three years before and after non-event years. During the same period, extreme heatwave events led to average yield declines of 9.0% for corn and 6.3% for soybean. Notably, we found no lagged yield-level responses in the years following either type of extreme climate event. Crop yield losses from extreme drought events were generally more severe than those from extreme heatwaves. Furthermore, the simultaneous occurrence of droughts and heatwaves exacerbated yield losses

more than those caused by isolated events, leading to additional yield reductions of 12.2% and 20.6% for corn, and 8.4% and 19.1% for soybean, during droughts and heatwaves, respectively. Overall, corn yields are more susceptible to extreme climate disasters compared to soybean yields. Additionally, our results suggest that the DLEM is generally capable of reproducing observed yield responses to extreme drought and heatwave events.

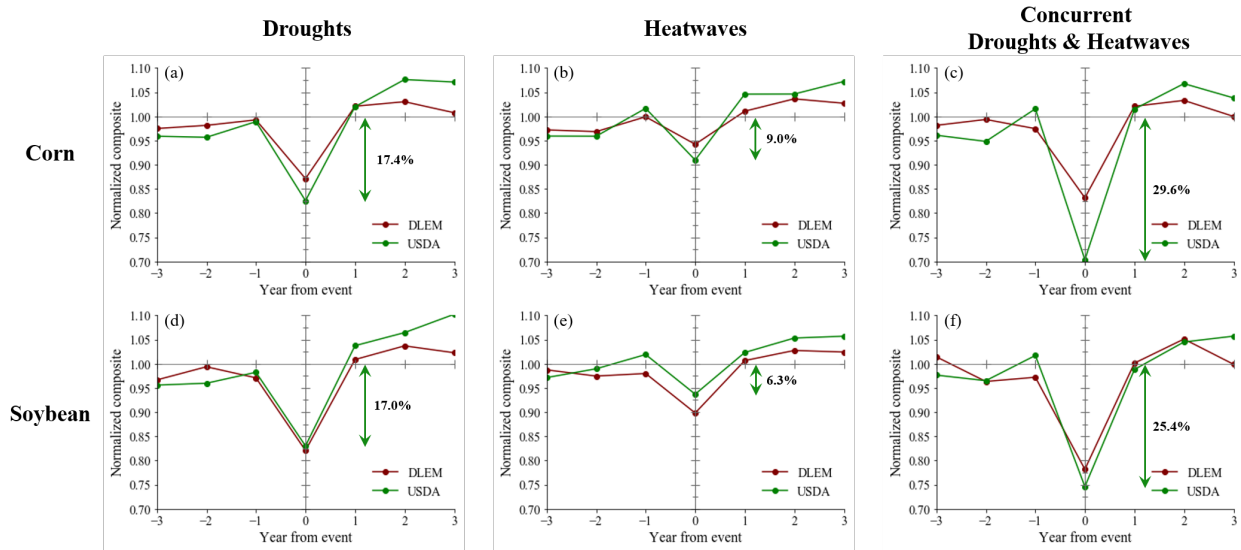


Figure 4-4. Influence of extreme droughts, heatwaves, and their co-occurrence on observed (i.e., USDA) and simulated (i.e., DLEM) crop yields. Composites are based on 7-year time windows of county-level yields centered on the respective event.

We also analyzed the influence of extreme weather disasters on crop yields across different USDA climate hubs. Our results revealed significant regional differences in the impact of extreme weather disasters on crop yields. Specifically, the Midwest and Southeast hubs are most vulnerable to corn yield losses due to extreme droughts and heatwaves (Figure 4-5), while the South Plains and Southeast hubs exhibit the most substantial yield reductions for soybean resulting from extreme droughts and heatwaves (Figure 4-6). These regional differences may be attributed to differences in local crop management practices as well as variations in local climate and soil moisture conditions.

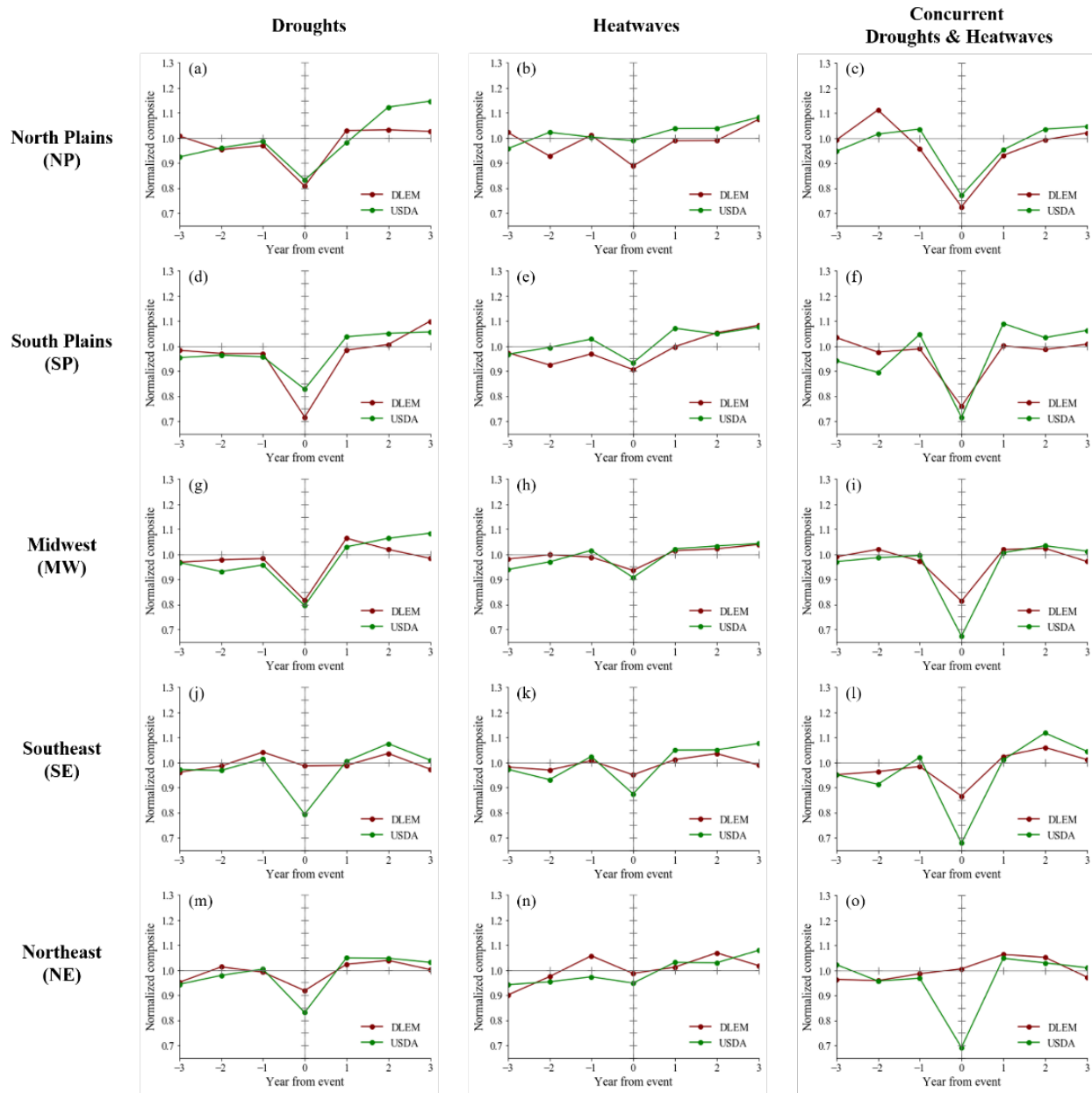


Figure 4-5. Influence of extreme droughts, heatwaves, and their co-occurrence on observed (i.e., USDA) and simulated (i.e., DLEM) corn yields over different climate hubs.

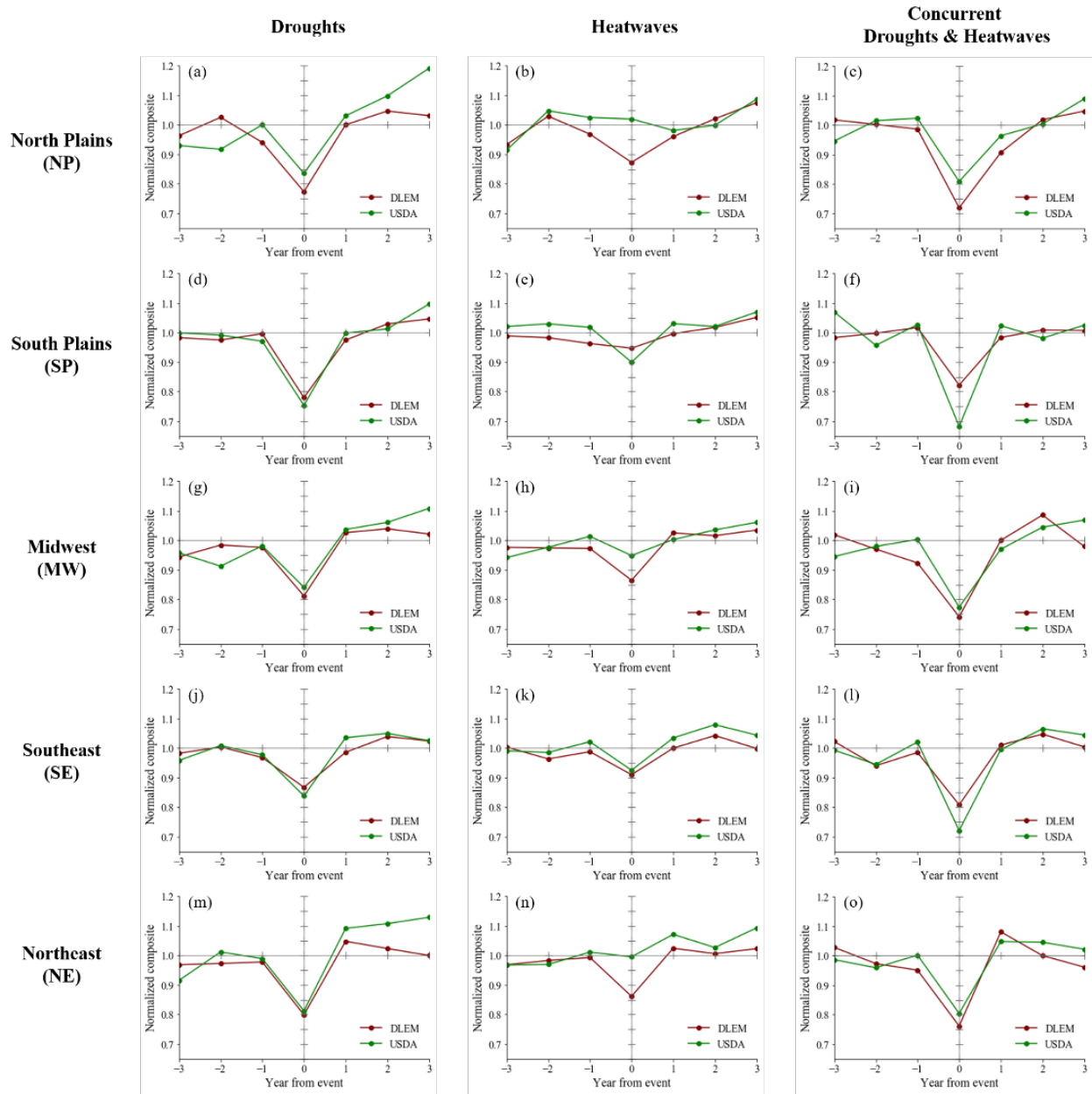


Figure 4-6. Influence of extreme droughts, heatwaves, and their co-occurrence on observed (i.e., USDA) and simulated (i.e., DLEM) soybean yields across different climate hubs.

4.3.3 Sensitivity of corn and soybean yields to concurrent drought and heatwave events

Before analyzing sensitivity changes, we examined potential nonlinearities and asymmetries in the response of crop yields to droughts and heatwaves using the multivariate adaptive regression

splines (MARS) method (Lobell et al. 2014). Our results indicate that the impact of droughts on crop yields is nonlinear: both extremely low and high SPEI values adversely affect the yields of corn and soybean (Figure 4-7). Regarding heatwaves, our findings show a direct negative impact on the yields of both crops. Moreover, the severity of yield loss is proportional to the intensity of the heatwaves, indicating a dose-response relationship.

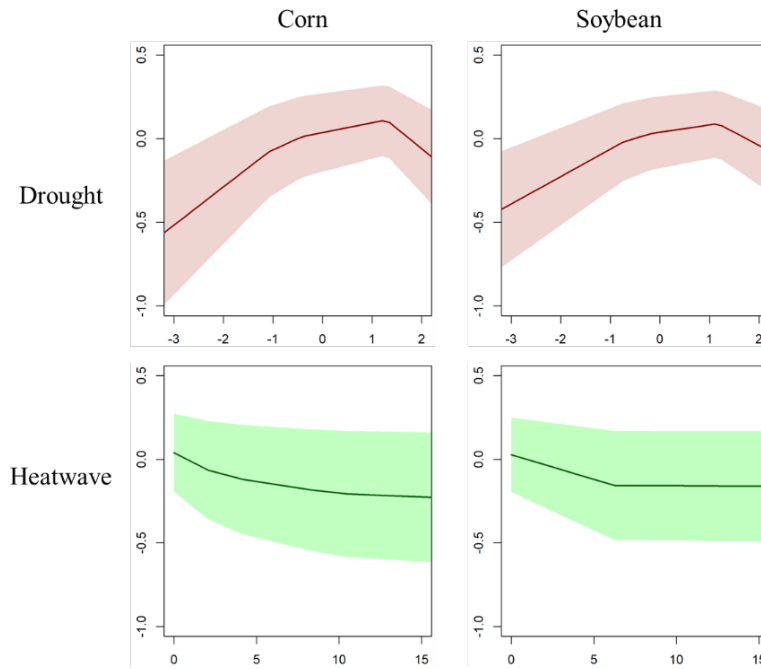


Figure 4-7. Nonlinear responses of crop yields to droughts and heatwaves from multivariate adaptive regression splines analysis for corn and soybean, where shaded areas show 10–90% confidence interval.

We further evaluated whether the sensitivity of the corn and soybean yields to extreme drought, heatwave, and their concurrent occurrences has changed during the past six decades (Figure 4-8). According to our analysis using USDA yield datasets, we found that median estimates of sensitivity have significantly decreased for heatwaves and their combinations (i.e., concurrent droughts and heatwaves). These estimates were generally consistent across different bootstrap samples of the data, that is, both the ranges of bootstrap estimates for heatwaves and the

combinations are negative, suggesting decreased sensitivity. Conversely, for drought sensitivity, we found a wide range of bootstrap estimates for both corn and soybean yields. These estimates ranged from significant increases to significant decreases in sensitivity, suggesting that the panel model was unable to precisely estimate changes in drought sensitivity over time. One potential reason for this could be attributed to the fact that the SPEI includes both positive (extremely wet) and negative (extremely dry) values, reflecting both drought and wet conditions and therefore leading to biased estimations. In addition, according to the analysis derived from DLEM-simulated yield datasets, we found that median estimates of sensitivity have also significantly decreased for heatwaves and their combinations. However, these estimates were not consistent across different bootstrap samples of the data. A similar inconsistency was also reflected in the drought sensitivity results, suggesting that the DLEM may not accurately reproduce the time trends of corn and soybean yield sensitivities to extreme climate disasters.

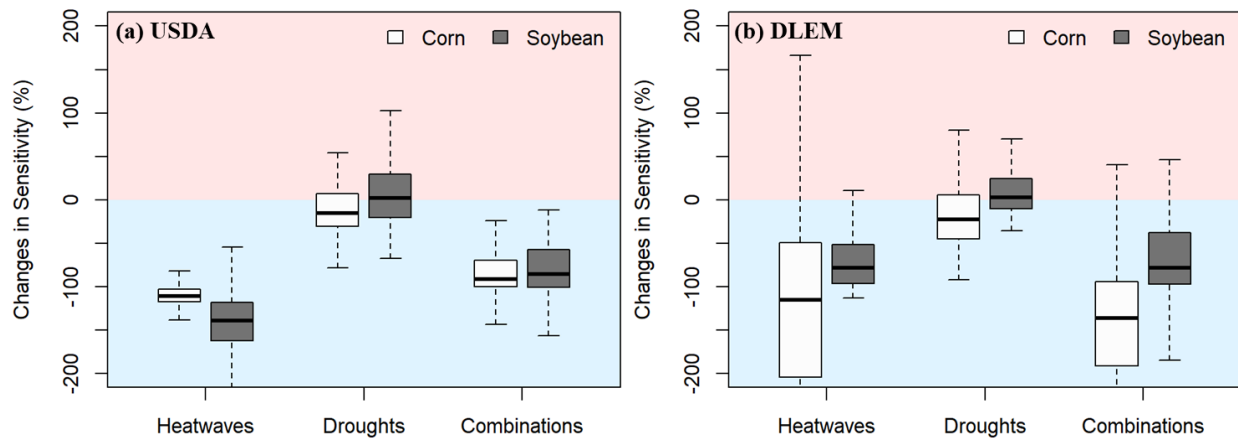


Figure 4-8. Time trends in yield sensitivity to heatwaves, droughts, and their combinations (i.e., concurrent droughts and heatwaves). The panel model estimates the time trend in sensitivity to SPEI (Standardized Precipitation Evapotranspiration Index) and HWMId (Heat Wave Magnitude Index daily), using county-level data during 1964-2018 in the conterminous US. Trends are expressed as a percentage of the value at the start of the time period. Vertical lines show the median estimate, boxes represent the 25th–75th percentiles, and whiskers show the range of bootstrap estimates, with block bootstrapping conducted by year.

We also evaluated the time trends in the sensitivity of corn and soybean yields to extreme droughts, heatwaves, and their combinations across various USDA climate hubs (Figure 4-9). We found that in major planting areas such as the Midwest hub, our conclusions remain consistent: both corn and soybean yields have exhibited decreased sensitivity to extreme heatwaves as well as to concurrent droughts and heatwaves. However, our results over other regions suggest that alternative methods might be necessary for examining changes in crop yield sensitivity to extreme climate disasters. Additionally, there are significant differences between the results derived from the DLEM-simulated yield dataset and those from the USDA. This suggests that further improvements to the DLEM model may be required for more accurate simulation of the impacts of extreme climate events on crop yields. Such improvements are also crucial for accurately projecting crop yields under future climate change scenarios.

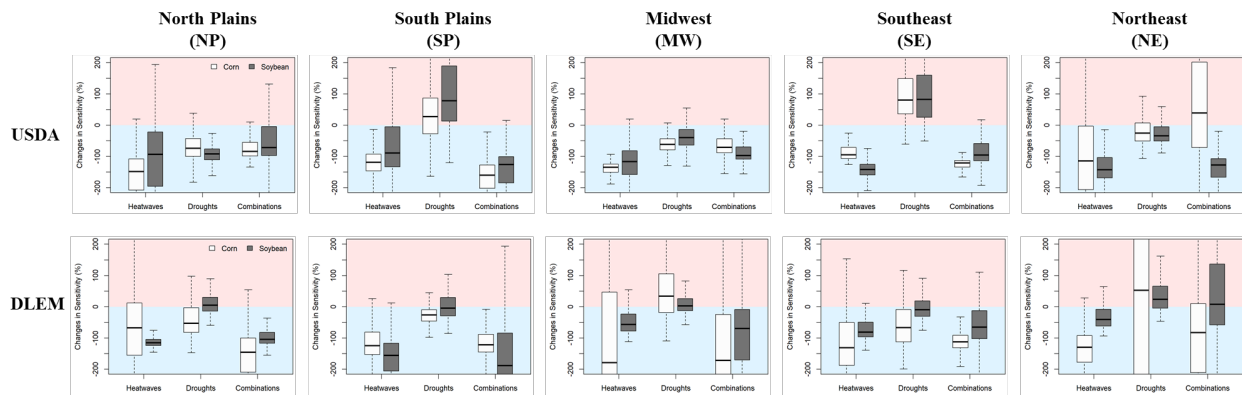


Figure 4-9. Time trends in yield sensitivity to heatwaves, droughts, and their combinations (i.e., concurrent droughts and heatwaves) across different climate hubs.

4.4 Discussion

Ensuring global food security in the context of exacerbated climate change requires the development of effective adaptation strategies within agricultural systems (IPCC 2014b). Achieving this goal necessitates an in-depth understanding of the impact of climate change—

particularly the simultaneous occurrence of extreme climate events such as droughts and heatwaves—on crop productivity (Rosenzweig and Tubiello 2007; Zipper et al. 2016). To this end, this study quantified the impact of concurrent droughts and heatwaves on U.S. corn and soybean yields, and it further assessed the temporal trends in the sensitivity of crop yields to these concurrent events.

4.4.1 Timescale and timing of drought and heatwave impacts

Our results reveal that both corn and soybean yields exhibit significant vulnerability to short-term droughts (i.e., lasting from 1 to 3 months), occurring during the pivotal reproductive phases of crop development (Figure 4-1). These critical phenological phases typically span from July to August for corn (corresponding to tasseling and silking phases) and from August to September for soybean (corresponding to pod setting and filling phases). Our identified critical timing for corn in July and for soybean in August aligns well with existing studies, which suggest that the period around pollination is of paramount importance for crop yield (Çakir 2004; Campos et al. 2004; Otegui et al. 1995; Zipper et al. 2016). This finding highlights the need for the implementation of precision agricultural techniques to accurately, and in a timely manner, monitor soil moisture conditions during these critical developmental phases (Zipper et al. 2016). Meanwhile, our results demonstrate that short-term droughts have a greater impact on the yields of annual crops than long-term droughts, which may be because crop growth and development are more sensitive to rapid and substantial alterations in soil moisture induced by short-term weather events (Illston and Basara 2003; Wu and Wilhite 2004). Notably, our findings diverge from previous research highlighting the importance of long-term droughts on perennial plants such as trees and shrubs (Anderegg et al. 2013; Anderegg et al. 2020; Barbeta et al. 2015). This distinction underscores the imperative of strategically managing short-term droughts in agricultural systems.

Regarding the impact of the timing of heatwaves on crop yields, our results indicate that both corn and soybean yields are highly susceptible to heatwaves occurring during July and August (Figure 4-2). The reproductive phase of corn, particularly the pollination, often falls within July and early August. Pollination is a crucial stage for the fertilization of ovules that will develop into kernels. Heatwave during this phase can compromise pollen viability, which would adversely affect the number of kernels per ear and, in turn, the yield (John et al. 1987; Liu et al. 2020b). Meanwhile, heatwave can also cause silk desiccation, thereby hindering successful pollination (Herrero and Johnson 1980). For soybean, the July-August period coincides with the flowering and pod-setting stages. Heatwave occurred during these stages could result in flower abortion and fewer pods, thereby leading to reduced yield (Heatherly and Elmore 2004; Specht et al. 1999). Moreover, heatwave can also lead to increased rates of plant respiration, affecting the allocation of assimilated carbon, which would otherwise contribute to grain filling in both corn and soybeans (Crafts-Brandner and Salvucci 2002).

4.4.2 Crop yield responses to droughts and heatwaves

The adverse impacts of extreme climate events, including droughts and heatwaves, on crop yields are well-documented in the literature (Haqiqi et al. 2021; Lesk et al. 2022; Lesk et al. 2016; Lobell et al. 2011; Schlenker and Roberts 2009a; Troy et al. 2015). Consistent with previous research, our findings demonstrate that extreme climate events have significantly reduced crop yields. Specifically, our analysis show that extreme drought events have led to an average yield reduction of 17.4% in corn and 17.0% in soybean, and extreme heatwaves have resulted in yield reductions of 9.0% and 6.3% for corn and soybean, respectively. Extreme droughts have a more adverse impact on crop yields than extreme heatwaves, possibly due to the extended duration of droughts that usually span substantial portions of the growing season. Such extended exposure

could have more devastating consequences than the relatively short-lived heatwaves (Lesk et al. 2016). Furthermore, our results indicate that the synergistic effect of simultaneous droughts and heatwaves exacerbates yield losses compared with a single event, consistent with previous studies (Cohen et al. 2020; Glotter and Elliott 2016; Jin et al. 2017; Lesk et al. 2016). The concurrent droughts and heatwaves synergistically impact the crop life cycle, for example, by reducing the time to anthesis and hastening the overall maturation process (Awasthi et al. 2014; Qaseem et al. 2019). The simultaneous occurrence of these events can create a feedback loop whereby each exacerbates the impact of the other on relevant processes such as photosynthesis and nutrient uptake, resulting in compounded yield losses (Lesk et al. 2022; Zampieri et al. 2017). Additionally, the absence of lagged yield-level responses in our study corroborates with findings from Lesk et al. (2016), which reported immediate rather than delayed impacts of weather extremes on crop productivity.

Our findings also elucidate the heterogeneity in the vulnerability of crop yields to extreme climate across different USDA climate hubs, corroborating existing research that points to regional susceptibility of crops to climate change (Hatfield et al. 2011; Lobell et al. 2011; Wheeler and von Braun 2013a). The regional differences in the impacts of extreme climate events may be due to a variety of factors, including varying local agricultural management practices and varying local climate and soil conditions (Challinor et al. 2014). For instance, Tack et al. (2015) indicated that agricultural management practices such as irrigation, choice of crop varieties, and planting density can either mitigate or exacerbate the impacts of extreme climate events on crop yields. Furthermore, soil characteristics, such as water-holding capacity and texture, play a pivotal role in determining the resilience of crops to droughts (Saxton and Rawls 2006). Additionally, the local climate plays an integral role when assessing vulnerability to extreme climate. Different climate zones exhibit

unique weather patterns that influence the manifestation of extreme events such as heatwaves and droughts (IPCC 2014b). Hence, understanding these microclimates and ambient environments is essential for predicting regional differences in crop yield responses to extreme climate events.

4.4.3 Sensitivity of crop yields to droughts and heatwaves

Our results indicate that the impact of short-term drought on crop yields is nonlinear, where both extremely negative and positive SPEI values have adverse effects on corn and soybean yields (Figure 4-7). This finding is consistent with previous studies (Li et al. 2019; Lobell et al. 2014; Zampieri et al. 2017; Zipper et al. 2015), which have demonstrated that crop yields decline not only under extreme dry conditions (represented by highly negative SPEI values) but also under extreme wet conditions (represented by highly positive SPEI values). Specifically, extremely negative SPEI values indicate severe drought conditions, leading to a series of physiological changes in crops, including stomatal closure, reduced photosynthesis, and lower nutrient uptake, which collectively lead to reduced yield (Farooq et al. 2009). Conversely, extremely high SPEI values denote excessive moisture conditions, which often result in waterlogging, nutrient leaching, and increased disease pressure (Booth et al. 2016; Nosetto et al. 2009; Zipper et al. 2015). Overall, potential nonlinear effects of drought underscore the necessity for more nuanced risk management strategies to maintain optimal soil moisture conditions. For heatwaves, our findings indicate a direct negative impact on crop yields, and this impact is exacerbated with increased heatwave intensity (Figure 4-7). Heatwaves can impair critical physiological processes such as photosynthesis, water uptake, and nutrient assimilation, which invariably leads to reduced yields (Lobell and Field 2007). Our findings are in line with previous research (Cohen et al. 2021; Lesk et al. 2022; Zhao et al. 2017). Notably, the severity of yield loss generally follows a dose-response relationship with the intensity of the heatwaves, suggesting the adverse impact of heatwaves is

magnified as their intensity increases. Consequently, our findings advocate for the refinement of agricultural management practices, such as the deployment of heat-tolerant crop varieties (Tadesse et al. 2019) and the implementation of targeted irrigation techniques that account for higher evapotranspiration rates during heatwaves (Feres and Soriano 2007), to reduce adverse heatwave impacts.

Additionally, we found that both corn and soybean yields have exhibited decreased sensitivity to extreme heatwaves as well as to concurrent droughts and heatwaves. One possible explanation for this decreased sensitivity is the significant technological advancement in crop breeding and genetics (Gaffney et al. 2015; Lobell et al. 2011). For example, drought-resistant and heat-tolerant cultivars are increasingly being adopted by farmers (McFadden et al. 2018), enabling crops to survive and even thrive in harsh climatic conditions. Another possible explanation is adaptive farming practices, such as optimized irrigation, conservation tillage, and appropriate timing of planting, that help to retain soil moisture (Howell 2001; Ortiz et al. 2008; Smith and Olesen 2010). These practices can mitigate the impact of heatwaves and droughts on crop yields. Moreover, some research has suggested that crops can undergo a form of acclimation, adjusting their physiological processes to better cope with elevated temperatures and reduced water availability (Dan et al. 2008; Hussain et al. 2013; Leakey et al. 2009). However, it should be noted that some limitations exist in our study, as our current results were unable to draw conclusive findings regarding changes in drought sensitivity over time. The bootstrap estimates of drought sensitivity showed a wide range of values, from significant increases to significant decreases (Figure 4-8). This suggests that either the panel model used or the SPEI and HWMId metrics was unable to precisely quantify changes in drought sensitivity over time. Notably, Lobell et al. (2020) used a different metric—the plant-available water storage—to investigate temporal changes in drought sensitivity for U.S. corn, and

their findings indicated an increased sensitivity to drought conditions. In summary, our results underscore the increasing resilience of corn and soybean yields to concurrent droughts and heatwaves, possibly due to both genetic improvements and adaptive farming practices. However, more effective methodologies and metrics are still needed to accurately evaluate changes in drought sensitivity over time.

4.4.4 Model uncertainties

The inconsistency in sensitivity estimates between the USDA and the DLEM may be attributed to a variety of factors, including model forcing datasets, structures, and parameters. Firstly, the input data used to drive the DLEM may introduce uncertainty to both simulated crop yields and losses due to extreme climate events. For example, the crop-specific irrigation dataset was downscaled from the county-level irrigation reanalysis dataset, which lacked detailed spatial information and would inevitably influence the accuracy of yield simulations. Secondly, the simplifications or omissions of real-world biophysical, biogeochemical, and hydrological processes in the DLEM may also cause simulation biases in crop yields. For example, the current DLEM's representation of groundwater and irrigation practice is relatively simple (e.g., without considering irrigation amount and frequency), which could lead to biased simulated soil moisture that, in turn, could affect crop yield simulation, particularly under extreme climate conditions. Moreover, the DLEM currently does not account for improvements in crop genetic and breeding technologies that enhance crop resistance to extreme climates (Bailey-Serres et al. 2019; Hammer et al. 2002), nor does it consider human adaptive behaviors such as farmers' preparedness and response strategies related to extreme weather events (Annan and Schlenker 2015). The exclusion of these adaptive processes within the model may further contribute to uncertainties in sensitivity estimates. Finally, uncertainties in model parameterization could also introduce additional bias in

crop yield simulations (You et al. 2022), further affecting yield responses to extreme climate events. Addressing these limitations is critical for enhancing the DLEM's ability to accurately reproduce time trends of crop yield sensitivities to extreme climate disasters.

4.5 Conclusion

In this study, we analyzed U.S. corn and soybean yield vulnerabilities to compound climate events, namely, concurrent droughts and heatwaves. Our findings indicate that both crops are most sensitive to short-term droughts (spanning 1-3 months) and heatwaves during their critical reproductive stages, typically occurring from July to September for droughts and July to August for heatwaves. Among these extreme disasters, droughts tend to have a more detrimental impact on yields compared to heatwaves. Moreover, the concurrence of both disasters exacerbates yield loss substantially, surpassing the effects of single extreme events. Additionally, our study indicates a declining trend in crop sensitivity to both heatwaves and concurrent drought-heatwave events, possibly due to the adoption of drought-resistant and heat-tolerant cultivars, and the implementation of adaptive farming practices such as optimized irrigation and conservation tillage. While the DLEM is capable of reproducing the observed yield loss caused by extreme events, it cannot accurately reproduce the time trends of yield sensitivity to these extreme climate disasters. This highlights the imperative need to refine the DLEM to improve its simulation capabilities. Overall, our research serves as an instrumental foundation for understanding crop yield vulnerabilities to concurrent extreme climate events, while also identifying critical limitations in DLEM that need to be addressed for more accurate and reliable future projections.

References

- Allen, S., Barros, V., Cardona, O., Cutter, S., Dube, O.P., Ebi, K., Handmer, J., Lavell, A., Mastrandrea, M., McBean, G., Mechler, R., & Nicholls, N. (2012). Managing the Risks of Extreme Events and Disasters to Advance Climate Change Adaptation. Special Report of Working Groups I and II of the Intergovernmental Panel on Climate Change. Cambridge Univ. Press
- Anderegg, W.R.L., Kane, J.M., & Anderegg, L.D.L. (2013). Consequences of widespread tree mortality triggered by drought and temperature stress. *Nature Climate Change*, *3*, 30-36
- Anderegg, W.R.L., Trugman, A.T., Badgley, G., Konings, A.G., & Shaw, J. (2020). Divergent forest sensitivity to repeated extreme droughts. *Nature Climate Change*, *10*, 1091-1095
- Anderson, R., Bayer, P.E., & Edwards, D. (2020). Climate change and the need for agricultural adaptation. *Current Opinion in Plant Biology*, *56*, 197-202
- Annan, F., & Schlenker, W. (2015). Federal crop insurance and the disincentive to adapt to extreme heat. *American Economic Review*, *105*, 262-266
- Awasthi, R., Kaushal, N., Vadez, V., Turner, N.C., Berger, J., Siddique, K.H.M., & Nayyar, H. (2014). Individual and combined effects of transient drought and heat stress on carbon assimilation and seed filling in chickpea. *Functional Plant Biology*, *41*, 1148-1167
- Bailey-Serres, J., Parker, J.E., Ainsworth, E.A., Oldroyd, G.E.D., & Schroeder, J.I. (2019). Genetic strategies for improving crop yields. *Nature*, *575*, 109-118
- Barbeta, A., Mejía-Chang, M., Ogaya, R., Voltas, J., Dawson, T.E., & Peñuelas, J. (2015). The combined effects of a long-term experimental drought and an extreme drought on the use of plant-water sources in a Mediterranean forest. *Global Change Biology*, *21*, 1213-1225
- Bassu, S., Brisson, N., Durand, J.-L., Boote, K., Lizaso, J., Jones, J.W., Rosenzweig, C., Ruane, A.C., Adam, M., Baron, C., Basso, B., Biernath, C., Boogaard, H., Conijn, S., Corbeels, M., Deryng, D., De Sanctis, G., Gayler, S., Grassini, P., Hatfield, J., Hoek, S., Izaurralde, C., Jongschaap, R., Kemanian, A.R., Kersebaum, K.C., Kim, S.-H., Kumar, N.S., Makowski, D., Müller, C., Nendel, C., Priesack, E., Pravia, M.V., Sau, F., Shcherbak, I., Tao, F., Teixeira, E., Timlin, D., & Waha, K. (2014). How do various maize crop models vary in their responses to climate change factors? *Global Change Biology*, *20*, 2301-2320
- Battisti, D.S., & Naylor, R.L. (2009). Historical Warnings of Future Food Insecurity with Unprecedented Seasonal Heat. *Science*, *323*, 240-244
- Beguéría, S., Vicente-Serrano, S.M., Reig, F., & Latorre, B. (2014). Standardized precipitation evapotranspiration index (SPEI) revisited: parameter fitting, evapotranspiration models, tools, datasets and drought monitoring. *International Journal of Climatology*, *34*, 3001-3023
- Bolaños, J., & Edmeades, G.O. (1996). The importance of the anthesis-silking interval in breeding for drought tolerance in tropical maize. *Field Crops Research*, *48*, 65-80
- Booth, E.G., Zipper, S.C., Loheide, S.P., & Kucharik, C.J. (2016). Is groundwater recharge always serving us well? Water supply provisioning, crop production, and flood attenuation in conflict in Wisconsin, USA. *Ecosystem Services*, *21*, 153-165
- Çakir, R. (2004). Effect of water stress at different development stages on vegetative and reproductive growth of corn. *Field Crops Research*, *89*, 1-16
- Campos, H., Cooper, M., Habben, J.E., Edmeades, G.O., & Schussler, J.R. (2004). Improving drought tolerance in maize: a view from industry. *Field Crops Research*, *90*, 19-34
- Ceccherini, G., Russo, S., Ameztoy, I., Marchese, A.F., & Carmona-Moreno, C. (2017). Heat waves in Africa 1981-2015, observations and reanalysis. *Natural Hazards & Earth System Sciences*, *17*
- Challinor, A.J., Watson, J., Lobell, D.B., Howden, S.M., Smith, D.R., & Chhetri, N. (2014). A meta-analysis of crop yield under climate change and adaptation. *Nature Climate Change*, *4*, 287-291
- Cohen, I., Zandalinas, S.I., Huck, C., Fritschi, F.B., & Mittler, R. (2020). Meta-analysis of drought and heat stress combination impact on crop yield and yield components. *Physiologia Plantarum*, *n/a*
- Cohen, I., Zandalinas, S.I., Huck, C., Fritschi, F.B., & Mittler, R. (2021). Meta-analysis of drought and heat stress combination impact on crop yield and yield components. *Physiologia Plantarum*, *171*, 66-76
- Crafts-Brandner, S.J., & Salvucci, M.E. (2002). Sensitivity of Photosynthesis in a C4 Plant, Maize, to Heat Stress. *Plant physiology*, *129*, 1773-1780
- Dan, W., Heckathorn, S.A., Barua, D., Joshi, P., Hamilton, E.W., & LaCroix, J.J. (2008). Effects of elevated CO2 on the tolerance of photosynthesis to acute heat stress in C3, C4, and CAM species. *American Journal of Botany*, *95*, 165-176

- Drewniak, B., Song, J., Prell, J., Kotamarthi, V.R., & Jacob, R. (2013). Modeling agriculture in the Community Land Model. *Geosci. Model Dev.*, 6, 495-515
- Egli, D.B. (2008). Comparison of Corn and Soybean Yields in the United States: Historical Trends and Future Prospects. *Agronomy journal*, 100, S-79-S-88
- Eyshi Rezaei, E., Webber, H., Gaiser, T., Naab, J., & Ewert, F. (2015). Heat stress in cereals: Mechanisms and modelling. *European Journal of Agronomy*, 64, 98-113
- Farooq, M., Wahid, A., Kobayashi, N., Fujita, D., & Basra, S.M.A. (2009). Plant Drought Stress: Effects, Mechanisms and Management. In E. Lichtfouse, M. Navarrete, P. Debaeke, S. Véronique, & C. Alberola (Eds.), *Sustainable Agriculture* (pp. 153-188). Dordrecht: Springer Netherlands
- Fereres, E., & Soriano, M.A. (2007). Deficit irrigation for reducing agricultural water use. *Journal of Experimental Botany*, 58, 147-159
- Gaffney, J., Schussler, J., Löffler, C., Cai, W., Paszkiewicz, S., Messina, C., Groeteke, J., Keaschall, J., & Cooper, M. (2015). Industry-Scale Evaluation of Maize Hybrids Selected for Increased Yield in Drought-Stress Conditions of the US Corn Belt. *Crop Science*, 55, 1608-1618
- Glatter, M., & Elliott, J. (2016). Simulating US agriculture in a modern Dust Bowl drought. *Nature Plants*, 3, 16193
- Hammer, G.L., Kropff, M.J., Sinclair, T.R., & Porter, J.R. (2002). Future contributions of crop modelling—from heuristics and supporting decision making to understanding genetic regulation and aiding crop improvement. *European Journal of Agronomy*, 18, 15-31
- Haqiqi, I., Grogan, D.S., Hertel, T.W., & Schlenker, W. (2021). Quantifying the impacts of compound extremes on agriculture. *Hydrol. Earth Syst. Sci.*, 25, 551-564
- Hatfield, J.L., Boote, K.J., Kimball, B.A., Ziska, L.H., Izaurralde, R.C., Ort, D., Thomson, A.M., & Wolfe, D. (2011). Climate Impacts on Agriculture: Implications for Crop Production. *Agronomy journal*, 103, 351-370
- Heatherly, L.G., & Elmore, R.W. (2004). Managing Inputs for Peak Production. *Soybeans: Improvement, production, and uses* (pp. 451-536)
- Herrero, M.P., & Johnson, R.R. (1980). High Temperature Stress and Pollen Viability of Maize1. *Crop Science*, 20, crops1980.0011183X002000060030x
- Howden, S.M., Soussana, J.-F., Tubiello, F.N., Chhetri, N., Dunlop, M., & Meinke, H. (2007). Adapting agriculture to climate change. *Proceedings of the National Academy of Sciences*, 104, 19691
- Howell, T.A. (2001). Enhancing Water Use Efficiency in Irrigated Agriculture. *Agronomy journal*, 93, 281-289
- Hussain, M.Z., VanLoocke, A., Siebers, M.H., Ruiz-Vera, U.M., Cody Markelz, R.J., Leakey, A.D.B., Ort, D.R., & Bernacchi, C.J. (2013). Future carbon dioxide concentration decreases canopy evapotranspiration and soil water depletion by field-grown maize. *Global Change Biology*, 19, 1572-1584
- Illston, B.G., & Basara, J.B. (2003). Analysis of short-term droughts in Oklahoma. *Eos, Transactions American Geophysical Union*, 84, 157-161
- IPCC (2014). *Climate Change 2014: Impacts, Adaptation, and Vulnerability. Part A: Global and Sectoral Aspects. Contribution of Working Group II to the Fifth Assessment Report of the Intergovernmental Panel on Climate Change*. [Field, C.B., V.R. Barros, D.J. Dokken, K.J. Mach, M.D. Mastrandrea, T.E. Bilir, M. Chatterjee, K.L. Ebi, Y.O. Estrada, R.C. Genova, B. Girma, E.S. Kissel, A.N. Levy, S. MacCracken, P.R. Mastrandrea, and L.L. White (eds.)]. Cambridge University Press, Cambridge, United Kingdom and New York, NY, USA, 1132 pp.
- Jägermeyr, J., & Frieler, K. (2018). Spatial variations in crop growing seasons pivotal to reproduce global fluctuations in maize and wheat yields. *Science advances*, 4, eaat4517
- Janssen, E., Wuebbles, D.J., Kunkel, K.E., Olsen, S.C., & Goodman, A. (2014). Observational- and model-based trends and projections of extreme precipitation over the contiguous United States. *Earth's Future*, 2, 99-113
- Jin, Z., Zhuang, Q., Wang, J., Archontoulis, S.V., Zobel, Z., & Kotamarthi, V.R. (2017). The combined and separate impacts of climate extremes on the current and future US rainfed maize and soybean production under elevated CO2. *Global Change Biology*, 23, 2687-2704
- John, B.S., Lambert, R.J., Bruce, L.V., & Mark, E.W. (1987). Plant Factors Controlling Seed Set in Maize: The Influence of Silk, Pollen, and Ear-Leaf Water Status and Tassel Heat Treatment at Pollination. *Plant physiology*, 83, 121-125
- Leakey, A.D.B., Ainsworth, E.A., Bernacchi, C.J., Rogers, A., Long, S.P., & Ort, D.R. (2009). Elevated CO2 effects on plant carbon, nitrogen, and water relations: six important lessons from FACE. *Journal of Experimental Botany*, 60, 2859-2876
- Lesk, C., Anderson, W., Rigden, A., Coast, O., Jägermeyr, J., McDermid, S., Davis, K.F., & Konar, M. (2022). Compound heat and moisture extreme impacts on global crop yields under climate change. *Nature Reviews Earth & Environment*, 3, 872-889

- Lesk, C., Rowhani, P., & Ramankutty, N. (2016). Influence of extreme weather disasters on global crop production. *Nature*, *529*, 84-87
- Li, Y., Guan, K., Schnitkey, G.D., DeLucia, E., & Peng, B. (2019). Excessive rainfall leads to maize yield loss of a comparable magnitude to extreme drought in the United States. *Global Change Biology*, *25*, 2325-2337
- Liu, X., Wang, X., Wang, X., Gao, J., Luo, N., Meng, Q., & Wang, P. (2020). Dissecting the critical stage in the response of maize kernel set to individual and combined drought and heat stress around flowering. *Environmental and Experimental Botany*, *179*, 104213
- Lobell, D.B. (2014). Climate change adaptation in crop production: Beware of illusions. *Global Food Security*, *3*, 72-76
- Lobell, D.B., Deines, J.M., & Tommaso, S.D. (2020). Changes in the drought sensitivity of US maize yields. *Nature Food*, *1*, 729-735
- Lobell, D.B., & Field, C.B. (2007). Global scale climate–crop yield relationships and the impacts of recent warming. *Environmental Research Letters*, *2*, 014002
- Lobell, D.B., Hammer, G.L., McLean, G., Messina, C., Roberts, M.J., & Schlenker, W. (2013). The critical role of extreme heat for maize production in the United States. *Nature Climate Change*, *3*, 497-501
- Lobell, D.B., Roberts, M.J., Schlenker, W., Braun, N., Little, B.B., Rejesus, R.M., & Hammer, G.L. (2014). Greater Sensitivity to Drought Accompanies Maize Yield Increase in the U.S. Midwest. *Science*, *344*, 516
- Lobell, D.B., Schlenker, W., & Costa-Roberts, J. (2011). Climate Trends and Global Crop Production Since 1980. *Science*, *333*, 616-620
- Lu, J., Carbone, G.J., & Gao, P. (2017). Detrending crop yield data for spatial visualization of drought impacts in the United States, 1895–2014. *Agricultural and Forest Meteorology*, *237-238*, 196-208
- Mazdiyasi, O., & AghaKouchak, A. (2015). Substantial increase in concurrent droughts and heatwaves in the United States. *Proceedings of the National Academy of Sciences*, *112*, 11484
- McFadden, J., Smith, D.J., & Wallander, S. (2018). Adoption of drought-tolerant corn in the US: A field-level analysis of adoption patterns and emerging trends. *2018 Agricultural & Applied Economics Association Annual Meeting, Washington, D.C.*
- Meehl, G.A., & Tebaldi, C. (2004). More Intense, More Frequent, and Longer Lasting Heat Waves in the 21st Century. *Science*, *305*, 994
- NASS, N.A.S.S. (2013). Crop Production 2012 Summary. *US Department of Agriculture, Washington DC.*
- Nosetto, M.D., Jobbágy, E.G., Jackson, R.B., & Sznajder, G.A. (2009). Reciprocal influence of crops and shallow ground water in sandy landscapes of the Inland Pampas. *Field Crops Research*, *113*, 138-148
- Ortiz, R., Sayre, K.D., Govaerts, B., Gupta, R., Subbarao, G.V., Ban, T., Hodson, D., Dixon, J.M., Iván Ortiz-Monasterio, J., & Reynolds, M. (2008). Climate change: Can wheat beat the heat? *Agriculture, Ecosystems & Environment*, *126*, 46-58
- Otegui, M.E., Andrade, F.H., & Suero, E.E. (1995). Growth, water use, and kernel abortion of maize subjected to drought at silking. *Field Crops Research*, *40*, 87-94
- Pan, S., Bian, Z., Tian, H., Yao, Y., Najjar, R.G., Friedrichs, M.A.M., Hofmann, E.E., Xu, R., & Zhang, B. (2021). Impacts of Multiple Environmental Changes on Long-term Nitrogen Loading from the Chesapeake Bay Watershed. *Journal of Geophysical Research: Biogeosciences*, *126*, e2020JG005826
- Parent, B., & Tardieu, F. (2012). Temperature responses of developmental processes have not been affected by breeding in different ecological areas for 17 crop species. *New Phytologist*, *194*, 760-774
- Peng, B., Guan, K., Tang, J., Ainsworth, E.A., Asseng, S., Bernacchi, C.J., Cooper, M., DeLucia, E.H., Elliott, J.W., Ewert, F., Grant, R.F., Gustafson, D.I., Hammer, G.L., Jin, Z., Jones, J.W., Kimm, H., Lawrence, D.M., Li, Y., Lombardozzi, D.L., Marshall-Colon, A., Messina, C.D., Ort, D.R., Schnable, J.C., Vallejos, C.E., Wu, A., Yin, X., & Zhou, W. (2020). Towards a multiscale crop modelling framework for climate change adaptation assessment. *Nature Plants*, *6*, 338-348
- Prasad, P.V.V., Staggenborg, S.A., & Ristic, Z. (2008). Impacts of Drought and/or Heat Stress on Physiological, Developmental, Growth, and Yield Processes of Crop Plants. *Response of Crops to Limited Water* (pp. 301-355)
- Qaseem, M.F., Qureshi, R., & Shaheen, H. (2019). Effects of Pre-Anthesis Drought, Heat and Their Combination on the Growth, Yield and Physiology of diverse Wheat (*Triticum aestivum* L.) Genotypes Varying in Sensitivity to Heat and drought stress. *Scientific Reports*, *9*, 6955
- Reichstein, M., Bahn, M., Ciais, P., Frank, D., Mahecha, M.D., Seneviratne, S.I., Zscheischler, J., Beer, C., Buchmann, N., Frank, D.C., Papale, D., Rammig, A., Smith, P., Thonicke, K., van der Velde, M., Vicca, S., Walz, A., & Wattenbach, M. (2013). Climate extremes and the carbon cycle. *Nature*, *500*, 287-295

- Ridder, N.N., Ukkola, A.M., Pitman, A.J., & Perkins-Kirkpatrick, S.E. (2022). Increased occurrence of high impact compound events under climate change. *npj Climate and Atmospheric Science*, 5, 3
- Rosenzweig, C., Elliott, J., Deryng, D., Ruane, A.C., Müller, C., Arneth, A., Boote, K.J., Folberth, C., Glotter, M., & Khabarov, N. (2014). Assessing agricultural risks of climate change in the 21st century in a global gridded crop model intercomparison. *Proceedings of the National Academy of Sciences*, 111, 3268-3273
- Rosenzweig, C., Jones, J.W., Hatfield, J.L., Ruane, A.C., Boote, K.J., Thorburn, P., Antle, J.M., Nelson, G.C., Porter, C., Janssen, S., Asseng, S., Basso, B., Ewert, F., Wallach, D., Baigorría, G., & Winter, J.M. (2013). The Agricultural Model Intercomparison and Improvement Project (AgMIP): Protocols and pilot studies. *Agricultural and Forest Meteorology*, 170, 166-182
- Rosenzweig, C., & Tubiello, F.N. (2007). Adaptation and mitigation strategies in agriculture: an analysis of potential synergies. *Mitigation and adaptation strategies for global change*, 12, 855-873
- Russo, S., Dosio, A., Graversen, R.G., Sillmann, J., Carrao, H., Dunbar, M.B., Singleton, A., Montagna, P., Barbola, P., & Vogt, J.V. (2014). Magnitude of extreme heat waves in present climate and their projection in a warming world. *Journal of Geophysical Research: Atmospheres*, 119, 5005-5012
- Russo, S., Sillmann, J., & Fischer, E.M. (2015). Top ten European heatwaves since 1950 and their occurrence in the coming decades. *Environmental Research Letters*, 10, 124003
- Saxton, K.E., & Rawls, W.J. (2006). Soil Water Characteristic Estimates by Texture and Organic Matter for Hydrologic Solutions. *Soil Science Society of America Journal*, 70, 1569-1578
- Schlenker, W., & Roberts, M.J. (2009). Nonlinear temperature effects indicate severe damages to U.S. crop yields under climate change. *Proceedings of the National Academy of Sciences*, 106, 15594-15598
- Shi, W., Wang, M., & Liu, Y. (2021). Crop yield and production responses to climate disasters in China. *Science of the Total Environment*, 750, 141147
- Smith, P., & Olesen, J.E. (2010). Synergies between the mitigation of, and adaptation to, climate change in agriculture. *The Journal of Agricultural Science*, 148, 543-552
- Specht, J.E., Hume, D.J., & Kumudini, S.V. (1999). Soybean Yield Potential—A Genetic and Physiological Perspective. *Crop Science*, 39, 1560-1570
- Tack, J., Barkley, A., & Nalley, L.L. (2015). Effect of warming temperatures on US wheat yields. *Journal of Agricultural Science*, 155, 6931-6936
- Tadesse, W., Suleiman, S., Tahir, I., Sanchez-Garcia, M., Jighly, A., Hagra, A., Thabet, S., & Baum, M. (2019). Heat-Tolerant QTLs Associated with Grain Yield and Its Components in Spring Bread Wheat under Heat-Stressed Environments of Sudan and Egypt. *Crop Science*, 59, 199-211
- Tian, H., Chen, G., Liu, M., Zhang, C., Sun, G., Lu, C., Xu, X., Ren, W., Pan, S., & Chappelka, A. (2010). Model estimates of net primary productivity, evapotranspiration, and water use efficiency in the terrestrial ecosystems of the southern United States during 1895–2007. *Forest Ecology and Management*, 259, 1311-1327
- Tian, H., Xu, R., Pan, S., Yao, Y., Bian, Z., Cai, W.-J., Hopkinson, C.S., Justic, D., Lohrenz, S., Lu, C., Ren, W., & Yang, J. (2020). Long-Term Trajectory of Nitrogen Loading and Delivery From Mississippi River Basin to the Gulf of Mexico. *Global Biogeochemical Cycles*, 34, e2019GB006475
- Troy, T.J., Kipgen, C., & Pal, I. (2015). The impact of climate extremes and irrigation on US crop yields. *Environmental Research Letters*, 10, 054013
- USDA (2015). World Agricultural Supply and Demand Estimates Report. *USDA, Washington, DC*.
- Vicente-Serrano, S.M., Beguería, S., & López-Moreno, J.I. (2010). A Multiscalar Drought Index Sensitive to Global Warming: The Standardized Precipitation Evapotranspiration Index. *Journal of Climate*, 23, 1696-1718
- Wheeler, T., & von Braun, J. (2013). Climate Change Impacts on Global Food Security. *Science*, 341, 508-513
- Wu, H., & Wilhite, D.A. (2004). An Operational Agricultural Drought Risk Assessment Model for Nebraska, USA. *Natural Hazards*, 33, 1-21
- Yao, Y., Tian, H., Shi, H., Pan, S., Xu, R., Pan, N., & Canadell, J.G. (2020). Increased global nitrous oxide emissions from streams and rivers in the Anthropocene. *Nature Climate Change*, 10, 138-142
- You, Y., Tian, H., Pan, S., Shi, H., Bian, Z., Gurgel, A., Huang, Y., Kicklighter, D., Liang, X.-Z., Lu, C., Melillo, J., Miao, R., Pan, N., Reilly, J., Ren, W., Xu, R., Yang, J., Yu, Q., & Zhang, J. (2022). Incorporating dynamic crop growth processes and management practices into a terrestrial biosphere model for simulating crop production in the United States: Toward a unified modeling framework. *Agricultural and Forest Meteorology*, 325, 109144
- Zampieri, M., Ceglar, A., Dentener, F., & Toret, A. (2017). Wheat yield loss attributable to heat waves, drought and water excess at the global, national and subnational scales. *Environmental Research Letters*, 12, 064008
- Zhao, C., Liu, B., Piao, S., Wang, X., Lobell, D.B., Huang, Y., Huang, M., Yao, Y., Bassu, S., Ciais, P., Durand, J.-L., Elliott, J., Ewert, F., Janssens, I.A., Li, T., Lin, E., Liu, Q., Martre, P., Müller, C., Peng, S., Peñuelas, J.,

- Ruane, A.C., Wallach, D., Wang, T., Wu, D., Liu, Z., Zhu, Y., Zhu, Z., & Asseng, S. (2017). Temperature increase reduces global yields of major crops in four independent estimates. *Proceedings of the National Academy of Sciences*, *114*, 9326
- Zipper, S.C., Qiu, J., & Kucharik, C.J. (2016). Drought effects on US maize and soybean production: spatiotemporal patterns and historical changes. *Environmental Research Letters*, *11*, 094021
- Zipper, S.C., Soylu, M.E., Booth, E.G., & Loheide II, S.P. (2015). Untangling the effects of shallow groundwater and soil texture as drivers of subfield-scale yield variability. *Water Resources Research*, *51*, 6338-6358

Chapter 5. Net greenhouse gas balance in U.S. croplands: How can soils be a part of the climate solution?

Abstract

Agricultural soils play a dual role in regulating the Earth's climate by releasing or sequestering carbon dioxide (CO₂) in soil organic carbon (SOC) and emitting non-CO₂ greenhouse gases (GHGs) such as nitrous oxide (N₂O) and methane (CH₄). To understand how agricultural soils can play a role in climate solutions requires a comprehensive assessment of net soil GHG balance (i.e., sum of SOC-sequestered CO₂ and non-CO₂ GHG emissions) and the underlying controls. Herein, we used a model-data integration approach to understand and quantify how natural and anthropogenic factors have affected the magnitude and spatiotemporal variations of the net soil GHG balance in U.S. croplands during 1960-2018. Specifically, we used the Dynamic Land Ecosystem Model (DLEM) for regional simulations and used field observations of SOC sequestration rates and N₂O and CH₄ emissions to calibrate, validate, and corroborate model simulations. Results show that U.S. agricultural soils sequestered 13.2 ± 1.16 Tg CO₂-C yr⁻¹ in SOC (at a depth of 3.5 m) during 1960-2018 and emitted 0.39 ± 0.02 Tg N₂O-N yr⁻¹ and 0.21 ± 0.01 Tg CH₄-C yr⁻¹, respectively. Based on the GWP100 metric (global warming potential on a 100-year time horizon), the estimated national net GHG emission rate from agricultural soils was 121.9 ± 11.46 Tg CO₂-eq yr⁻¹, thus contributing to climate warming. The sequestered SOC offset ~28% of the climate-warming effects resulting from non-CO₂ GHG emissions, and this offsetting effect increased over time. Increased nitrogen fertilizer use was the dominant factor contributing to the increase in net GHG emissions during 1960-2018, explaining ~47% of total changes. In contrast, the adoption of agricultural conservation practices (e.g., reduced tillage) and rising

atmospheric CO₂ attenuated net GHG emissions from U.S. croplands. Our study highlights the importance of concurrently quantifying SOC-sequestered CO₂ and non-CO₂ GHG emissions for developing effective agricultural climate change mitigation measures.

5.1 Introduction

Contemporary agriculture is facing multiple challenges such as feeding a growing world population and mitigating climate change (Chen et al. 2014; Foley et al. 2011; Pittelkow et al. 2015a). By 2050, global food production may need to increase by 25%-70% (Hunter et al. 2017), or even double the current production levels (Tilman et al. 2011), to meet projected food demands, which would inevitably lead to substantial increases in greenhouse gas (GHG) emissions due to nitrogen (N) fertilizer use and cropland expansion (Cavigelli et al. 2012; Molotoks et al. 2018; Thompson et al. 2019; Zabel et al. 2019). To date, agriculture has been a major force in anthropogenic global warming, contributing about 25%-30% and 35%-50% of global land biogenic emissions of nitrous oxide (N₂O) and methane (CH₄), respectively (Tian et al. 2016). This constitutes a great challenge to achieve the Paris climate goal of limiting global warming to well below 2°C by the end of this century (Tian et al. 2020a). Therefore, reducing GHG emissions from the agricultural sector is an imminent need for mitigating climate change. Global croplands account for about 10% of the terrestrial soil organic carbon (SOC) stock (IPCC 2019; Watson et al. 2000) and could potentially sequester 0.90~1.85 Pg C/yr in the top 0.3m of soils, which is equivalent to 26-53% of the soil carbon sequestration target of 3.5 Pg C/yr established by the 4p1000 Initiative for climate mitigation (Zomer et al. 2017). Increasing SOC stock is considered to be the most important countermeasure for GHG mitigation in agriculture (Mosier et al. 2006; Smith et al. 2010). Besides sequestering atmospheric CO₂, enhancing SOC stocks can also provide multiple co-benefits, such as reducing soil erosion, strengthening climate resilience, and improving

soil fertility and health (Lal 2018; Sohi 2012). Thus, advancing our understanding of the magnitude and spatiotemporal variations of net GHG balance (i.e., sum of SOC sequestration of CO₂ and emissions of N₂O and CH₄) in agricultural soils, as well as drivers of their change, is critical for measuring the cumulative radiative forcing of non-CO₂ GHG emissions and CO₂ uptake (Robertson and Grace 2004) and developing effective agricultural climate change mitigation strategies. Meanwhile, improved understanding could contribute to the achievement of Sustainable Development Goals including “Climate Action” and “Zero Hunger”.

As one of the most important agricultural producers in the world, U.S. agriculture contributed a significant portion of global agricultural GHG emissions. Numerous studies have measured and quantified N₂O and CH₄ emissions and SOC sequestration in U.S. croplands (Del Grosso et al. 2010; EPA 2021; Linnquist et al. 2018; Lokupitiya et al. 2012; Lu et al. 2021; Ogle et al. 2010; Penman et al. 2000; Yu et al. 2018). For example, it is reported that agriculture emitted ~10% of the national total GHG emissions in 2019 in the U.S. and was the largest source of N₂O emissions (~75%) (EPA 2021). Nonetheless, these estimates are highly uncertain and wide-ranging, largely due to differences in quantification methods and data sources (Ogle et al. 2010; Tian et al. 2018; Tian et al. 2019; Xu et al. 2012). Specifically, uncertainty in SOC stock changes in U.S. croplands could range from $-4.6 \text{ Tg C yr}^{-1}$ to $+4.9 \text{ Tg C yr}^{-1}$ (Ogle et al. 2010; Ogle et al. 2006), and uncertainty in U.S. agricultural soil N₂O emissions range from $-0.07 \text{ Tg N yr}^{-1}$ to $+0.1 \text{ Tg N yr}^{-1}$ (Cavigelli et al. 2012; Del Grosso et al. 2010). In addition, most of these studies have focused on estimating either individual GHG fluxes or SOC sequestration rate, while much less work has been done in quantifying magnitude and spatiotemporal variations in net soil GHG balance in U.S. croplands (EPA 2021). Due to possible trade-offs between SOC sequestration and GHG emissions under different agricultural management practices (Guenet et al. 2021; Tian et al. 2015a; Tian et

al. 2011), simultaneous quantification of SOC-sequestered CO₂ and non-CO₂ GHG emissions is crucial to accurately assess the overall climate abatement potential of mitigation measures. Furthermore, whether SOC sequestration of CO₂ in U.S. croplands can offset non-CO₂ GHG emissions and how far we are from achieving carbon-neutral agriculture remains unclear.

Climate-smart agriculture (CSA) management practices (e.g., reduced tillage, optimized N fertilizer use, and alternate wetting and drying irrigation) have been advocated to reduce GHG emissions without compromising crop yield (FAO 2013; Miralles-Wilhelm 2021). Various field investigations and meta-analyses have explored the effects and efficacy of these practices (Bai et al. 2019; Gerber et al. 2016; Shang et al. 2021; Sun et al. 2020). However, most existing work assessing the impact of CSA measures on GHG emissions has focused on a single management practice and one or two GHG fluxes (e.g., CO₂ or N₂O) at a time (Huang et al. 2022; Lu et al. 2022; Yu et al. 2020). Relatively few studies have simultaneously quantified the integrated effects of multiple management practices on net soil GHG balance, especially at large spatial scales (e.g., national and continental scales). Notably, EPA (2013) comprehensively quantified all three major GHG emissions and the abatement potential of non-CO₂ GHGs on both national and global scales. Considering that some CSA management practices may have antagonistic effects on SOC sequestration and non-CO₂ GHG emissions (Guenet et al. 2021), and the resulting effects of different practices typically have large variations and may be non-additive (Yue et al. 2019), studies that fail to combine SOC sequestration and non-CO₂ GHG emissions (as well as multiple practices together) may lead to inconsistencies when making comparisons that would not provide effective assessments (Shang et al. 2021).

Global environmental changes such as climate change, elevated atmospheric CO₂ concentration, and N deposition have also substantially affected agricultural GHG emissions (Ren

et al. 2020; Ren et al. 2011). These factors vary over space and time in a highly heterogeneous geographical environment (e.g., diverse soil types and cropping systems) that can affect the effectiveness of CSA practices (Abdalla et al. 2013; Sun et al. 2020). This means a mitigation practice that is effective in one location or under certain conditions may not be effective elsewhere or under other conditions (Shang et al. 2021). In an example illustrating the importance of considering interactions between environmental factors and agricultural management practices, Huang et al. (2018) found that conversion from conventional tillage to no-tillage reduced GHG emissions in dry but not in humid climates. However, relatively few studies have quantitatively attributed changes in the net soil GHG balance of U.S. croplands to different drivers (including multiple management practices and environmental factors) over long-term periods (Moore et al., 2022), although such factorial contribution analyses are essential for accurately assessing impacts of these CSA practices and developing effective climate mitigation measures.

Field experiments provide feasible and reliable means of elucidating complex relationships of agricultural management practices and net soil GHG balance under multiple environmental changes (Plaza-Bonilla et al. 2018). However, directly extrapolating site-specific findings to large spatial areas is difficult due to unique environmental and management conditions of each site (Huang et al. 2022). Process-based terrestrial biosphere models (TBMs), with well-represented crop growth processes and agricultural management practices (e.g., N fertilization, tillage, irrigation, and rotation), as well as detailed hydrological, biophysical, and biogeochemical processes, can account for effects of spatial and temporal variations in environmental and management conditions on net soil GHG balance at large scales (Bondeau et al. 2007; McDermid et al. 2017; You et al. 2022). However, the simulation performance of TBMs is largely limited by the availability of high-quality model forcing datasets (i.e., introducing uncertainties in input data),

the lack of sufficient data for model calibration and validation (i.e., introducing uncertainties in model parameters), and the inadequate representation of relevant processes in the model (i.e., introducing uncertainties in model structures) (Fisher et al. 2014; Gurung et al. 2020; Ogle et al. 2010). In view of respective strengths and weaknesses of field observations and TBMs simulations, the integration of modeling and data would provide promising means to overcome these bottlenecks (Fer et al. 2021; Peng et al. 2011).

In this study, we quantified the combined effects of multiple management practices and environmental changes on the magnitude and spatiotemporal variations of net soil GHG balance in U.S. croplands using a model-data integration approach. The model used here is the Dynamic Land Ecosystem Model v4.0 (DLEM v4.0), which is a highly integrated process-based TBM. DLEM v4.0 is capable of simultaneously depicting biosphere-atmosphere exchanges of CO₂, N₂O, and CH₄, driven by multiple environmental forcings and management factors across site, regional, and global scales (Pan et al. 2021; Tian et al. 2010a; Tian et al. 2020b; Yao et al. 2020; You et al. 2022). High-resolution model forcing datasets were developed to drive the DLEM. Field observations of SOC sequestration rates and non-CO₂ GHG emissions under various management practices and environmental conditions on U.S. croplands were compiled to calibrate, validate, and corroborate model simulations. The objectives of this work were (1) to estimate the net soil GHG balance of U.S. croplands as driven by changes in multiple management practices (e.g., N fertilization, tillage, and irrigation), climate conditions, historical land use, atmospheric CO₂ concentration, and N deposition spanning from 1960 to 2018, (2) to examine the relative contributions of SOC sequestration of CO₂ and non-CO₂ GHG emissions to the net soil GHG balance of U.S. croplands, and (3) to quantify factorial contributions of different drivers to the spatial and temporal variations in net soil GHG balance across the country.

5.2 Materials and methods

5.2.1 Meta-data collection

A comprehensive literature search was conducted to identify peer-reviewed publications reporting *in-situ* soil GHG emissions from U.S. croplands using several databases including Google Scholar, Web of Science, and Scopus. Search keywords included “cropland or crop or corn or maize or soybean or wheat or rice”, “the United States or America or U.S. or USA”, “soil organic carbon or SOC”, “nitrous oxide or N₂O”, “methane or CH₄”, and/or “greenhouse gases or GHG”. To ensure the quality of compiled datasets, papers identified were further refined by the following criteria: (1) measurements were made in the field rather than in the laboratory; (2) ancillary information such as cropping systems, experimental year and duration, and applied management practices (e.g., N fertilizer use rate, tillage type, and irrigation) were provided; and (3) replicated field experiments were performed.

This search identified a total of 576 site-years of data representing 79 locations from 91 peer-reviewed publications (Figure 5-1), including 296 observations of N₂O emissions, 198 observations of CH₄ emissions, 19 observations of SOC sequestration rate, and 63 observations of SOC stock. Multiple management practices were involved in these observations, such as tillage, N fertilizer use, irrigation, manure application, and cover cropping. In addition, GetData Graph Digitizer software was used to extract exact values when data was presented in graphical form. Further details of the data compiled by meta-data collection can be found in You et al. (2023).

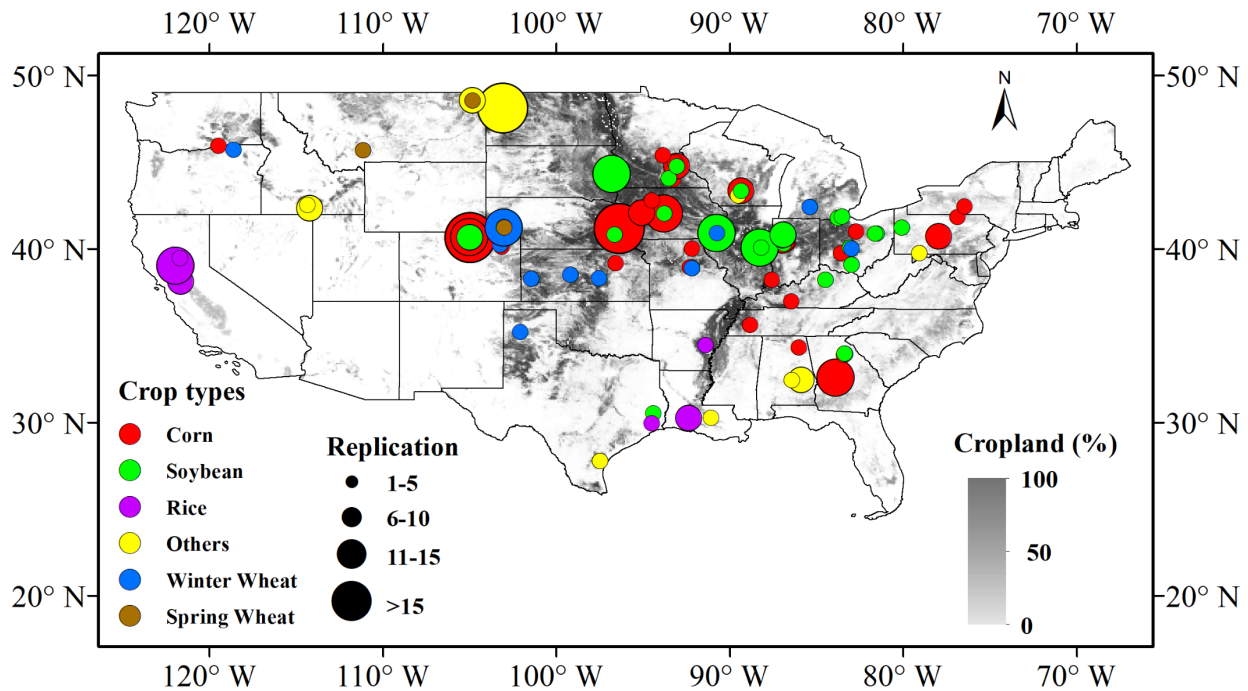


Figure 5-1. Spatial distribution of field sites included in this study. Different colors represent different crop types, in which “others” represent crop types not listed in the legend (e.g., barley, cotton, and sorghum). Point size represents the number of replications/observations at each site.

5.2.2 Model and forcing datasets

DLEM v4.0 is a highly integrated TBM that couples major biophysical, biogeochemical, and hydrological processes to quantify daily, spatially explicit carbon, water, and nutrient stocks and fluxes in terrestrial ecosystems and inland water systems at site, regional, and global scales (Pan et al. 2021; Tian et al. 2010a; Tian et al. 2020b; You et al. 2022). The simulation of terrestrial carbon, water, and nutrient dynamics is driven by multiple environmental forcings (e.g., climate change, atmospheric CO₂ concentration and N deposition) and various management factors (e.g., N fertilizer use rate, irrigation, and manure application). To meet cross-scale agricultural application needs (e.g., management guidance, climate change mitigation and adaptation), DLEM

v4.0 also includes mechanistic representations of dynamic crop growth and development processes, such as crop-specific phenological development, carbon allocation, yield formation, and biological N fixation (You et al. 2022). Additionally, agricultural management practices such as N fertilizer use, irrigation, tillage, manure application, dynamic crop rotation, cover cropping, and genetic improvements are also included. The well-represented crop growth processes and management practices enable DLEM v4.0 to simulate crop state variables (e.g., leaf area index and tissue biomass) across growth stages and biogeochemical fluxes and pools of carbon, N, and water related to agroecosystems (e.g., crop yield, GHG emissions, SOC, and nutrient leaching) across various spatial and temporal scales. More details about the representation of crop growth processes and different agricultural management practices in DLEM v4.0 are provided in You et al. (2022).

To drive DLEM v4.0, four types of long-term datasets at 5×5 arc-min spatial resolution were developed. These datasets include agricultural management practices (e.g., N fertilizer use rate, crop rotation, tillage, irrigation, and manure application), land use and land cover change (LULC), natural environmental changes (e.g., climate conditions, atmospheric CO₂ concentration, and N deposition), and other auxiliary data (e.g., soil properties and topography). More details about these datasets are presented in Section 2.3 in Chapter 2.

5.2.3 Model calibration, validation, and uncertainty analysis

DLEM has been widely validated and applied to estimate N₂O and CH₄ emissions and SOC stocks at multiple sites and large-scale regions including the U.S. (Huang et al. 2020; Lu et al. 2021; Tian et al. 2012a; Yu et al. 2018), North America (Tian et al. 2010b; Xu 2010; Xu et al. 2012), China (Ren et al. 2011; Zhang et al. 2020a), and across the globe (Friedlingstein et al. 2020b; Ren et al. 2020; Saunio et al. 2020a; Tian et al. 2020a). In this study, we rigorously

calibrated and validated DLEM, as driven by the forcing datasets developed in section 2.3, to better simulate SOC stock, and N₂O and CH₄ emissions in U.S. croplands using field observations compiled by the meta-data collection described in section 2.1. We calculated SOC sequestration rates as the differences in SOC stocks between two adjacent years. The potential loss or accumulation of SOC resulting from changes in soil properties due to conversions between different biome types (e.g., from forest to cropland) was not considered in our analysis. That means, the changes in SOC sequestration rate calculated in this study are entirely attributable to natural environmental factors and agricultural management activities. Several metrics were used to quantify model performance, including coefficient of determination (R^2), root mean square error (RMSE), and normalized root mean square error (NRMSE).

In total, 576 site-year measurements representing 79 U.S. cropland sites covering major cropping systems were used to calibrate, validate, and corroborate model simulations (Figure 5-1). The values of major parameters related to N₂O, CH₄, and SOC processes were determined through model calibration within a reasonable range of reported values in literature. Specifically, we first used default parameter values to run the model, and then we manually tuned the parameters within the reported ranges to obtain a close match between observed and simulated values for N₂O, CH₄, and SOC. We adopted the parameter set that obtained the minimal bias between the simulated and measured values across all calibration sites as the optimal parameters and used it for the regional simulation. Additionally, apart from calibrating parameters related to N₂O, CH₄, and SOC processes, we also calibrated the model with a focus on crop yields using data collected from the AmeriFlux Network, the Resilient Economic Agricultural Practices Project, and the United States Department of Agriculture-National Agricultural Statistics Service (further details can be found in You et al. (2022)). After model calibration, field observed N₂O, CH₄, and SOC data (excluding

the data used for model calibration) were utilized to evaluate the model performance. Generally, DLEM can well-simulate emissions of N_2O and CH_4 , SOC sequestration rates, and SOC stocks compared with field observations from the meta-data collection, in which RMSE (NRMSE) values were 0.16 g N/m^2 (9.6%), 1.5 g C/m^2 (4.4%), 156.9 g C/m^2 (19.3%), and 1929.1 g C/m^2 (17.6%), respectively, and the R^2 values were 0.6, 0.91, 0.46, and 0.64, respectively (Figure 5-2).

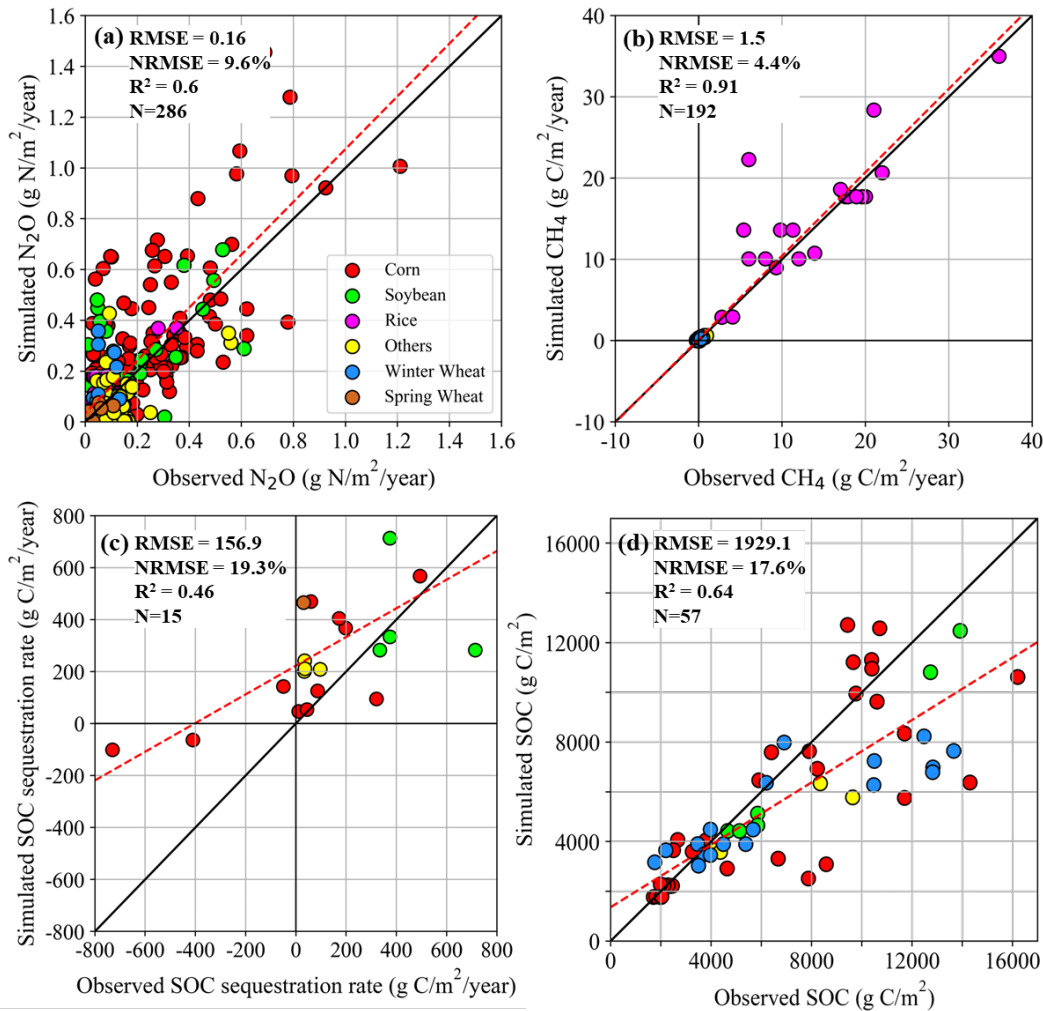


Figure 5-2. Site-scale comparisons of model estimates and field observations of N_2O (a), CH_4 (b), SOC sequestration rate (c), and SOC stocks (d) across different crop types. Dashed line is the regression of observed data and modeled results, and the solid line is the 1:1 line. Note that the SOC sequestration rates and SOC stocks here were reported by studies at various soil depths (e.g., 0~20 cm or 0~30 cm), thus we outputted simulation results at corresponding soil depths for

validation. “Others” represent all crop types not listed in the legend (e.g., barley, cotton, and sorghum). Additionally, due to the small amount of N₂O and CH₄ emissions (close to 0) at many sites, these datapoints are stacked near the origin, resulting in the number of datapoints on the graph appearing to be fewer than the actual number of datapoints involved in the statistical analysis.

We also quantified uncertainties in simulated regional SOC sequestration rate and N₂O and CH₄ fluxes in U.S. croplands due to uncertainties in model parameters (Tian et al. 2011; Xu 2010). Specifically, we first conducted a variance-based global sensitivity analysis for each major crop type to quantify the relative importance of model parameters in simulating SOC sequestration rate and N₂O and CH₄ emissions using the Sobol’ method (Sobol 1993b). We then identified parameters having a significant impact on simulated SOC sequestration rate and N₂O and CH₄ fluxes. Next, we used the Monte Carlo sampling scheme to generate an ensemble of 100 sets of these sensitive parameters by randomly varying their values within a 20% range of their calibrated values based on their respective probability distribution functions (Tian et al. 2011; You et al. 2022). Finally, we used the generated parameter sets as inputs for DLEM to simulate regional SOC sequestration rate and N₂O and CH₄ emissions from U.S. croplands. Uncertainties in simulated SOC sequestration rate and N₂O and CH₄ fluxes resulting from model parameters were represented by ± 1 standard deviations derived from these simulations.

5.2.4 Model implementation and experimental design

Implementation of DLEM v4.0 included three major steps: an equilibrium run, a spin-up run, and a transient run. The equilibrium run was driven by average annual climate data during the 1860s and other environmental factors in 1860. The equilibrium state was assumed to be reached when changes in carbon, N, and water pools between two consecutive 20-year periods were less than 0.5 g C m⁻² year⁻¹, 0.5 g N m⁻² year⁻¹, and 0.5 mm year⁻¹, respectively. The spin-up run was

driven by detrended climate data during the 1860s to eliminate fluctuations due to the transition from equilibrium run to transient run. Finally, the transient run was driven by historical data from 1860 to 2018. In this study, simulation results from 1960 to 2018 will be analyzed, so the model run during 1860-1959 is considered as a spin up for the slow soil biogeochemical cycles.

We designed 11 simulation experiments to distinguish factorial contributions of different drivers to spatial and temporal variations in the net soil GHG balance of U.S. croplands (Table 5-1). Attribution factors included N fertilization, tillage, irrigation, manure application, climate change, atmospheric CO₂ concentration and N deposition, and LULC. A reference run (S0) was performed by keeping all factors at the 1860 level to examine model fluctuations resulting from internal system dynamics. This run yielded background emissions with little human perturbation. An all-combined run (S1) was implemented by driving the model using all historically varying input forcings during 1860-2018 to represent the “best estimates” of SOC sequestration rate and N₂O and CH₄ emissions from U.S. croplands. Net changes in SOC sequestration rate and N₂O and CH₄ emissions driven by all factors were calculated as the difference between S1 and S0 simulations. Meanwhile, we performed 7 additional simulations (S2-S8) to investigate individual contributions of changes in each factor to annual variations in SOC sequestration rate and N₂O and CH₄ fluxes. Specifically, in each simulation one particular factor was kept constant at the 1860 level, while all other factors were set to vary over time, and the factorial contribution of this fixed factor was obtained by subtracting the simulation from the “all-combined” simulation (S1). Since LULC is usually accompanied by changes in the total input of management practices (e.g., manure and mineral fertilizer application), we calculated the factorial contribution of LULC by keeping all management factors constant at the 1860 level while varying other environmental factors with LULC turned on and off (Lu et al. 2021). Thus, the factorial contribution of LULC was calculated

as the difference between S9 and S10 (Table 5-1). In addition, because our analysis focused on the period 1960-2018, we calculated the factorial contribution of each factor relative to the average state in the 1950s. That means, the factorial contribution of each factor from 1960 to 2018 was calculated by subtracting the average state of the 1950s from its original factorial contribution.

Table 5-1. Factorial experiments to quantify the relative contributions of different drivers to changes in carbon dioxide, nitrous oxide, and methane emissions from U.S. croplands.

No.	Scenario	Nfer ^a	Tillage ^b	Irrigation ^c	Manure	Climate ^d	CO ₂	Ndep	LULC
S0	Reference	1860	1860	1860	1860	1860	1860	1860	1860
S1	All Combined	1860-2018	1860-2018	1860-2018	1860-2018	1860-2018	1860-2018	1860-2018	1860-2018
S2	Without N fertilization (Nfer)	1860	1860-2018	1860-2018	1860-2018	1860-2018	1860-2018	1860-2018	1860-2018
S3	Without Tillage	1860-2018	1860	1860-2018	1860-2018	1860-2018	1860-2018	1860-2018	1860-2018
S4	Without Irrigation	1860-2018	1860-2018	1860	1860-2018	1860-2018	1860-2018	1860-2018	1860-2018
S5	Without Manure	1860-2018	1860-2018	1860-2018	1860	1860-2018	1860-2018	1860-2018	1860-2018
S6	Without Climate	1860-2018	1860-2018	1860-2018	1860-2018	1860	1860-2018	1860-2018	1860-2018
S7	Without CO ₂	1860-2018	1860-2018	1860-2018	1860-2018	1860-2018	1860	1860-2018	1860-2018
S8	Without N deposition (Ndep)	1860-2018	1860-2018	1860-2018	1860-2018	1860-2018	1860-2018	1860	1860-2018
S9	Climate+CO ₂ +Ndep	1860	1860	1860	1860	1860-2018	1860-2018	1860-2018	1860
S10	Climate+CO ₂ +Ndep+LULC	1860	1860	1860	1860	1860-2018	1860-2018	1860-2018	1860-2018

^aWe assumed N fertilization rate before 1910 was kept constant at the 1910 level.

^bWe assumed tillage data before 1960 was kept constant at the 1960 level.

^cWe assumed irrigation data before 1950 was kept constant at the 1950 level.

^dClimate data in 1860 was the average climate condition during the 1860s.

5.2.5 Global warming potential calculation

The global warming potential (GWP) is an index to measure the integrated radiative forcing from the emission of 1 kg of a trace gas relative to that of CO₂ (Myhre et al. 2013). In GWP conversions, CO₂ is typically considered the reference gas with a GWP constant of 1. CH₄ and N₂O emissions can be converted to ‘CO₂-equivalents’ based on their respective GWP constants over a specified time horizon. To obtain a comprehensive assessment of the climatic impact of net soil GHG balance, we adopted the following equation to calculate the combined GWPs for SOC sequestration of CO₂ and N₂O and CH₄ emissions:

$$GWP = F_{CO_2-C} \times \frac{44}{12} \times GWP_{CO_2} + F_{N_2O-N} \times \frac{44}{28} \times GWP_{N_2O} + F_{CH_4-C} \times \frac{16}{12} \times GWP_{CH_4} \quad (1)$$

$$F_{CO_2-C} = -SOC_{CSR} \quad (2)$$

where F_{CO_2-C} , F_{N_2O-N} , and F_{CH_4-C} were annual fluxes of CO₂, N₂O, and CH₄, respectively; SOC_{CSR} was SOC sequestration rate; molecular weight conversion fractions 44/12, 44/28, and 16/12 were used to convert the mass of CO₂-C, N₂O-N, and CH₄-C into CO₂, N₂O, and CH₄, respectively; GWP_{CO_2} , GWP_{N_2O} and GWP_{CH_4} were GWP constants indicating radiative forcing of CO₂, N₂O, and CH₄ in terms of their CO₂ equivalents, and this study used the GWP values integrated over a time horizon of 100 years for CO₂, N₂O, and CH₄, which were 1, 265, and 28, respectively (Myhre et al. 2013).

5.3 Results

5.3.1 National budget and dynamics of net GHG balance in U.S. croplands

Our simulations showed that U.S. croplands acted as a net carbon sink during 1960-2018 with an average SOC sequestration rate of 13.2 ± 1.16 Tg C year⁻¹ (at a depth of 3.5m), and acted as a net source of N₂O and CH₄ with average emission rates of 0.39 ± 0.02 Tg N year⁻¹ and 0.21 ± 0.01 Tg C year⁻¹, respectively (Figure 5-3). Both SOC sequestration and N₂O and CH₄ fluxes in U.S. croplands exhibited large interannual variations during 1960-2018, but showed overall significant increasing trends (with respective rates of 0.429 Tg C year⁻², 0.003 Tg N year⁻², and 0.001 Tg C year⁻²).

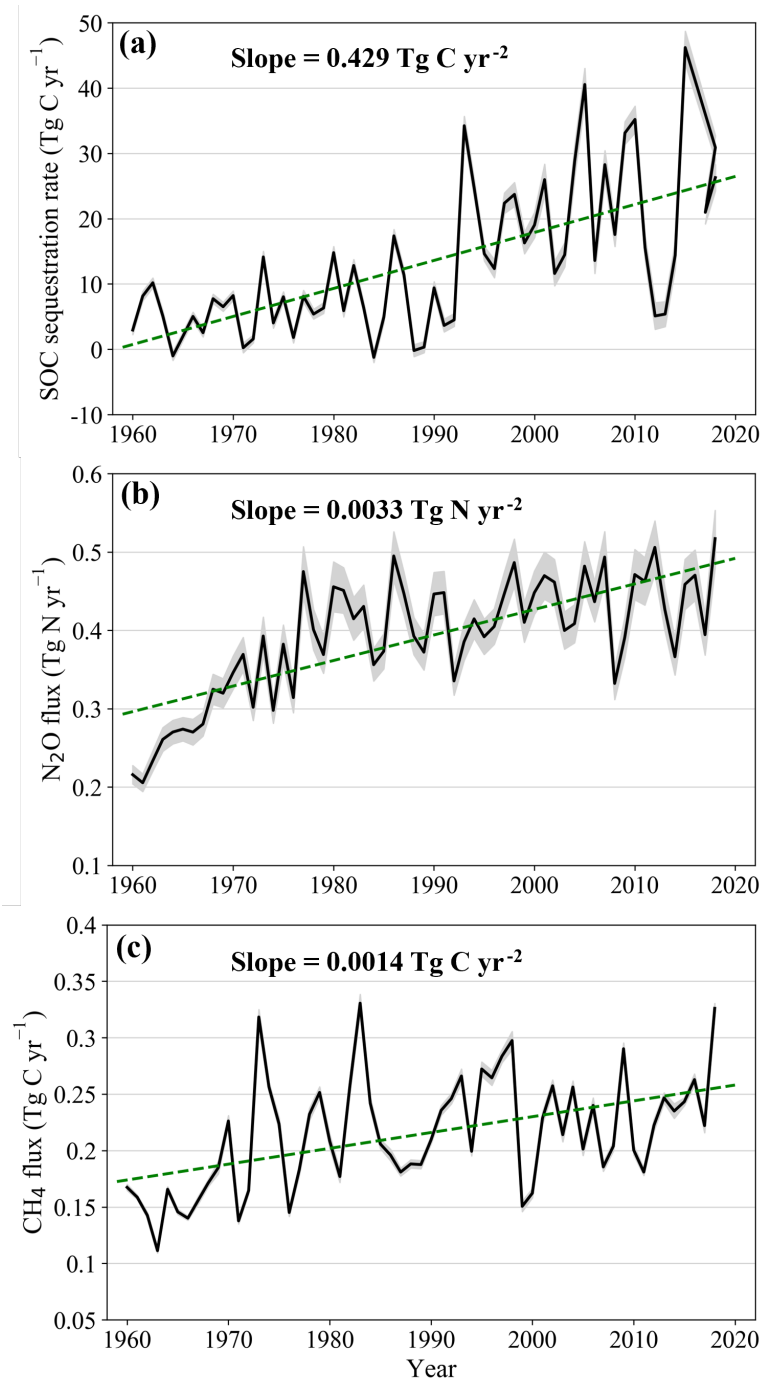


Figure 5-3. Temporal variations in national SOC sequestration rate (a) and fluxes of N₂O (b) and CH₄ (c) in U.S. agricultural soils from 1960 to 2018. Shaded area denotes the uncertainty ranges of SOC sequestration rate and N₂O and CH₄ fluxes (represented by ± 1 standard deviation).

Using the GWP100 metric (global warming potential on a 100-year time horizon), sequestered SOC in U.S. agricultural soils reduced national net GHG balance at an average rate of 48.4 ± 4.25 Tg CO₂-eq year⁻¹ during 1960-2018, whereas N₂O and CH₄ emissions contributed to net GHG balance at average rates of 162.41 ± 8.33 Tg CO₂-eq year⁻¹ and 7.84 ± 0.37 Tg CO₂-eq year⁻¹, respectively (Figure 5-4). Thus, non-CO₂ GHG emissions (i.e., sum of N₂O and CH₄ emissions) from U.S. croplands surpassed SOC sequestered, indicating that U.S. croplands acted as a net source of GHGs. Statistically, sequestered SOC offset ~28% of climate-warming effects resulting from non-CO₂ GHG emissions during 1960-2018, and the proportion of the offset increased over time. When considering both SOC sequestration and non-CO₂ GHG emissions, the average net GHG balance during 1960-2018 was estimated to be a GHG source of 121.9 ± 11.46 Tg CO₂-eq year⁻¹ and exhibited a substantial decadal variability, increasing from 98.32 ± 7.13 Tg CO₂-eq year⁻¹ in the 1960s to 156.01 ± 11.48 Tg CO₂-eq year⁻¹ in the 1980s and gradually decreasing to 115.87 ± 16.18 Tg CO₂-eq year⁻¹ in the 2010s.

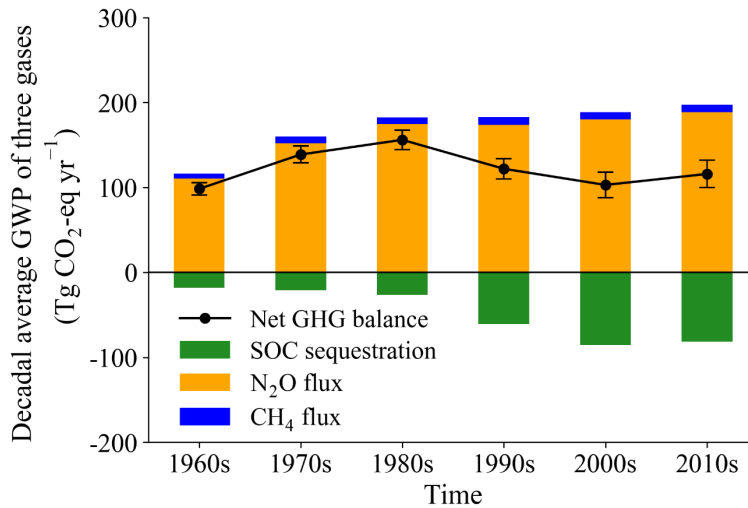


Figure 5-4. Temporal variations in national net greenhouse gas balance of U.S. croplands from the 1960s to the 2010s. Note that error bars represent ± 1 standard deviation of net greenhouse gas balance in each decade.

5.3.2 Spatial patterns of net GHG balance in U.S. croplands

With an average SOC sequestration rate of $\sim 12.5 \text{ g C m}^{-2} \text{ year}^{-1}$, simulation results over the study period indicated that most U.S. croplands acted as carbon sinks, with the Midwest, Southeast, and Northwest regions having relatively high SOC sequestration rates (Figure 5-5). The spatial pattern of N_2O emissions varied substantially across the country, with hotspots in the Midwest region having peak N_2O emission rates as high as $0.8 \text{ g N m}^{-2} \text{ year}^{-1}$. In contrast, the distribution of CH_4 flux was polarized, with a high CH_4 emission rate of $\sim 13 \text{ g C m}^{-2} \text{ year}^{-1}$ in the Mississippi Delta and the Sacramento Valley regions due to rice cultivation and rates approaching zero in other areas.

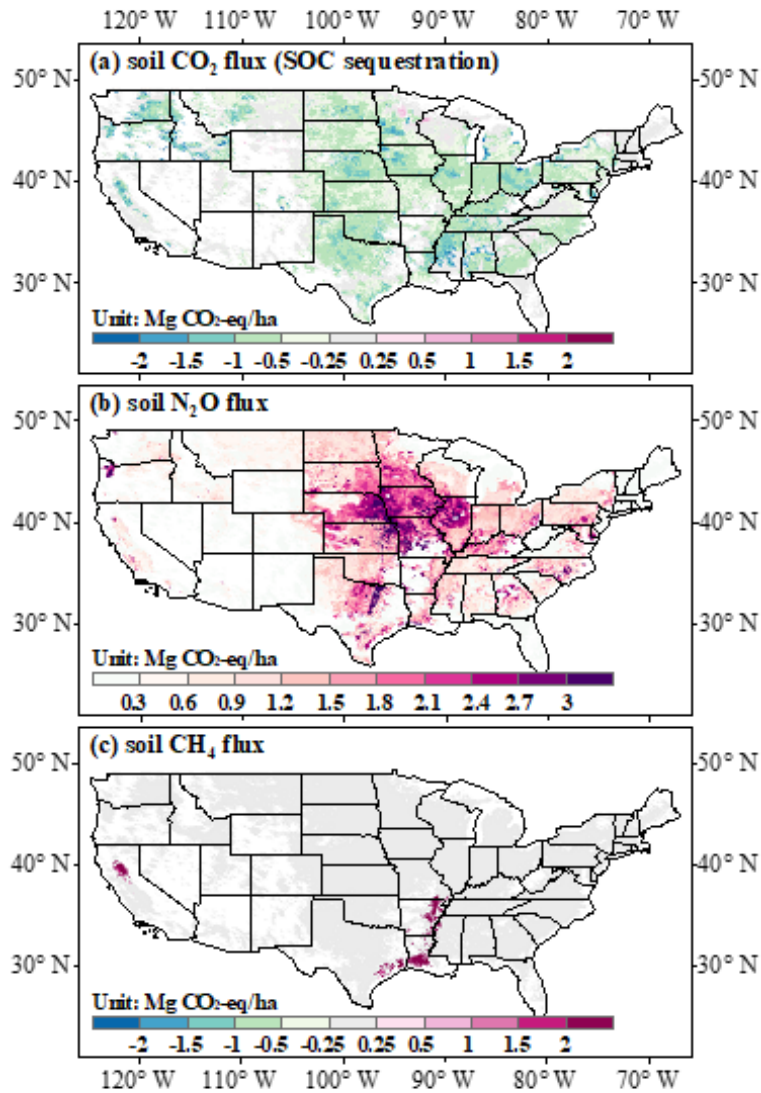


Figure 5-5. Spatial patterns of average annual SOC sequestration rate (a) and fluxes of N₂O (b) and CH₄ (c) in U.S. agricultural soils from 1960 to 2018. Note that negative values in soil fluxes represent uptake and positive values represent release. Therefore, negative soil CO₂ flux indicates SOC sequestration.

When simultaneously taking SOC sequestration and non-CO₂ GHG emissions into account, we found that the distribution of net soil GHG balance showed large spatial heterogeneity, with hotspots in the Midwest and Mississippi Delta regions where peak net soil GHG emissions were estimated to be higher than 2.5 Mg CO₂-eq ha⁻¹ year⁻¹ (Figure 5-6). In contrast, some U.S.

croplands (primarily located in Northwest regions) acted as a net sink of GHGs during the study period (representing ~38% of national cropland area), suggesting that sequestered SOC in these regions completely offset non-CO₂ GHG emissions. The net GHG balance of croplands varied substantially across different regional hubs of distinct climate characteristics. The Midwest hub was the largest contributor, accounting for ~47% of the national total net GHG balance during 1960-2018. The Northern Plains hub had the second largest share (~21%), followed by the Southern Plains and Southeast climate hubs (~14% each), while the Northwest, Southwest, and Northeast hubs accounted for less than 5%. The net GHG balance of the Midwest hub averaged 66.61 Tg CO₂-eq year⁻¹ over the study period, and its contribution to the national total net GHG balance exhibited large decadal variations, first increasing and then decreasing. In addition, simulation results showed that N₂O emissions greatly enhanced net GHG balance in all hubs, while CH₄ emissions only promoted net GHG balance in the Southeast and Southwest hubs.

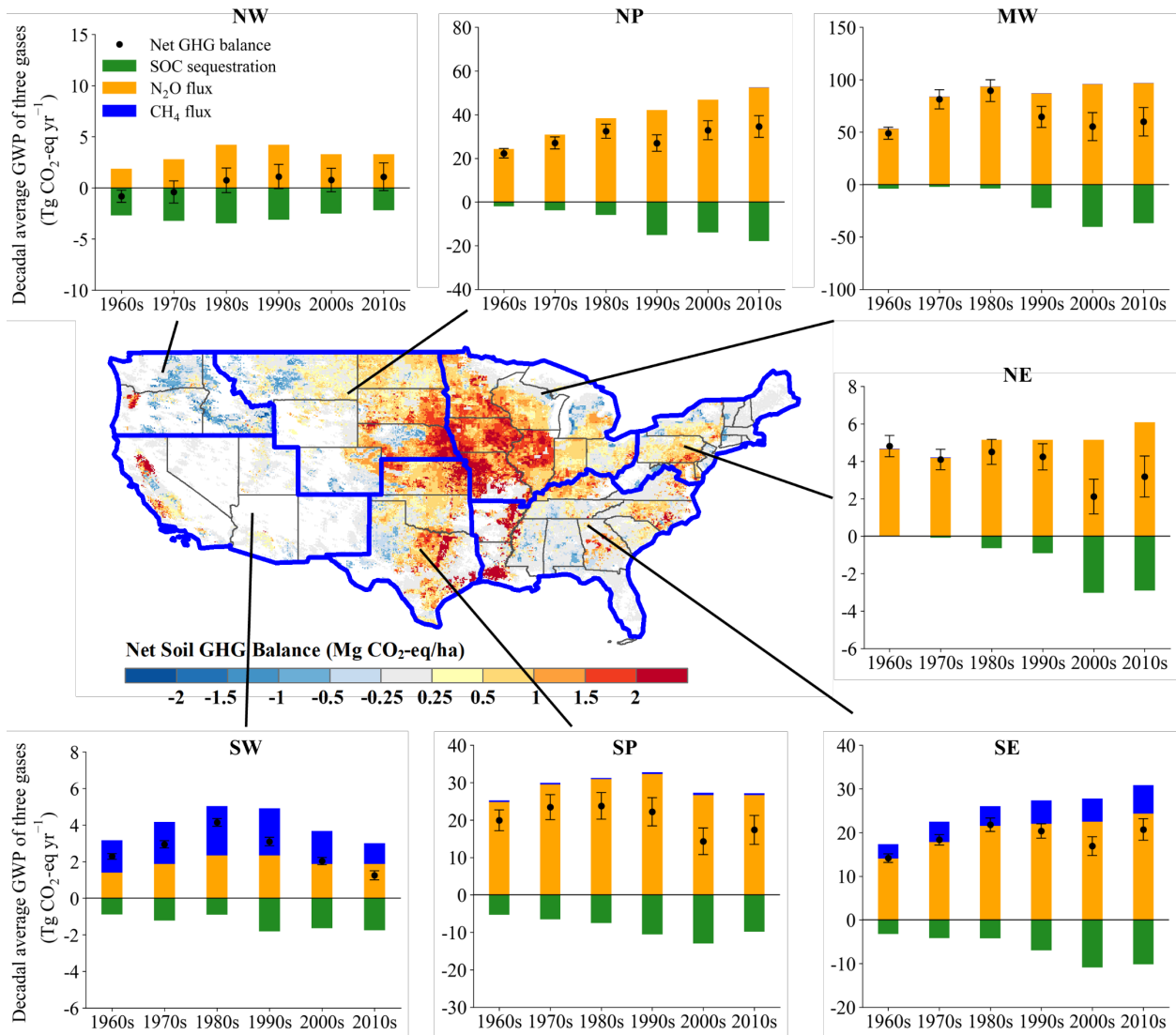


Figure 5-6. Spatial pattern of average annual net greenhouse gas balance of U.S. croplands from the 1960s to the 2010s. Note that error bars in insets represent ± 1 standard deviation of the net greenhouse gas balance in each decade. NW, NP, MW, NE, SW, SP, and SE represent the Northwest, Northern Plains, Midwest, Northeast, Southwest, Southern Plains, and Southeast climate hubs, respectively.

5.3.3 Relative contributions of SOC sequestration and N₂O and CH₄ emissions to net GHG balance

Given that non-CO₂ GHG emissions have surpassed the amount of SOC sequestered in U.S. croplands (Figure 5-4), we conducted a more comprehensive analysis of the spatial distribution of the relative contribution of SOC sequestration and N₂O and CH₄ emissions to the net GHG balance of U.S. croplands (Figure 5-7). Over the study period, soil N₂O emissions played a dominant role in controlling the net GHG balance of most croplands (e.g., the Midwest, Northern and Southern Plains hubs), followed by SOC sequestration, while CH₄ emissions only controlled the net GHG balance in the Mississippi Delta and Sacramento Valley regions, which are major rice growing areas. Meanwhile, the proportion of areas in the U.S. dominated by SOC sequestration increased over time, indicating an increasing role of SOC sequestration in controlling the net GHG balance across the country. For example, most Midwest croplands were dominated by N₂O emissions (red color) in the 1960s, but was controlled jointly by N₂O emission and SOC sequestration (yellow and green colors) in the 2010s.

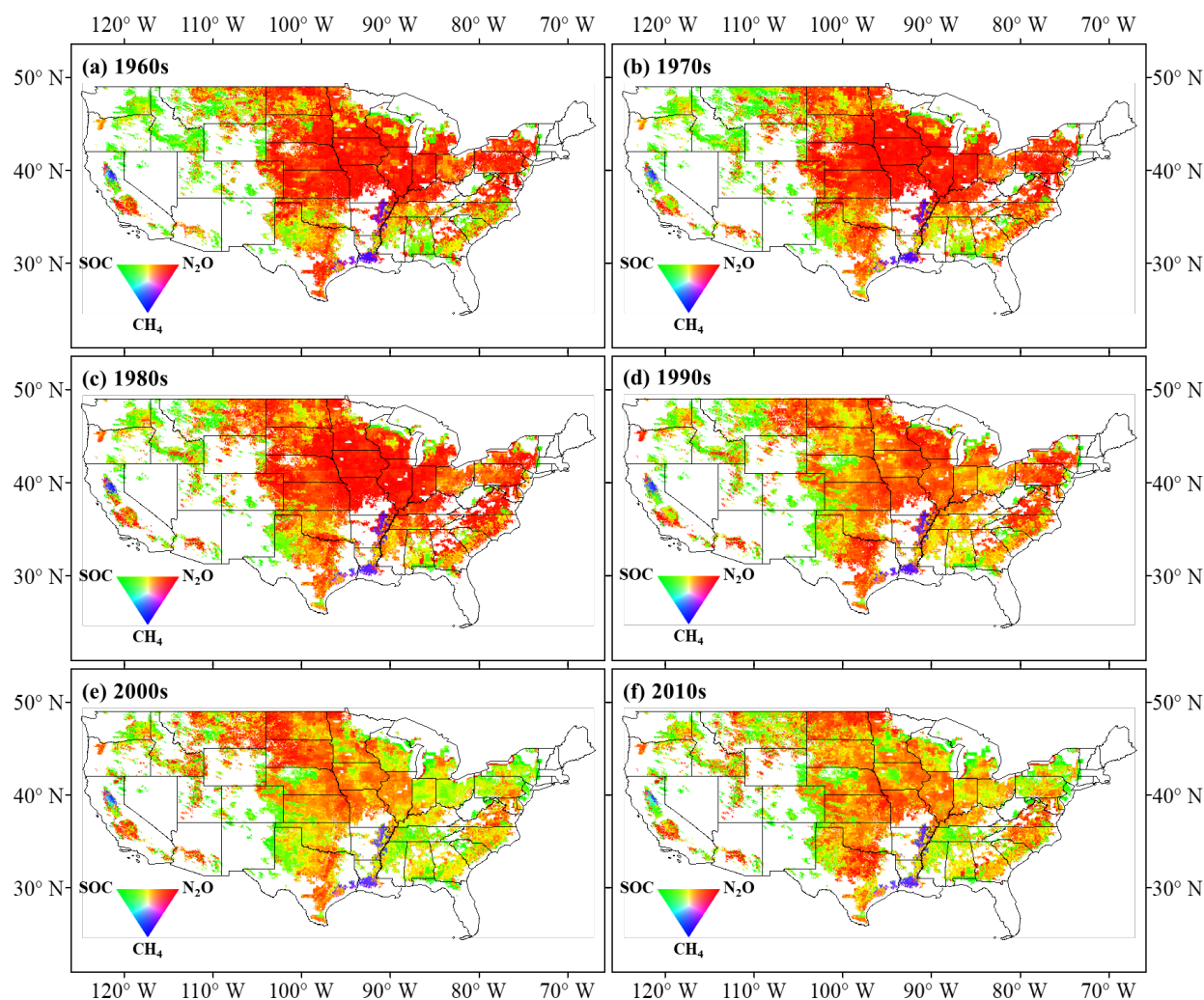


Figure 5-7. Spatial distributions of the relative contribution of SOC sequestration and emissions of N_2O and CH_4 to the net greenhouse gas balance of U.S. croplands from the 1960s to the 2010s.

5.3.4 Factorial contributions of multi-driver changes to net GHG balance in U.S. croplands

We further quantified the factorial contributions of key drivers, including multiple agricultural management practices and environmental forcings, to changes in the net soil GHG balance of U.S. croplands from 1960 to 2018 by setting up a series of simulation experiments (Table 5-1). Our results revealed that increased use of N fertilizer was the dominant factor driving changes in the net GHG balance of U.S. croplands in comparison to the average state in the 1950s. This increase

contributed to a net GHG balance increase of 79.9 Tg CO₂-eq year⁻¹ and roughly explained 47% of the total changes (Figure 5-8). Increased atmospheric N deposition and manure application also contributed to the increase in net GHG balance, with average rates of 8.3 Tg CO₂-eq year⁻¹ and 2.7 Tg CO₂-eq year⁻¹, respectively. Conversely, LULC resulted in a substantial reduction in the net GHG balance in U.S. croplands, with an average mitigation rate of 42.2 Tg CO₂-eq year⁻¹, which explained ~23% of the total changes. Rising atmospheric CO₂ concentration was the second-largest mitigator, reducing the net GHG balance at an average rate of 20.1 Tg CO₂-eq year⁻¹ and accounting for ~9% of the total changes. Reduced tillage and increased irrigated area were also effective in mitigating the net GHG balance in U.S. croplands, with average mitigation rates of 3.1 Tg CO₂-eq year⁻¹ and 1.9 Tg CO₂-eq year⁻¹, respectively. Additionally, compared to the 1950s, climate change initially reduced net GHG balance in U.S. croplands by an average rate of 12.5 Tg CO₂-eq year⁻¹ from the 1960s to the 1990s, but later increased net GHG balance at an average rate of 36.5 Tg CO₂-eq year⁻¹.

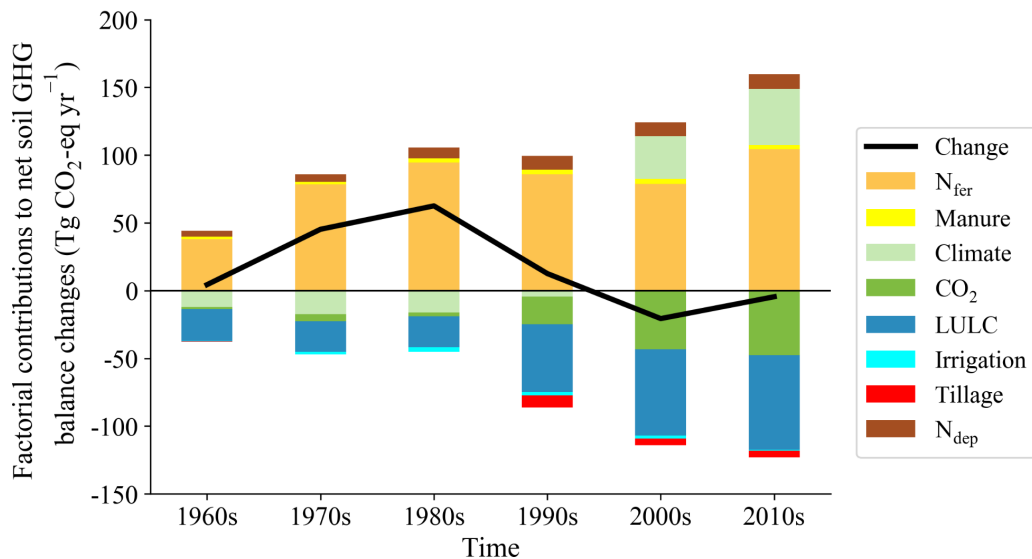


Figure 5-8. Factorial contributions of multiple agricultural management practices and environmental forcings to changes in the net greenhouse gas balance of U.S. croplands from the 1960s to the 2010s, in comparison to the average state in the 1950s. N_{fer} represents nitrogen

fertilizer use; Ndep represents atmospheric nitrogen deposition; LULC represents land use and land cover change (reflecting both cropland abandonment and expansion, as well as interannual crop rotation changes); and CO₂ represents atmospheric carbon dioxide concentration. Note that the sum of factorial contributions of individual drivers (i.e., stacked bars) does not equal net changes in the net greenhouse gas balance (i.e., black line) due to interaction effects.

5.4 Discussion

5.4.1 Comparison with previous studies

We compared our estimates of SOC sequestration rate and N₂O and CH₄ emissions in U.S. croplands with other regional estimates published (Table 5-2). Over the past six decades, our estimated SOC sequestration rate in U.S. croplands ranged from 4.9 ± 0.66 Tg C yr⁻¹ in the 1960s to 22.2 ± 1.91 Tg C yr⁻¹ in the 2010s and fell within the rate change reported by others (Ogle et al. 2010; Ogle et al. 2006; Pacala et al. 2001; Sleeter et al. 2018; West et al. 2008; Zhang et al. 2015a). For instance, Pacala et al. (2001) estimated the range of SOC sequestration rate in U.S. croplands to be 0~40 Tg C yr⁻¹, Ogle et al. (2010) estimated a net increase in SOC of 17.5 ± 2.9 Tg C yr⁻¹ during 1995-2000, and Sleeter et al. (2018) estimated a net accumulation of SOC in U.S. croplands of 32 Tg C yr⁻¹ during 1973-2010. Our estimated SOC sequestration rate was generally consistent with these studies. In addition, our estimated SOC sequestration rate showed an increasing trend during 1960-2018, partly due to the increasing atmospheric CO₂ concentration (Walker et al. 2021), improved crop management practices (e.g., N fertilizer use and irrigation) (Christopher and Lal 2007), and advancements in crop technologies (e.g., genetics and breeding). These factors have resulted in significant increases in biomass production and grain yield, leading to greater crop residue inputs into soils. For instance, productions of major crops such as corn and soybean have nearly tripled to quadrupled in the U.S. over the past several decades (USDA 2018). Despite the carbon allocation process in DLEM is driven by photosynthetic carbon supply and subject to

multiple environmental stresses (You et al. 2022), the simulated ratio of yield to whole plant biomass has remained relatively stable over time, suggesting that the simulated crop residues would have also significantly increased during the same period. Although the DLEM have accounted for the removal of a certain percentage of crop residues from the agroecosystem through tillage practices (50%, 25%, and 0% for conventional tillage, reduced tillage, and no tillage, respectively), we acknowledge that large uncertainties still exist concerning these residue removal percentages, potentially biasing the simulated residue inputs into soils and SOC sequestration rate. In terms of N₂O emissions, our estimates ranged from 0.27 ± 0.02 Tg N yr⁻¹ in the 1960s to 0.45 ± 0.03 Tg N yr⁻¹ in the 2010s, which were also comparable to previous studies (Chen et al. 2016; Del Grosso et al. 2006; EPA 2018; Griffis et al. 2013; Lu et al. 2021; Mummey et al. 1998; Tian et al. 2019). For example, the direct N₂O emissions from U.S. agricultural soils estimated by the Global N₂O Model Inter-comparison Project (NMIP) ranged from 0.3 Tg N yr⁻¹ to 0.62 Tg N yr⁻¹ during 2007-2016 (Tian et al. 2019; Xu et al. 2021), and our estimate of 0.44 Tg N yr⁻¹ fell well within this range. Additionally, our estimated CH₄ emissions (averaged to 0.23 Tg C yr⁻¹ over the last two decades) was also close to previous estimates centered on an annual emission rate of ~0.25 Tg C yr⁻¹ (EPA 2015; Sass et al. 1999; Tian et al. 2015a).

Overall, our individual estimates of SOC sequestration rate and N₂O and CH₄ emissions in U.S. croplands were in similar magnitudes and variation ranges as other regional estimates, but differences still exist, possibly due to uncertainties in forcing data and differences in estimation methods. However, unlike previous studies that focused solely on individual GHGs or SOC, our work quantified both SOC-sequestered CO₂ and non-CO₂ GHG emissions in U.S. croplands simultaneously. In this way, we could gain a more complete picture of the magnitude and spatiotemporal variations of the net soil GHG balance in U.S. croplands and uncover new insights.

For instance, by disentangling changes in the relative contribution of SOC sequestration and N₂O and CH₄ emissions in the net GHG balance of U.S. croplands over the past few decades, we found that N₂O emission and SOC sequestration jointly controlled the net GHG balance over most croplands in recent decades (Figure 5-7), highlighting the importance of considering both non-CO₂ GHG emissions and SOC sequestration when developing climate mitigation strategies. Meanwhile, our results revealed that the proportion of regions dominated by SOC sequestration increased over time. Possible explanations for this trend may include a gradual flattening of soil N₂O emissions due to stabilized N fertilization amounts, as well as increased crop biomass due to improved management practices and breeding and genetic technologies that in turn enhanced residue inputs into soils and promoted SOC sequestration. However, given that meeting growing food demand will inevitably lead to increased non-CO₂ GHG emissions due to fertilization (Cavigelli et al. 2012; Molotoks et al. 2018), and significant increases in crop biomass may be limited by advances in crop breeding and genetic technologies, our findings therefore re-emphasize the necessity of concurrently reducing non-CO₂ GHG emissions and enhancing SOC sequestration to achieve the goal of carbon-neutral agriculture, which is particularly important since non-CO₂ GHG emissions have already surpassed the amount of SOC-sequestered CO₂ in U.S. croplands. Additionally, our results showed that the adoption of reduced tillage practices led to a decrease in net GHG balance, which underscores the potential of leveraging CSA management practices (e.g., no-tillage and cover cropping) to mitigate net GHG balance in U.S. croplands (Huggins and Reganold 2008; Prokopy et al. 2019). Considering that some CSA practices could have quite different impacts (or even antagonistic) on SOC sequestration and N₂O and CH₄ emissions (Guenet et al. 2021), our estimation of net GHG balance also allows for more comprehensive and effective mitigation efforts to combat climate change.

Table 5-2. Comparisons of SOC sequestration rate and fluxes of N₂O and CH₄ from other studies.

Fluxes	Reported value	Reported region	Time period	Approaches	References
SOC sequestration rate (Tg C yr ⁻¹)	0 ~ 40	Entire U.S. croplands	1980-1990	Model + extrapolation	Pacala et al. (2001)
	13.5 ± 5.3	Entire U.S. croplands	1982-1997	Model	Ogle et al. (2006)
	14.4	U.S. Midwest croplands	1991-2000	Statistical approach	West et al. (2008)
	14.6 ± 3.2	Entire U.S. croplands	1990-1995	Process-based model	Ogle et al. (2010)
	17.5 ± 2.9	Entire U.S. croplands	1995-2000	Process-based model	Ogle et al. (2010)
	14	U.S. Midwest croplands	2000-2008	Process-based model	Zhang et al. (2015a)
	32	Entire U.S. croplands	1973-2010	Integrated model	Sleeter et al. (2018)
	7.2 ± 0.82	Entire U.S. croplands	1980s	Process-based model	This study
	16.6 ± 1.26	Entire U.S. croplands	1990s	Process-based model	This study
	23.3 ± 2.01	Entire U.S. croplands	2000s	Process-based model	This study
22.2 ± 1.91	Entire U.S. croplands	2010s	Process-based model	This study	
N ₂ O (Tg N yr ⁻¹)	0.448 ~ 0.478	Entire U.S. croplands	1990s	Model + extrapolation	Mummey et al. (1998)
	0.439	Entire U.S. croplands	1990-2003	Process-based model	Del Grosso et al. (2006)
	0.42 ± 0.05	U.S. Corn Belt croplands	2010	Extrapolation	Griffis et al. (2013)
	0.23 ± 0.18	U.S. Corn Belt croplands	2010	IPCC-based emission factor	Griffis et al. (2013)
	0.319 ± 0.184	U.S. Corn Belt croplands	2010	Atmospheric inversion	Chen et al. (2016)
	0.471 ± 0.326	U.S. Corn Belt croplands	2011	Atmospheric inversion	Chen et al. (2016)
	0.47 ~ 0.51	Entire U.S. croplands	1990-2016	IPCC Guidelines	EPA (2018)
	0.3 ± 0.2	Entire U.S. croplands	2007-2016	Model ensemble (NMIP)	Tian et al. (2019)
	0.51 ± 0.05	Entire U.S. croplands	2010s	Process-based model	Lu et al. (2021)
	0.43 ± 0.03	Entire U.S. croplands	2000s	Process-based model	This study
0.45 ± 0.03	Entire U.S. croplands	2010s	Process-based model	This study	
CH ₄ (Tg C yr ⁻¹)	0.04 ~ 0.47	U.S. rice paddies	/	IPCC Guidelines	Sass et al. (1999)
	0.3	North America croplands	1979-2018	Process-based model	Tian et al. (2015a)
	0.276	U.S. rice paddies	1990	IPCC Guidelines	EPA (2015)
	0.267	U.S. rice paddies	2005	IPCC Guidelines	EPA (2015)
	0.255	U.S. rice paddies	2011	IPCC Guidelines	EPA (2015)
	0.279	U.S. rice paddies	2012	IPCC Guidelines	EPA (2015)
	0.249	U.S. rice paddies	2013	IPCC Guidelines	EPA (2015)
	0.22 ± 0.0026	Entire U.S. croplands	2000s	Process-based model	This study
0.24 ± 0.0023	Entire U.S. croplands	2010s	Process-based model	This study	

5.4.2 Impacts of agricultural management factors and environmental changes on net GHG balance

Leveraging agricultural management practices to curb net GHG emissions from croplands has recently come under sharp focus due to their large mitigation potential, low cost and accompanying co-benefits such as improved soil and water quality and biodiversity maintenance (Fargione et al. 2018). As seen in other studies (Christopher and Lal 2007; Gerber et al. 2016; Lu et al. 2021), our factorial analysis indicated that N fertilization (including both synthetic N fertilizer use and manure application) contributed significantly to net GHG emissions from U.S. croplands (Figure 5-8). For instance, Lu et al. (2021) reported that N fertilization was the dominant driver contributing to N₂O emissions from U.S. agricultural soils, which increased N₂O emissions by 0.33 Tg N year⁻¹ since 1900. Synthetic N fertilizer use in U.S. croplands increased substantially (Figure 5-10(a) and Figure 5-11(a)), from 2.48 Tg N year⁻¹ in 1960 to 11.8 Tg N year⁻¹ in 2015, which greatly promoted non-CO₂ GHG emissions (especially N₂O) and exacerbated global climate warming. Although N addition could simultaneously stimulate SOC accumulation in croplands, we found that SOC climate benefits were largely offset by non-CO₂ GHG emissions (Figures 5-9(a) and (b)). Therefore, optimizing N fertilizer use rates is an imminent need for achieving overall maximum benefits among enhancing SOC sequestration, improving crop yields, and curbing non-CO₂ GHG emissions (Gerber et al. 2016; Xia et al. 2017). According to CRM's survey data, the proportion of U.S. croplands adopting no-tillage practices increased significantly over the past three decades (Figure 5-10(c) and Figure 5-11(c)). Our factorial analysis suggested that the tillage intensity reduction suppressed net GHG emissions, which was consistent with other U.S. studies (Huang et al. 2022; Lu et al. 2022; Yu et al. 2020). For instance, Yu et al. (2020) found that reduced tillage intensity in U.S. corn-soybean cropping systems contributed to a net SOC accumulation of 1.0 Tg

C year⁻¹ during 1998-2008. Lu et al. (2022) reported a reduction rate of -5.5 Tg CO₂-eq year⁻¹ in GHG emissions from U.S. corn-soybean cropping systems during 1998-2008 as a result of tillage intensity reduction. Huang et al. (2022) suggested attenuated soil CO₂ and N₂O emissions from Kentucky croplands under no-tillage compared to conventional tillage. Reduced net GHG emissions were also associated with an increase in irrigated U.S. cropland acreage over 1960-2018 (Figure 5-10(e) and Figure 5-11(e)). Irrigation possibly increased aboveground and belowground biomass and led to higher soil carbon inputs and SOC content (Bai et al. 2019; Blanco-Canqui et al. 2011). Additionally, we found that LULC reduced net GHG emissions from U.S. croplands (Figure 5-8) at an average mitigation rate of 42.2 Tg CO₂-eq year⁻¹, primarily due to the enhanced SOC sequestration amount in recent decades compared to the average state in the 1950s (Figure 5-9). Specifically, when compared with the 1950s, there has been a decrease in cropland area during recent decades (Figure 5-11(b)), coinciding with a notable increase in the SOC sequestration rate. However, it is worth noting that the national total accumulated SOC amount is determined by the multiplication of cropland area and the average SOC sequestration rate. Consequently, the recent reduction in cropland area is counterbalanced by the concurrent increase in SOC sequestration rate, to the extent that the total amount of SOC sequestered in U.S. croplands during recent decades still surpasses that of the 1950s. This dynamic interplay has ultimately led to a reduction in net GHG emissions due to LULC relative to the average state of the 1950s. Nevertheless, it should be noted that our current factorial analysis did not account for potential loss or accumulation of SOC resulting from changes in soil properties due to conversions between different biome types (e.g., from forest to cropland) and thus may lead to a biased contribution. Overall, our factorial analysis of multiple agricultural management practices indicated large potential for CSA practices (e.g., optimized N fertilizer use and reduced tillage) to mitigate non-

CO₂ GHG emissions and enhance SOC sequestration in agricultural soils, thereby leading to an overall reduction in net GHG emissions.

Changes in environmental factors, including elevated atmospheric N deposition and climatic conditions over the past two decades, also contributed significantly to net GHG emissions in U.S. croplands, while rising atmospheric CO₂ concentration served to mitigate GHG emissions (Figure 5-8). Despite considerable interannual variability, the increase in average surface air temperature in U.S. croplands over the past two decades compared with the 1950s (Figure 5-10(h) and Figure 5-11(h)) suggested a positive response of net GHG emissions to this climate warming. Similar positive responses were reported in other studies. For example, a meta-analysis by Liu et al. (2020a) found that an warming of ~1.5°C in rice paddies accelerated SOC decomposition by 12.9% and stimulated N₂O and CH₄ emissions by 35.2% and 23.4%, respectively. Xu et al. (2020) found that climate warming resulted in a net N₂O emission increase of 0.3 Tg N year⁻¹ in global croplands during 2000-2014. Warming can accelerate SOC decomposition, which enriches soil carbon substrate and N availability to promote soil microbial CO₂ production, methanogenesis, and denitrification processes (Carey et al. 2016; Pärn et al. 2018; Weier et al. 1993; Yvon-Durocher et al. 2014). Our factorial analysis of each individual gas also indicated a positive response of climate warming on SOC decomposition, and N₂O and CH₄ emissions (Figure 5-9). Additionally, the contrasting impacts of climate change on net GHG balance before and after the 1990s can be illustrated by the different response of N₂O emissions to climate change (Figure 5-9(b)). Positive effects of increased N deposition on net GHG emissions were also reported in other studies (Xu et al. 2020; Yang et al. 2021), where increased N availability can promote nitrification and denitrification processes and thereby N₂O emissions. Similar to findings of others (Ren et al. 2011; van Groenigen et al. 2011; Xu et al. 2020), our study showed a negative response to rising

atmospheric CO₂ levels, which can be ascribed to increased soil carbon inputs from CO₂ enhanced crop biomass production (van Groenigen et al. 2011).

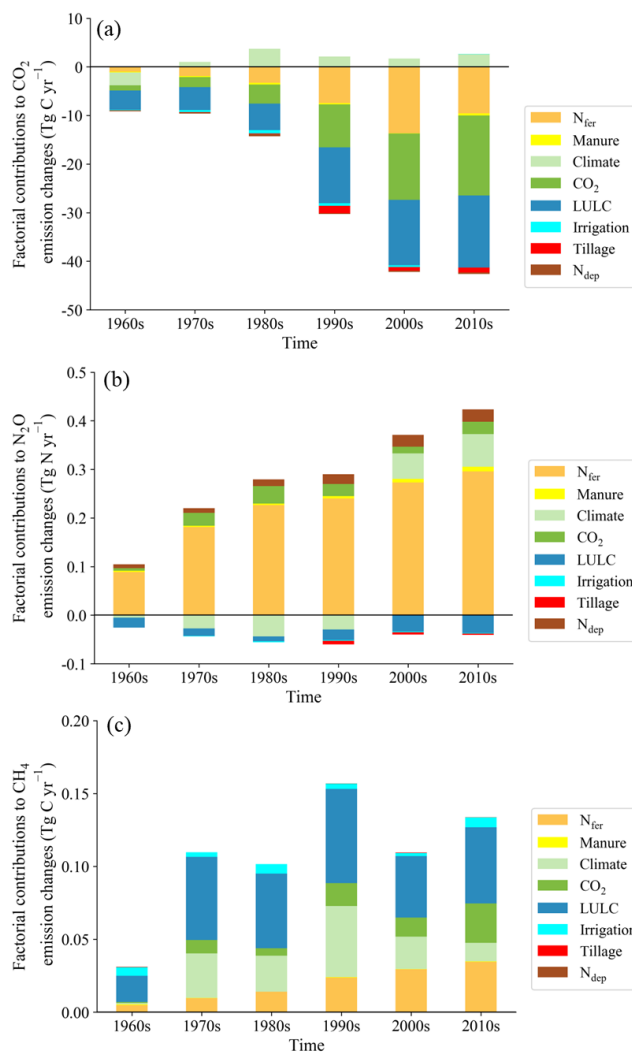


Figure 5-9. Factorial contributions of multiple agricultural management practices and environmental forcings to changes in CO₂ emission, N₂O emission, and CH₄ emission in U.S. croplands from the 1960s to the 2010s, in comparison to the average state in the 1950s. Note that the negative impact on CO₂ emissions indicates a positive impact on soil organic carbon sequestration. N_{fer} represents nitrogen fertilizer use; N_{dep} represents atmospheric nitrogen deposition; LULC represents land use and land cover change (reflecting both cropland abandonment and expansion, as well as interannual crop rotation changes); and CO₂ represents atmospheric carbon dioxide concentration.

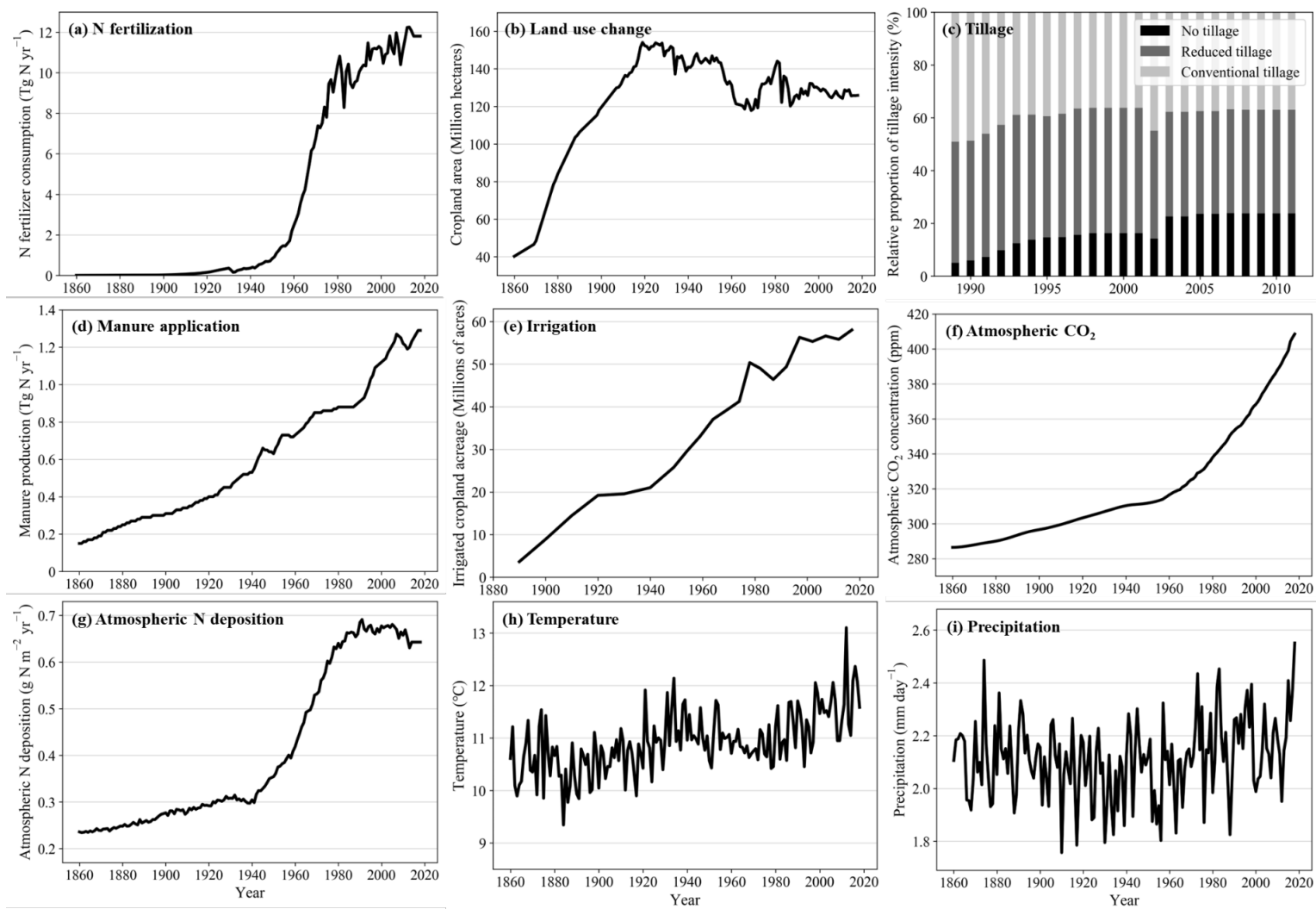


Figure 5-10. Temporal changes in nitrogen fertilization amount (a), cropland area (b), tillage intensity (c), manure production (d), irrigated cropland acreage (e), atmospheric CO₂ concentration (f), atmospheric nitrogen deposition (g), temperature (h), and precipitation (i) over the study period.

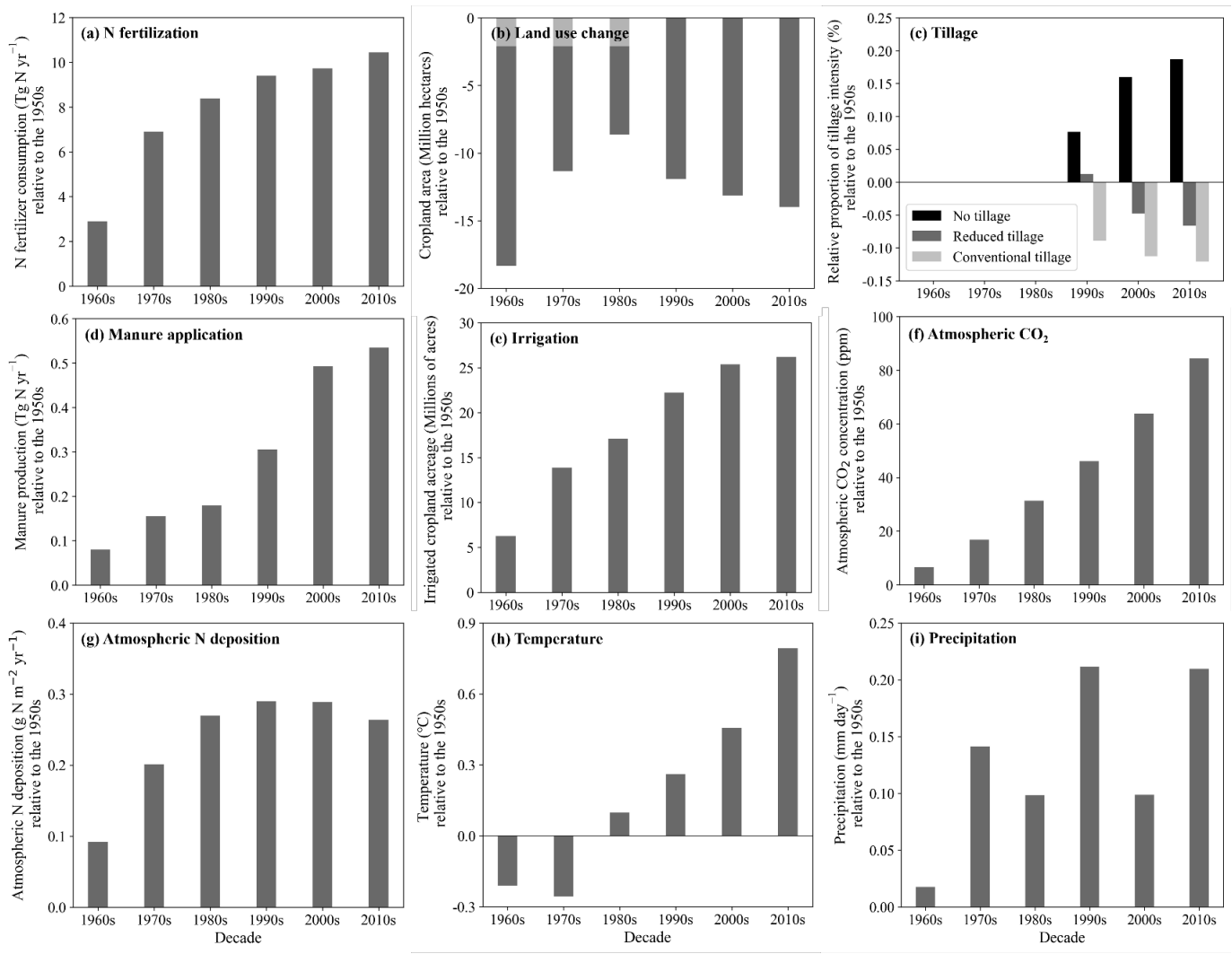


Figure 5-11. Decadal changes in various factors relative to the 1950s, including nitrogen fertilization amount (a), cropland area (b), tillage intensity (c), manure production (d), irrigated cropland acreage (e), atmospheric CO₂ concentration (f), atmospheric nitrogen deposition (g), temperature (h), and precipitation (i).

5.4.3 Uncertainty and future work

We have quantified uncertainty in the simulated net GHG balance associated with model parameters. However, other uncertainties persist (e.g., arising from input datasets and model structures), and further improvements are needed to enhance predictions. First, model forcing datasets could introduce some uncertainties. For example, the crop-specific N fertilization data was reconstructed based on state-level surveys, which could not reflect actual spatial variations of fertilizer use in both magnitude and timing. Tillage intensity data were only available at the county-level for recent decades, which lacked detailed spatial information and would inevitably introduce extrapolation errors in earlier years. Additionally, the assumption of crop residue removal percentage associated with tillage practices could also result in large uncertainties in the amount of crop residue inputs into soils, as it may diverge substantially from actual patterns. Therefore, joint community efforts to further improve model forcing datasets are needed. Second, the simplifications or omissions of real-world biophysical, biogeochemical, and hydrological processes in the DLEM, along with the under-representation of individual gas responses to various environmental factors, may also cause simulation biases. For example, the current DLEM representation of groundwater and irrigation practice (i.e., without considering irrigation amount and frequency) is relatively simple, which could lead to biased simulated soil moisture that, in turn, could affect GHG emission predictions. Furthermore, several studies have shown that soil freezing and thawing events induced non-negligible amounts of N₂O emissions (Del Grosso et al. 2022; Wagner-Riddle et al. 2017); nevertheless, the effects of soil freeze-thaw cycles on GHG emissions were not included in our current simulations and therefore constituted a possible source of deviation in our results. It is important to acknowledge that our model structures are inherently incomplete and uncertain, contributing significantly to the overall uncertainty in model simulations.

Accurately quantifying the uncertainty associated with model structures is a challenging task. Some studies have proposed using Bayesian methods to address this issue through conditioning model behavior on measurements (Engeland et al. 2005; Gurung et al. 2020). A notable example is the work of Gurung et al. (2020), who applied a Bayesian model analysis framework incorporating the sampling importance resampling scheme to assess uncertainties in both model parameters and structures. However, we concur with Marshall et al. (2007) that a robust estimation of model structural uncertainty requires the use of multiple models. Initiatives such as the Coupled Model Intercomparison Project (Eyring et al. 2016) and the Global N₂O Model Intercomparison Project (Tian et al. 2018) provide valuable templates for this purpose. Therefore, we call for the initiation of multiple model inter-comparison projects, with a specific focus on net GHG balance, to comprehensively quantify uncertainty from model structures. Finally, the lack of available spatialized and temporal datasets on SOC sequestration rate to constrain our model simulations over space and time could also result in significant uncertainty in our results, as SOC sequestration rates are typically much smaller than the magnitude of SOC pools. We will address these limitations in future studies to improve future simulation estimates.

5.5 Conclusion

This study quantified the magnitude and spatiotemporal variations of the net soil GHG balance in U.S. croplands from 1960 to 2018 using a model-data integration approach. We found that U.S. croplands acted as a net carbon sink during 1960-2018 with an average SOC sequestration rate of $13.2 \pm 1.16 \text{ Tg C year}^{-1}$ but a net source of N₂O and CH₄ with average emission rates of $0.39 \pm 0.02 \text{ Tg N year}^{-1}$ and $0.21 \pm 0.01 \text{ Tg C year}^{-1}$, respectively. When translated into the GWP100 metric, the simulated national average net GHG emission rate of U.S. agricultural soils was $121.9 \pm 11.46 \text{ Tg CO}_2\text{-eq yr}^{-1}$. Thus, net effort of soil GHG emission during this study period

was a contributor of climate warming. Sequestered SOC offset ~28% of the climate-warming effects resulting from non-CO₂ GHG emissions, and the proportion of this offset increased over time. The Midwest hub contributed ~47% of the national total net GHG balance, followed by the Northern Plains hub at ~21%. Our factorial analysis over 1960-2018 indicated that N fertilization use was the dominant factor promoting net GHG emissions from U.S. croplands and explained ~47% of the total changes, while reduced tillage and rising atmospheric CO₂ attenuated net GHG emissions from U.S. croplands. Our study emphasizes the need to consider both SOC sequestration and non-CO₂ GHG emissions when examining the role of soils in addressing climate change. It also underscores the critical role of CSA management practices (e.g., reduced tillage and optimized N fertilization) in mitigating the net GHG balance of U.S. croplands. Given the pressing need to curb climate change, future work could focus on predicting the long-term impacts and mitigation potential of various CSA management practices on the net GHG balance and crop production under different climate scenarios, with the ultimate goal of achieving carbon neutrality and sustainable agriculture.

References

- Abdalla, M., Osborne, B., Lanigan, G., Forristal, D., Williams, M., Smith, P., & Jones, M.B. (2013). Conservation tillage systems: a review of its consequences for greenhouse gas emissions. *Soil Use and Management*, 29, 199-209
- Bai, X., Huang, Y., Ren, W., Coyne, M., Jacinthe, P.A., Tao, B., Hui, D., Yang, J., & Matocha, C. (2019). Responses of soil carbon sequestration to climate-smart agriculture practices: A meta-analysis. *Global Change Biology*, 25, 2591-2606
- Blanco-Canqui, H., Mikha, M.M., Presley, D.R., & Claassen, M.M. (2011). Addition of cover crops enhances no-till potential for improving soil physical properties. *Soil Science Society of America Journal*, 75, 1471-1482
- Bondeau, A., Smith, P.C., Zaehle, S., Schaphoff, S., Lucht, W., Cramer, W., Gerten, D., Lotze-Campen, H., Müller, C., & Reichstein, M. (2007). Modelling the role of agriculture for the 20th century global terrestrial carbon balance. *Global Change Biology*, 13, 679-706
- Carey, J.C., Tang, J., Templer, P.H., Kroeger, K.D., Crowther, T.W., Burton, A.J., Dukes, J.S., Emmett, B., Frey, S.D., Hessel, M.A., Jiang, L., Machmuller, M.B., Mohan, J., Panetta, A.M., Reich, P.B., Reinsch, S., Wang, X., Allison, S.D., Bamminger, C., Bridgham, S., Collins, S.L., de Dato, G., Eddy, W.C., Enquist, B.J., Estiarte, M., Harte, J., Henderson, A., Johnson, B.R., Larsen, K.S., Luo, Y., Marhan, S., Melillo, J.M., Peñuelas, J., Pfeifer-Meister, L., Poll, C., Rastetter, E., Reinmann, A.B., Reynolds, L.L., Schmidt, I.K., Shaver, G.R., Strong, A.L., Suseela, V., & Tietema, A. (2016). Temperature response of soil respiration

- largely unaltered with experimental warming. *Proceedings of the National Academy of Sciences*, *113*, 13797-13802
- Cavigelli, M.A., Grosso, S.J.D., Liebig, M.A., Snyder, C.S., Fixen, P.E., Venterea, R.T., Leytem, A.B., McLain, J.E., & Watts, D.B. (2012). US agricultural nitrous oxide emissions: context, status, and trends. *Frontiers in Ecology and the Environment*, *10*, 537-546
- Chen, X., Cui, Z., Fan, M., Vitousek, P., Zhao, M., Ma, W., Wang, Z., Zhang, W., Yan, X., & Yang, J. (2014). Producing more grain with lower environmental costs. *Nature*, *514*, 486-489
- Chen, Z., Griffis, T.J., Millet, D.B., Wood, J.D., Lee, X., Baker, J.M., Xiao, K., Turner, P.A., Chen, M., Zobitz, J., & Wells, K.C. (2016). Partitioning N₂O emissions within the U.S. Corn Belt using an inverse modeling approach. *Global Biogeochemical Cycles*, *30*, 1192-1205
- Christopher, S.F., & Lal, R. (2007). Nitrogen management affects carbon sequestration in North American cropland soils. *Critical Reviews in Plant Sciences*, *26*, 45-64
- Del Grosso, S.J., Ogle, S.M., Nevison, C., Gurung, R., Parton, W.J., Wagner-Riddle, C., Smith, W., Winiwarter, W., Grant, B., Tenuta, M., Marx, E., Spencer, S., & Williams, S. (2022). A gap in nitrous oxide emission reporting complicates long-term climate mitigation. *Proceedings of the National Academy of Sciences*, *119*, e2200354119
- Del Grosso, S.J., Ogle, S.M., Parton, W.J., & Breidt, F.J. (2010). Estimating uncertainty in N₂O emissions from US cropland soils. *Global Biogeochemical Cycles*, *24*
- Del Grosso, S.J., Parton, W.J., Mosier, A.R., Walsh, M.K., Ojima, D.S., & Thornton, P.E. (2006). DAYCENT national-scale simulations of nitrous oxide emissions from cropped soils in the United States. *Journal of environmental quality*, *35*, 1451-1460
- Engeland, K., Xu, C.-Y., & Gottschalk, L. (2005). Assessing uncertainties in a conceptual water balance model using Bayesian methodology. *Hydrological Sciences Journal*, *50*, null-63
- EPA (2013). Chapter V: Agriculture Sector. In *Global Mitigation of Non-CO₂ Greenhouse Gases: 2010–2030*. United States Environmental Protection Agency (EPA), Office of Atmospheric Programs, Washington, DC.
- EPA (2015). Inventory of US greenhouse gas emissions and sinks: 1990–2013. *Tech. Rep. EPA 430-R-15-003*
- EPA (2018). Inventory of US greenhouse gas emissions and sinks: 1990–2016. *Tech. Rep. EPA 430-R-18-003*
- EPA (2021). Inventory of US greenhouse gas emissions and sinks: 1990–2019. *Tech. Rep. EPA 430-R-21-003*
- Eyring, V., Bony, S., Meehl, G.A., Senior, C.A., Stevens, B., Stouffer, R.J., & Taylor, K.E. (2016). Overview of the Coupled Model Intercomparison Project Phase 6 (CMIP6) experimental design and organization. *Geosci. Model Dev.*, *9*, 1937-1958
- FAO (2013). *Climate-smart agriculture: sourcebook*. Rome, Italy: Food and Agriculture Organization of the United Nations (FAO)
- Fargione, J.E., Bassett, S., Boucher, T., Bridgham, S.D., Conant, R.T., Cook-Patton, S.C., Ellis, P.W., Falcucci, A., Fourqurean, J.W., & Gopalakrishna, T. (2018). Natural climate solutions for the United States. *Science advances*, *4*, eaat1869
- Fer, I., Gardella, A.K., Shiklomanov, A.N., Campbell, E.E., Cowdery, E.M., De Kauwe, M.G., Desai, A., Duveneck, M.J., Fisher, J.B., Haynes, K.D., Hoffman, F.M., Johnston, M.R., Kooper, R., LeBauer, D.S., Mantooth, J., Parton, W.J., Poulter, B., Quaife, T., Raiho, A., Schaefer, K., Serbin, S.P., Simkins, J., Wilcox, K.R., Viskari, T., & Dietze, M.C. (2021). Beyond ecosystem modeling: A roadmap to community cyberinfrastructure for ecological data-model integration. *Global Change Biology*, *27*, 13-26
- Fisher, J.B., Huntzinger, D.N., Schwalm, C.R., & Sitch, S. (2014). Modeling the terrestrial biosphere. *Annual review of environment and resources*, *39*, 91-123
- Foley, J.A., Ramankutty, N., Brauman, K.A., Cassidy, E.S., Gerber, J.S., Johnston, M., Mueller, N.D., O'Connell, C., Ray, D.K., West, P.C., Balzer, C., Bennett, E.M., Carpenter, S.R., Hill, J., Monfreda, C., Polasky, S., Rockström, J., Sheehan, J., Siebert, S., Tilman, D., & Zaks, D.P.M. (2011). Solutions for a cultivated planet. *Nature*, *478*, 337-342
- Friedlingstein, P., O'Sullivan, M., Jones, M.W., Andrew, R.M., Hauck, J., Olsen, A., Peters, G.P., Peters, W., Pongratz, J., Sitch, S., Le Quééré, C., Canadell, J.G., Ciais, P., Jackson, R.B., Alin, S., Aragão, L.E.O.C., Arneeth, A., Arora, V., Bates, N.R., Becker, M., Benoit-Cattin, A., Bittig, H.C., Bopp, L., Bultan, S., Chandra, N., Chevallier, F., Chini, L.P., Evans, W., Florentie, L., Forster, P.M., Gasser, T., Gehlen, M., Gilfillan, D., Gkritzalis, T., Gregor, L., Gruber, N., Harris, I., Hartung, K., Haverd, V., Houghton, R.A., Ilyina, T., Jain, A.K., Joetzjer, E., Kadono, K., Kato, E., Kitidis, V., Korsbakken, J.I., Landschützer, P., Lefèvre, N., Lenton, A., Lienert, S., Liu, Z., Lombardozzi, D., Marland, G., Metzl, N., Munro, D.R., Nabel, J.E.M.S., Nakaoka, S.I., Niwa, Y., O'Brien, K., Ono, T., Palmer, P.I., Pierrot, D., Poulter, B., Resplandy, L., Robertson, E., Rödenbeck, C., Schwinger, J., Séférian, R., Skjelvan, I., Smith, A.J.P., Sutton, A.J.,

- Tanhua, T., Tans, P.P., Tian, H., Tilbrook, B., van der Werf, G., Vuichard, N., Walker, A.P., Wanninkhof, R., Watson, A.J., Willis, D., Wiltshire, A.J., Yuan, W., Yue, X., & Zaehle, S. (2020). Global Carbon Budget 2020. *Earth System Science Data*, *12*, 3269-3340
- Gerber, J.S., Carlson, K.M., Makowski, D., Mueller, N.D., Garcia de Cortazar-Atauri, I., Havlík, P., Herrero, M., Launay, M., O'Connell, C.S., & Smith, P. (2016). Spatially explicit estimates of N₂O emissions from croplands suggest climate mitigation opportunities from improved fertilizer management. *Global Change Biology*, *22*, 3383-3394
- Griffis, T.J., Lee, X., Baker, J.M., Russelle, M.P., Zhang, X., Venterea, R., & Millet, D.B. (2013). Reconciling the differences between top-down and bottom-up estimates of nitrous oxide emissions for the U.S. Corn Belt. *Global Biogeochemical Cycles*, *27*, 746-754
- Guenet, B., Gabrielle, B., Chenu, C., Arrouays, D., Balesdent, J., Bernoux, M., Bruni, E., Caliman, J.-P., Cardinael, R., Chen, S., Ciais, P., Desbois, D., Fouche, J., Frank, S., Henault, C., Lugato, E., Naipal, V., Nesme, T., Obersteiner, M., Pellerin, S., Powlson, D.S., Rasse, D.P., Rees, F., Soussana, J.-F., Su, Y., Tian, H., Valin, H., & Zhou, F. (2021). Can N₂O emissions offset the benefits from soil organic carbon storage? *Global Change Biology*, *27*, 237-256
- Gurung, R.B., Ogle, S.M., Breidt, F.J., Williams, S.A., & Parton, W.J. (2020). Bayesian calibration of the DayCent ecosystem model to simulate soil organic carbon dynamics and reduce model uncertainty. *Geoderma*, *376*, 114529
- Huang, Y., Ren, W., Grove, J., Poffenbarger, H., Jacobsen, K., Tao, B., Zhu, X., & McNear, D. (2020). Assessing synergistic effects of no-tillage and cover crops on soil carbon dynamics in a long-term maize cropping system under climate change. *Agricultural and Forest Meteorology*, *291*, 108090
- Huang, Y., Ren, W., Wang, L., Hui, D., Grove, J.H., Yang, X., Tao, B., & Goff, B. (2018). Greenhouse gas emissions and crop yield in no-tillage systems: A meta-analysis. *Agriculture, Ecosystems & Environment*, *268*, 144-153
- Huang, Y., Tao, B., Yang, Y., Zhu, X., Yang, X., Grove, J.H., & Ren, W. (2022). Simulating no-tillage effects on crop yield and greenhouse gas emissions in Kentucky corn and soybean cropping systems: 1980–2018. *Agricultural systems*, *197*, 103355
- Huggins, D.R., & Reganold, J.P. (2008). No-till: the quiet revolution. *Scientific American*, *299*, 70-77
- Hunter, M.C., Smith, R.G., Schipanski, M.E., Atwood, L.W., & Mortensen, D.A. (2017). Agriculture in 2050: Recalibrating Targets for Sustainable Intensification. *Bioscience*, *67*, 386-391
- IPCC (2019). Climate Change and Land: an IPCC special report on climate change, desertification, land degradation, sustainable land management, food security, and greenhouse gas fluxes in terrestrial ecosystems [P.R. Shukla, J. Skea, E. Calvo Buendia, V. Masson-Delmotte, H.-O. Pörtner, D. C. Roberts, P. Zhai, R. Slade, S. Connors, R. van Diemen, M. Ferrat, E. Haughey, S. Luz, S. Neogi, M. Pathak, J. Petzold, J. Portugal Pereira, P. Vyas, E. Huntley, K. Kissick, M. Belkacemi, J. Malley, (eds.)]
- Lal, R. (2018). Digging deeper: A holistic perspective of factors affecting soil organic carbon sequestration in agroecosystems. *Global Change Biology*, *24*, 3285-3301
- Linquist, B.A., Marcos, M., Adviento-Borbe, M.A., Anders, M., Harrell, D., Linscombe, S., Reba, M.L., Runkle, B.R.K., Tarpley, L., & Thomson, A. (2018). Greenhouse gas emissions and management practices that affect emissions in US rice systems. *Journal of environmental quality*, *47*, 395-409
- Liu, S., Zheng, Y., Ma, R., Yu, K., Han, Z., Xiao, S., Li, Z., Wu, S., Li, S., & Wang, J. (2020). Increased soil release of greenhouse gases shrinks terrestrial carbon uptake enhancement under warming. *Global Change Biology*, *26*, 4601-4613
- Lokupitiya, E., Paustian, K., Easter, M., Williams, S., Andrén, O., & Kätterer, T. (2012). Carbon balances in US croplands during the last two decades of the twentieth century. *Biogeochemistry*, *107*, 207-225
- Lu, C., Yu, Z., Hennessy, D.A., Feng, H., Tian, H., & Hui, D. (2022). Emerging weed resistance increases tillage intensity and greenhouse gas emissions in the US corn–soybean cropping system. *Nature Food*, *3*, 266-274
- Lu, C., Yu, Z., Zhang, J., Cao, P., Tian, H., & Nevison, C. (2021). Century-long changes and drivers of soil nitrous oxide (N₂O) emissions across the contiguous United States. *Global Change Biology*, *28*, 2505– 2524
- Marshall, L., Nott, D., & Sharma, A. (2007). Towards dynamic catchment modelling: a Bayesian hierarchical mixtures of experts framework. *Hydrological Processes*, *21*, 847-861
- McDermid, S.S., Mearns, L.O., & Ruane, A.C. (2017). Representing agriculture in Earth System Models: Approaches and priorities for development. *Journal of Advances in Modeling Earth Systems*, *9*, 2230-2265
- Miralles-Wilhelm, F. (2021). Nature-based solutions in agriculture: Sustainable management and conservation of land, water and biodiversity. In Rome, Italy: Food and Agriculture Organization of the United Nations

- Molotoks, A., Stehfest, E., Doelman, J., Albanito, F., Fitton, N., Dawson, T.P., & Smith, P. (2018). Global projections of future cropland expansion to 2050 and direct impacts on biodiversity and carbon storage. *Global Change Biology*, *24*, 5895-5908
- Mosier, A.R., Halvorson, A.D., Reule, C.A., & Liu, X.J. (2006). Net global warming potential and greenhouse gas intensity in irrigated cropping systems in northeastern Colorado. *Journal of environmental quality*, *35*, 1584-1598
- Mumme, D.L., Smith, J.L., & Bluhm, G. (1998). Assessment of alternative soil management practices on N₂O emissions from US agriculture. *Agriculture, Ecosystems & Environment*, *70*, 79-87
- Myhre, G., Shindell, D., Bréon, F.M., Collins, W., Fuglestedt, J., Huang, J., Koch, D., Lamarque, J.F., Lee, D., Mendoza, B., Nakajima, T., Robock, A., Stephens, G., Takemura, T., & Zhang, H. (2013). Anthropogenic and natural radiative forcing. In *Climate Change 2013: The Physical Science Basis. Contribution of Working Group I to the Fifth Assessment Report of the Intergovernmental Panel on Climate Change*. T.F. Stocker, D. Qin, G.-K. Plattner, M. Tignor, S.K. Allen, J. Doschung, A. Nauels, Y. Xia, V. Bex, and P.M. Midgley, Eds. Cambridge University Press, pp. 659-740.
- Ogle, S.M., Breidt, F.J., Easter, M., Williams, S., Killian, K., & Paustian, K. (2010). Scale and uncertainty in modeled soil organic carbon stock changes for US croplands using a process-based model. *Global Change Biology*, *16*, 810-822
- Ogle, S.M., Breidt, F.J., & Paustian, K. (2006). Bias and variance in model results associated with spatial scaling of measurements for parameterization in regional assessments. *Global Change Biology*, *12*, 516-523
- Pacala, S.W., Hurtt, G.C., Baker, D., Peylin, P., Houghton, R.A., Birdsey, R.A., Heath, L., Sundquist, E.T., Stallard, R.F., Ciais, P., Moorcroft, P., Caspersen, J.P., Shevliakova, E., Moore, B., Kohlmaier, G., Holland, E., Gloor, M., Harmon, M.E., Fan, S.M., Sarmiento, J.L., Goodale, C.L., Schimel, D., & Field, C.B. (2001). Consistent Land- and Atmosphere-Based U.S. Carbon Sink Estimates. *Science*, *292*, 2316-2320
- Pan, S., Bian, Z., Tian, H., Yao, Y., Najjar, R.G., Friedrichs, M.A.M., Hofmann, E.E., Xu, R., & Zhang, B. (2021). Impacts of Multiple Environmental Changes on Long-term Nitrogen Loading from the Chesapeake Bay Watershed. *Journal of Geophysical Research: Biogeosciences*, *126*, e2020JG005826
- Pärn, J., Verhoeven, J.T.A., Butterbach-Bahl, K., Dise, N.B., Ullah, S., Aasa, A., Egorov, S., Espenberg, M., Järveoja, J., & Jauhiainen, J. (2018). Nitrogen-rich organic soils under warm well-drained conditions are global nitrous oxide emission hotspots. *Nature Communications*, *9*, 1-8
- Peng, C., Guiot, J., Wu, H., Jiang, H., & Luo, Y. (2011). Integrating models with data in ecology and palaeoecology: advances towards a model–data fusion approach. *Ecology Letters*, *14*, 522-536
- Penman, J., Kruger, D., Galbally, I.E., Hiraishi, T., Nyenzi, B., Emmanuel, S., Buendia, L., Hoppaus, R., Martinsen, T., & Meijer, J. (2000). Good practice guidance and uncertainty management in national greenhouse gas inventories
- Pittelkow, C.M., Liang, X., Linquist, B.A., van Groenigen, K.J., Lee, J., Lundy, M.E., van Gestel, N., Six, J., Venterea, R.T., & van Kessel, C. (2015). Productivity limits and potentials of the principles of conservation agriculture. *Nature*, *517*, 365-368
- Plaza-Bonilla, D., Álvaro-Fuentes, J., Bareche, J., Pareja-Sánchez, E., Justes, É., & Cantero-Martínez, C. (2018). No-tillage reduces long-term yield-scaled soil nitrous oxide emissions in rainfed Mediterranean agroecosystems: A field and modelling approach. *Agriculture, Ecosystems & Environment*, *262*, 36-47
- Prokopy, L.S., Floress, K., Arbuckle, J.G., Church, S.P., Eanes, F.R., Gao, Y., Gramig, B.M., Ranjan, P., & Singh, A.S. (2019). Adoption of agricultural conservation practices in the United States: Evidence from 35 years of quantitative literature. *Journal of Soil and Water Conservation*, *74*, 520-534
- Ren, W., Banger, K., Tao, B., Yang, J., Huang, Y., & Tian, H. (2020). Global pattern and change of cropland soil organic carbon during 1901-2010: Roles of climate, atmospheric chemistry, land use and management. *Geography and Sustainability*, *1*, 59-69
- Ren, W., Tian, H., Xu, X., Liu, M., Lu, C., Chen, G., Melillo, J., Reilly, J., & Liu, J. (2011). Spatial and temporal patterns of CO₂ and CH₄ fluxes in China's croplands in response to multifactor environmental changes. *Tellus B: Chemical and Physical Meteorology*, *63*, 222-240
- Robertson, G.P., & Grace, P.R. (2004). Greenhouse gas fluxes in tropical and temperate agriculture: the need for a full-cost accounting of global warming potentials. *Tropical Agriculture in Transition—Opportunities for Mitigating Greenhouse Gas Emissions?* (pp. 51-63): Springer
- Sass, R.L., Fisher Jr, F.M., Ding, A., & Huang, Y. (1999). Exchange of methane from rice fields: National, regional, and global budgets. *Journal of Geophysical Research: Atmospheres*, *104*, 26943-26951
- Saunio, M., Stavert, A.R., Poulter, B., Bousquet, P., Canadell, J.G., Jackson, R.B., Raymond, P.A., Dlugokencky, E.J., Houweling, S., Patra, P.K., Ciais, P., Arora, V.K., Bastviken, D., Bergamaschi, P., Blake, D.R.,

- Brailsford, G., Bruhwiler, L., Carlson, K.M., Carrol, M., Castaldi, S., Chandra, N., Crevoisier, C., Crill, P.M., Covey, K., Curry, C.L., Etiope, G., Frankenberg, C., Gedney, N., Hegglin, M.I., Höglund-Isaksson, L., Hugelius, G., Ishizawa, M., Ito, A., Janssens-Maenhout, G., Jensen, K.M., Joos, F., Kleinen, T., Krummel, P.B., Langenfelds, R.L., Laruelle, G.G., Liu, L., Machida, T., Maksyutov, S., McDonald, K.C., McNorton, J., Miller, P.A., Melton, J.R., Morino, I., Müller, J., Murguía-Flores, F., Naik, V., Niwa, Y., Noce, S., O'Doherty, S., Parker, R.J., Peng, C., Peng, S., Peters, G.P., Prigent, C., Prinn, R., Ramonet, M., Regnier, P., Riley, W.J., Rosentreter, J.A., Segers, A., Simpson, I.J., Shi, H., Smith, S.J., Steele, L.P., Thornton, B.F., Tian, H., Tohjima, Y., Tubiello, F.N., Tsuruta, A., Viovy, N., Voulgarakis, A., Weber, T.S., van Weele, M., van der Werf, G.R., Weiss, R.F., Worthy, D., Wunch, D., Yin, Y., Yoshida, Y., Zhang, W., Zhang, Z., Zhao, Y., Zheng, B., Zhu, Q., Zhu, Q., & Zhuang, Q. (2020). The Global Methane Budget 2000–2017. *Earth System Science Data*, *12*, 1561-1623
- Shang, Z., Abdalla, M., Xia, L., Zhou, F., Sun, W., & Smith, P. (2021). Can cropland management practices lower net greenhouse emissions without compromising yield? *Global Change Biology*, *27*, 4657–4670
- Sleeter, B.M., Liu, J., Daniel, C., Rayfield, B., Sherba, J., Hawbaker, T.J., Zhu, Z., Selmants, P.C., & Loveland, T.R. (2018). Effects of contemporary land-use and land-cover change on the carbon balance of terrestrial ecosystems in the United States. *Environmental Research Letters*, *13*, 045006
- Smith, P., Lanigan, G., Kutsch, W.L., Buchmann, N., Eugster, W., Aubinet, M., Ceschia, E., Béziat, P., Yeluripati, J.B., & Osborne, B. (2010). Measurements necessary for assessing the net ecosystem carbon budget of croplands. *Agriculture, Ecosystems & Environment*, *139*, 302-315
- Sobol, I.M. (1993). Sensitivity Estimates for Nonlinear Mathematical Models. *Math Modeling & Computational Experiment*, *1*, 407-414
- Sohi, S.P. (2012). Carbon storage with benefits. *Science*, *338*, 1034-1035
- Sun, W., Canadell, J.G., Yu, L., Yu, L., Zhang, W., Smith, P., Fischer, T., & Huang, Y. (2020). Climate drives global soil carbon sequestration and crop yield changes under conservation agriculture. *Global Change Biology*, *26*, 3325-3335
- Thompson, R.L., Lassaletta, L., Patra, P.K., Wilson, C., Wells, K.C., Gressent, A., Koffi, E.N., Chipperfield, M.P., Winiwarter, W., Davidson, E.A., Tian, H., & Canadell, J.G. (2019). Acceleration of global N₂O emissions seen from two decades of atmospheric inversion. *Nature Climate Change*, *9*, 993-998
- Tian, H., Chen, G., Liu, M., Zhang, C., Sun, G., Lu, C., Xu, X., Ren, W., Pan, S., & Chappelka, A. (2010a). Model estimates of net primary productivity, evapotranspiration, and water use efficiency in the terrestrial ecosystems of the southern United States during 1895–2007. *Forest Ecology and Management*, *259*, 1311-1327
- Tian, H., Chen, G., Lu, C., Xu, X., Hayes, D.J., Ren, W., Pan, S., Huntzinger, D.N., & Wofsy, S.C. (2015). North American terrestrial CO₂ uptake largely offset by CH₄ and N₂O emissions: toward a full accounting of the greenhouse gas budget. *Climatic Change*, *129*, 413-426
- Tian, H., Chen, G., Zhang, C., Liu, M., Sun, G., Chappelka, A., Ren, W., Xu, X., Lu, C., Pan, S., Chen, H., Hui, D., McNulty, S., Lockaby, G., & Vance, E. (2012). Century-Scale Responses of Ecosystem Carbon Storage and Flux to Multiple Environmental Changes in the Southern United States. *Ecosystems*, *15*, 674-694
- Tian, H., Lu, C., Ciais, P., Michalak, A.M., Canadell, J.G., Saikawa, E., Huntzinger, D.N., Gurney, K.R., Sitch, S., Zhang, B., Yang, J., Bousquet, P., Bruhwiler, L., Chen, G., Dlugokencky, E., Friedlingstein, P., Melillo, J., Pan, S., Poulter, B., Prinn, R., Saunio, M., Schwalm, C.R., & Wofsy, S.C. (2016). The terrestrial biosphere as a net source of greenhouse gases to the atmosphere. *Nature*, *531*, 225-228
- Tian, H., Xu, R., Canadell, J.G., Thompson, R.L., Winiwarter, W., Suntharalingam, P., Davidson, E.A., Ciais, P., Jackson, R.B., Janssens-Maenhout, G., Prather, M.J., Regnier, P., Pan, N., Pan, S., Peters, G.P., Shi, H., Tubiello, F.N., Zaehle, S., Zhou, F., Arneth, A., Battaglia, G., Berthet, S., Bopp, L., Bouwman, A.F., Buitenhuis, E.T., Chang, J., Chipperfield, M.P., Dangal, S.R.S., Dlugokencky, E., Elkins, J.W., Eyre, B.D., Fu, B., Hall, B., Ito, A., Joos, F., Krummel, P.B., Landolfi, A., Laruelle, G.G., Lauerwald, R., Li, W., Lienert, S., Maavara, T., MacLeod, M., Millet, D.B., Olin, S., Patra, P.K., Prinn, R.G., Raymond, P.A., Ruiz, D.J., van der Werf, G.R., Vuichard, N., Wang, J., Weiss, R.F., Wells, K.C., Wilson, C., Yang, J., & Yao, Y. (2020a). A comprehensive quantification of global nitrous oxide sources and sinks. *Nature*, *586*, 248-256
- Tian, H., Xu, R., Pan, S., Yao, Y., Bian, Z., Cai, W.-J., Hopkinson, C.S., Justic, D., Lohrenz, S., Lu, C., Ren, W., & Yang, J. (2020b). Long-Term Trajectory of Nitrogen Loading and Delivery From Mississippi River Basin to the Gulf of Mexico. *Global Biogeochemical Cycles*, *34*, e2019GB006475

- Tian, H., Xu, X., Liu, M., Ren, W., Zhang, C., Chen, G., & Lu, C. (2010b). Spatial and temporal patterns of CH₄ and N₂O fluxes in terrestrial ecosystems of North America during 1979–2008: application of a global biogeochemistry model. *Biogeosciences*, *7*, 2673-2694
- Tian, H., Xu, X., Lu, C., Liu, M., Ren, W., Chen, G., Melillo, J., & Liu, J. (2011). Net exchanges of CO₂, CH₄, and N₂O between China's terrestrial ecosystems and the atmosphere and their contributions to global climate warming. *Journal of Geophysical Research: Biogeosciences*, *116*
- Tian, H., Yang, J., Lu, C., Xu, R., Canadell, J.G., Jackson, R.B., Arneeth, A., Chang, J., Chen, G., & Ciais, P. (2018). The global N₂O model intercomparison project. *Bulletin of the American Meteorological Society*, *99*, 1231-1251
- Tian, H., Yang, J., Xu, R., Lu, C., Canadell, J.G., Davidson, E.A., Jackson, R.B., Arneeth, A., Chang, J., & Ciais, P. (2019). Global soil nitrous oxide emissions since the preindustrial era estimated by an ensemble of terrestrial biosphere models: Magnitude, attribution, and uncertainty. *Global Change Biology*, *25*, 640-659
- Tilman, D., Balzer, C., Hill, J., & Befort, B.L. (2011). Global food demand and the sustainable intensification of agriculture. *Proceedings of the National Academy of Sciences*, *108*, 20260
- USDA, N. (2018). Crop production historical track records. In: United States Department of Agriculture, National Agricultural Statistics ...
- van Groenigen, K.J., Osenberg, C.W., & Hungate, B.A. (2011). Increased soil emissions of potent greenhouse gases under increased atmospheric CO₂. *Nature*, *475*, 214-216
- Wagner-Riddle, C., Congreves, K.A., Abalos, D., Berg, A.A., Brown, S.E., Ambadan, J.T., Gao, X., & Tenuta, M. (2017). Globally important nitrous oxide emissions from croplands induced by freeze–thaw cycles. *Nature Geoscience*, *10*, 279-283
- Walker, A.P., De Kauwe, M.G., Bastos, A., Belmecheri, S., Georgiou, K., Keeling, R.F., McMahon, S.M., Medlyn, B.E., Moore, D.J.P., Norby, R.J., Zaehle, S., Anderson-Teixeira, K.J., Battipaglia, G., Brienen, R.J.W., Cabugao, K.G., Cailleret, M., Campbell, E., Canadell, J.G., Ciais, P., Craig, M.E., Ellsworth, D.S., Farquhar, G.D., Fatichi, S., Fisher, J.B., Frank, D.C., Graven, H., Gu, L., Haverd, V., Heilman, K., Heimann, M., Hungate, B.A., Iversen, C.M., Joos, F., Jiang, M., Keenan, T.F., Knauer, J., Körner, C., Leshyk, V.O., Leuzinger, S., Liu, Y., MacBean, N., Malhi, Y., McVicar, T.R., Penuelas, J., Pongratz, J., Powell, A.S., Riutta, T., Sabot, M.E.B., Schleucher, J., Sitch, S., Smith, W.K., Sulman, B., Taylor, B., Terrer, C., Torn, M.S., Treseder, K.K., Trugman, A.T., Trumbore, S.E., van Mantgem, P.J., Voelker, S.L., Whelan, M.E., & Zuidema, P.A. (2021). Integrating the evidence for a terrestrial carbon sink caused by increasing atmospheric CO₂. *New Phytologist*, *229*, 2413-2445
- Watson, R.T., Noble, I.R., Bolin, B., Ravindranath, N.H., Verardo, D.J., & Dokken, D.J. (2000). *Land use, land-use change and forestry: a special report of the Intergovernmental Panel on Climate Change*. Cambridge University Press
- Weier, K.L., Doran, J.W., Power, J.F., & Walters, D.T. (1993). Denitrification and the dinitrogen/nitrous oxide ratio as affected by soil water, available carbon, and nitrate. *Soil Science Society of America Journal*, *57*, 66-72
- West, T.O., Brandt, C.C., Wilson, B.S., Hellwinckel, C.M., Tyler, D.D., Marland, G., De La Torre Ugarte, D.G., Larson, J.A., & Nelson, R.G. (2008). Estimating Regional Changes in Soil Carbon with High Spatial Resolution. *Soil Science Society of America Journal*, *72*, 285-294
- Xia, L., Lam, S.K., Chen, D., Wang, J., Tang, Q., & Yan, X. (2017). Can knowledge-based N management produce more staple grain with lower greenhouse gas emission and reactive nitrogen pollution? A meta-analysis. *Global Change Biology*, *23*, 1917-1925
- Xu, R., Tian, H., Pan, N., Thompson, R.L., Canadell, J.G., Davidson, E.A., Nevison, C., Winiwarter, W., Shi, H., Pan, S., Chang, J., Ciais, P., Dangal, S.R.S., Ito, A., Jackson, R.B., Joos, F., Lauerwald, R., Lienert, S., Maavara, T., Millet, D.B., Raymond, P.A., Regnier, P., Tubiello, F.N., Vuichard, N., Wells, K.C., Wilson, C., Yang, J., Yao, Y., Zaehle, S., & Zhou, F. (2021). Magnitude and Uncertainty of Nitrous Oxide Emissions From North America Based on Bottom-Up and Top-Down Approaches: Informing Future Research and National Inventories. *Geophysical Research Letters*, *48*, e2021GL095264
- Xu, R., Tian, H., Pan, S., Prior, S.A., Feng, Y., & Dangal, S.R.S. (2020). Global N₂O Emissions From Cropland Driven by Nitrogen Addition and Environmental Factors: Comparison and Uncertainty Analysis. *Global Biogeochemical Cycles*, *34*, e2020GB006698
- Xu, X. (2010). Modeling methane and nitrous oxide exchanges between the atmosphere and terrestrial ecosystems over North America in the context of multifactor global change. In: Auburn University
- Xu, X.F., Tian, H.Q., Chen, G.S., Liu, M.L., Ren, W., Lu, C.Q., & Zhang, C. (2012). Multifactor controls on terrestrial N₂O flux over North America from 1979 through 2010. *Biogeosciences*, *9*, 1351-1366

- Yang, Y., Liu, L., Zhang, F., Zhang, X., Xu, W., Liu, X., Wang, Z., & Xie, Y. (2021). Soil Nitrous Oxide Emissions by Atmospheric Nitrogen Deposition over Global Agricultural Systems. *Environmental Science & Technology*, *55*, 4420-4429
- Yao, Y., Tian, H., Shi, H., Pan, S., Xu, R., Pan, N., & Canadell, J.G. (2020). Increased global nitrous oxide emissions from streams and rivers in the Anthropocene. *Nature Climate Change*, *10*, 138-142
- You, Y., Tian, H., Pan, S., Shi, H., Bian, Z., Gurgel, A., Huang, Y., Kicklighter, D., Liang, X.-Z., Lu, C., Melillo, J., Miao, R., Pan, N., Reilly, J., Ren, W., Xu, R., Yang, J., Yu, Q., & Zhang, J. (2022). Incorporating dynamic crop growth processes and management practices into a terrestrial biosphere model for simulating crop production in the United States: Toward a unified modeling framework. *Agricultural and Forest Meteorology*, *325*, 109144
- You, Y., Tian, H., Pan, S., Shi, H., Lu, C., Batchelor, W.D., Cheng, B., Hui, D., Kicklighter, D., Liang, X.-Z., Li, X., Melillo, J., Pan, N., Prior, S.A., & Reilly, J. (2023). Net greenhouse gas balance in U.S. croplands: How can soils be a part of the climate solution? *Global Change Biology* (Under Review)
- Yu, Z., Lu, C., Cao, P., & Tian, H. (2018). Long-term terrestrial carbon dynamics in the Midwestern United States during 1850–2015: Roles of land use and cover change and agricultural management. *Global Change Biology*, *24*, 2673-2690
- Yu, Z., Lu, C., Hennessy, D.A., Feng, H., & Tian, H. (2020). Impacts of tillage practices on soil carbon stocks in the US corn-soybean cropping system during 1998 to 2016. *Environmental Research Letters*, *15*, 014008
- Yue, K., Peng, Y., Fornara, D.A., Van Meerbeek, K., Vesterdal, L., Yang, W., Peng, C., Tan, B., Zhou, W., & Xu, Z. (2019). Responses of nitrogen concentrations and pools to multiple environmental change drivers: A meta-analysis across terrestrial ecosystems. *Global Ecology and Biogeography*, *28*, 690-724
- Yvon-Durocher, G., Allen, A.P., Bastviken, D., Conrad, R., Gudas, C., St-Pierre, A., Thanh-Duc, N., & Del Giorgio, P.A. (2014). Methane fluxes show consistent temperature dependence across microbial to ecosystem scales. *Nature*, *507*, 488-491
- Zabel, F., Delzeit, R., Schneider, J.M., Seppelt, R., Mauser, W., & Václavík, T. (2019). Global impacts of future cropland expansion and intensification on agricultural markets and biodiversity. *Nature Communications*, *10*, 2844
- Zhang, J., Tian, H., Shi, H., Zhang, J., Wang, X., Pan, S., & Yang, J. (2020). Increased greenhouse gas emissions intensity of major croplands in China: Implications for food security and climate change mitigation. *Global Change Biology*, *26*, 6116-6133
- Zhang, X., Izaurralde, R.C., Manowitz, D.H., Sahajpal, R., West, T.O., Thomson, A.M., Xu, M., Zhao, K., LeDuc, S.D., & Williams, J.R. (2015). Regional scale cropland carbon budgets: Evaluating a geospatial agricultural modeling system using inventory data. *Environmental Modelling & Software*, *63*, 199-216
- Zomer, R.J., Bossio, D.A., Sommer, R., & Verchot, L.V. (2017). Global Sequestration Potential of Increased Organic Carbon in Cropland Soils. *Scientific Reports*, *7*, 15554

Chapter 6. Projected dynamics of crop production and greenhouse gas balance in U.S. croplands: The imperative of sustainable agriculture

Abstract

Contemporary agriculture faces a dual challenge under climate change: ensuring food security while reducing net greenhouse gas (GHG) emissions. While numerous studies have independently predicted food production and GHG emissions under future climate scenarios, few have examined their complex interrelationship. To bridge this gap, this study used the Dynamic Land Ecosystem Model (DLEM), driven by climate forcings from the CMIP6 climate model, to predict future crop production, net GHG balance, and net GHG emissions intensity (GHGI: net soil GHGs emissions per unit of crop production) in U.S. croplands under three climate scenarios (i.e., SSP126, SSP245, and SSP585) from 2020 to 2100. Our results show a significant increase in the national net GHG balance across the SSP245 and SSP585 scenarios, with the most pronounced increase occurring under the high-emission trajectory SSP585, averaging 236 Tg CO₂-eq year⁻¹. In contrast, the net GHG balance under the 126 scenario remains relatively stable throughout the study period. Crop production shows significant interannual variations but does not exhibit significant trends across all scenarios. This imbalance, where the net GHG balance increases disproportionately compared to crop production, leads to an increased GHGI, which is estimated to be 0.26 CO₂-eq Tg⁻¹, 0.34 CO₂-eq Tg⁻¹, and 0.42 CO₂-eq Tg⁻¹ under the SSP126, SSP245, and SSP585 scenarios, respectively. Increased temperatures and atmospheric CO₂ concentrations are the primary contributors to the significant increase in net GHG balance and GHGI. The predicted increase in GHGI underscores the urgent need for immediate intervention through climate-smart agricultural practices. Our study offers a comprehensive prediction of the intricate relationship between climate

change and agriculture, advocating for conservative agricultural practices to maintain food security while mitigating net GHG emissions.

6.1 Introduction

Climate change poses an increasing threat to the world's food supply. As global temperatures rise and the frequency of extreme weather events increases, agricultural systems around the world face a variety of risks, such as decreased crop yields, soil degradation, and increased susceptibility to pests and diseases (IPCC 2018). Additionally, agriculture has played a pivotal role in anthropogenic global warming, contributing about 25%-30% and 35%-50% of global land biogenic emissions of nitrous oxide (N₂O) and methane (CH₄), respectively (Tian et al. 2016). This constitutes a significant obstacle to achieving the Paris climate goal of limiting global warming to well below 2°C by the end of this century (Tian et al. 2020a). As a leading global producer of staple crops such as corn, soybean, and wheat, the United States (U.S.) plays a crucial role in both domestic and global food systems (Dohlman et al. 2020). However, its agricultural system has been significantly impacted by climate change (Lobell et al. 2014; Ortiz-Bobea et al. 2019; Schlenker and Roberts 2009b). According to EPA (2021), U.S. agriculture contributed ~10% of the national total greenhouse gas (GHG) emissions in 2019 and was the largest source of N₂O emissions (~75%). Considering the increasing climate-related risks in the future coupled with the U.S.'s pivotal role in global food supply, it is imperative to quantify the effects of future climate change on U.S. agricultural systems (e.g., crop yields and net GHG emissions), thereby informing policy-making ranging from localized farm management strategies to international trade accords.

The magnitude, rate, and pattern of future climate change on agricultural productivity have been extensively studied at both field and regional scales using models that range from highly process-based to relatively empirical in their formulation (Challinor et al. 2018; Fei et al. 2023;

Liu et al. 2021; Rosenzweig et al. 2014; Rosenzweig et al. 2013). Among them, process-based crop models have been widely recognized as effective tools for simulating crop yields and investigating the impacts of future climate change and agricultural management practices on the exchange of carbon, water, nitrogen (N) and energy fluxes between the agroecosystem and the atmosphere (Bondeau et al. 2007; Lutz et al. 2019a; McDermid et al. 2017; Rosenzweig et al. 2014). Previously, many agronomic crop models (e.g., CERES, APSIM, EPIC, and DSSAT) have been developed to simulate crop yields and provide guidance for agricultural decision-making, with the aim of reducing potential risks and evaluating adaptation strategies (Holzworth et al. 2014; Jones et al. 2003; Keating et al. 2003; Ritchie et al. 1998; Williams et al. 1989). However, since crop models are originally designed for farmer's decision support, they generally focus on field-scale yield simulation over homogeneous plot conditions. Meanwhile, they typically have a reduced-form representation of hydrologic, energy and biogeochemical cycles. These properties limit their ability to simulate regional crop production, assess mitigation potential in the agriculture sector, and evaluate the environmental impacts of agricultural management activities. In recent years, with the increasing attention to the impact of agricultural activities on the Earth's climate, there is a growing trend for terrestrial biosphere models (TBMs) to include detailed crop growth processes and agricultural management practices (Drewniak et al. 2013; Peng et al. 2018; Van den Hoof et al. 2011; Wu et al. 2016; Zhang et al. 2018). The TBM with well-represented crop phenological development and growth processes, as well as agricultural management practices, not only benefits yield simulation, but also improves the estimation of regional-scale carbon, water and energy exchanges between the biosphere and the atmosphere (Boas et al. 2021; Lokupitiya et al. 2009; Lu et al. 2017b; McDermid et al. 2017; Osborne et al. 2015; Song et al. 2013). Notably, You et al. (2022) integrated the strengths of crop models and TBMs into a unified agricultural

modeling framework, which was achieved by incorporating detailed and mechanistic representations of dynamic crop growth processes and agricultural management practices into the Dynamic Land Ecosystem Model (DLEM). This unified modeling framework has led to improved simulation accuracy of various fluxes and stocks such as crop yield, biomass, leaf area index, soil organic carbon (SOC), and GHG emissions.

GHG emission is another crucial factor closely related to agricultural productivity. By 2050, global food production may need to increase by 25%-70% (Hunter et al. 2017), or even double current production levels (Tilman et al. 2011), to meet projected food demands. This would inevitably lead to substantial increases in GHG emissions due to predicted increases in N fertilizer use and cropland expansion (Cavigelli et al. 2012; Molotoks et al. 2018; Thompson et al. 2019; Zabel et al. 2019). For example, Stocker et al. (2013) used the LPX-Bern 1.0 model to estimate global N₂O and CH₄ emissions under two contrasting scenarios: a climate mitigation scenario (RCP 2.6) and a high-emission scenario (RCP 8.5). Kanter et al. (2016) used the GFDL-LM3 N.1 model to evaluate the impact of variations in climate scenarios, land use, and N fertilizer use rates on agricultural N₂O emissions before 2050. However, it should be noted that agriculture also has the capability to sequester carbon in soils through practices such as no tillage and cover cropping (Bai et al. 2019; EPA 2021). In light of the dual role of agriculture—both impacted by and impacting climate change—it becomes imperative to study food production and GHG emissions simultaneously (Garnett et al. 2013; Parry 2019). GHG emissions intensity (GHGI), defined as the amount of GHG emitted per unit of food produced, can be used to assess the relationship between food production and GHG emissions (Carlson et al. 2017). As the climate continues to change, it is therefore imperative to comprehend and predict the future relationship between food production and GHG emissions (i.e., changes in GHGI) under future climate change scenarios. This prediction

could provide farmers and policymakers with valuable insights to mitigate the negative effects of climate change on food security and to ensure environmental sustainability (IPCC 2019; Rosenzweig et al. 2014; Wheeler and von Braun 2013a).

While previous studies have mainly focused on either crop production or GHG emissions in isolation, there is limited work that integrates the two, namely GHGI (net soil GHGs emissions per unit of crop production), within the context of future climate change scenarios (Arora 2019; Laborde et al. 2021; Smith et al. 2014; Zhang et al. 2020a). These research gaps hinder the development of comprehensive mitigation and adaptation strategies for the agricultural sector (Carlson et al. 2017; Mrówczyńska-Kamińska et al. 2021; Schmidhuber and Tubiello 2007). Projections that integrate food production, GHG emissions, and GHGI could provide valuable insights into the resilience of the U.S. food production system under various climate change scenarios. Therefore, it is imperative to bridge this gap to develop robust, data-driven policy interventions that can mitigate the environmental impacts of agriculture while ensuring food security.

This study aims to predict crop production, net GHG balance, and GHGI in U.S. croplands under various future climate scenarios, including SSP126, SSP245, and SSP585. To this end, we used climate forcings derived from a CMIP6 climate model IPSL-CM6A-LR to drive the unified agricultural modeling framework within the Dynamic Land Ecosystem Model (DLEM). The objectives of this work are twofold: (1) to estimate the net GHG balance, crop production, and GHGI in U.S. croplands under various climate change scenarios from 2020 to 2100, and (2) to quantify factorial contributions of different climate drivers (i.e., climate change, atmospheric CO₂, and N deposition) to the spatial and temporal variations in net GHG balance and crop production across the country.

6.2 Materials and methods

6.2.1 Model descriptions

DLEM v4.0 is a highly integrated TBM that is capable of quantifying daily, spatially explicit carbon, water, and nutrient stocks and fluxes in terrestrial ecosystems and inland water systems across site, regional, and global scales (Pan et al. 2021; Tian et al. 2010a; Tian et al. 2020b; Yao et al. 2020). To meet cross-scale agricultural application needs (e.g., management guidance, climate change mitigation and adaptation), DLEM v4.0 has incorporated explicit and mechanistic representations of dynamic crop growth processes and multiple agricultural management practices. These include but are not limited to crop-specific phenological development, carbon allocation, yield formation, and biological nitrogen fixation processes, as well as management practices such as nitrogen fertilization, irrigation, rotation, manure application, tillage, cover cropping, and crop genetic improvements (You et al. 2022). By fully coupling these agricultural processes with biogeochemical, biophysical, and hydrological processes, DLEM v4.0 is capable of simulating and predicting the exchange of carbon (including crop yield), water, nutrient and energy fluxes within the agriculture-climate-environment system. A thorough description of the processes incorporated into the agricultural module of DLEM v4.0 is presented in Chapter 2.

6.2.2 Future climate scenarios and other input data

6.2.2.1 Future climate scenarios

The Shared Socioeconomic Pathways (SSPs) consist of five narratives, namely SSP1, SSP2, SSP3, SSP4, and SSP5, that describe a variety of societal trajectories. Various societal factors, including but not limited to socio-economic conditions, demographic patterns, lifestyle choices, and policy influences, characterize these trajectories (Riahi et al. 2017). In conjunction with the

four Representative Concentration Pathways (RCPs), namely RCP2.6, RCP4.5, RCP6, and RCP8.5, which cover a range of radiative forcing scenarios and consequently GHG emissions trajectories (Moss et al. 2010), these combinations of SSP-RCP pathways serve as the fundamental basis for the climate projections used in the Intergovernmental Panel on Climate Change's (IPCC) Fifth Assessment Report (IPCC 2014a) and the recent IPCC Special Report on 1.5 degrees (IPCC 2018).

In this study, we used CMIP6 climate forcing output from the IPSL-CM6A-LR model under different combined SSP and RCP scenarios to estimate future variations in U.S. crop production and GHG emissions. These SSP-RCP combinations include SSP585, SSP245, and SSP126 (Boucher et al. 2020; Lurton et al. 2020). The climate forcing data include precipitation, shortwave solar radiation, mean, maximum and minimum temperature. Among them, SSP585 represents a worst-case scenario with an additional radiative forcing of 8.5 W/m² by the year 2100 and is an extension of the CMIP5's RCP8.5 scenario. It depicts a picture of high GHG emissions that are exacerbated by a variety of socioeconomic factors. SSP245 represents a “middle-of-the-road” scenario, accounting for some climate protection measures, and projects an additional radiative forcing of 4.5 W/m² by 2100. This is an update of the RCP4.5 scenario. SSP126 represents the “best case” future from the sustainability perspective, with radiative forcing limited to 2.6 W/m² by the year 2100. This scenario is designed to be consistent with the goal of limiting global warming to 2°C and is a revised version of the RCP2.6 scenario. Each of these pathways not only captures the potential future states of the Earth's climate, but also reflects how climate science is intertwined with societal decisions and developmental trajectories (O'Neill et al. 2016). These future climate datasets were further bias-corrected at a daily time-step and a 5 arc-min spatial resolution, using the historical climate dataset reconstructed in Section 2.3 in Chapter 2.

Future atmospheric CO₂ concentration data for the three scenarios were generated by the climate-carbon cycle model MAGICC7.0 (Meinshausen et al. 2020). Under the SSP126 scenario, the increase in atmospheric CO₂ concentration slows to a peak of 474 ppm in 2063, then decreases to 446 ppm in 2100 as a result of significant emission mitigation and land-based carbon removal. Under the SSP245 scenario, the atmospheric CO₂ concentration continues increasing, but the increase slows down after the 2060s. In 2100, the CO₂ concentration will reach 603 ppm. Under the SSP585 scenario, the CO₂ concentration in the atmosphere increases significantly, reaching 1135 ppm in 2100.

Future atmospheric N deposition data for the three scenarios were derived from the IMAGE3.0 model, which is a comprehensive integrated framework that incorporates interactions between human and natural systems and is characterized by biophysical processes such as water, carbon, and nutrient cycles and various environmental indicators (Stehfest et al. 2014).

6.2.2.2 Other input data

Details of other model forcing datasets, such as agricultural management practices (e.g., N fertilizer use rate, crop rotation, tillage, irrigation, and manure application), land use change, and soil properties, can be found in Section 2.3 in Chapter 2.

6.2.3 Model implementation and experimental design

Implementation of DLEM v4.0 consisted of three major steps: an equilibrium run, a spin-up run, and a transient run. The equilibrium run was driven by average annual climate data during the 1860s and other environmental factors in 1860. The equilibrium state was assumed to be reached when changes in carbon, N, and water pools between two consecutive 20-year periods were less than 0.5 g C m⁻² year⁻¹, 0.5 g N m⁻² year⁻¹, and 0.5 mm year⁻¹, respectively. The spin-up run was

driven by detrended climate data during the 1860s to eliminate fluctuations due to the transition from equilibrium run to transient run. Finally, the transient run was driven by historical and future data from 1860 to 2100 for the three SSP-RCP combinations (i.e., SSP585, SSP245, and SSP126). Note that land use change and agricultural management practices data were maintained at the 2020 level when the model was run for the period 2020-2100.

For each future climate scenario, we designed four simulation experiments to distinguish the factorial contributions of different drivers to the inter-annual variations of crop production and net soil GHG balance (Table 6-1), including climate change, atmospheric CO₂ concentration, and N deposition. Specifically, S0 denotes the all-combined experiment, where the DLEM was driven by all historically and future-varying factors. S1 denotes the climate-controlled experiment, where the climate conditions after 2020 were kept the same as those in 2020, while other factors were time-varying. The contribution of climate change can be calculated as the difference between S0 and S1. S2 and S3 denote the atmospheric CO₂ concentration-controlled and N deposition-controlled experiments, respectively, in which the atmospheric CO₂ concentration and N deposition after 2020 were kept the same as in 2020, whereas other factors varied over time. The contribution of atmospheric CO₂ concentration and N deposition are determined by the difference between S0 and S2 and S0 and S3, respectively.

Table 6-1. Factorial experiments in this study.

Scenario	Climate	Atmospheric CO₂ Concentration	Atmospheric N Deposition
S0 All-Combined	1860-2100	1860-2100	1860-2100
S1 Climate-Controlled	1860-2020*	1860-2100	1860-2100
S2 Atmospheric CO ₂ -Controlled	1860-2100	1860-2020*	1860-2100
S3 Atmospheric N Deposition-Controlled	1860-2100	1860-2100	1860-2020*

*Data after 2020 was kept the same as 2020.

6.2.4 Global warming potential and GHGI calculation

The global warming potential (GWP) is an index to measure the integrated radiative forcing from the emission of 1 kg of a trace gas relative to that of CO₂ (Myhre et al. 2013). In GWP conversions, CO₂ is typically considered the reference gas with a GWP constant of 1. CH₄ and N₂O emissions can be converted to ‘CO₂-equivalents’ based on their respective GWP constants over a specified time horizon. To obtain a comprehensive assessment of the climatic impact of net soil GHG balance, we adopted the following equation to calculate the combined GWPs for SOC sequestration of CO₂ and N₂O and CH₄ emissions:

$$GWP = F_{CO_2-C} \times \frac{44}{12} \times GWP_{CO_2} + F_{N_2O-N} \times \frac{44}{28} \times GWP_{N_2O} + F_{CH_4-C} \times \frac{16}{12} \times GWP_{CH_4} \quad (1)$$

$$F_{CO_2-C} = -SOCSR \quad (2)$$

where F_{CO_2-C} , F_{N_2O-N} , and F_{CH_4-C} were annual fluxes of CO₂, N₂O, and CH₄, respectively; $SOCSR$ was SOC sequestration rate; molecular weight conversion fractions 44/12, 44/28, and 16/12 were used to convert the mass of CO₂-C, N₂O-N, and CH₄-C into CO₂, N₂O, and CH₄, respectively; GWP_{CO_2} , GWP_{N_2O} and GWP_{CH_4} were GWP constants indicating radiative forcing of CO₂, N₂O, and CH₄ in terms of their CO₂ equivalents, and this study used the GWP values integrated over a time horizon of 100 years for CO₂, N₂O, and CH₄, which were 1, 273, and 27, respectively (Myhre et al. 2013).

GHGI, defined as the amount of net soil GHGs emitted per unit of food produced, can be used to assess the efficiency of agricultural systems in emitting GHGs relative to their productivity:

$$GHGI = GHG / Crop Production \quad (3)$$

where GHG is the GWP value of net soil GHG balance, and crop production is the simulated crop yield.

6.3 Results

6.3.1 National budget and spatiotemporal variations in net GHG balance

Our simulations indicate that U.S. croplands exhibit divergent temporal variations in GHG fluxes under various future climate scenarios (Figure 6-1). In terms of SOC sequestration, U.S. croplands continuously serve as a net carbon sink between 2020 and 2100 under the SSP126 and SSP245 scenarios, with average SOC sequestration rates of $30.1 \text{ Tg C year}^{-1}$ and $31.9 \text{ Tg C year}^{-1}$, respectively. However, under the SSP585 scenario, U.S. croplands act as a net carbon sink from 2020 to 2090, with an average SOC sequestration rate of $26.7 \text{ Tg C year}^{-1}$, but transition to a net carbon source during the 2090s, with an average SOC decomposition rate of $1.8 \text{ Tg C year}^{-1}$. Additionally, under the SSP126 and SSP245 scenarios, the SOC sequestration rate remains relatively stable from 2020 to 2100 without significant trends, while under the SSP585 scenario, it remains stable from 2020 to 2070 and then shows a declining trend.

As for N_2O , U.S. croplands consistently act as a net source during 2020-2100, with average emission rates of $0.58 \text{ Tg N year}^{-1}$, $0.66 \text{ Tg N year}^{-1}$, and $0.74 \text{ Tg N year}^{-1}$ under the SSP126, SSP245, and SSP585 scenarios, respectively. Notably, N_2O emissions under the SSP245 and SSP585 scenarios show a significant increasing trend, with increasing rates of $0.003 \text{ Tg N year}^{-2}$ and $0.005 \text{ Tg N year}^{-2}$, respectively. In contrast, N_2O emissions under the SSP126 scenario exhibit fluctuations but generally remain relatively stable during 2020-2100.

For CH_4 , U.S. croplands consistently act as a net source during 2020-2100, with average emission rates of $0.28 \text{ Tg C year}^{-1}$, $0.35 \text{ Tg C year}^{-1}$, and $0.31 \text{ Tg C year}^{-1}$ under SSP126, SSP245, and SSP585 scenarios, respectively. Although large interannual variations in CH_4 emissions were observed for all scenarios, only the SSP585 scenario showed a statistically significant increasing trend, at a rate of $0.001 \text{ Tg C year}^{-2}$.

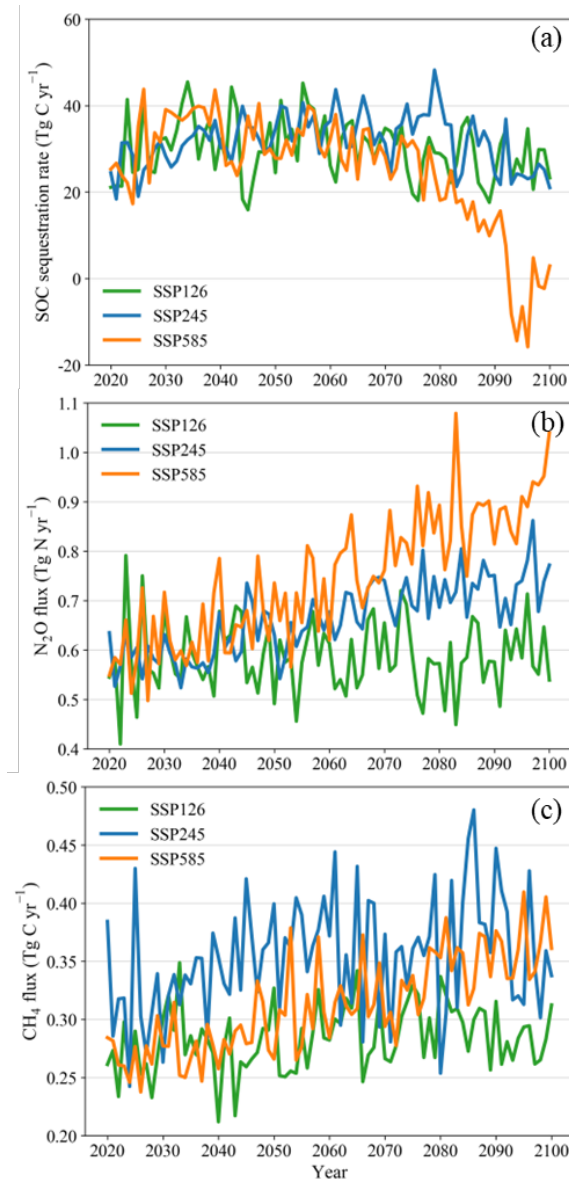


Figure 6-1. Temporal variations in national SOC sequestration rate (a) and fluxes of N_2O (b) and CH_4 (c) in U.S. agricultural soils from 2020 to 2100. Note that negative values in SOC sequestration rate represent carbon release.

Using the GWP100 (GWP over a 100-year time horizon) metric, sequestered SOC in U.S. agricultural soils reduces the national net GHG balance during 2020–2100 at average rates of 110 $\text{Tg CO}_2\text{-eq year}^{-1}$, 117 $\text{Tg CO}_2\text{-eq year}^{-1}$, and 94 $\text{Tg CO}_2\text{-eq year}^{-1}$ for the SSP126, SSP245, and SSP585 scenarios, respectively. In contrast, non- CO_2 GHG emissions (i.e., the sum of N_2O and

CH₄ emissions) contribute to the net GHG balance at average rates of 262 Tg CO₂-eq year⁻¹, 297 Tg CO₂-eq year⁻¹, and 330 Tg CO₂-eq year⁻¹ for the SSP126, SSP245, and SSP585 scenarios, respectively. Consequently, non-CO₂ GHG emissions from U.S. croplands consistently exceed SOC sequestered across all climate scenarios, indicating that U.S. croplands continue to act as a net source of GHGs during 2020-2100. Statistically, under the SSP126, SSP245, and SSP585 scenarios, sequestered SOC offset approximately 42%, 39%, and 28% of climate-warming effects resulting from non-CO₂ GHG emissions during 2020-2100, respectively. When integrating both SOC sequestration and non-CO₂ GHG emissions, the average net GHG balance during 2020-2100 is estimated to be a GHG source of 151 Tg CO₂-eq year⁻¹, 180 Tg CO₂-eq year⁻¹, and 236 Tg CO₂-eq year⁻¹ under the SSP126, SSP245, and SSP585 scenarios, respectively. Moreover, it exhibits a significant increasing trend under the SSP245 and SSP585 scenarios but remains relatively stable under the SSP126 scenario (Figure 6-2).

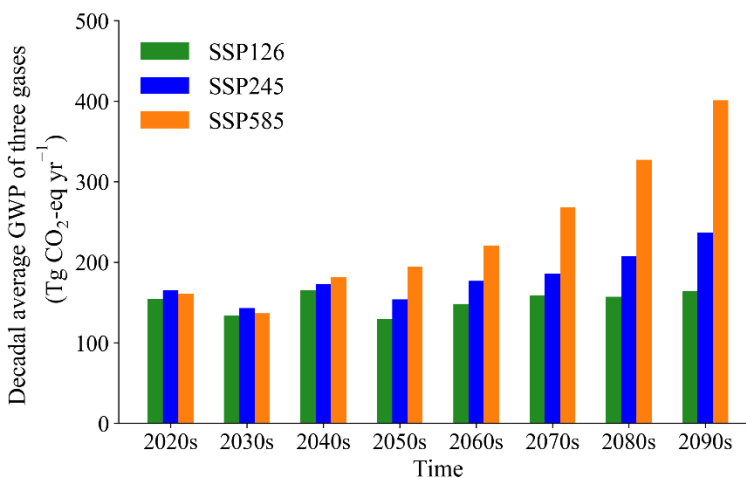


Figure 6-2. Temporal variations in national net greenhouse gas balance of U.S. croplands from the 2020s to the 2090s.

The spatial distribution of the net soil GHG balance showed large spatial variations under all scenarios. Notably, emission hotspots are concentrated in the Midwest and central U.S. regions, where peak net soil GHG emissions reach up to 4 Mg CO₂-eq ha⁻¹ year⁻¹ (Figure 6-3). Generally,

the SSP585 scenario results in the highest net GHG emissions across the majority of U.S. croplands, and the SSP245 scenario leads to medium emissions, while the SSP126 scenario yields the lowest emissions.

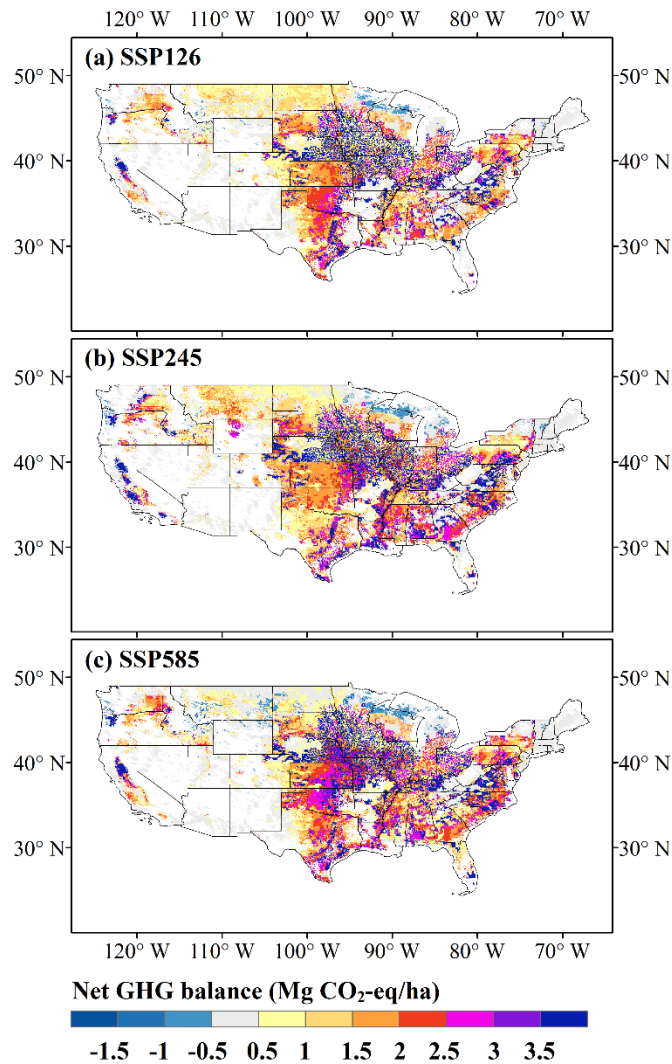


Figure 6-3. Spatial pattern of the average annual net greenhouse gas balance of U.S. croplands during 2020-2100 under the SSP126 (a), SSP245 (b), and SSP585 (c) scenarios.

6.3.2 Spatial and temporal variations in crop production

Our simulation results reveal that national crop production exhibits substantial interannual variations and shows no significant trends across all climate scenarios (Figure 6-4). Specifically,

the average national crop production during 2020-2100 is estimated to be 593 Tg year⁻¹ under the SSP126 scenario, 531 Tg year⁻¹ under the SSP245 scenario, and 568 Tg year⁻¹ under the SSP585 scenario. Notably, the SSP126 scenario leads to the highest national crop production, followed by the SSP585 and SSP245 scenarios, respectively. However, it is worth noting that crop production in the 2090s experiences a substantial decrease under the SSP585 scenario.

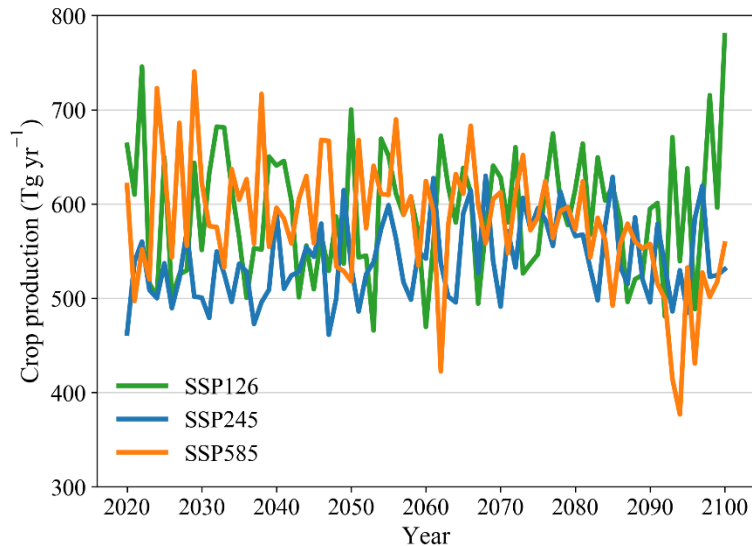


Figure 6-4. Temporal variations in national crop production in U.S. croplands from 2020 to 2100 under the SSP126, SSP245, and SSP585 scenarios.

The spatial distribution of average annual crop production during 2020-2100 exhibits substantial variability across all scenarios (Figure 6-5). Notably, regions such as the Midwest, the central U.S., and the Mississippi Delta display high levels of production. Additionally, our simulation results suggest that the spatial patterns of crop production remain generally consistent across different climate scenarios.

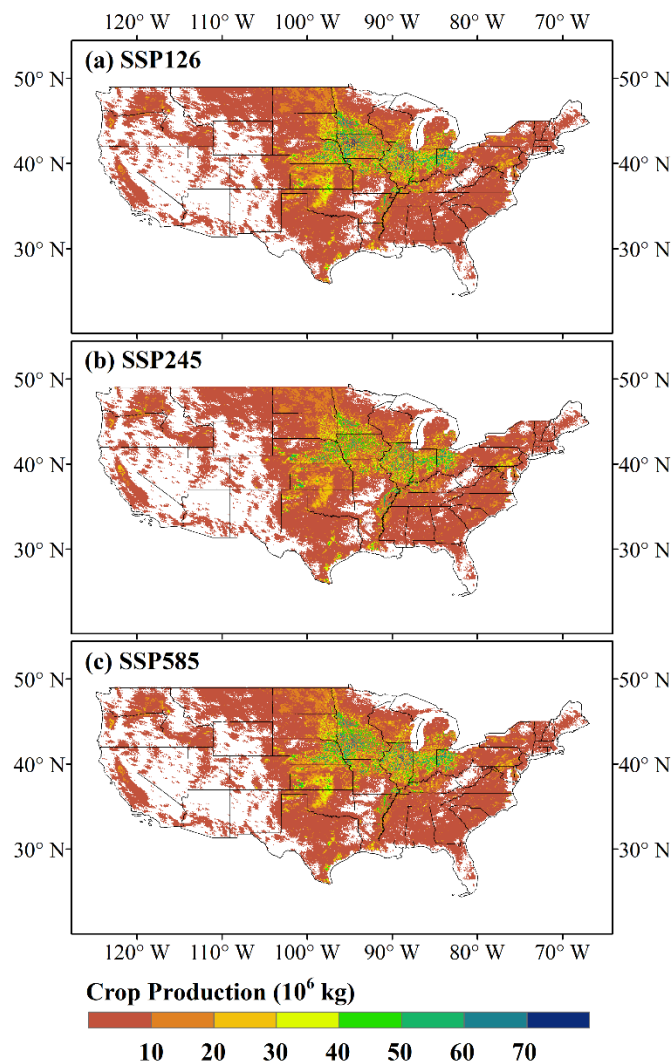


Figure 6-5. Spatial pattern of the average annual crop production in U.S. croplands during 2020-2100 under the SSP126 (a), SSP245 (b), and SSP585 (c) scenarios.

6.3.3 Spatial and temporal variations in net GHG emissions intensity

We analyzed the temporal variations in the GHGI of U.S. croplands (Figure 6-6). Under the SSP126, SSP245, and SSP585 scenarios, the average annual GHGI for the period 2020-2100 is estimated to be $0.26 \text{ CO}_2\text{-eq Tg}^{-1}$, $0.34 \text{ CO}_2\text{-eq Tg}^{-1}$, and $0.42 \text{ CO}_2\text{-eq Tg}^{-1}$, respectively. National GHGI shows an increasing trend in both the SSP245 and SSP585 scenarios. Specifically, for the SSP245 scenario, GHGI increases from an initial level of $0.31 \text{ Tg CO}_2\text{-eq Tg}^{-1}$ in the 2020s to

0.44 Tg CO₂-eq Tg⁻¹ in the 2090s. For the SSP585 scenario, it increases from 0.26 Tg CO₂-eq Tg⁻¹ in the 2020s to 0.81 Tg CO₂-eq Tg⁻¹ in the 2090s. Additionally, the SSP585 scenario exhibits the most substantial increase in GHGI between 2020 and 2100 (especially during the 2090s), whereas GHGI under the SSP126 scenario remains relatively stable over the study period.

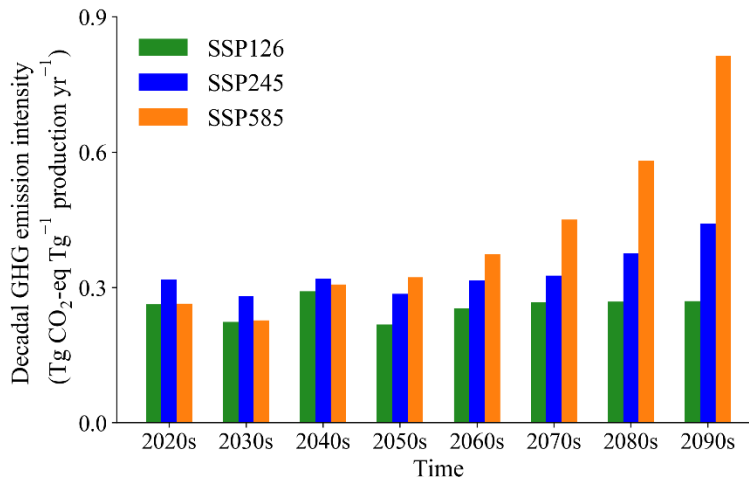


Figure 6-6. Temporal variations in greenhouse gas emissions intensity in U.S. croplands from the 2020s to the 2090s under the SSP126, SSP245, and SSP585 scenarios.

Similar to the net GHG balance and crop production, the spatial distribution of GHGI in U.S. croplands also exhibits substantial heterogeneity under all climate scenarios (Figure 6-7). For the SSP126 scenario, high GHGI is mainly located in the western and northwestern regions, as well as the Mississippi Delta, where GHGI can reach up to 0.8 Mg CO₂-eq Mg⁻¹. In contrast, low GHGI is primarily concentrated in the northeastern U.S. However, under the SSP245 and SSP585 scenarios, regions with high GHGI not only include the western and northwestern regions as well as the Mississippi Delta, but also expand to the Midwest and southeastern regions. Notably, the proportion of croplands with high GHGI (e.g., > 0.8 Mg CO₂-eq Mg⁻¹) is significantly larger under the SSP245 and SSP585 scenarios than under the SSP126 scenario.

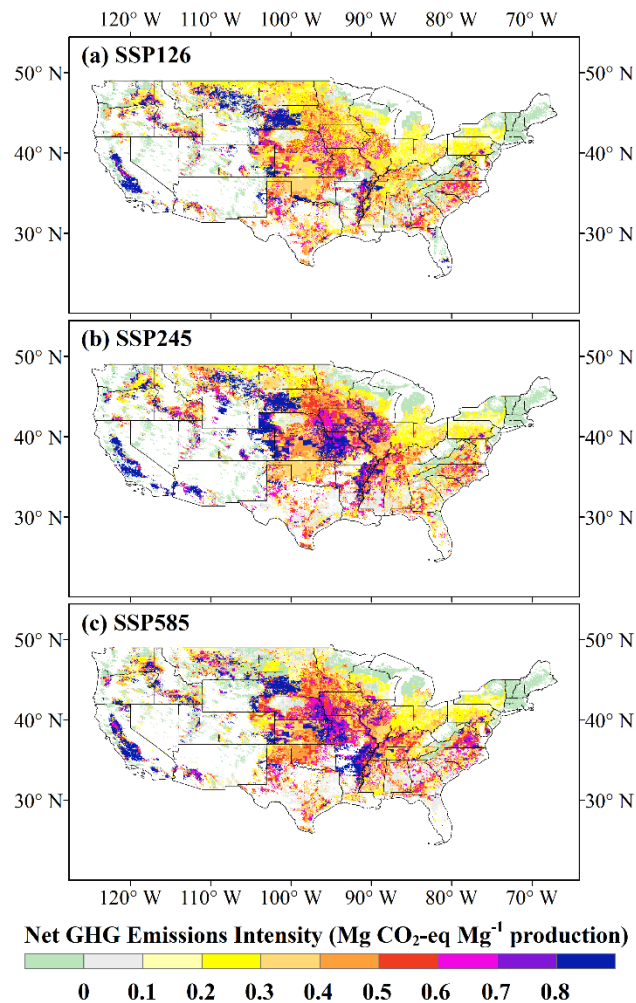


Figure 6-7. Spatial pattern of net greenhouse gas emissions intensity in U.S. croplands during 2020-2100 under the SSP126 (a), SSP245 (b), and SSP585 (c) scenarios.

6.3.4 Factorial contributions of multi-driver changes to net GHG balance and crop production

By setting up a series of simulation experiments (Table 6-1), we further quantified the factorial contributions of key drivers—climate change, atmospheric CO_2 , and N deposition—to the changes in net soil GHG balance and crop production in U.S. croplands during the period 2020-2100. Our results indicate that climate change is the dominant driver of variations in net soil GHG emissions across all scenarios, with the SSP585 scenario exhibiting the greatest impact (Figure 6-8). During

2020-2100, climate change is projected to account for an increase in the net GHG balance of 69 Tg CO₂-eq year⁻¹, 136 Tg CO₂-eq year⁻¹, and 229 Tg CO₂-eq year⁻¹, representing approximately 81%, 87%, and 82% of the total changes under the SSP126, SSP245, and SSP585 scenarios, respectively. Notably, under the SSP585 scenario, the impact of climate change increases substantially over time, from 47 Tg CO₂-eq year⁻¹ in the 2020s to 524 Tg CO₂-eq year⁻¹ in the 2090s. Under the SSP245 scenario, the contribution increases slightly over the study period, whereas under the SSP126 scenario, the contribution increases slightly from the 2020s to the 2040s and then decreases continuously thereafter. In all scenarios, increased atmospheric CO₂ concentration is the second most significant factor, with the SSP585 exhibiting the most significant impact. Nevertheless, it should be noted that rising atmospheric CO₂ initially reduces the net GHG balance and then promotes it across all scenarios. In contrast, variations in N deposition have a negligible impact on the net GHG balance. In particular, while future N deposition slightly reduces the net GHG balance under the SSP126 scenario compared to the 2020 level, it slightly increases the net GHG balance under the SSP245 and SSP585 scenarios.

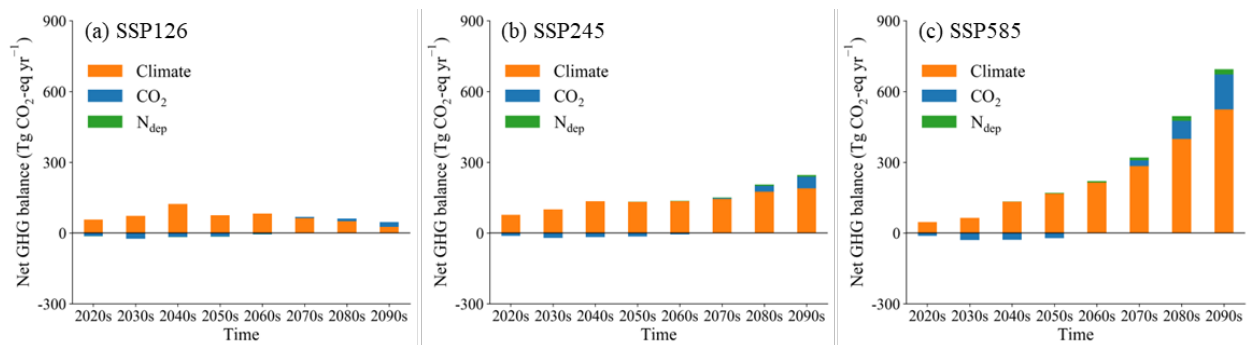


Figure 6-8. Factorial contributions of climate change, atmospheric CO₂, and N deposition to the changes in net soil GHG balance of U.S. croplands during 2020-2100 under the SSP126 (a), SSP245 (b), and SSP585 (c) scenarios.

For crop production, our attribution analysis reveals that climate change remains the dominant factor driving its variations, followed by atmospheric CO₂, while N deposition has a negligible

impact (Figure 6-9). Specifically, climate change is projected to reduce crop production by 125 Tg year⁻¹, 186 Tg year⁻¹, and 189 Tg year⁻¹ during 2020-2100, accounting for approximately 73%, 71%, and 56% of total changes under the SSP126, SSP245, and SSP585 scenarios, respectively. Furthermore, the negative impacts of climate change on crop production generally show an increasing trend under all scenarios. In contrast, increases in atmospheric CO₂ concentration result in substantial increases in crop production, especially under the SSP245 and SSP585 scenarios. Specifically, atmospheric CO₂ is projected to increase crop production by 45 Tg year⁻¹, 85 Tg year⁻¹, 160 Tg year⁻¹, representing approximately 26%, 28%, and 42% of total changes under the SSP126, SSP245, and SSP585 scenarios, respectively. Additionally, under the SSP245 and SSP585 scenarios, the promoting impact of atmospheric CO₂ on crop production increases significantly over time, whereas under the SSP126 scenario, this positive effect increases slightly from the 2020s to the 2070s and then decreases continuously thereafter. Future changes in N deposition are estimated to decrease crop production by 1 Tg year⁻¹ under the SSP126 scenario, while marginally increasing crop production by 2 Tg year⁻¹ and 3 Tg year⁻¹ under the SSP245 and SSP585 scenarios, respectively.

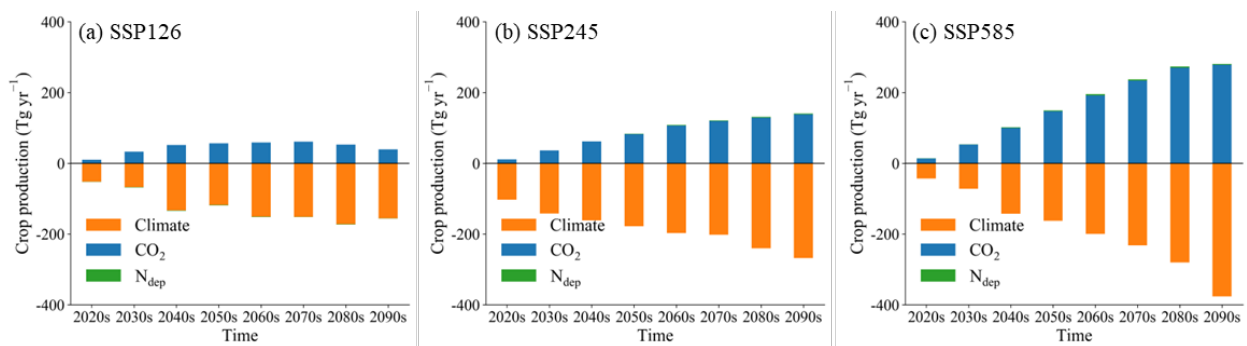


Figure 6-9. Factorial contributions of climate change, atmospheric CO₂, and N deposition to the changes in crop production of U.S. croplands during 2020-2100 under the SSP126 (a), SSP245 (b), and SSP585 (c) scenarios.

6.4 Discussion

6.4.1 Impacts of future climate change on net GHG balance, crop production, and GHGI

This study predicted the future trajectory of net GHG balance, crop production, and GHGI in U.S. croplands from 2020 to 2100 under three different climate scenarios: SSP126, SSP245, and SSP585. Our predictions indicate that both the national net GHG balance and GHGI increase significantly under the SSP245 and SSP585 scenarios over the study period (Figure 6-2 and Figure 6-6). The SSP585 scenario demonstrates the most significant increases in both net GHG balance and GHGI, consistent with its characterization as an extreme, high-emission trajectory. In contrast, the national net GHG balance and GHGI under the 126 scenario remains relatively stable over the study period. Additionally, national crop production exhibits substantial interannual variations and shows no significant trends across all climate scenarios (Figure 6-4).

The major drivers of the increase in the net GHG balance include increased temperature and rising atmospheric CO₂ concentration relative to current levels (Figure 6-8 and Figure 6-10). For example, under the SSP585 scenario, the average annual temperature is projected to increase from 13.6 °C in 2020 to 20.5 °C in 2100, and the average CO₂ concentration increases from 414.9 ppm to 1135.2 ppm. Increased temperature has a direct impact on microbial activity and root respiration, boosting their metabolic processes. This often results in accelerated SOC decomposition, which enriches soil carbon substrate and nutrient availability like N to promote soil microbial CO₂ production, methanogenesis, and denitrification processes (Carey et al. 2016; Pärn et al. 2018; Weier et al. 1993; Yvon-Durocher et al. 2014). Our factorial analysis of each individual gas also revealed a positive response of climate warming on SOC decomposition and N₂O emissions (Figure 6-11 (a-f)), while a positive impact of warming on CH₄ emissions was observed only under the SSP245 scenario. This may be due to the reduced precipitation levels associated with the

SSP126 and SSP585 scenarios, which are likely to inhibit methanogenesis processes, in contrast to conditions under the SSP245 scenario (Figure 6-11 (g-i)). Similar positive responses of rising temperature to GHG emissions are also observed in previous studies. For example, a meta-analysis by Liu et al. (2020a) found that a warming of $\sim 1.5^{\circ}\text{C}$ in rice paddies accelerated SOC decomposition by 12.9% and stimulated N_2O and CH_4 emissions by 35.2% and 23.4%, respectively. Xu et al. (2020) found that climate warming resulted in a net N_2O emission increase of $0.3 \text{ Tg N year}^{-1}$ in global croplands during 2000-2014.

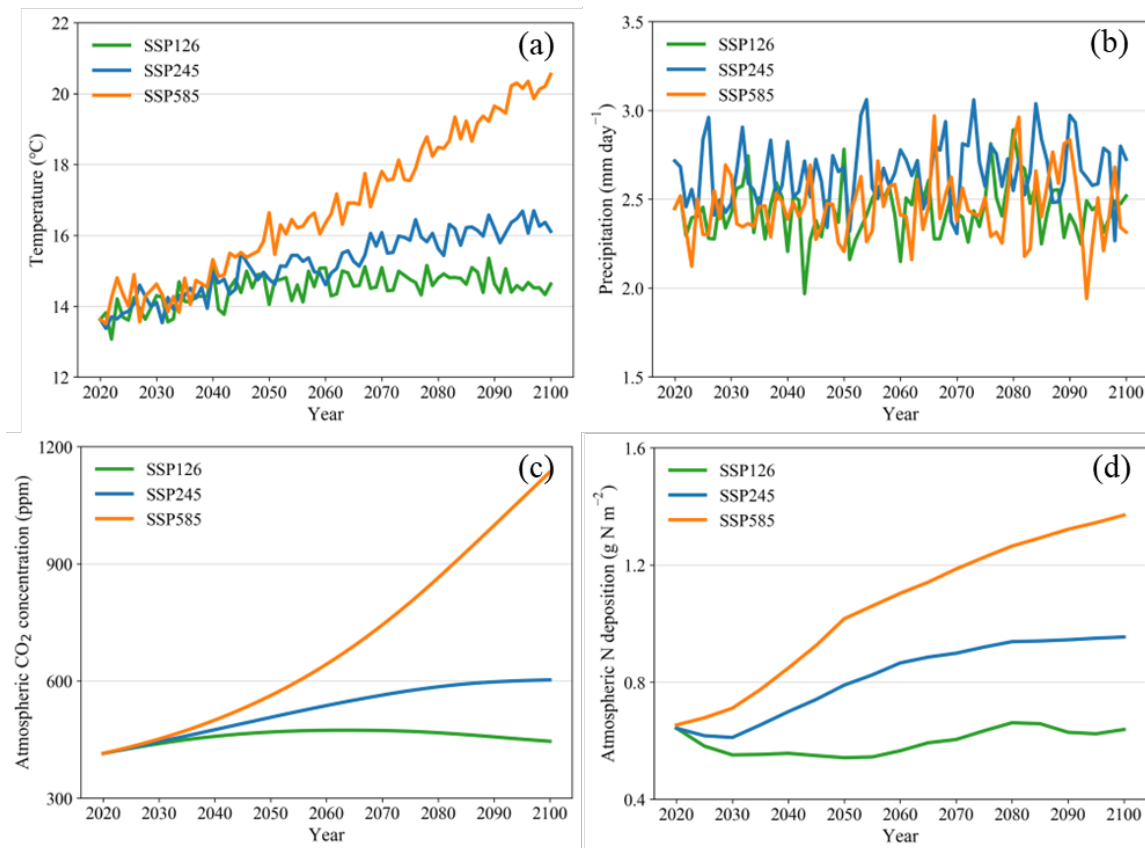


Figure 6-10. Temporal changes in temperature (a), precipitation (b), atmospheric carbon dioxide concentration (c), and atmospheric nitrogen deposition (d) under the SSP126, SSP245, and SSP585 scenarios during the 2020-2100 period.

In contrast, increasing atmospheric CO_2 concentration has complex and multi-faceted effects on the net GHG balance. On the one hand, elevated CO_2 levels can promote crop growth and

photosynthesis, leading to greater root exudation and crop residue, thereby adding more carbon to the soil (Ren et al. 2011; van Groenigen et al. 2011; Xu et al. 2020). On the other hand, this added soil carbon may also stimulate N₂O and CH₄ emissions due to the increased availability of carbon substrates and nutrients for microbial activity (Kammann et al. 2008; van Groenigen et al. 2011). These findings are further corroborated by our factorial analysis of each individual gas (Figure 6-11), which shows that rising CO₂ concentration promotes SOC sequestration but also stimulates N₂O and CH₄ emissions. Therefore, the net impact of rising atmospheric CO₂ concentration on the net GHG balance depends on the balance between SOC sequestration rates and non-CO₂ GHG emissions, emphasizing the need to consider both carbon sequestration and GHG emissions when developing mitigation strategies.

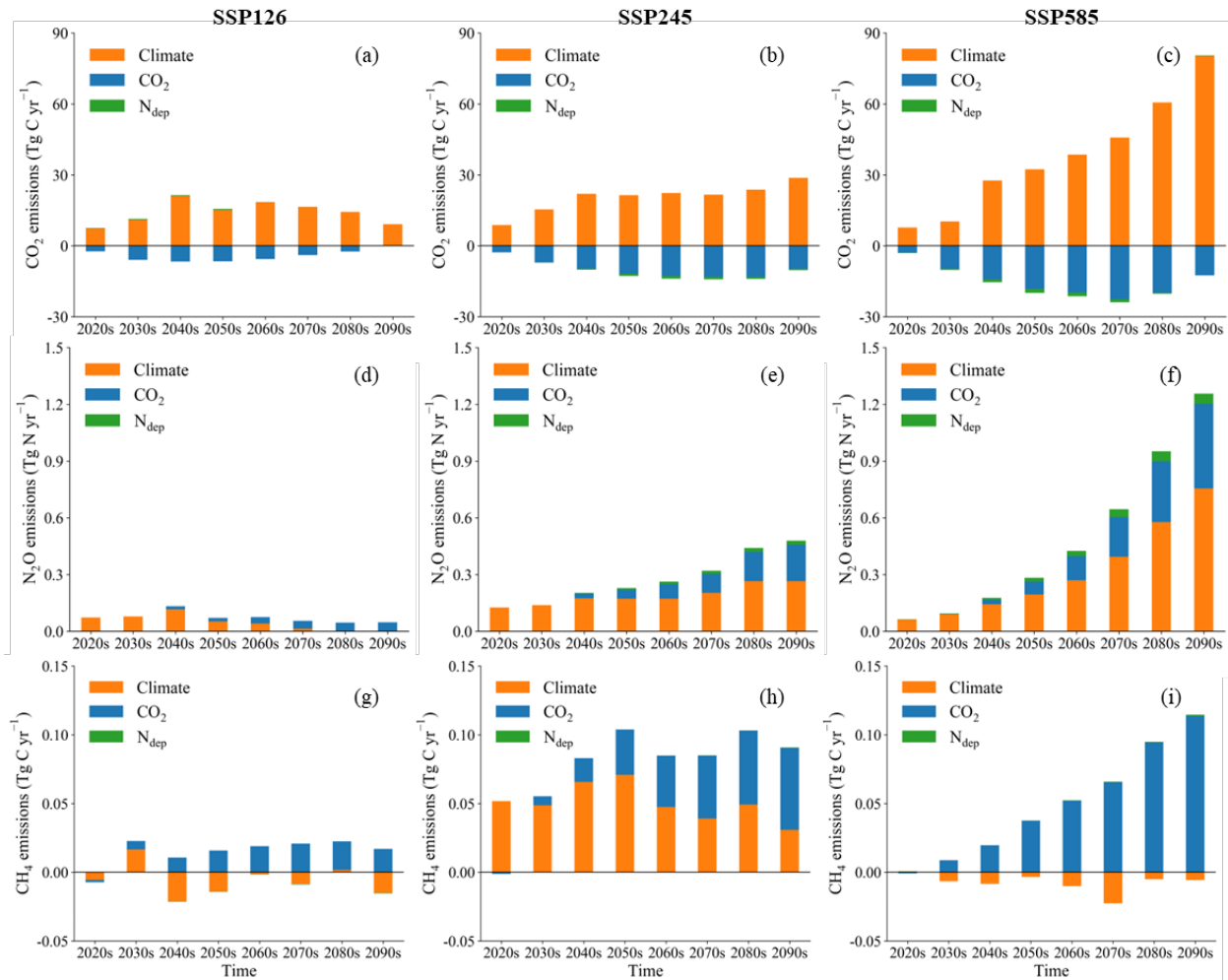


Figure 6-11. Factorial contributions of climate change, atmospheric CO₂, and N deposition to the changes in CO₂ emission (a-c), N₂O emission (d-f), and CH₄ emission (g-i) from U.S. croplands during 2020-2100 under the SSP126, SSP245, and SSP585 scenarios.

Interannual variations in crop productivity are primarily attributable to changes in climate and atmospheric CO₂ concentration (Figure 6-4 and Figure 6-9). Consistent with previous studies (IPCC 2019; Jägermeyr et al. 2021; Liu et al. 2021), our attribution analysis reveals that future climate change will have a negative impact on crop production. This negative impact is mainly due to elevated temperatures associated with all climate scenarios (Figure 6-10). Specifically, higher temperatures can lead to increased evapotranspiration rates, which in turn reduces soil

moisture and causes water stress in crops (Battisti and Naylor 2009; Ottman et al. 2012). Extreme heat can also directly damage plant tissues, reduce pollen production and viability, and hasten crop maturity, all of which contribute to decreased crop yields (Barlow et al. 2015; Prasad et al. 2006; Ugarte et al. 2007). In contrast, our results indicate that rising atmospheric CO₂ concentration has a positive impact on crop production. Higher CO₂ levels can enhance photosynthesis, allowing crops to convert more CO₂ into plant biomass (Jaggard et al. 2010; Kimball and Idso 1983; Long et al. 2006). Additionally, increased CO₂ could enhance the water-use efficiency of crops, making them more resilient to drought (Allen et al. 2011; Conley et al. 2001). Interestingly, our results suggest that the beneficial effects of increased CO₂ may partially offset the negative consequences of climate change. While this finding is promising, it is important to note that the CO₂ fertilization effect has its limits and may not scale linearly with ever-increasing levels of atmospheric CO₂ (Leakey et al. 2009). Additionally, our results indicate that crop production under the SSP245 scenario is the lowest compared to all other scenarios (Figure 6-4), which can be attributed to the balance between the negative impact of rising temperatures and the positive impact of elevated atmospheric CO₂ concentration on crop production. While the SSP585 scenario exhibits a more substantial increase in temperature than the SSP245 scenario, it also exhibits a higher level of CO₂ concentration. Consequently, the negative impact of rising temperatures is largely offset by the positive impact of elevated atmospheric CO₂ concentration under the SSP585 scenario, whereas the SSP245 scenario does not, leading to lower crop production compared to the SSP585 scenario. The interaction between elevated CO₂ concentration and climate change on crop production is inherently complex. Future research should aim to identify thresholds beyond which these impacts might become irreversible and explore mitigation strategies to safeguard global crop production.

Combining net GHG balance and crop production, our results indicate that national GHGI increases under the SSP245 and SSP585 scenarios (Figure 6-6). The increasing trend is primarily attributed to a significant increase in the net GHG balance, while the corresponding crop production shows only small changes. This finding is of particular concern as it contradicts the sustainable agriculture goal of reducing GHG emissions while ensuring food security. Given that global food production may need to increase by 25%-70% (Hunter et al. 2017) or even double current production levels (Tilman et al. 2011) by 2050 to meet the demands of the growing global population, the increasing trend in national GHGI underscores the need for a concerted global effort to make agriculture more sustainable (Beltran-Peña et al. 2020; Rockström et al. 2017). Without mitigation measures, increasing GHGI will likely exacerbate climate change while failing to adequately address global food security.

6.4.2 Uncertainty and future work

Several types of uncertainties persist in this study, including model parameter uncertainty, model structure uncertainty, and model forcing data uncertainty. Firstly, the DLEM includes a large number of parameters, whereas the lack of sufficient data for model calibration and validation causes uncertainties, particularly regarding the responses of crop yield and GHG emissions to future climate change and elevated CO₂ concentrations. Secondly, the lack or simplified representation of some key processes in the DLEM also introduces uncertainty to the simulation results. For example, the current DLEM representation of groundwater and irrigation practice (i.e., without considering irrigation amount and frequency) is relatively simple, which could lead to biased simulated soil moisture that, in turn, could affect crop yield and GHG emission predictions. Moreover, the DLEM currently does not account for improvements in crop genetic and breeding technologies that enhance crop resistance to extreme climates (Bailey-Serres et al. 2019; Hammer

et al. 2002), nor does it consider human adaptive behaviors such as farmers' preparedness and response strategies related to extreme weather events (Annan and Schlenker 2015). The exclusion of these adaptive processes within the model may further contribute to uncertainties in future projections. Lastly, the input data driving the DLEM introduces uncertainty as well. For example, future climate scenarios (i.e., SSP126, SSP245, and SSP585) contain significant uncertainties due to their dependence on unpredictable variables such as human behavior, policy decisions, and technological advancements (O'Neill et al. 2016). These climate scenarios are also subject to the inherent limitations of current climate models, particularly in their handling of complex Earth system feedbacks like cloud formation and ocean circulation (Flato et al. 2014). We will address these limitations in future studies to further improve future simulation estimates.

6.5 Conclusion

This study provides a comprehensive projection of the effects of different climate change scenarios—SSP126, SSP245, and SSP585—on net GHG balance, crop production, and GHGI in U.S. croplands from 2020 to 2100. Our analysis reveals that the SSP245 and SSP585 scenarios result in a substantial increase in both net GHG balance and GHGI. In contrast, they remain relatively stable under the SSP126 scenario. Elevated temperatures and atmospheric CO₂ concentrations are the primary contributors to the significant increase in GHG and GHGI. Crop production, however, exhibits significant interannual variations but shows no significant trends across all scenarios. The heightened GHGI raises serious concerns about deviating from the sustainable agriculture goal of mitigating climate change and ensuring food security. Consequently, our findings emphasize the urgent need for the adoption of climate-smart agricultural management practices that simultaneously address the imperatives of reducing GHG emissions and sustaining food production.

References

- Allen, L.H., Kakani, V.G., Vu, J.C.V., & Boote, K.J. (2011). Elevated CO₂ increases water use efficiency by sustaining photosynthesis of water-limited maize and sorghum. *Journal of Plant Physiology*, *168*, 1909-1918
- Annan, F., & Schlenker, W. (2015). Federal crop insurance and the disincentive to adapt to extreme heat. *American Economic Review*, *105*, 262-266
- Arora, N.K. (2019). Impact of climate change on agriculture production and its sustainable solutions. *Environmental Sustainability*, *2*, 95-96
- Bai, X., Huang, Y., Ren, W., Coyne, M., Jacinthe, P.A., Tao, B., Hui, D., Yang, J., & Matocha, C. (2019). Responses of soil carbon sequestration to climate-smart agriculture practices: A meta-analysis. *Global Change Biology*, *25*, 2591-2606
- Bailey-Serres, J., Parker, J.E., Ainsworth, E.A., Oldroyd, G.E.D., & Schroeder, J.I. (2019). Genetic strategies for improving crop yields. *Nature*, *575*, 109-118
- Barlow, K.M., Christy, B.P., O'Leary, G.J., Riffkin, P.A., & Nuttall, J.G. (2015). Simulating the impact of extreme heat and frost events on wheat crop production: A review. *Field Crops Research*, *171*, 109-119
- Battisti, D.S., & Naylor, R.L. (2009). Historical warnings of future food insecurity with unprecedented seasonal heat. *Science*, *323*, 240-244
- Beltran-Peña, A., Rosa, L., & D'Odorico, P. (2020). Global food self-sufficiency in the 21st century under sustainable intensification of agriculture. *Environmental Research Letters*, *15*, 095004
- Boas, T., Bogena, H., Grünwald, T., Heinesch, B., Ryu, D., Schmidt, M., Vereecken, H., Western, A., & Hendricks Franssen, H.J. (2021). Improving the representation of cropland sites in the Community Land Model (CLM) version 5.0. *Geosci. Model Dev.*, *14*, 573-601
- Bondeau, A., Smith, P.C., Zaehle, S., Schaphoff, S., Lucht, W., Cramer, W., Gerten, D., Lotze-Campen, H., Müller, C., & Reichstein, M. (2007). Modelling the role of agriculture for the 20th century global terrestrial carbon balance. *Global Change Biology*, *13*, 679-706
- Boucher, O., Servonnat, J., Albright, A.L., Aumont, O., Balkanski, Y., Bastrikov, V., Bekki, S., Bonnet, R., Bony, S., & Bopp, L. (2020). Presentation and evaluation of the IPSL-CM6A-LR climate model. *Journal of Advances in Modeling Earth Systems*, *12*, e2019MS002010
- Carey, J.C., Tang, J., Templer, P.H., Kroeger, K.D., Crowther, T.W., Burton, A.J., Dukes, J.S., Emmett, B., Frey, S.D., Heskell, M.A., Jiang, L., Machmuller, M.B., Mohan, J., Panetta, A.M., Reich, P.B., Reinsch, S., Wang, X., Allison, S.D., Bamminger, C., Bridgham, S., Collins, S.L., de Dato, G., Eddy, W.C., Enquist, B.J., Estiarte, M., Harte, J., Henderson, A., Johnson, B.R., Larsen, K.S., Luo, Y., Marhan, S., Melillo, J.M., Peñuelas, J., Pfeifer-Meister, L., Poll, C., Rastetter, E., Reinmann, A.B., Reynolds, L.L., Schmidt, I.K., Shaver, G.R., Strong, A.L., Susceala, V., & Tietema, A. (2016). Temperature response of soil respiration largely unaltered with experimental warming. *Proceedings of the National Academy of Sciences*, *113*, 13797-13802
- Carlson, K.M., Gerber, J.S., Mueller, N.D., Herrero, M., MacDonald, G.K., Brauman, K.A., Havlik, P., O'Connell, C.S., Johnson, J.A., & Saatchi, S. (2017). Greenhouse gas emissions intensity of global croplands. *Nature Climate Change*, *7*, 63-68
- Cavigelli, M.A., Grosso, S.J.D., Liebig, M.A., Snyder, C.S., Fixen, P.E., Venterea, R.T., Leytem, A.B., McLain, J.E., & Watts, D.B. (2012). US agricultural nitrous oxide emissions: context, status, and trends. *Frontiers in Ecology and the Environment*, *10*, 537-546
- Challinor, A.J., Müller, C., Asseng, S., Deva, C., Nicklin, K.J., Wallach, D., Vanuytrecht, E., Whitfield, S., Ramirez-Villegas, J., & Koehler, A.-K. (2018). Improving the use of crop models for risk assessment and climate change adaptation. *Agricultural systems*, *159*, 296-306
- Conley, M.M., Kimball, B.A., Brooks, T.J., Pinter Jr, P.J., Hunsaker, D.J., Wall, G.W., Adam, N.R., LaMorte, R.L., Matthias, A.D., & Thompson, T.L. (2001). CO₂ enrichment increases water-use efficiency in sorghum. *New Phytologist*, *151*, 407-412
- Dohlman, E., Hansen, J., & Boussios, D. (2020). USDA agricultural projections to 2029. *USDA agricultural projections to 2029*.
- Drewniak, B., Song, J., Prell, J., Kotamarthi, V.R., & Jacob, R. (2013). Modeling agriculture in the Community Land Model. *Geosci. Model Dev.*, *6*, 495-515
- EPA (2021). Inventory of US greenhouse gas emissions and sinks: 1990–2019. *Tech. Rep. EPA 430-R-21-003*
- Fei, C., Jägermeyr, J., McCarl, B., Contreras, E.M., Muttter, C., Phillips, M., Ruane, A.C., Sarofim, M.C., Schultz, P., & Vargo, A. (2023). Future climate change impacts on U.S. agricultural yields, production, and market. *Anthropocene*, *42*, 100386

- Flato, G., Marotzke, J., Abiodun, B., Braconnot, P., Chou, S.C., Collins, W., Cox, P., Driouech, F., Emori, S., & Eyring, V. (2014). Evaluation of climate models. *Climate change 2013: the physical science basis. Contribution of Working Group I to the Fifth Assessment Report of the Intergovernmental Panel on Climate Change* (pp. 741-866): Cambridge University Press
- Garnett, T., Appleby, M.C., Balmford, A., Bateman, I.J., Benton, T.G., Bloomer, P., Burlingame, B., Dawkins, M., Dolan, L., & Fraser, D. (2013). Sustainable intensification in agriculture: premises and policies. *Science*, *341*, 33-34
- Hammer, G.L., Kropff, M.J., Sinclair, T.R., & Porter, J.R. (2002). Future contributions of crop modelling—from heuristics and supporting decision making to understanding genetic regulation and aiding crop improvement. *European Journal of Agronomy*, *18*, 15-31
- Holzworth, D.P., Huth, N.I., deVoil, P.G., Zurcher, E.J., Herrmann, N.I., McLean, G., Chenu, K., van Oosterom, E.J., Snow, V., & Murphy, C. (2014). APSIM—evolution towards a new generation of agricultural systems simulation. *Environmental Modelling & Software*, *62*, 327-350
- Hunter, M.C., Smith, R.G., Schipanski, M.E., Atwood, L.W., & Mortensen, D.A. (2017). Agriculture in 2050: Recalibrating Targets for Sustainable Intensification. *Bioscience*, *67*, 386-391
- IPCC (2014). *Climate Change 2014 – Impacts, Adaptation and Vulnerability: Part A: Global and Sectoral Aspects: Working Group II Contribution to the IPCC Fifth Assessment Report: Volume I: Global and Sectoral Aspects*. Cambridge: Cambridge University Press
- IPCC (2018). *Impacts of 1.5°C Global Warming on Natural and Human Systems. In: Global Warming of 1.5°C. An IPCC Special Report on the impacts of global warming of 1.5°C above pre-industrial levels and related global greenhouse gas emission pathways, in the context of strengthening the global response to the threat of climate change, sustainable development, and efforts to eradicate poverty* [Masson-Delmotte, V., P. Zhai, H.-O. Pörtner, D. Roberts, J. Skea, P.R. Shukla, A. Pirani, W. Moufouma-Okia, C. Péan, R. Pidcock, S. Connors, J.B.R. Matthews, Y. Chen, X. Zhou, M.I. Gomis, E. Lonnoy, T. Maycock, M. Tignor, and T. Waterfield (eds.)]. Cambridge University Press, Cambridge, UK and New York, NY, USA, pp. 175-312, doi:10.1017/9781009157940.005.
- IPCC (2019). *Climate Change and Land: an IPCC special report on climate change, desertification, land degradation, sustainable land management, food security, and greenhouse gas fluxes in terrestrial ecosystems* [P.R. Shukla, J. Skea, E. Calvo Buendia, V. Masson-Delmotte, H.-O. Pörtner, D. C. Roberts, P. Zhai, R. Slade, S. Connors, R. van Diemen, M. Ferrat, E. Haughey, S. Luz, S. Neogi, M. Pathak, J. Petzold, J. Portugal Pereira, P. Vyas, E. Huntley, K. Kissick, M. Belkacemi, J. Malley, (eds.)]
- Jägermeyr, J., Müller, C., Ruane, A.C., Elliott, J., Balkovic, J., Castillo, O., Faye, B., Foster, I., Folberth, C., Franke, J.A., Fuchs, K., Guarin, J.R., Heinke, J., Hoogenboom, G., Iizumi, T., Jain, A.K., Kelly, D., Khabarov, N., Lange, S., Lin, T.-S., Liu, W., Mialyk, O., Minoli, S., Moyer, E.J., Okada, M., Phillips, M., Porter, C., Rabin, S.S., Scheer, C., Schneider, J.M., Schyns, J.F., Skalsky, R., Smerald, A., Stella, T., Stephens, H., Webber, H., Zabel, F., & Rosenzweig, C. (2021). Climate impacts on global agriculture emerge earlier in new generation of climate and crop models. *Nature Food*, *2*, 873-885
- Jaggard, K.W., Qi, A., & Ober, E.S. (2010). Possible changes to arable crop yields by 2050. *Philosophical Transactions of the Royal Society B: Biological Sciences*, *365*, 2835-2851
- Jones, J.W., Hoogenboom, G., Porter, C.H., Boote, K.J., Batchelor, W.D., Hunt, L.A., Wilkens, P.W., Singh, U., Gijssman, A.J., & Ritchie, J.T. (2003). The DSSAT cropping system model. *European Journal of Agronomy*, *18*, 235-265
- Kammann, C., Müller, C., Grünhage, L., & Jäger, H.-J. (2008). Elevated CO₂ stimulates N₂O emissions in permanent grassland. *Soil Biology and Biochemistry*, *40*, 2194-2205
- Kanter, D.R., Zhang, X., Mauzerall, D.L., Malyshev, S., & Shevliakova, E. (2016). The importance of climate change and nitrogen use efficiency for future nitrous oxide emissions from agriculture. *Environmental Research Letters*, *11*, 094003
- Keating, B.A., Carberry, P.S., Hammer, G.L., Probert, M.E., Robertson, M.J., Holzworth, D., Huth, N.I., Hargreaves, J.N.G., Meinke, H., Hochman, Z., McLean, G., Verburg, K., Snow, V., Dimes, J.P., Silburn, M., Wang, E., Brown, S., Bristow, K.L., Asseng, S., Chapman, S., McCown, R.L., Freebairn, D.M., & Smith, C.J. (2003). An overview of APSIM, a model designed for farming systems simulation. *European Journal of Agronomy*, *18*, 267-288
- Kimball, B.A., & Idso, S.B. (1983). Increasing atmospheric CO₂: effects on crop yield, water use and climate. *Agricultural water management*, *7*, 55-72
- Laborde, D., Mamun, A., Martin, W., Piñeiro, V., & Vos, R. (2021). Agricultural subsidies and global greenhouse gas emissions. *Nature Communications*, *12*, 2601

- Leakey, A.D.B., Ainsworth, E.A., Bernacchi, C.J., Rogers, A., Long, S.P., & Ort, D.R. (2009). Elevated CO₂ effects on plant carbon, nitrogen, and water relations: six important lessons from FACE. *Journal of Experimental Botany*, *60*, 2859-2876
- Liu, S., Zheng, Y., Ma, R., Yu, K., Han, Z., Xiao, S., Li, Z., Wu, S., Li, S., & Wang, J. (2020). Increased soil release of greenhouse gases shrinks terrestrial carbon uptake enhancement under warming. *Global Change Biology*, *26*, 4601-4613
- Liu, W., Ye, T., Jägermeyr, J., Müller, C., Chen, S., Liu, X., & Shi, P. (2021). Future climate change significantly alters interannual wheat yield variability over half of harvested areas. *Environmental Research Letters*, *16*, 094045
- Lobell, D.B., Roberts, M.J., Schlenker, W., Braun, N., Little, B.B., Rejesus, R.M., & Hammer, G.L. (2014). Greater Sensitivity to Drought Accompanies Maize Yield Increase in the U.S. Midwest. *Science*, *344*, 516
- Lokupitiya, E., Denning, S., Paustian, K., Baker, I., Schaefer, K., Verma, S.B., Meyers, T., Bernacchi, C.J., Suyker, A.E., & Fischer, M.L. (2009). Incorporation of crop phenology in Simple Biosphere Model (SiBcrop) to improve land-atmosphere carbon exchanges from croplands
- Long, S.P., Ainsworth, E.A., Leakey, A.D.B., Nosberger, J., & Ort, D.R. (2006). Food for thought: lower-than-expected crop yield stimulation with rising CO₂ concentrations. *Science*, *312*, 1918-1921
- Lu, Y., Williams, I.N., Bagley, J.E., Torn, M.S., & Kueppers, L.M. (2017). Representing winter wheat in the Community Land Model (version 4.5). *Geosci. Model Dev.*, *10*, 1873-1888
- Lurton, T., Balkanski, Y., Bastrikov, V., Bekki, S., Bopp, L., Braconnot, P., Brockmann, P., Cadule, P., Contoux, C., & Cozic, A. (2020). Implementation of the CMIP6 Forcing Data in the IPSL-CM6A-LR Model. *Journal of Advances in Modeling Earth Systems*, *12*, e2019MS001940
- Lutz, F., Herzfeld, T., Heinke, J., Rolinski, S., Schaphoff, S., von Bloh, W., Stoorvogel, J.J., & Müller, C. (2019). Simulating the effect of tillage practices with the global ecosystem model LPJmL (version 5.0-tillage). *Geosci. Model Dev.*, *12*, 2419-2440
- McDermid, S.S., Mearns, L.O., & Ruane, A.C. (2017). Representing agriculture in Earth System Models: Approaches and priorities for development. *Journal of Advances in Modeling Earth Systems*, *9*, 2230-2265
- Meinshausen, M., Nicholls, Z.R.J., Lewis, J., Gidden, M.J., Vogel, E., Freund, M., Beyerle, U., Gessner, C., Nauels, A., & Bauer, N. (2020). The shared socio-economic pathway (SSP) greenhouse gas concentrations and their extensions to 2500. *Geoscientific Model Development*, *13*, 3571-3605
- Molotoks, A., Stehfest, E., Doelman, J., Albanito, F., Fitton, N., Dawson, T.P., & Smith, P. (2018). Global projections of future cropland expansion to 2050 and direct impacts on biodiversity and carbon storage. *Global Change Biology*, *24*, 5895-5908
- Moss, R.H., Edmonds, J.A., Hibbard, K.A., Manning, M.R., Rose, S.K., Van Vuuren, D.P., Carter, T.R., Emori, S., Kainuma, M., & Kram, T. (2010). The next generation of scenarios for climate change research and assessment. *Nature*, *463*, 747-756
- Mrówczyńska-Kamińska, A., Bajan, B., Pawłowski, K.P., Genstwa, N., & Zmyślona, J. (2021). Greenhouse gas emissions intensity of food production systems and its determinants. *Plos One*, *16*, e0250995
- Myhre, G., Shindell, D., Bréon, F.M., Collins, W., Fuglestedt, J., Huang, J., Koch, D., Lamarque, J.F., Lee, D., Mendoza, B., Nakajima, T., Robock, A., Stephens, G., Takemura, T., & Zhang, H. (2013). Anthropogenic and natural radiative forcing. In *Climate Change 2013: The Physical Science Basis. Contribution of Working Group I to the Fifth Assessment Report of the Intergovernmental Panel on Climate Change*. T.F. Stocker, D. Qin, G.-K. Plattner, M. Tignor, S.K. Allen, J. Doschung, A. Nauels, Y. Xia, V. Bex, and P.M. Midgley, Eds. Cambridge University Press, pp. 659-740. In
- O'Neill, B.C., Tebaldi, C., Van Vuuren, D.P., Eyring, V., Friedlingstein, P., Hurtt, G., Knutti, R., Kriegler, E., Lamarque, J.-F., & Lowe, J. (2016). The scenario model intercomparison project (ScenarioMIP) for CMIP6. *Geoscientific Model Development*, *9*, 3461-3482
- Ortiz-Bobea, A., Wang, H., Carrillo, C.M., & Ault, T.R. (2019). Unpacking the climatic drivers of US agricultural yields. *Environmental Research Letters*, *14*, 064003
- Osborne, T., Gornall, J., Hooker, J., Williams, K., Wiltshire, A., Betts, R., & Wheeler, T. (2015). JULES-crop: a parametrisation of crops in the Joint UK Land Environment Simulator. *Geoscientific Model Development*, *8*, 1139-1155
- Ottman, M.J., Kimball, B.A., White, J.W., & Wall, G.W. (2012). Wheat growth response to increased temperature from varied planting dates and supplemental infrared heating. *Agronomy journal*, *104*, 7-16
- Pan, S., Bian, Z., Tian, H., Yao, Y., Najjar, R.G., Friedrichs, M.A.M., Hofmann, E.E., Xu, R., & Zhang, B. (2021). Impacts of Multiple Environmental Changes on Long-term Nitrogen Loading from the Chesapeake Bay Watershed. *Journal of Geophysical Research: Biogeosciences*, *126*, e2020JG005826

- Pärn, J., Verhoeven, J.T.A., Butterbach-Bahl, K., Dise, N.B., Ullah, S., Aasa, A., Egorov, S., Espenberg, M., Järveoja, J., & Jauhiainen, J. (2018). Nitrogen-rich organic soils under warm well-drained conditions are global nitrous oxide emission hotspots. *Nature Communications*, 9, 1-8
- Parry, M.L. (2019). *Climate change and world agriculture*. Routledge
- Peng, B., Guan, K., Chen, M., Lawrence, D.M., Pokhrel, Y., Suyker, A., Arkebauer, T., & Lu, Y. (2018). Improving maize growth processes in the community land model: Implementation and evaluation. *Agricultural and Forest Meteorology*, 250, 64-89
- Prasad, P.V.V., Boote, K.J., & Allen Jr, L.H. (2006). Adverse high temperature effects on pollen viability, seed-set, seed yield and harvest index of grain-sorghum [*Sorghum bicolor* (L.) Moench] are more severe at elevated carbon dioxide due to higher tissue temperatures. *Agricultural and Forest Meteorology*, 139, 237-251
- Ren, W., Tian, H., Xu, X., Liu, M., Lu, C., Chen, G., Melillo, J., Reilly, J., & Liu, J. (2011). Spatial and temporal patterns of CO₂ and CH₄ fluxes in China's croplands in response to multifactor environmental changes. *Tellus B: Chemical and Physical Meteorology*, 63, 222-240
- Riahi, K., Van Vuuren, D.P., Kriegler, E., Edmonds, J., O'neill, B.C., Fujimori, S., Bauer, N., Calvin, K., Dellink, R., & Fricko, O. (2017). The Shared Socioeconomic Pathways and their energy, land use, and greenhouse gas emissions implications: An overview. *Global Environmental Change*, 42, 153-168
- Ritchie, J.T., Singh, U., Godwin, D.C., & Bowen, W.T. (1998). Cereal growth, development and yield. In G.Y. Tsuji, G. Hoogenboom, & P.K. Thornton (Eds.), *Understanding Options for Agricultural Production* (pp. 79-98). Dordrecht: Springer Netherlands
- Rockström, J., Williams, J., Daily, G., Noble, A., Matthews, N., Gordon, L., Wetterstrand, H., DeClerck, F., Shah, M., & Steduto, P. (2017). Sustainable intensification of agriculture for human prosperity and global sustainability. *Ambio*, 46, 4-17
- Rosenzweig, C., Elliott, J., Deryng, D., Ruane, A.C., Müller, C., Arneth, A., Boote, K.J., Folberth, C., Glotter, M., & Khabarov, N. (2014). Assessing agricultural risks of climate change in the 21st century in a global gridded crop model intercomparison. *Proceedings of the National Academy of Sciences*, 111, 3268-3273
- Rosenzweig, C., Jones, J.W., Hatfield, J.L., Ruane, A.C., Boote, K.J., Thorburn, P., Antle, J.M., Nelson, G.C., Porter, C., Janssen, S., Asseng, S., Basso, B., Ewert, F., Wallach, D., Baigorria, G., & Winter, J.M. (2013). The Agricultural Model Intercomparison and Improvement Project (AgMIP): Protocols and pilot studies. *Agricultural and Forest Meteorology*, 170, 166-182
- Schlenker, W., & Roberts, M.J. (2009). Nonlinear temperature effects indicate severe damages to US crop yields under climate change. *Proceedings of the National Academy of Sciences*, 106, 15594-15598
- Schmidhuber, J., & Tubiello, F.N. (2007). Global food security under climate change. *Proceedings of the National Academy of Sciences*, 104, 19703-19708
- Smith, P., Bustamante, M., Ahammad, H., Clark, H., Dong, H., Elsiddig, E.A., Haberl, H., Harper, R., House, J., & Jafari, M. (2014). Agriculture, forestry and other land use (AFOLU). *Climate change 2014: mitigation of climate change. Contribution of Working Group III to the Fifth Assessment Report of the Intergovernmental Panel on Climate Change* (pp. 811-922): Cambridge University Press
- Song, Y., Jain, A.K., & McIsaac, G.F. (2013). Implementation of dynamic crop growth processes into a land surface model: evaluation of energy, water and carbon fluxes under corn and soybean rotation. *Biogeosciences*, 10, 8039-8066
- Stehfest, E., van Vuuren, D., Bouwman, L., & Kram, T. (2014). *Integrated assessment of global environmental change with IMAGE 3.0: Model description and policy applications*. Netherlands Environmental Assessment Agency (PBL)
- Stocker, B.D., Roth, R., Joos, F., Spahni, R., Steinacher, M., Zaehle, S., Bouwman, L., Xu, R., & Prentice, I.C. (2013). Multiple greenhouse-gas feedbacks from the land biosphere under future climate change scenarios. *Nature Climate Change*, 3, 666-672
- Thompson, R.L., Lassaletta, L., Patra, P.K., Wilson, C., Wells, K.C., Gressent, A., Koffi, E.N., Chipperfield, M.P., Winiwarter, W., Davidson, E.A., Tian, H., & Canadell, J.G. (2019). Acceleration of global N₂O emissions seen from two decades of atmospheric inversion. *Nature Climate Change*, 9, 993-998
- Tian, H., Chen, G., Liu, M., Zhang, C., Sun, G., Lu, C., Xu, X., Ren, W., Pan, S., & Chappelka, A. (2010). Model estimates of net primary productivity, evapotranspiration, and water use efficiency in the terrestrial ecosystems of the southern United States during 1895–2007. *Forest Ecology and Management*, 259, 1311-1327
- Tian, H., Lu, C., Ciais, P., Michalak, A.M., Canadell, J.G., Saikawa, E., Huntzinger, D.N., Gurney, K.R., Sitch, S., Zhang, B., Yang, J., Bousquet, P., Bruhwiler, L., Chen, G., Dlugokencky, E., Friedlingstein, P., Melillo, J.,

- Pan, S., Poulter, B., Prinn, R., Saunio, M., Schwalm, C.R., & Wofsy, S.C. (2016). The terrestrial biosphere as a net source of greenhouse gases to the atmosphere. *Nature*, *531*, 225-228
- Tian, H., Xu, R., Canadell, J.G., Thompson, R.L., Winiwarter, W., Suntharalingam, P., Davidson, E.A., Ciais, P., Jackson, R.B., Janssens-Maenhout, G., Prather, M.J., Regnier, P., Pan, N., Pan, S., Peters, G.P., Shi, H., Tubiello, F.N., Zaehle, S., Zhou, F., Arneeth, A., Battaglia, G., Berthet, S., Bopp, L., Bouwman, A.F., Buitenhuis, E.T., Chang, J., Chipperfield, M.P., Dangal, S.R.S., Dlugokencky, E., Elkins, J.W., Eyre, B.D., Fu, B., Hall, B., Ito, A., Joos, F., Krummel, P.B., Landolfi, A., Laruelle, G.G., Lauerwald, R., Li, W., Lienert, S., Maavara, T., MacLeod, M., Millet, D.B., Olin, S., Patra, P.K., Prinn, R.G., Raymond, P.A., Ruiz, D.J., van der Werf, G.R., Vuichard, N., Wang, J., Weiss, R.F., Wells, K.C., Wilson, C., Yang, J., & Yao, Y. (2020a). A comprehensive quantification of global nitrous oxide sources and sinks. *Nature*, *586*, 248-256
- Tian, H., Xu, R., Pan, S., Yao, Y., Bian, Z., Cai, W.-J., Hopkinson, C.S., Justic, D., Lohrenz, S., Lu, C., Ren, W., & Yang, J. (2020b). Long-Term Trajectory of Nitrogen Loading and Delivery From Mississippi River Basin to the Gulf of Mexico. *Global Biogeochemical Cycles*, *34*, e2019GB006475
- Tilman, D., Balzer, C., Hill, J., & Befort, B.L. (2011). Global food demand and the sustainable intensification of agriculture. *Proceedings of the National Academy of Sciences*, *108*, 20260
- Ugarte, C., Calderini, D.F., & Slafer, G.A. (2007). Grain weight and grain number responsiveness to pre-anthesis temperature in wheat, barley and triticale. *Field Crops Research*, *100*, 240-248
- Van den Hoof, C., Hanert, E., & Vidale, P.L. (2011). Simulating dynamic crop growth with an adapted land surface model—JULES-SUCROS: Model development and validation. *Agricultural and Forest Meteorology*, *151*, 137-153
- van Groenigen, K.J., Osenberg, C.W., & Hungate, B.A. (2011). Increased soil emissions of potent greenhouse gases under increased atmospheric CO₂. *Nature*, *475*, 214-216
- Weier, K.L., Doran, J.W., Power, J.F., & Walters, D.T. (1993). Denitrification and the dinitrogen/nitrous oxide ratio as affected by soil water, available carbon, and nitrate. *Soil Science Society of America Journal*, *57*, 66-72
- Wheeler, T., & von Braun, J. (2013). Climate Change Impacts on Global Food Security. *Science*, *341*, 508-513
- Williams, J.R., Jones, C.A., Kiniry, J.R., & Spanel, D.A. (1989). The EPIC crop growth model. *Transactions of the ASAE*, *32*, 497-0511
- Wu, X., Vuichard, N., Ciais, P., Viovy, N., Noblet-Ducoudré, N.d., Wang, X., Magliulo, V., Wattenbach, M., Vitale, L., & Tommasi, P.D. (2016). ORCHIDEE-CROP (v0), a new process-based agro-land surface model: model description and evaluation over Europe. *Geoscientific Model Development*, *9*, 857-873
- Xu, R., Tian, H., Pan, S., Prior, S.A., Feng, Y., & Dangal, S.R.S. (2020). Global N₂O Emissions From Cropland Driven by Nitrogen Addition and Environmental Factors: Comparison and Uncertainty Analysis. *Global Biogeochemical Cycles*, *34*, e2020GB006698
- Yao, Y., Tian, H., Shi, H., Pan, S., Xu, R., Pan, N., & Canadell, J.G. (2020). Increased global nitrous oxide emissions from streams and rivers in the Anthropocene. *Nature Climate Change*, *10*, 138-142
- You, Y., Tian, H., Pan, S., Shi, H., Bian, Z., Gurgel, A., Huang, Y., Kicklighter, D., Liang, X.-Z., Lu, C., Melillo, J., Miao, R., Pan, N., Reilly, J., Ren, W., Xu, R., Yang, J., Yu, Q., & Zhang, J. (2022). Incorporating dynamic crop growth processes and management practices into a terrestrial biosphere model for simulating crop production in the United States: Toward a unified modeling framework. *Agricultural and Forest Meteorology*, *325*, 109144
- Yvon-Durocher, G., Allen, A.P., Bastviken, D., Conrad, R., Gudasz, C., St-Pierre, A., Thanh-Duc, N., & Del Giorgio, P.A. (2014). Methane fluxes show consistent temperature dependence across microbial to ecosystem scales. *Nature*, *507*, 488-491
- Zabel, F., Delzeit, R., Schneider, J.M., Seppelt, R., Mauser, W., & Václavík, T. (2019). Global impacts of future cropland expansion and intensification on agricultural markets and biodiversity. *Nature Communications*, *10*, 2844
- Zhang, J., Tian, H., Shi, H., Zhang, J., Wang, X., Pan, S., & Yang, J. (2020). Increased greenhouse gas emissions intensity of major croplands in China: Implications for food security and climate change mitigation. *Global Change Biology*, *26*, 6116-6133
- Zhang, J., Tian, H., Yang, J., & Pan, S. (2018). Improving representation of crop growth and yield in the Dynamic Land Ecosystem Model and its application to China. *Journal of Advances in Modeling Earth Systems*, *10*, 1680-1707

Chapter 7. Impacts of climate-smart agricultural practices on crop production and greenhouse gas balance in U.S. croplands under future climate predictions

Abstract

Climate-smart agricultural (CSA) practices, such as no tillage and cover cropping, have recently gained widespread advocacy for their potential to curb GHG emissions and enhance soil organic carbon (SOC) sequestration. Nevertheless, the long-term impacts of CSA practices on the regional net GHG balance (i.e., sum of SOC sequestration and emissions of nitrous oxide (N₂O) and methane (CH₄)) and crop production under future climate scenarios are still uncertain, although such a comprehensive analysis could offer valuable insights towards achieving sustainable agriculture. In this study, we used the Dynamic Land Ecosystem Model (DLEM) to predict the long-term impacts of four CSA practices—no tillage, crop rotation, cover cropping, and N fertilizer reduction—on crop production and net GHG balance in U.S. croplands across various future climate scenarios, including SSP126, SSP245, and SSP585. Our results indicate that these CSA practices significantly reduced the net GHG balance in U.S. croplands, with average reductions of 18.9%, 10.3%, 28.6%, and 17.8% for no tillage, N fertilizer reduction, cover cropping, and crop rotation, respectively, across the three climate scenarios. Moreover, while no tillage and N fertilizer reduction only marginally impacted crop production, cover cropping and crop rotation diminished crop production by about 14.7% and 18.5%, respectively. Our results underscore the imperative for comprehensive, scenario-specific CSA strategies to meet the dual goals of climate change mitigation and food security. Our study holds important implications for effectively implementing CSA practices to address climate change issues in the agricultural sector,

which also aligns with carbon neutrality goals and supports the achievement of climate-resilient agricultural systems.

7.1 Introduction

Limiting global warming below the 2°C threshold established by the Paris Climate Agreement requires both efforts to reduce greenhouse gas (GHG) emissions and to remove carbon dioxide (CO₂) from the atmosphere (Rogelj et al. 2016; United Nations 2015). Agriculture plays a crucial role in achieving this objective due to its dual role: it not only contributes significantly to climate change but also offers substantial potential for climate mitigation. Specifically, agriculture is a primary source of anthropogenic GHG emissions, contributing approximately 25%-30% and 35%-50% of global land biogenic emissions of nitrous oxide (N₂O) and methane (CH₄), respectively, during the 2000s (Tian et al. 2016). Furthermore, it is anticipated that these emissions will continue to rise as global fertilizer use increases to meet the projected increase in food demand (Cavigelli et al. 2012; Thompson et al. 2019). On the other hand, agriculture also offers substantial potential for climate mitigation. Global croplands account for about 10% of terrestrial soil organic carbon (SOC) stock (IPCC 2019; Watson et al. 2000) and could potentially sequester 0.90~1.85 Pg C/yr in the top 0.3 m of soils, which is equivalent to 26-53% of the soil carbon sequestration target of 3.5 Pg C/yr established by the 4p1000 Initiative for climate mitigation (Zomer et al. 2017). Notably, by implementing conservation agriculture practices (e.g., reduced tillage and optimized nitrogen (N) fertilization), croplands can mitigate climate change by reducing GHG emissions and enhancing SOC sequestration without compromising crop yield (Bai et al. 2019; Hutchinson et al. 2007; Sun et al. 2020). Net soil GHG emissions, a metric defined as the balance of SOC sequestration, N₂O and CH₄ emissions, can be used to measure the overall climate effect resulting from the cumulative radiative forcing of all three major GHGs (i.e., CO₂, N₂O and CH₄)

(Robertson and Grace 2004). Therefore, it is imperative to seek optimal agricultural management practices that can reduce net soil GHG emissions while sustaining or boosting crop production, which could result in a win-win situation for stabilizing the global climate system and safeguarding food security.

Climate-smart agriculture (CSA) management practices, such as reduced tillage, straw return, cover cropping, and biochar application, have been widely advocated for their potential to enhance SOC sequestration (Bai et al. 2019; FAO 2013; Lipper et al. 2014). For example, reduced tillage and straw return generally minimize soil disturbance and promote soil aggregation, which can reduce SOC losses from soil erosion and protect SOC from microbial degradation, thereby decreasing SOC decomposition rate and increasing SOC stock (Abdalla et al. 2013; Montgomery 2007; Salinas-Garcia et al. 1997). Cover cropping provides additional biomass input to the soil, thereby increasing SOC and N contents (Lal 2004). Moreover, it can promote soil aggregation and structure (Sainju et al. 2003), thereby indirectly reducing SOC loss from erosion (De Baets et al. 2011). However, despite the increase in SOC, these CSA practices have also raised concerns because they could potentially stimulate N₂O and CH₄ emissions, thereby offsetting their climate benefits (Shakoor et al. 2021; Shang et al. 2021; Tian et al. 2012b; Zhou et al. 2017). Specifically, CSA practices, such as reduced tillage and cover cropping, usually lead to improved soil water content (i.e., higher soil water-filled pore space) and increased crop residue coverage, which favor the formation of anaerobic soil conditions and increase substrate concentrations, thereby promoting microbial processes like denitrification and methanogenesis, ultimately facilitating N₂O and CH₄ production (Sheehy et al. 2013; Zhang et al. 2015b). Furthermore, these practices could also impact crop yields, but their effects remain highly debated and are largely dependent on background environmental conditions (Pittelkow et al. 2015a; Schneider et al. 2017). For example,

it has been reported that, under rainfed conditions in dry climates, reduced tillage tends to lead to higher crop yields compared to conventional tillage due to improved soil water conservation and retention (Farooq et al. 2011; Pittelkow et al. 2015b); however, under humid and poor-drained conditions, reduced tillage may negatively impact crop yield due to enhanced soil compaction that inhibits root growth and promotes soil waterlogging (Howeler et al. 1993a). Overall, effective mitigation practices should provide comprehensive benefits on both net GHG emissions and crop yields, not just focusing on one or two agricultural components (e.g., SOC or yield).

In addition to the aforementioned CSA practices aimed at enhancing SOC sequestration, nutrient management and crop rotation have also gained wide attention for their potential in mitigating GHG emissions. Numerous studies have demonstrated that the indiscriminate use of N fertilizers can lead to extra GHG emissions, rather than further boosting crop yield (Cui et al. 2013; Liu and Greaver 2009; Xia et al. 2017; Zhang et al. 2020a). In terms of crop rotation involving legumes, it has great potential to improve water quality and achieve climate targets compared to monocultures. This is due to the legume crops' ability to biologically fix N from the atmosphere, which can reduce both nutrient runoff and GHG emissions by decreasing the need for synthetic N fertilizers (Reckling et al. 2016a; Reckling et al. 2016b).

Many studies have investigated the impacts of CSA practices (e.g., reduced tillage, straw return, cover cropping, N fertilization management, and crop rotation) on various agricultural components (i.e., SOC, N₂O, CH₄, and yield) (Bai et al. 2019; Beillouin et al. 2021; Huang et al. 2020; Sun et al. 2020; Yu et al. 2020; Zhang et al. 2020a). However, most of these studies have focused on one or two agricultural components (e.g., SOC or yield) and are often limited to small spatial scales, such as site- and landscape-scales. Conversely, few studies have quantified the integrated effects of CSA practices on all these agricultural components simultaneously, especially

at large spatial scales (e.g., national- and continental- scales). Due to possible trade-offs between SOC sequestration and GHG emissions under various CSA practices (Guenet et al. 2021; Tian et al. 2015a; Tian et al. 2011), studies fail to simultaneously quantify SOC-sequestered CO₂ and non-CO₂ GHG emissions, as well as crop yields may lead to inconsistency when making comparisons and may not provide effective mitigation assessments (Shang et al. 2021). Additionally, both natural and human-induced environmental changes such as climate change, atmospheric CO₂ fertilization, and N deposition have substantially influenced agricultural GHG emissions and crop yields in complex ways (Ren et al. 2012; Ren et al. 2011; Zhang et al. 2020a). These environmental factors often interact with the local geographical environment (e.g., diverse soil types and climatic conditions) to influence the efficacy of CSA practices. This implies that a CSA practice effective in one location under certain environmental conditions may not be effective elsewhere (Shang et al. 2021). Therefore, to accurately and comprehensively assess the mitigation potential of CSA practices, it is crucial to evaluate their impacts on both net GHG emissions and crop yields at large spatial scales, taking into account multiple environmental changes simultaneously (e.g., climate change and atmospheric CO₂ fertilization).

Greenhouse gas emission intensity (GHGI), a CO₂ equivalents-based metric defined as net soil GHG emissions per unit of crop production (Grassini and Cassman 2012; Mosier et al. 2006), can be used to measure the balance between net soil GHG emissions and crop yields. CSA practices that can decrease GHGI are vital for resolving the conflict between climate change mitigation and food security. While field experiments offer a practical way to unravel the complex relationships between changes in GHGI and management practices under diverse environmental conditions (Plaza-Bonilla et al. 2018), extrapolating these site-specific findings to broader spatial scales using statistical methods is challenging due to the unique environmental and management

conditions at each experimental site. Furthermore, there is still a lack of long-term and spatially explicit assessments examining the effects of multiple CSA practices and environmental factors on GHGI at the regional scale—information that is critical for developing effective mitigation strategies. Process-based terrestrial biosphere models (TBMs) with well-represented biophysical, biogeochemical, hydrological, and crop growth processes, as well as key agricultural management practices, can address these limitations and provide a promising tool for climate change mitigation and adaptation in agriculture (Bondeau et al. 2007; McDermid et al. 2017; You et al. 2022). Therefore, employing TBMs to study the effects of different CSA practices on net GHG emissions, crop yields, and GHGI under various future climate scenarios is essential for accurately assessing the overall climate mitigation potential of these practices.

As one of the world's leading agricultural producers, the U.S. contributes a significant portion of global agricultural GHG emissions and plays a pivotal role in the global agricultural system. Taking the U.S. as a representative area, this study aims to assess the impact of four CSA practices—namely, no tillage, crop rotation, cover cropping (planting peas in the fallow period), and N fertilizer reduction—on crop production, net GHG balance, and GHGI in U.S. croplands across various future climate scenarios, including SSP126, SSP245, and SSP585. To perform these simulations, we used climate forcings derived from a CMIP6 climate model, IPSL-CM6A-LR, to drive a highly integrated TBM, the Dynamic Land Ecosystem Model v4.0 (DLEM v4.0). Our work may provide valuable insights into the overall climate mitigation potential of these CSA practices under different future climate scenarios.

7.2 Materials and methods

7.2.1 Model and forcing datasets

DLEM v4.0 is a highly integrated TBM that is capable of quantifying daily, spatially explicit carbon, water, and nutrient stocks and fluxes in terrestrial ecosystems and inland water systems across site, regional, and global scales (Pan et al. 2021; Tian et al. 2010a; Tian et al. 2020b; Yao et al. 2020). To meet cross-scale agricultural application needs (e.g., management guidance, climate change mitigation and adaptation), DLEM v4.0 has incorporated explicit and mechanistic representations of dynamic crop growth processes and multiple agricultural management practices. These include but are not limited to crop-specific phenological development, carbon allocation, yield formation, and biological N fixation processes, as well as management practices such as N fertilization, irrigation, rotation, manure application, tillage, cover cropping, and crop genetic improvements (You et al. 2022). By fully coupling these agricultural processes with biogeochemical, biophysical, and hydrological processes, DLEM v4.0 is capable of simulating and predicting the exchange of carbon (including crop yield), water, nutrient and energy fluxes within the agriculture-climate-environment system. A thorough description of the processes incorporated into the agricultural module of DLEM v4.0 is presented in Chapter 2.

To predict future variations in U.S. crop production and GHG emissions, we used climate forcings (e.g., climate conditions, atmospheric CO₂ concentration, and N deposition) from CMIP6 to drive DLEM. A detailed description of the three climate scenarios (i.e., SSP126, SSP245, and SSP585) is provided in Section 6.2.2.1 in Chapter 6. Details of other model forcing datasets such as land use change and soil properties can be found in Section 2.3 in Chapter 2.

7.2.2 CSA practices scenarios

In this study, we evaluated the impacts of four CSA practices—namely, no tillage, reduced N fertilizer use, cover cropping, and crop rotation with legume crops—on crop production, GHG, and GHGI. To assess these impacts, we assumed that all croplands would adopt these CSA practices separately under various future climate scenarios. Specifically, for the no tillage practice, all croplands would implement no tillage during the future simulation period 2020-2100, and all crop residues would be left on the soil surface. For the reduction of N fertilizer use, all croplands would reduce the N fertilizer use rate to 75% of the fertilizer level in 2020 during the future simulation period. For the cover cropping practice, all croplands would plant peas (i.e., an annual, relatively drought tolerant legume crop used for cover crops) during the normal fallow period and leave all crop biomass in the field at the beginning of the following main crop growing season. For crop rotation with legume crops, all corn sites would follow a consistent corn-soybean rotation pattern, alternating between planting corn and soybean each year. In this sequence, if corn was planted in the first year, soybean would be planted in the following year, followed by another year of corn, and then soybean, and so on. Additionally, we conducted four comparative experiments, examining the following experimental pairs: “no tillage vs. conventional tillage”, “75% N fertilizer use vs. 100% N fertilizer use”, “with cover cropping vs. without cover cropping”, and “with crop rotation vs. without crop rotation”.

7.2.3 Model implementation and experimental design

Implementation of DLEM v4.0 consisted of three major steps: an equilibrium run, a spin-up run, and a transient run. The equilibrium run was driven by average annual climate data during the 1860s and other environmental factors in 1860. The equilibrium state was assumed to be reached when changes in carbon, N, and water pools between two consecutive 20-year periods were less

than $0.5 \text{ g C m}^{-2} \text{ year}^{-1}$, $0.5 \text{ g N m}^{-2} \text{ year}^{-1}$, and 0.5 mm year^{-1} , respectively. The spin-up run was driven by detrended climate data during the 1860s to eliminate fluctuations due to the transition from equilibrium run to transient run. Finally, the transient run was driven by historical and future data from 1860 to 2100 for the three SSP-RCP combinations (i.e., SSP585, SSP245, and SSP126). Note that, when the model was run for the period 2020-2100, management practices (excluding CSA practices) and land use change data were maintained at the 2020 level.

We designed eight experiments to assess the impacts of CSA practices on crop production, GHG, and GHGI under different future climate scenarios (Table 7-1), namely SSP126, SSP245, and SSP585. These scenario pairs include “no tillage (S1) vs. conventional tillage (S2)”, “75% N fertilizer use (S3) vs. 100% N fertilizer use (S4)”, “with cover cropping (S5) vs. without cover cropping (S6)”, and “with crop rotation (S7) vs. without crop rotation (S8)”. Among these experiments, climate conditions, atmospheric CO_2 concentration, and N deposition were derived from future climate scenarios and were time-varying. Conversely, the implementation of CSA practices was adjusted correspondingly for each experiment. For example, S1 represents the no tillage scenario, where no tillage practice was implemented in all croplands during 2020-2100, and all other management practices were maintained at the 2020 level. Similarly, S3 represents the N fertilizer reduction scenario, where 75% of the 2020 fertilizer level was applied in all croplands during 2020-2100, while all other management practices were maintained at the 2020 level. The mitigation potential of each CSA practice is determined by the difference between these paired experiments.

Table 7-1. Comparative experiments of climate-smart agriculture practices in this study.

Scenario	Climate, CO ₂ concentration, and N deposition	Tillage	N fertilizer use	Cover cropping	Rotation
S1 No tillage	1860-2100 ^Δ	No tillage [#]	1860-2020*	None	None
S2 Conventional tillage	1860-2100 ^Δ	Conventional tillage [#]	1860-2020*	None	None
S3 75% N fertilizer use	1860-2100 ^Δ	1860-2020*	75% of the 2020 fertilizer level [#]	None	None
S4 100% N fertilizer use	1860-2100 ^Δ	1860-2020*	100% of the 2020 fertilizer level [#]	None	None
S5 With cover cropping	1860-2100 ^Δ	1860-2020*	1860-2020*	With cover cropping [#]	None
S6 Without cover cropping	1860-2100 ^Δ	1860-2020*	1860-2020*	Without cover cropping [#]	None
S7 With crop rotation	1860-2100 ^Δ	1860-2020*	1860-2020*	None	With rotation [#]
S8 Without crop rotation	1860-2100 ^Δ	1860-2020*	1860-2020*	None	Without rotation [#]

^ΔClimate conditions, atmospheric CO₂ concentration, and N deposition after 2020 were derived from various future climate scenarios (i.e., SSP126, SSP245, and SSP585), and data before 2020 were derived from historically real-world datasets.

[#]Simulations after 2020 were driven by the corresponding climate-smart practices, and simulations before 2020 were driven by historically varying practices datasets.

*Data after 2020 was kept the same as 2020.

7.2.4 Global warming potential and GHGI calculation

The global warming potential (GWP) is an index to measure the integrated radiative forcing from the emission of 1 kg of a trace gas relative to that of CO₂ (Myhre et al. 2013). In GWP conversions, CO₂ is typically considered the reference gas with a GWP constant of 1. CH₄ and N₂O emissions can be converted to ‘CO₂-equivalents’ based on their respective GWP constants over a specified time horizon. To obtain a comprehensive assessment of the climatic impact of net soil GHG balance, we adopted the following equation to calculate the combined GWPs for SOC sequestration of CO₂ and N₂O and CH₄ emissions:

$$GWP = F_{CO_2-C} \times \frac{44}{12} \times GWP_{CO_2} + F_{N_2O-N} \times \frac{44}{28} \times GWP_{N_2O} + F_{CH_4-C} \times \frac{16}{12} \times GWP_{CH_4} \quad (1)$$

$$F_{CO_2-C} = -SOCSR \quad (2)$$

where F_{CO_2-C} , F_{N_2O-N} , and F_{CH_4-C} were annual fluxes of CO₂, N₂O, and CH₄, respectively; $SOCSR$ was SOC sequestration rate; molecular weight conversion fractions 44/12, 44/28, and 16/12 were used to convert the mass of CO₂-C, N₂O-N, and CH₄-C into CO₂, N₂O, and CH₄, respectively; GWP_{CO_2} , GWP_{N_2O} and GWP_{CH_4} were GWP constants indicating radiative forcing of CO₂, N₂O, and CH₄ in terms of their CO₂ equivalents, and this study used the GWP values integrated over a time horizon of 100 years for CO₂, N₂O, and CH₄, which were 1, 273, and 27, respectively (Myhre et al. 2013).

GHGI, defined as the amount of net soil GHGs emitted per unit of food produced, can be used to assess the efficiency of agricultural systems in emitting GHGs relative to their productivity:

$$GHGI = GHG / Crop \text{ Production} \quad (3)$$

where GHG is the GWP value of net soil GHG balance, and crop production is the simulated crop yield.

7.3 Results

7.3.1 Impacts of no tillage on net GHG balance, crop production, and GHGI

We analyzed the impacts of no tillage and conventional tillage practices on the future net GHG balance, crop production, and GHGI of U.S. croplands under various future climate scenarios (Figure 7-1). Under no tillage, the estimated national net GHG balance during 2020-2100 was 137 Tg CO₂-eq year⁻¹, 168 Tg CO₂-eq year⁻¹, and 221 Tg CO₂-eq year⁻¹ under the SSP126, SSP245, and SSP585 scenarios, respectively. Conversely, under conventional tillage, the estimated national net GHG balance was 170 Tg CO₂-eq year⁻¹, 212 Tg CO₂-eq year⁻¹, and 263 Tg CO₂-eq year⁻¹ under the respective scenarios. When compared to the estimated future net GHG balance under

natural environmental changes (i.e., no CSA practices were implemented), no tillage resulted in a reduction of 9.3%, 7.1%, and 7.2% in net GHG balance under the SSP126, SSP245, and SSP585 scenarios, respectively. In contrast, conventional tillage increased net GHG balance by 12.7%, 17.8%, and 10.6% under the respective scenarios. Generally, no tillage significantly reduced the net soil GHG balance of U.S. croplands by 19.5% under SSP126, 21.1% under SSP245, and 16% under SSP585 scenarios, compared to conventional tillage. Furthermore, our findings suggest no significant temporal variations in the mitigation potential of no tillage, with the largest mitigation potential exhibited under the SSP126 scenario.

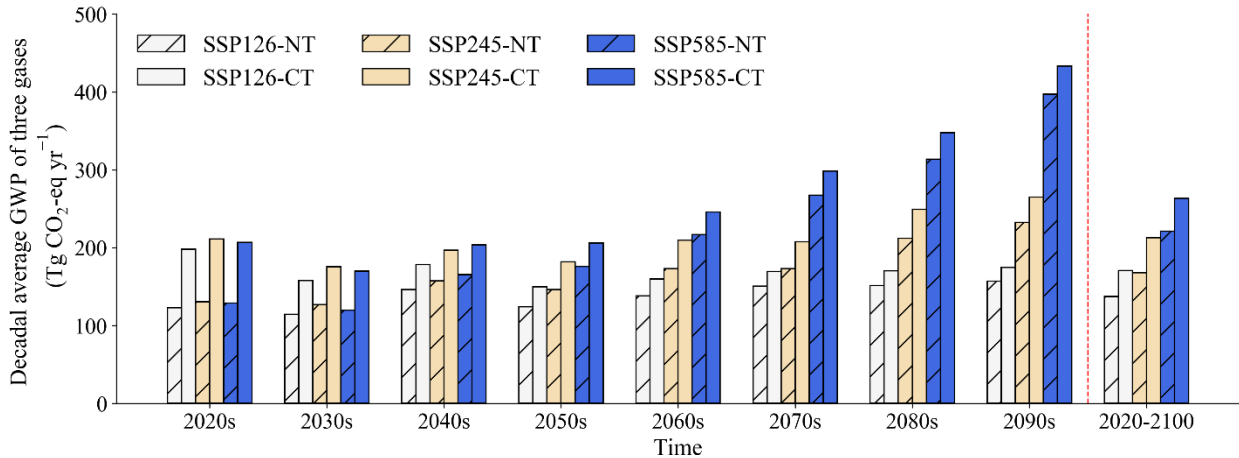


Figure 7-1. Temporal variations in national net greenhouse gas balance of U.S. croplands from the 2020s to the 2090s under the implementation of no tillage and conventional tillage across various future scenarios (i.e., SSP126, SSP245, and SSP585). Note that NT and CT represent no tillage and conventional tillage, respectively.

Under no tillage, national crop production during 2020-2100 was estimated to be 582 Tg year⁻¹ under the SSP126 scenario, 535 Tg year⁻¹ under the SSP245 scenario, and 558 Tg year⁻¹ under the SSP585 scenario. In comparison, under conventional tillage, the estimates were 601 Tg year⁻¹, 556 Tg year⁻¹, and 578 Tg year⁻¹ under the SSP126, SSP245, and SSP585 scenarios, respectively. The implementation of no tillage resulted in a slight reduction in national crop

production by 3.2%, 3.6%, and 3.3% under the respective scenarios, respectively, compared to conventional tillage (Figure 7-2). Additionally, we observed no significant temporal variations in the impacts of no tillage and conventional tillage on national crop production.

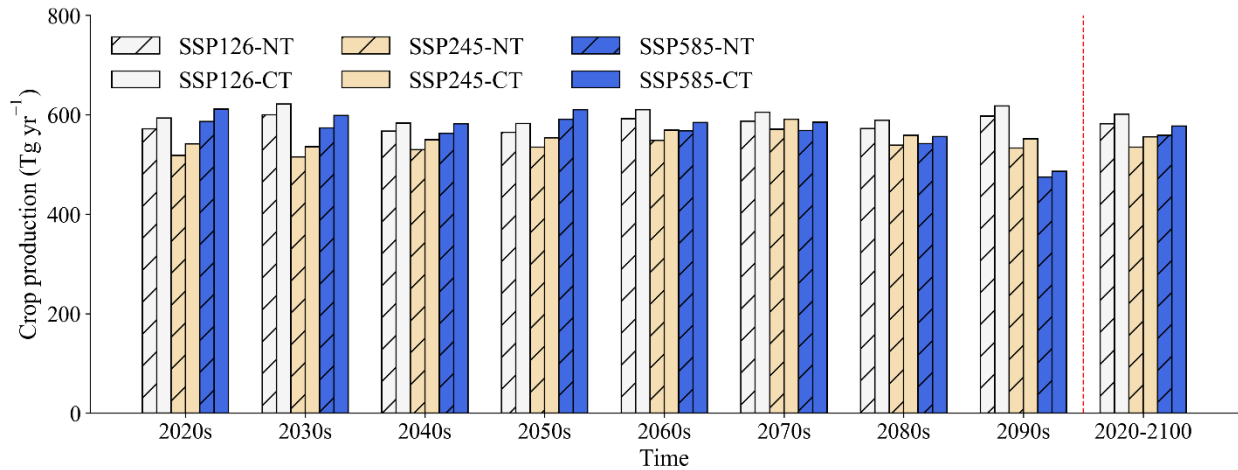


Figure 7-2. Temporal variations in national crop production of U.S. croplands from the 2020s to the 2090s under the implementation of no tillage and conventional tillage across various future scenarios (i.e., SSP126, SSP245, and SSP585). Note that NT and CT represent no tillage and conventional tillage, respectively.

Combining crop production and net GHG balance, the national GHGI during 2020-2100 under no tillage was estimated to be 0.24 Tg CO₂-eq Tg⁻¹ under the SSP126 scenario, 0.31 Tg CO₂-eq Tg⁻¹ under the SSP245 scenario, and 0.4 Tg CO₂-eq Tg⁻¹ under the SSP585 scenario (Figure 7-3). Relative to the GHGI estimated under natural environmental changes, our results suggest that no tillage reduces national GHGI by 7.6%, 7.8%, and 5.7% for the SSP126, SSP245, and SSP585 scenarios, respectively. When compared to conventional tillage, no tillage reduces national GHGI by 16.8%, 18.1%, and 13.3% under the respective scenarios. Additionally, we found no significant temporal variations in the mitigation potential of no tillage regarding GHGI, and no tillage exhibited the largest mitigation potential under the SSP126 and SSP245 scenarios.

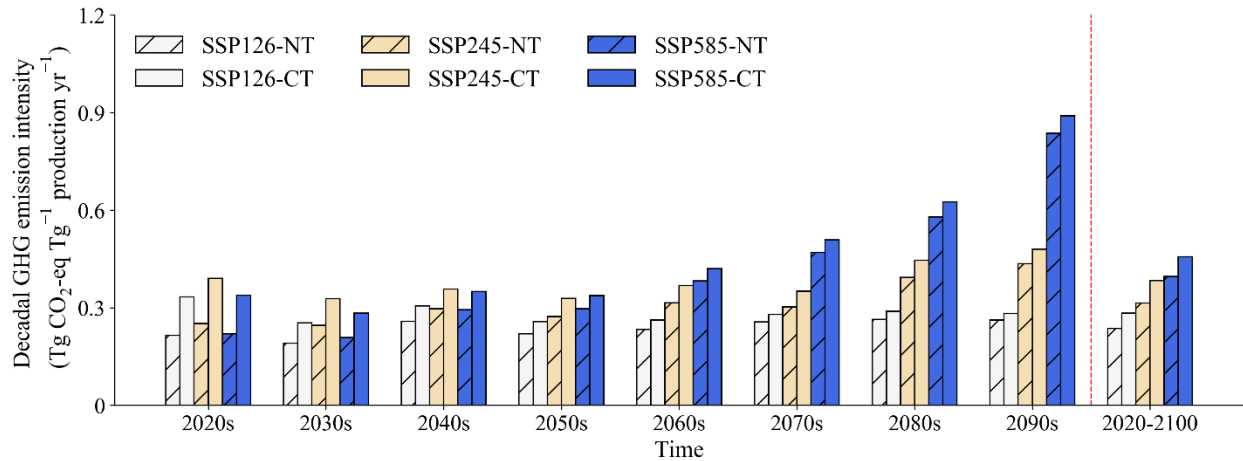


Figure 7-3. Temporal variations in national greenhouse gas emissions intensity of U.S. croplands from the 2020s to the 2090s under the implementation of no tillage and conventional tillage across various future scenarios (i.e., SSP126, SSP245, and SSP585). Note that NT and CT represent no tillage and conventional tillage, respectively.

7.3.2 Impacts of N fertilizer reduction on net GHG balance, crop production, and GHGI

Our results indicate that reducing N fertilizer by 25% could lead to a lower net GHG balance compared to scenarios with no N fertilizer reduction (Figure 7-4). Specifically, the estimated national net GHG balance during 2020-2100 under a 75% N fertilization level was 128 Tg CO₂-eq year⁻¹, 171 Tg CO₂-eq year⁻¹, and 215 Tg CO₂-eq year⁻¹ under the SSP126, SSP245, and SSP585 scenarios, respectively. This reduction in N fertilizer mitigates the net GHG balance by 15.6%, 5.6%, and 9.8% under the respective scenarios compared to those with no N fertilizer reduction. Furthermore, our findings suggest that the mitigation potential of N fertilizer reduction does not exhibit significant temporal variations, with the largest mitigation potential observed under the SSP126 scenario.

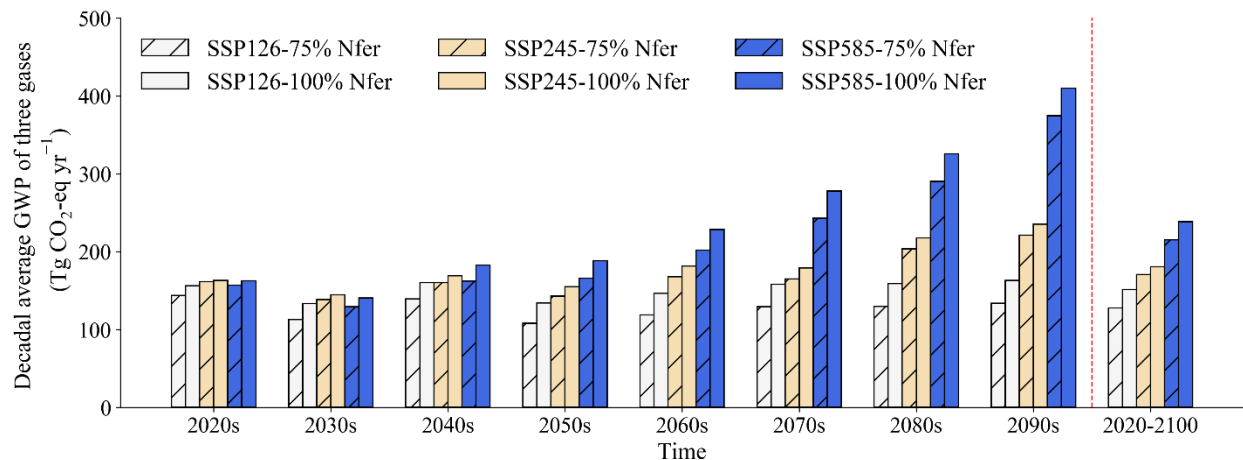


Figure 7-4. Temporal variations in national net greenhouse gas balance of U.S. croplands from the 2020s to the 2090s under a 25% reduction in nitrogen fertilizer (i.e., 75% Nfer) and no nitrogen fertilizer reduction (i.e., 100% Nfer) across various future scenarios (i.e., SSP126, SSP245, and SSP585).

Under the scenario of N fertilizer reduction, national crop production during 2020-2100 was estimated to be 573 Tg year⁻¹ under the SSP126 scenario, 528 Tg year⁻¹ under the SSP245 scenario, and 560 Tg year⁻¹ under the SSP585 scenario. In comparison, under the scenario of no N fertilizer reduction, the estimates were 593 Tg year⁻¹, 531 Tg year⁻¹, and 568 Tg year⁻¹ under the respective scenarios. A 25% reduction in N fertilizer resulted in a slight reduction in national crop production by 3.2%, 0.5%, and 1.4% under the SSP126, SSP245, and SSP585 scenarios, respectively (Figure 7-5). Additionally, our results showed no significant temporal variations in the impacts of N fertilizer reduction on national crop production.

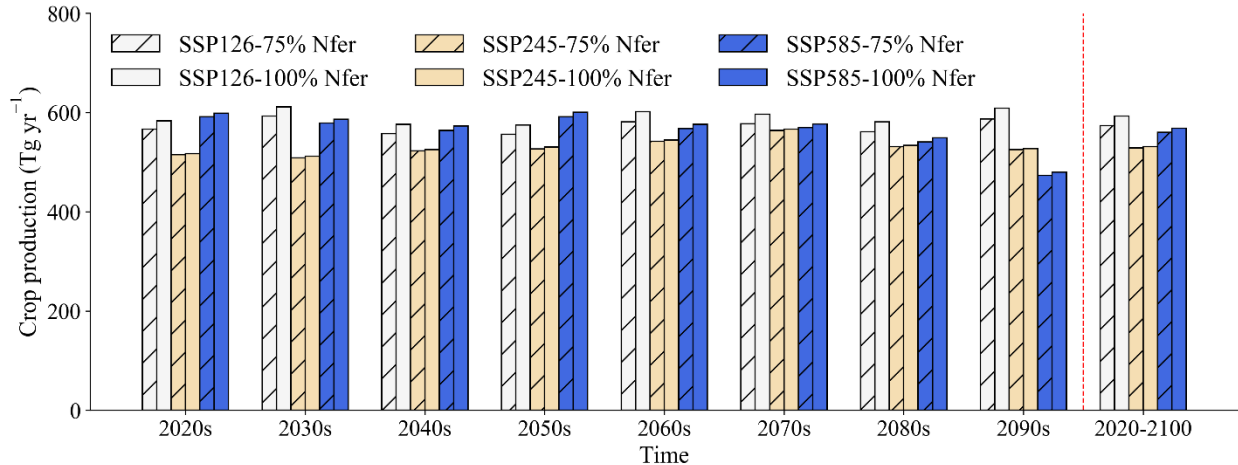


Figure 7-5. Temporal variations in national crop production of U.S. croplands from the 2020s to the 2090s under a 25% reduction in nitrogen fertilizer (i.e., 75% Nfer) and no nitrogen fertilizer reduction (i.e., 100% Nfer) across various future scenarios (i.e., SSP126, SSP245, and SSP585).

Combining crop production and net GHG balance, the national GHGI during 2020-2100, under the scenario of a 25% reduction in N fertilizer, was estimated to be 0.22 Tg CO₂-eq Tg⁻¹, 0.32 Tg CO₂-eq Tg⁻¹, and 0.38 Tg CO₂-eq Tg⁻¹ for the SSP126, SSP245, and SSP585 scenarios, respectively (Figure 7-6). Relative to the GHGI estimated without N fertilizer reduction, our results suggest that a 25% reduction in N fertilizer mitigates national GHGI by 12.8%, 5.1%, and 8.5% for the SSP126, SSP245, and SSP585 scenarios, respectively. Additionally, we found no significant temporal variations in the mitigation potential of N fertilizer reduction regarding GHGI, with the largest mitigation potential observed under the SSP126 scenario.

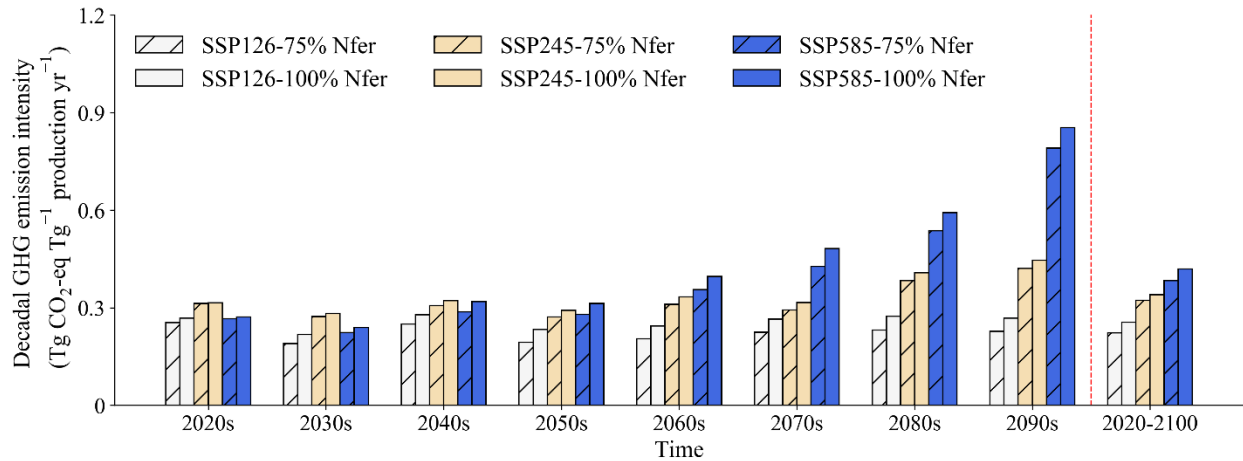


Figure 7-6. Temporal variations in national greenhouse gas emissions intensity of U.S. croplands from the 2020s to the 2090s under a 25% reduction in nitrogen fertilizer (i.e., 75% Nfer) and no nitrogen fertilizer reduction (i.e., 100% Nfer) across various future scenarios (i.e., SSP126, SSP245, and SSP585).

7.3.3 Impacts of cover cropping on net GHG balance, crop production, and GHGI

With the implementation of cover cropping practice (i.e., planting peas in the fallow period), the estimated national net GHG balance during 2020-2100 was 128 Tg CO₂-eq year⁻¹, 89 Tg CO₂-eq year⁻¹, and 192 Tg CO₂-eq year⁻¹ under the SSP126, SSP245, and SSP585 scenarios, respectively (Figure 7-7). In contrast, without cover cropping, the estimated national net GHG balance was 151 Tg CO₂-eq year⁻¹, 181 Tg CO₂-eq year⁻¹, and 238 Tg CO₂-eq year⁻¹ under the respective scenarios. Thus, cover cropping reduced the net GHG balance by 23 Tg CO₂-eq year⁻¹ (16%), 92 Tg CO₂-eq year⁻¹ (51%), and 46 Tg CO₂-eq year⁻¹ (19%) under the SSP126, SSP245, and SSP585 scenarios, respectively. In addition, our findings suggest that the largest mitigation potential is exhibited under the SSP245 scenario.

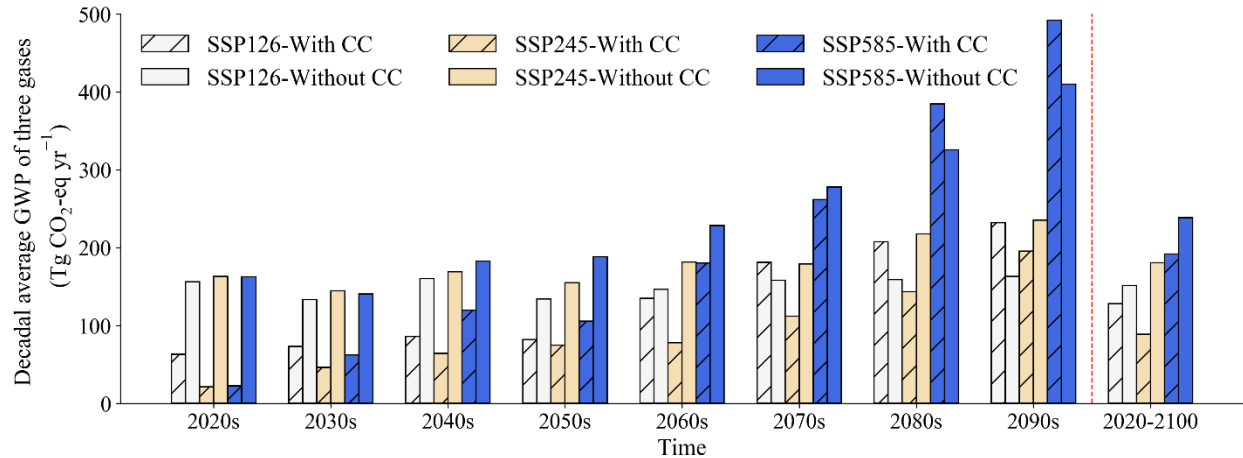


Figure 7-7. Temporal variations in national net greenhouse gas balance of U.S. croplands from the 2020s to the 2090s with cover cropping and without cover cropping practices across various future scenarios (i.e., SSP126, SSP245, and SSP585). Note that CC represents cover cropping.

With the implementation of cover cropping practice, national crop production during 2020-2100 was estimated to be 505 Tg year⁻¹, 458 Tg year⁻¹, and 478 Tg year⁻¹ under the SSP126, SSP245, and SSP585 scenarios, respectively. In comparison, without cover cropping, the estimates were 593 Tg year⁻¹, 531 Tg year⁻¹, and 568 Tg year⁻¹ under the respective scenarios. Cover cropping resulted in a reduction in national crop production by 14.8%, 13.7%, and 15.8% under the SSP126, SSP245, and SSP585 scenarios, respectively (Figure 7-8). Additionally, no significant temporal variations were observed in the impacts of cover cropping practice on national crop production.

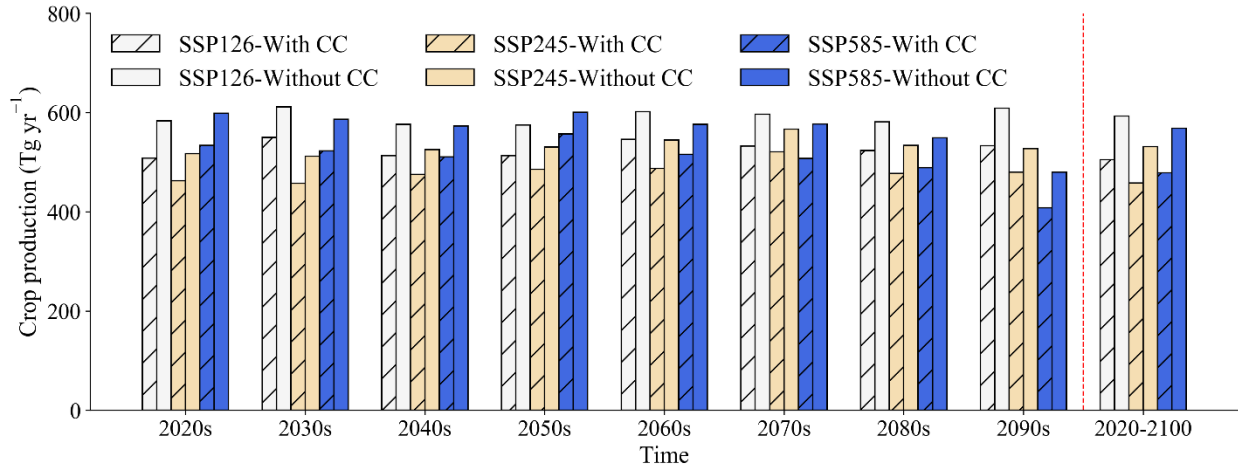


Figure 7-8. Temporal variations in national crop production of U.S. croplands from the 2020s to the 2090s with cover cropping and without cover cropping practices across various future scenarios (i.e., SSP126, SSP245, and SSP585). Note that CC represents cover cropping.

The national GHGI during 2020-2100 under the implementation of cover cropping practice was estimated to be 0.25 Tg CO₂-eq Tg⁻¹ for the SSP126 scenario, 0.19 Tg CO₂-eq Tg⁻¹ for the SSP245 scenario, and 0.4 Tg CO₂-eq Tg⁻¹ for the SSP585 scenario (Figure 7-9). Compared to the GHGI estimated without cover cropping, our results suggest that cover cropping reduced national GHGI by 0.002 Tg CO₂-eq Tg⁻¹, 0.146 Tg CO₂-eq Tg⁻¹, and 0.018 Tg CO₂-eq Tg⁻¹ for the SSP126, SSP245, and SSP585 scenarios, respectively. Additionally, we found that cover cropping exhibited the largest mitigation potential under the SSP245 scenario.

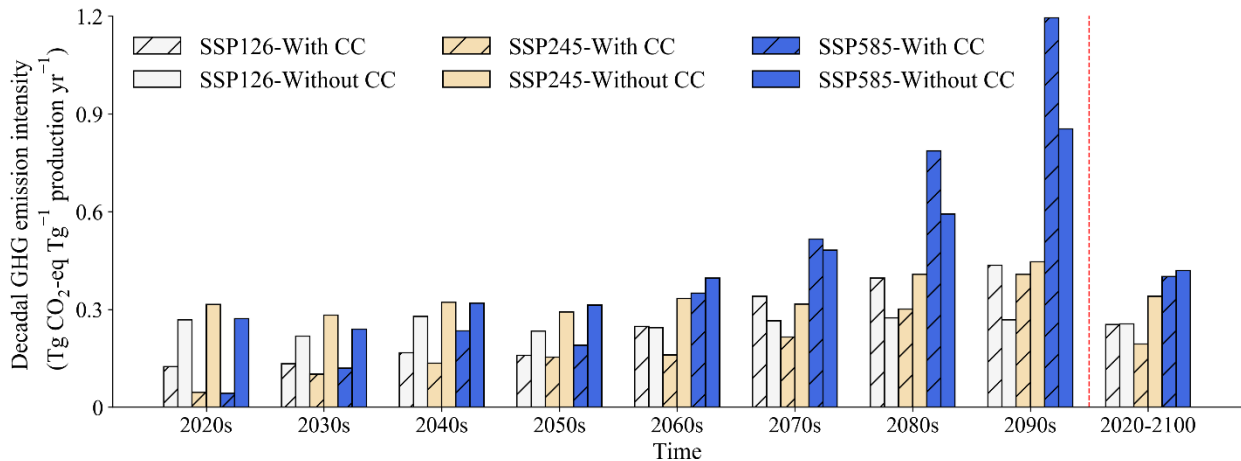


Figure 7-9. Temporal variations in national greenhouse gas emissions intensity of U.S. croplands from the 2020s to the 2090s with cover cropping and without cover cropping practices across various future scenarios (i.e., SSP126, SSP245, and SSP585). Note that CC represents cover cropping.

7.3.4 Impacts of crop rotation on net GHG balance, crop production, and GHGI

Our results demonstrate that implementing crop rotation could result in a lower net GHG balance compared to scenarios that do not employ this practice (Figure 7-10). Specifically, when employing corn-soybean rotation, the national net GHG balance during 2020-2100 was estimated to be 117 Tg CO₂-eq year⁻¹, 149 Tg CO₂-eq year⁻¹, and 207 Tg CO₂-eq year⁻¹ under the SSP126, SSP245, and SSP585 scenarios, respectively. Crop rotation resulted in reductions of 22.9%, 17.4%, and 13.1% in net GHG balance under the respective scenarios. Furthermore, our findings suggest no significant temporal variations in the mitigation potential of crop rotation, with the largest mitigation potential exhibited under the SSP126 scenario.

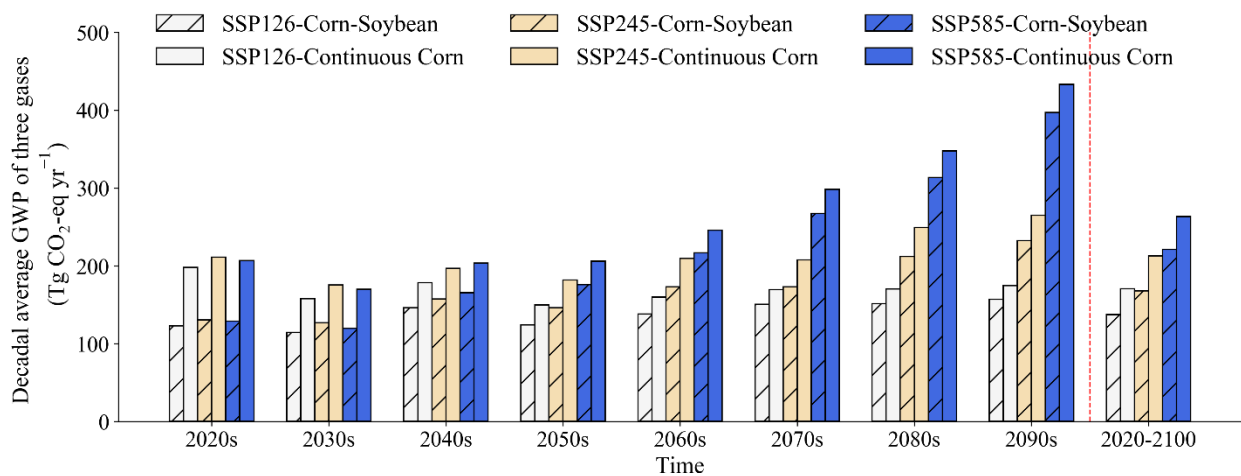


Figure 7-10. Temporal variations in national net greenhouse gas balance of U.S. croplands from the 2020s to the 2090s with crop rotation (i.e., corn-soybean rotation) and without crop rotation (i.e., continuous corn) practices across various future scenarios (i.e., SSP126, SSP245, and SSP585).

Under crop rotation, national crop production during 2020-2100 was estimated to be 475 Tg year⁻¹, 431 Tg year⁻¹, and 472 Tg year⁻¹ under the SSP126, SSP245, and SSP585 scenarios, respectively. Compared to the scenario without crop rotation, the implementation of crop rotation practice resulted in reductions in national crop production by 19.8%, 18.9%, and 16.9% under the respective scenarios (Figure 7-11). Additionally, we observed no significant temporal variations in the impacts of crop rotation on national crop production.

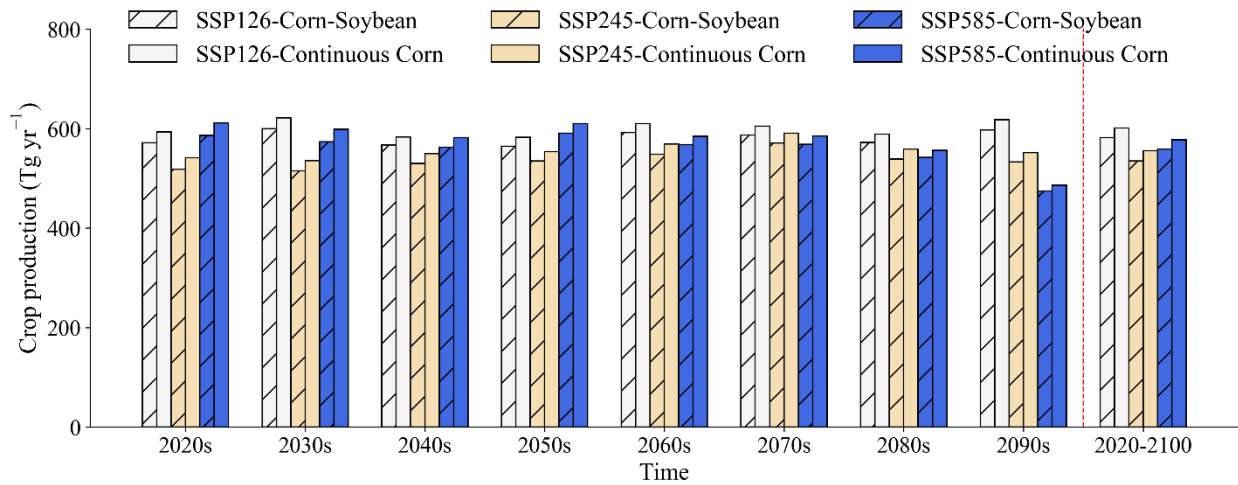


Figure 7-11. Temporal variations in national crop production of U.S. croplands from the 2020s to the 2090s with crop rotation (i.e., corn-soybean) and without crop rotation (i.e., continuous corn) practices across various future scenarios (i.e., SSP126, SSP245, and SSP585).

The national GHGI for the period 2020-2100, under the implementation of crop rotation, was estimated to be 0.25 Tg CO₂-eq Tg⁻¹, 0.35 Tg CO₂-eq Tg⁻¹, and 0.44 Tg CO₂-eq Tg⁻¹ for the SSP126, SSP245, and SSP585 scenarios, respectively (Figure 7-12). When compared to the GHGI estimated without crop rotation, our results suggest that crop rotation reduced national GHGI by 3.9% under the SSP126 scenario, but increased it by 1.9% and 4.7% under the SSP245 and SSP585 scenarios, respectively. Overall, our findings demonstrate that the largest mitigation potential of crop rotation is exhibited under the SSP126 scenario.

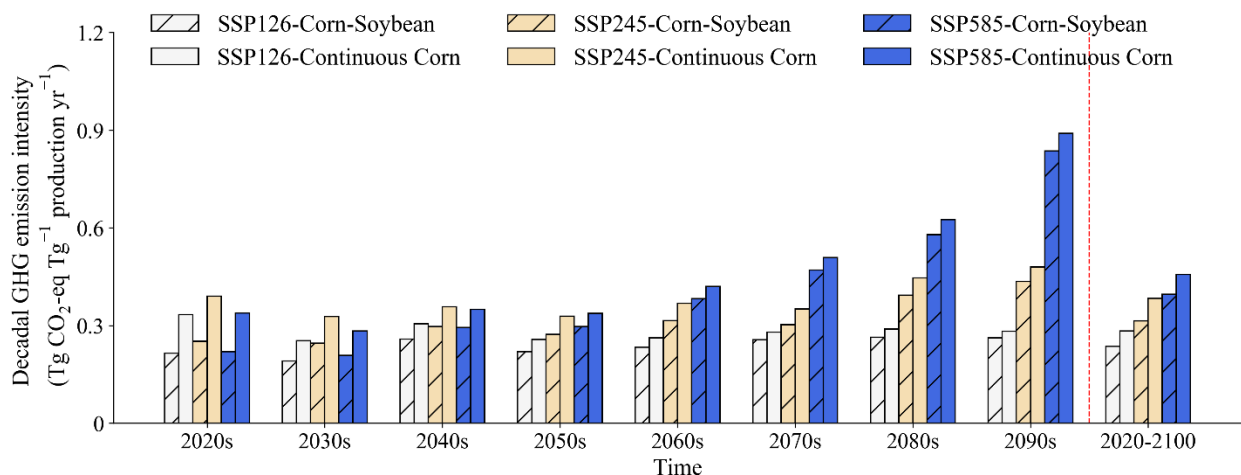


Figure 7-12. Temporal variations in national greenhouse gas emissions intensity of U.S. croplands from the 2020s to the 2090s with crop rotation (i.e., corn-soybean) and without crop rotation (i.e., continuous corn) practices across various future scenarios (i.e., SSP126, SSP245, and SSP585).

7.4 Discussion

7.4.1 Comparison with previous studies

Our analysis of the impacts of CSA practices on net GHG balance, crop yield, and GHGI provides pivotal insights imperative for simultaneously addressing climate change issues and ensuring food security. In terms of no tillage, our findings indicate that implementing this practice could reduce the net GHG balance, while implementing conventional tillage would increase it. Specifically, compared to 2020, implementing no tillage during 2020-2100 resulted in a reduction of 9.3%, 7.1%, and 7.2% in net GHG balance under the SSP126, SSP245, and SSP585 scenarios, respectively, whereas conventional tillage increased net GHG balance by 12.7%, 17.8%, and 10.6% under the respective scenarios (Figure 7-1). Compared to conventional tillage, no tillage significantly reduced the net soil GHG balance of U.S. croplands by 19.5% under SSP126, 21.1% under SSP245, and 16% under SSP585 scenarios. Our findings are consistent with previous studies. For example, Del Grosso et al. (2005) reported a 33% reduction in GWP under no tillage compared

to tilled soil for major non-rice cropping systems in the U.S.; Mangalassery et al. (2014) found that tilled soil produced 20% greater net GWP than zero tilled soil. No tillage has large potential in increasing SOC storage and improving soil health and quality (Ogle et al. 2019; Powlson et al. 2014; Sun et al. 2020). It typically minimizes soil disturbance and promotes soil aggregation, which can reduce SOC losses from soil erosion and protect SOC from microbial attack, thereby decreasing the SOC decomposition rate and increasing SOC stock (Abdalla et al. 2013; Montgomery 2007; Salinas-Garcia et al. 1997). Nonetheless, no tillage may simultaneously influence N₂O and CH₄ emissions (Shakoor et al. 2021) by altering soil water content (i.e., higher soil water-filled pore space) and crop residue coverage. Our results revealed reduced N₂O emissions under no tillage, consistent with some previous studies (Plaza-Bonilla et al. 2018; Yoo et al. 2016) but contradictory to others (Huang et al. 2018; Lutz et al. 2019b). The reduction in N₂O emissions may be attributed to the well-aerated farmland soils (Rochette 2008), coupled with lower N mineralization rates due to the retention of crop residues on the soil surface under no tillage. Conversely, our results indicated increased CH₄ emissions under no tillage, potentially due to increased substrate concentration promoting the methanogenesis process and thereby enhancing CH₄ production (Sheehy et al. 2013; Zhang et al. 2015b). In addition, our results indicate that no tillage slightly reduced crop production (Figure 7-2), aligning with previous studies (Ogle et al. 2012; Pittelkow et al. 2015b; Van Kessel et al. 2013). This reduction is possibly due to increased soil compaction that potentially inhibits root growth and promotes soil waterlogging (Alvarez and Steinbach 2009; Howeler et al. 1993b; Van den Putte et al. 2010).

Our analyses also underscored the climate benefits of a 25% reduction in N fertilizer, which significantly mitigated the national net GHG balance by 15.6%, 5.6%, and 9.8% under the SSP126, SSP245, and SSP585 scenarios, respectively (Figure 7-4). Notably, this reduction in N fertilizer

led to only a slight decrease in crop production, with decreases ranging between 0.5% and 3.2% under the three scenarios (Figure 7-5). The slight decline in crop production, in contrast with the substantial decrease in net GHG balance, suggests that N fertilization in U.S. croplands could potentially be further optimized to mitigate climate change without causing substantial detriment to U.S. food security (Mueller et al. 2012; Roy et al. 2021). This is consistent with previous field-based studies demonstrating that the excessive use of N fertilizer would increase N₂O and CH₄ emissions without proportionately increasing crop yield (Liu and Greaver 2009; Luo et al. 2017; Zaehle et al. 2011; Zhang et al. 2020a). For example, Hu et al. (2023) found that a reduction of up to 10% in N fertilizer for wheat and up to 30% for corn and rice was neutral for crop yield but would reduce net GHG emissions by 14.5%-25%. Therefore, our results highlight the tangible benefits of N fertilizer optimization for sustainable agricultural development, as evidenced by a reduction of up to 12.8% in GHGI under the SSP126 scenario (Figure 7-6).

The adoption of cover cropping practices, exemplified by planting peas in the fallow period, also contributed to climate change mitigation (Figure 7-7). Our results indicate that, on average, the adoption of cover cropping practices increased SOC sequestration rates by about 31 Tg C yr⁻¹ and N₂O emissions by about 0.15 Tg N yr⁻¹, respectively, across all future climate scenarios. Using peas as cover crops not only enriches soil N supply for subsequent crops through the process of biological N fixation but also increases carbon inputs into the soil. This, in turn, directly enhances both N₂O emissions and the SOC sequestration rate (Poeplau and Don 2015; Wortman et al. 2012). Meanwhile, it indirectly stimulates N₂O emissions by incorporating cover crop residues into the soil, thereby providing additional nutrients, or by increasing the carbon supply derived from photosynthesis in active growing root systems (Webb et al. 2000). Furthermore, our results suggest a reduction in CH₄ emissions when cover cropping practices are implemented. This reduction may

be attributed to the depletion of soil water, promoting the formation of aerobic soil environments that inhibit methanogenesis processes and CH₄ production. Notably, our results indicate that the largest mitigation potential for cover cropping is under the SSP245 scenario. This is mainly due to a substantially increased SOC sequestration rate, along with moderately increased N₂O emissions compared to the SSP126 and SSP585 scenarios. Specifically, non-CO₂ GHG emissions were estimated at 309 Tg CO₂-eq year⁻¹, 315 Tg CO₂-eq year⁻¹, and 445 Tg CO₂-eq year⁻¹ under the SSP126, SSP245, and SSP585 scenarios, respectively, and SOC-sequestered CO₂ under the three scenarios were estimated at 181 Tg CO₂-eq year⁻¹, 226 Tg CO₂-eq year⁻¹, and 253 Tg CO₂-eq year⁻¹, respectively. Consequently, the sequestered SOC under the SSP245 scenario largely offset the non-CO₂ GHG emissions when compared to the other two scenarios. Unraveling the effects of cover cropping on net GHG balance is complex because it influences both the SOC sequestration rate and non-CO₂ GHG emissions (Abdalla et al. 2019). Additionally, our analysis reveals that cover cropping practices have, on average, led to a 14.8% decrease in crop production across all future climate scenarios (Figure 7-8), aligning with existing research (Alvarez et al. 2017; Garba et al. 2022; Malone et al. 2022; Nielsen et al. 2016). For example, a review by Tonitto et al. (2006) reported a 10% yield reduction in primary crops after the implementation of cover cropping. Similarly, Alvarez et al. (2017) found an 8% reduction in corn yields following cover cropping compared to a fallow control. The reduction in crop yield can primarily be attributed to soil water depletion by cover crops. This, in turn, reduces plant-available soil moisture for subsequent crops, particularly exacerbating crop yield losses when this practice is implemented prior to dry growing seasons (Deines et al. 2023).

In terms of crop rotation practice, our results suggest that implementing this practice could also contribute to climate change mitigation; however, it concurrently reduced the overall crop

production (Figures 7-10 and 7-11). Specifically, implementing crop rotation (with legume crops) resulted in reductions of 22.9%, 17.4%, and 13.1% in net GHG balance under the SSP126, SSP245, and SSP585 scenarios, respectively, but it also reduced overall crop production by 19.8%, 18.9%, and 16.9% under these scenarios, respectively. The larger net GHG emissions from continuous corn are likely due to the increased N fertilizer amounts compared to corn-soybean rotations, as observed in other studies (Behnke et al. 2018; Halvorson et al. 2008; Hoben et al. 2011). Conversely, the reduced overall crop production is mainly due to the lower yield of soybean relative to corn. Our findings are consistent with previous studies (Behnke et al. 2018; Parkin and Kaspar 2006; Snyder et al. 2009). For example, Snyder et al. (2009) found that continuous corn resulted in two to three times higher N₂O emissions but produced four to five times the food yield in caloric value compared to the corn-soybean-wheat rotation. Behnke et al. (2018) reported that corn-soybean rotation diminished N₂O emissions by 2 kg ha⁻¹ yr⁻¹ compared to continuous corn. Consequently, our results suggest that the incorporation of crop rotation with legume crops could be a promising strategy for achieving sustainable agricultural intensification, potentially reducing both production risks and environmental impacts (Shah et al. 2021).

7.4.2 Uncertainty and implications

Several types of uncertainties persist in this study, including model parameter, structure, and forcing data uncertainties. Firstly, the DLEM includes a large number of parameters, whereas the lack of sufficient data for model calibration and validation causes uncertainties, particularly regarding the responses of crop yield and GHG emissions to various CSA practices (e.g., no tillage, crop rotation, and cover cropping). Secondly, the simplified representation of key processes in the DLEM also introduces uncertainty to the simulation results. For example, the current DLEM representation of groundwater and irrigation practice is relatively simple, which could lead to

biased simulated soil moisture that, in turn, could affect crop yield and GHG emission predictions under future climate scenarios. Moreover, the DLEM currently does not account for crop adaptation to climate change, as well as farmers' preparedness and response strategies to climate extremes (Annan and Schlenker 2015). The exclusion of these adaptive processes within the model may further induce uncertainties in future projections. Lastly, the input data driving the DLEM introduces uncertainty as well. For example, the CSA scenarios we assumed might diverge from the real-world situation due to economic considerations, which may compromise the effectiveness of our derived conclusions. Furthermore, future climate scenarios contain significant uncertainties due to their dependence on unpredictable variables such as human behavior and policy decisions (O'Neill et al. 2016). These climate scenarios are also subject to the inherent limitations of current climate models, particularly in their handling of complex Earth system feedbacks like cloud formation and ocean circulation (Flato et al. 2014). Addressing these limitations could further improve future simulation estimates.

Our analysis indicates that implementing CSA practices such as no tillage, N fertilizer reduction, cover cropping, and crop rotation practices significantly reduced the net GHG balance under future climate scenarios. These findings bring forth crucial implications, urging policymakers and agricultural practitioners to advocate for these practices for both environmental sustainability and climate change mitigation. While these CSA practices are promising in reducing net GHG emissions, some practices concurrently pose some challenges to food security due to associated reductions in crop yield. This necessitates the development of supportive strategies and innovative solutions to offset yield reduction and ensure sustainable food supplies. Additionally, given the diverse impacts under different climate scenarios, adaptive management strategies that consider the specific implications of each scenario are essential. The differences in outcomes under

these future climate scenarios underscore the importance of implementing context-specific strategies for climate mitigation within the agricultural sector. These implications collectively demonstrate that while the adoption of CSA practices is crucial for mitigating climate change and promoting sustainability, careful consideration and balance of associated challenges, particularly in food security, are essential.

7.5 Conclusion

This study assessed the long-term impacts of four CSA practices—no tillage, crop rotation, cover cropping, and N fertilizer reduction—on crop production, net GHG balance, and GHGI in U.S. croplands across various future climate scenarios, including SSP126, SSP245, and SSP585. Our results indicate that these CSA practices significantly reduced the net GHG balance in U.S. croplands, with average reductions of 18.9%, 10.3%, 28.6%, and 17.8% for no tillage, N fertilizer reduction, cover cropping, and crop rotation, respectively, across the three climate scenarios. Moreover, while no tillage and N fertilizer reduction only marginally impacted crop production, cover cropping and crop rotation resulted in substantial reductions, estimated at 14.7% and 18.5%, respectively. Consequently, our results underscore the need to consider the associated impacts on food security when implementing CSA practices. Additionally, the variations in mitigation potential under different climate scenarios emphasize the imperative for comprehensive, scenario-specific CSA strategies for climate change mitigation and sustainable development within the agricultural sector. Overall, our study provides invaluable insights and nuanced understanding of the implications of distinct CSA practices under varied future climate scenarios. These insights are crucial for informing policy and decision-making processes in aligning CSA practices with long-term sustainability and food security goals.

References

- Abdalla, M., Hastings, A., Cheng, K., Yue, Q., Chadwick, D., Espenberg, M., Truu, J., Rees, R.M., & Smith, P. (2019). A critical review of the impacts of cover crops on nitrogen leaching, net greenhouse gas balance and crop productivity. *Global Change Biology*, *25*, 2530-2543
- Abdalla, M., Osborne, B., Lanigan, G., Forristal, D., Williams, M., Smith, P., & Jones, M.B. (2013). Conservation tillage systems: a review of its consequences for greenhouse gas emissions. *Soil Use and Management*, *29*, 199-209
- Alvarez, R., & Steinbach, H.S. (2009). A review of the effects of tillage systems on some soil physical properties, water content, nitrate availability and crops yield in the Argentine Pampas. *Soil and Tillage Research*, *104*, 1-15
- Alvarez, R., Steinbach, H.S., & De Paepe, J.L. (2017). Cover crop effects on soils and subsequent crops in the pampas: A meta-analysis. *Soil and Tillage Research*, *170*, 53-65
- Annan, F., & Schlenker, W. (2015). Federal crop insurance and the disincentive to adapt to extreme heat. *American Economic Review*, *105*, 262-266
- Bai, X., Huang, Y., Ren, W., Coyne, M., Jacinthe, P.A., Tao, B., Hui, D., Yang, J., & Matocha, C. (2019). Responses of soil carbon sequestration to climate-smart agriculture practices: A meta-analysis. *Global Change Biology*, *25*, 2591-2606
- Behnke, G.D., Zuber, S.M., Pittelkow, C.M., Nafziger, E.D., & Villamil, M.B. (2018). Long-term crop rotation and tillage effects on soil greenhouse gas emissions and crop production in Illinois, USA. *Agriculture, Ecosystems & Environment*, *261*, 62-70
- Beillouin, D., Cardinael, R., Berre, D., Boyer, A., Corbeels, M., Fallot, A., Feder, F., & Demenois, J. (2021). A global overview of studies about land management, land-use change, and climate change effects on soil organic carbon. *Global Change Biology*, *n/a*
- Bondeau, A., Smith, P.C., Zaehle, S., Schaphoff, S., Lucht, W., Cramer, W., Gerten, D., Lotze-Campen, H., Müller, C., & Reichstein, M. (2007). Modelling the role of agriculture for the 20th century global terrestrial carbon balance. *Global Change Biology*, *13*, 679-706
- Cavigelli, M.A., Grosso, S.J.D., Liebig, M.A., Snyder, C.S., Fixen, P.E., Venterea, R.T., Leytem, A.B., McLain, J.E., & Watts, D.B. (2012). US agricultural nitrous oxide emissions: context, status, and trends. *Frontiers in Ecology and the Environment*, *10*, 537-546
- Cui, Z., Yue, S., Wang, G., Meng, Q., Wu, L., Yang, Z., Zhang, Q., Li, S., Zhang, F., & Chen, X. (2013). Closing the yield gap could reduce projected greenhouse gas emissions: a case study of maize production in China. *Global Change Biology*, *19*, 2467-2477
- De Baets, S., Poesen, J., Meersmans, J., & Serlet, L. (2011). Cover crops and their erosion-reducing effects during concentrated flow erosion. *CATENA*, *85*, 237-244
- Deines, J.M., Guan, K., Lopez, B., Zhou, Q., White, C.S., Wang, S., & Lobell, D.B. (2023). Recent cover crop adoption is associated with small maize and soybean yield losses in the United States. *Global Change Biology*, *29*, 794-807
- Del Grosso, S.J., Mosier, A.R., Parton, W.J., & Ojima, D.S. (2005). DAYCENT model analysis of past and contemporary soil N₂O and net greenhouse gas flux for major crops in the USA. *Soil and Tillage Research*, *83*, 9-24
- FAO (2013). *Climate-smart agriculture: sourcebook*. Rome, Italy: Food and Agriculture Organization of the United Nations (FAO)
- Farooq, M., Flower, K.C., Jabran, K., Wahid, A., & Siddique, K.H.M. (2011). Crop yield and weed management in rainfed conservation agriculture. *Soil and Tillage Research*, *117*, 172-183
- Flato, G., Marotzke, J., Abiodun, B., Braconnot, P., Chou, S.C., Collins, W., Cox, P., Driouech, F., Emori, S., & Eyring, V. (2014). Evaluation of climate models. *Climate change 2013: the physical science basis. Contribution of Working Group I to the Fifth Assessment Report of the Intergovernmental Panel on Climate Change* (pp. 741-866): Cambridge University Press
- Garba, I.I., Bell, L.W., & Williams, A. (2022). Cover crop legacy impacts on soil water and nitrogen dynamics, and on subsequent crop yields in drylands: a meta-analysis. *Agronomy for Sustainable Development*, *42*, 34
- Grassini, P., & Cassman, K.G. (2012). High-yield maize with large net energy yield and small global warming intensity. *Proceedings of the National Academy of Sciences*, *109*, 1074-1079
- Guenet, B., Gabrielle, B., Chenu, C., Arrouays, D., Balesdent, J., Bernoux, M., Bruni, E., Caliman, J.-P., Cardinael, R., Chen, S., Ciais, P., Desbois, D., Fouche, J., Frank, S., Henault, C., Lugato, E., Naipal, V., Nesme, T.,

- Obersteiner, M., Pellerin, S., Powelson, D.S., Rasse, D.P., Rees, F., Soussana, J.-F., Su, Y., Tian, H., Valin, H., & Zhou, F. (2021). Can N₂O emissions offset the benefits from soil organic carbon storage? *Global Change Biology*, *27*, 237-256
- Halvorson, A.D., Del Grosso, S.J., & Reule, C.A. (2008). Nitrogen, Tillage, and Crop Rotation Effects on Nitrous Oxide Emissions from Irrigated Cropping Systems. *Journal of environmental quality*, *37*, 1337-1344
- Hoben, J.P., Gehl, R.J., Millar, N., Grace, P.R., & Robertson, G.P. (2011). Nonlinear nitrous oxide (N₂O) response to nitrogen fertilizer in on-farm corn crops of the US Midwest. *Global Change Biology*, *17*, 1140-1152
- Howeler, R.H., Ezumah, H.C., & Midmore, D.J. (1993a). Tillage systems for root and tuber crops in the tropics. *Soil and Tillage Research*, *27*, 211-240
- Howeler, R.H., Ezumah, H.C., & Midmore, D.J. (1993b). Tillage systems for root and tuber crops in the tropics. *Soil and Tillage Research*, *27*, 211-240
- Hu, C., Sadras, V.O., Wang, Z., Du, W., Lei, X., Yang, M., Zhao, L., Zhang, P., Liu, J., Lu, G., Yang, X., & Zhang, S. (2023). Yield- and protein-neutral reduction in fertilizer rate for wheat, maize and rice can reduce the release of reactive nitrogen and greenhouse gas emissions in China. *Environmental Research Letters*, *18*, 064031
- Huang, Y., Ren, W., Grove, J., Poffenbarger, H., Jacobsen, K., Tao, B., Zhu, X., & McNear, D. (2020). Assessing synergistic effects of no-tillage and cover crops on soil carbon dynamics in a long-term maize cropping system under climate change. *Agricultural and Forest Meteorology*, *291*, 108090
- Huang, Y., Ren, W., Wang, L., Hui, D., Grove, J.H., Yang, X., Tao, B., & Goff, B. (2018). Greenhouse gas emissions and crop yield in no-tillage systems: A meta-analysis. *Agriculture, Ecosystems & Environment*, *268*, 144-153
- Hutchinson, J.J., Campbell, C.A., & Desjardins, R.L. (2007). Some perspectives on carbon sequestration in agriculture. *Agricultural and Forest Meteorology*, *142*, 288-302
- IPCC (2019). Climate Change and Land: an IPCC special report on climate change, desertification, land degradation, sustainable land management, food security, and greenhouse gas fluxes in terrestrial ecosystems [P.R. Shukla, J. Skea, E. Calvo Buendia, V. Masson-Delmotte, H.-O. Pörtner, D. C. Roberts, P. Zhai, R. Slade, S. Connors, R. van Diemen, M. Ferrat, E. Haughey, S. Luz, S. Neogi, M. Pathak, J. Petzold, J. Portugal Pereira, P. Vyas, E. Huntley, K. Kissick, M. Belkacemi, J. Malley, (eds.)]
- Lal, R. (2004). Soil carbon sequestration to mitigate climate change. *Geoderma*, *123*, 1-22
- Lipper, L., Thornton, P., Campbell, B.M., Baedeker, T., Braimoh, A., Bwalya, M., Caron, P., Cattaneo, A., Garrity, D., & Henry, K. (2014). Climate-smart agriculture for food security. *Nature Climate Change*, *4*, 1068-1072
- Liu, L., & Greaver, T.L. (2009). A review of nitrogen enrichment effects on three biogenic GHGs: the CO₂ sink may be largely offset by stimulated N₂O and CH₄ emission. *Ecology Letters*, *12*, 1103-1117
- Luo, Z., Wang, E., Xing, H., Smith, C., Wang, G., & Cresswell, H. (2017). Opportunities for enhancing yield and soil carbon sequestration while reducing N₂O emissions in rainfed cropping systems. *Agricultural and Forest Meteorology*, *232*, 400-410
- Lutz, F., Herzfeld, T., Heinke, J., Rolinski, S., Schaphoff, S., Von Bloh, W., Stoorvogel, J.J., & Müller, C. (2019). Simulating the effect of tillage practices with the global ecosystem model LPJmL (version 5.0-tillage). *Geoscientific Model Development*, *12*, 2419-2440
- Malone, L.C., Mourtzinis, S., Gaska, J.M., Lauer, J.G., Ruark, M.D., & Conley, S.P. (2022). Cover crops in a Wisconsin annual cropping system: Feasibility and yield effects. *Agronomy journal*, *114*, 1052-1067
- Mangalassery, S., Sjögersten, S., Sparkes, D.L., Sturrock, C.J., Craigon, J., & Mooney, S.J. (2014). To what extent can zero tillage lead to a reduction in greenhouse gas emissions from temperate soils? *Scientific Reports*, *4*, 4586
- McDermid, S.S., Mearns, L.O., & Ruane, A.C. (2017). Representing agriculture in Earth System Models: Approaches and priorities for development. *Journal of Advances in Modeling Earth Systems*, *9*, 2230-2265
- Montgomery, D.R. (2007). Soil erosion and agricultural sustainability. *Proceedings of the National Academy of Sciences*, *104*, 13268-13272
- Mosier, A.R., Halvorson, A.D., Reule, C.A., & Liu, X.J. (2006). Net global warming potential and greenhouse gas intensity in irrigated cropping systems in northeastern Colorado. *Journal of environmental quality*, *35*, 1584-1598
- Mueller, N.D., Gerber, J.S., Johnston, M., Ray, D.K., Ramankutty, N., & Foley, J.A. (2012). Closing yield gaps through nutrient and water management. *Nature*, *490*, 254-257
- Myhre, G., Shindell, D., Bréon, F.M., Collins, W., Fuglestedt, J., Huang, J., Koch, D., Lamarque, J.F., Lee, D., Mendoza, B., Nakajima, T., Robock, A., Stephens, G., Takemura, T., & Zhang, H. (2013). Anthropogenic and natural radiative forcing. In *Climate Change 2013: The Physical Science Basis. Contribution of Working*

- Group I to the Fifth Assessment Report of the Intergovernmental Panel on Climate Change. T.F. Stocker, D. Qin, G.-K. Plattner, M. Tignor, S.K. Allen, J. Doschung, A. Nauels, Y. Xia, V. Bex, and P.M. Midgley, Eds. Cambridge University Press, pp. 659-740. In
- Nielsen, D.C., Vigil, M.F., Lyon, D.J., Higgins, R.K., Hergert, G.W., & Holman, J.D. (2016). Cover crops can affect subsequent wheat yield in the Central Great Plains. *Crops & Soils*, *49*, 51-53
- O'Neill, B.C., Tebaldi, C., Van Vuuren, D.P., Eyring, V., Friedlingstein, P., Hurtt, G., Knutti, R., Kriegler, E., Lamarque, J.-F., & Lowe, J. (2016). The scenario model intercomparison project (ScenarioMIP) for CMIP6. *Geoscientific Model Development*, *9*, 3461-3482
- Ogle, S.M., Alsaker, C., Baldock, J., Bernoux, M., Breidt, F.J., McConkey, B., Regina, K., & Vazquez-Amabile, G.G. (2019). Climate and soil characteristics determine where no-till management can store carbon in soils and mitigate greenhouse gas emissions. *Scientific Reports*, *9*, 11665
- Ogle, S.M., Swan, A., & Paustian, K. (2012). No-till management impacts on crop productivity, carbon input and soil carbon sequestration. *Agriculture, Ecosystems & Environment*, *149*, 37-49
- Pan, S., Bian, Z., Tian, H., Yao, Y., Najjar, R.G., Friedrichs, M.A.M., Hofmann, E.E., Xu, R., & Zhang, B. (2021). Impacts of Multiple Environmental Changes on Long-term Nitrogen Loading from the Chesapeake Bay Watershed. *Journal of Geophysical Research: Biogeosciences*, *126*, e2020JG005826
- Parkin, T.B., & Kaspar, T.C. (2006). Nitrous Oxide Emissions from Corn–Soybean Systems in the Midwest. *Journal of environmental quality*, *35*, 1496-1506
- Pittelkow, C.M., Liang, X., Linquist, B.A., van Groenigen, K.J., Lee, J., Lundy, M.E., van Gestel, N., Six, J., Venterea, R.T., & van Kessel, C. (2015a). Productivity limits and potentials of the principles of conservation agriculture. *Nature*, *517*, 365-368
- Pittelkow, C.M., Linquist, B.A., Lundy, M.E., Liang, X., Van Groenigen, K.J., Lee, J., Van Gestel, N., Six, J., Venterea, R.T., & Van Kessel, C. (2015b). When does no-till yield more? A global meta-analysis. *Field Crops Research*, *183*, 156-168
- Plaza-Bonilla, D., Álvaro-Fuentes, J., Bareche, J., Pareja-Sánchez, E., Justes, É., & Cantero-Martínez, C. (2018). No-tillage reduces long-term yield-scaled soil nitrous oxide emissions in rainfed Mediterranean agroecosystems: A field and modelling approach. *Agriculture, Ecosystems & Environment*, *262*, 36-47
- Poepflau, C., & Don, A. (2015). Carbon sequestration in agricultural soils via cultivation of cover crops—A meta-analysis. *Agriculture, Ecosystems & Environment*, *200*, 33-41
- Powelson, D.S., Stirling, C.M., Jat, M.L., Gerard, B.G., Palm, C.A., Sanchez, P.A., & Cassman, K.G. (2014). Limited potential of no-till agriculture for climate change mitigation. *Nature Climate Change*, *4*, 678-683
- Reckling, M., Bergkvist, G., Watson, C.A., Stoddard, F.L., Zander, P.M., Walker, R.L., Pristeri, A., Toncea, I., & Bachinger, J. (2016a). Trade-offs between economic and environmental impacts of introducing legumes into cropping systems. *Frontiers in plant science*, *7*, 669
- Reckling, M., Hecker, J.-M., Bergkvist, G., Watson, C.A., Zander, P., Schläfke, N., Stoddard, F.L., Eory, V., Topp, C.F.E., & Maire, J. (2016b). A cropping system assessment framework—evaluating effects of introducing legumes into crop rotations. *European Journal of Agronomy*, *76*, 186-197
- Ren, W., Tian, H., Tao, B., Huang, Y., & Pan, S. (2012). China's crop productivity and soil carbon storage as influenced by multifactor global change. *Global Change Biology*, *18*, 2945-2957
- Ren, W., Tian, H., Xu, X., Liu, M., Lu, C., Chen, G., Melillo, J., Reilly, J., & Liu, J. (2011). Spatial and temporal patterns of CO₂ and CH₄ fluxes in China's croplands in response to multifactor environmental changes. *Tellus B: Chemical and Physical Meteorology*, *63*, 222-240
- Robertson, G.P., & Grace, P.R. (2004). Greenhouse gas fluxes in tropical and temperate agriculture: the need for a full-cost accounting of global warming potentials. *Tropical Agriculture in Transition—Opportunities for Mitigating Greenhouse Gas Emissions?* (pp. 51-63): Springer
- Rochette, P. (2008). No-till only increases N₂O emissions in poorly-aerated soils. *Soil and Tillage Research*, *101*, 97-100
- Rogelj, J., den Elzen, M., Höhne, N., Fransen, T., Fekete, H., Winkler, H., Schaeffer, R., Sha, F., Riahi, K., & Meinshausen, M. (2016). Paris Agreement climate proposals need a boost to keep warming well below 2 °C. *Nature*, *534*, 631-639
- Roy, E.D., Wagner, C.R.H., & Niles, M.T. (2021). Hot spots of opportunity for improved cropland nitrogen management across the United States. *Environmental Research Letters*, *16*, 035004
- Sainju, U.M., Whitehead, W.F., & Singh, B.P. (2003). Cover crops and nitrogen fertilization effects on soil aggregation and carbon and nitrogen pools. *Canadian Journal of Soil Science*, *83*, 155-165
- Salinas-Garcia, J.R., Hons, F.M., & Matocha, J.E. (1997). Long-term effects of tillage and fertilization on soil organic matter dynamics. *Soil Science Society of America Journal*, *61*, 152-159

- Schneider, F., Don, A., Hennings, I., Schmittmann, O., & Seidel, S.J. (2017). The effect of deep tillage on crop yield – What do we really know? *Soil and Tillage Research*, 174, 193-204
- Shah, K.K., Modi, B., Pandey, H.P., Subedi, A., Aryal, G., Pandey, M., & Shrestha, J. (2021). Diversified crop rotation: an approach for sustainable agriculture production. *Advances in Agriculture*, 2021, 1-9
- Shakoor, A., Shahbaz, M., Farooq, T.H., Sahar, N.E., Shahzad, S.M., Altaf, M.M., & Ashraf, M. (2021). A global meta-analysis of greenhouse gases emission and crop yield under no-tillage as compared to conventional tillage. *Science of the Total Environment*, 750, 142299
- Shang, Z., Abdalla, M., Xia, L., Zhou, F., Sun, W., & Smith, P. (2021). Can cropland management practices lower net greenhouse emissions without compromising yield? *Global Change Biology*, 27, 4657– 4670
- Sheehy, J., Six, J., Alakukku, L., & Regina, K. (2013). Fluxes of nitrous oxide in tilled and no-tilled boreal arable soils. *Agriculture, Ecosystems & Environment*, 164, 190-199
- Snyder, C.S., Bruulsema, T.W., Jensen, T.L., & Fixen, P.E. (2009). Review of greenhouse gas emissions from crop production systems and fertilizer management effects. *Agriculture, Ecosystems & Environment*, 133, 247-266
- Sun, W., Canadell, J.G., Yu, L., Yu, L., Zhang, W., Smith, P., Fischer, T., & Huang, Y. (2020). Climate drives global soil carbon sequestration and crop yield changes under conservation agriculture. *Global Change Biology*, 26, 3325-3335
- Thompson, R.L., Lassaletta, L., Patra, P.K., Wilson, C., Wells, K.C., Gressent, A., Koffi, E.N., Chipperfield, M.P., Winiwarter, W., Davidson, E.A., Tian, H., & Canadell, J.G. (2019). Acceleration of global N₂O emissions seen from two decades of atmospheric inversion. *Nature Climate Change*, 9, 993-998
- Tian, H., Chen, G., Liu, M., Zhang, C., Sun, G., Lu, C., Xu, X., Ren, W., Pan, S., & Chappelka, A. (2010). Model estimates of net primary productivity, evapotranspiration, and water use efficiency in the terrestrial ecosystems of the southern United States during 1895–2007. *Forest Ecology and Management*, 259, 1311-1327
- Tian, H., Chen, G., Lu, C., Xu, X., Hayes, D.J., Ren, W., Pan, S., Huntzinger, D.N., & Wofsy, S.C. (2015). North American terrestrial CO₂ uptake largely offset by CH₄ and N₂O emissions: toward a full accounting of the greenhouse gas budget. *Climatic Change*, 129, 413-426
- Tian, H., Lu, C., Ciais, P., Michalak, A.M., Canadell, J.G., Saikawa, E., Huntzinger, D.N., Gurney, K.R., Sitch, S., Zhang, B., Yang, J., Bousquet, P., Bruhwiler, L., Chen, G., Dlugokencky, E., Friedlingstein, P., Melillo, J., Pan, S., Poulter, B., Prinn, R., Saunio, M., Schwalm, C.R., & Wofsy, S.C. (2016). The terrestrial biosphere as a net source of greenhouse gases to the atmosphere. *Nature*, 531, 225-228
- Tian, H., Lu, C., Melillo, J., Ren, W., Huang, Y., Xu, X., Liu, M., Zhang, C., Chen, G., & Pan, S. (2012). Food benefit and climate warming potential of nitrogen fertilizer uses in China. *Environmental Research Letters*, 7, 044020
- Tian, H., Xu, R., Pan, S., Yao, Y., Bian, Z., Cai, W.-J., Hopkinson, C.S., Justic, D., Lohrenz, S., Lu, C., Ren, W., & Yang, J. (2020). Long-Term Trajectory of Nitrogen Loading and Delivery From Mississippi River Basin to the Gulf of Mexico. *Global Biogeochemical Cycles*, 34, e2019GB006475
- Tian, H., Xu, X., Lu, C., Liu, M., Ren, W., Chen, G., Melillo, J., & Liu, J. (2011). Net exchanges of CO₂, CH₄, and N₂O between China's terrestrial ecosystems and the atmosphere and their contributions to global climate warming. *Journal of Geophysical Research: Biogeosciences*, 116
- Tonitto, C., David, M.B., & Drinkwater, L.E. (2006). Replacing bare fallows with cover crops in fertilizer-intensive cropping systems: A meta-analysis of crop yield and N dynamics. *Agriculture, Ecosystems & Environment*, 112, 58-72
- United Nations, U.N. (2015). Framework Convention on Climate Change: Adoption of the Paris Agreement. In Van den Putte, A., Govers, G., Diels, J., Gillijns, K., & Demuzere, M. (2010). Assessing the effect of soil tillage on crop growth: A meta-regression analysis on European crop yields under conservation agriculture. *European Journal of Agronomy*, 33, 231-241
- Van Kessel, C., Venterea, R., Six, J., Adviento-Borbe, M.A., Linnquist, B., & van Groenigen, K.J. (2013). Climate, duration, and N placement determine N₂O emissions in reduced tillage systems: a meta-analysis. *Global Change Biology*, 19, 33-44
- Watson, R.T., Noble, I.R., Bolin, B., Ravindranath, N.H., Verardo, D.J., & Dokken, D.J. (2000). *Land use, land-use change and forestry: a special report of the Intergovernmental Panel on Climate Change*. Cambridge University Press
- Webb, J., Harrison, R., & Ellis, S. (2000). Nitrogen fluxes in three arable soils in the UK. *European Journal of Agronomy*, 13, 207-223

- Wortman, S.E., Francis, C.A., Bernards, M.L., Drijber, R.A., & Lindquist, J.L. (2012). Optimizing cover crop benefits with diverse mixtures and an alternative termination method. *Agronomy journal*, *104*, 1425-1435
- Xia, L., Lam, S.K., Chen, D., Wang, J., Tang, Q., & Yan, X. (2017). Can knowledge-based N management produce more staple grain with lower greenhouse gas emission and reactive nitrogen pollution? A meta-analysis. *Global Change Biology*, *23*, 1917-1925
- Yao, Y., Tian, H., Shi, H., Pan, S., Xu, R., Pan, N., & Canadell, J.G. (2020). Increased global nitrous oxide emissions from streams and rivers in the Anthropocene. *Nature Climate Change*, *10*, 138-142
- Yoo, J., Woo, S.-H., Park, K.-D., & Chung, K.-Y. (2016). Effect of no-tillage and conventional tillage practices on the nitrous oxide (N₂O) emissions in an upland soil: soil N₂O emission as affected by the fertilizer applications. *Applied Biological Chemistry*, *59*, 787-797
- You, Y., Tian, H., Pan, S., Shi, H., Bian, Z., Gurgel, A., Huang, Y., Kicklighter, D., Liang, X.-Z., Lu, C., Melillo, J., Miao, R., Pan, N., Reilly, J., Ren, W., Xu, R., Yang, J., Yu, Q., & Zhang, J. (2022). Incorporating dynamic crop growth processes and management practices into a terrestrial biosphere model for simulating crop production in the United States: Toward a unified modeling framework. *Agricultural and Forest Meteorology*, *325*, 109144
- Yu, Z., Lu, C., Hennessy, D.A., Feng, H., & Tian, H. (2020). Impacts of tillage practices on soil carbon stocks in the US corn-soybean cropping system during 1998 to 2016. *Environmental Research Letters*, *15*, 014008
- Zaehle, S., Ciais, P., Friend, A.D., & Prieur, V. (2011). Carbon benefits of anthropogenic reactive nitrogen offset by nitrous oxide emissions. *Nature Geoscience*, *4*, 601-605
- Zhang, J., Tian, H., Shi, H., Zhang, J., Wang, X., Pan, S., & Yang, J. (2020). Increased greenhouse gas emissions intensity of major croplands in China: Implications for food security and climate change mitigation. *Global Change Biology*, *26*, 6116-6133
- Zhang, Y., Sheng, J., Wang, Z., Chen, L., & Zheng, J. (2015). Nitrous oxide and methane emissions from a Chinese wheat-rice cropping system under different tillage practices during the wheat-growing season. *Soil and Tillage Research*, *146*, 261-269
- Zhou, M., Zhu, B., Wang, S., Zhu, X., Vereecken, H., & Brüggemann, N. (2017). Stimulation of N₂O emission by manure application to agricultural soils may largely offset carbon benefits: A global meta-analysis. *Global Change Biology*, *23*, 4068-4083
- Zomer, R.J., Bossio, D.A., Sommer, R., & Verchot, L.V. (2017). Global Sequestration Potential of Increased Organic Carbon in Cropland Soils. *Scientific Reports*, *7*, 15554

Chapter 8. Conclusions and future works

This study focuses on quantifying the impacts of multiple environmental forcings and climate-smart agricultural (CSA) practices on the magnitude and spatiotemporal variations of crop yield, net greenhouse gas (GHG) balance, and GHGI in U.S. croplands under both historical and future climate scenarios. To meet these objectives, we developed a unified agricultural model by integrating the strengths of conventional crop models in representing crop growth processes and agricultural management practices into a terrestrial biosphere model (TBM), the Dynamic Land Ecosystem Model (DLEM), to fulfill cross-scale agricultural application needs (e.g., adaptation and mitigation). Combining this new model and multi-source datasets, we used a data-driven systems approach to simulate the production of major crops in U.S., estimated yield losses caused by compound climate extremes, and analyzed the temporal variations in the sensitivity of U.S. agricultural systems to these extreme events over the past decades. Furthermore, we quantified the combined impacts of multiple management practices and environmental changes on the magnitude and spatiotemporal variations of net soil GHG balance in U.S. croplands. We also predicted future crop production, net GHG balance, and GHGI in U.S. croplands for the period 2020-2100 under various future climate scenarios, including SSP126, SSP245, and SSP585. Additionally, we evaluated the long-term impacts of four CSA practices—no tillage, crop rotation, cover cropping, and reduced N fertilization—on crop production, net GHG balance, and GHGI in U.S. croplands across these future climate scenarios.

The major conclusions are as follows:

- (1) Site-scale evaluations demonstrate that the newly developed agricultural model effectively simulates the seasonal variations and magnitudes of leaf area index and aboveground biomass and

annual yield. Regarding the regional-scale performance, the simulated spatial pattern of crop production is also consistent with ground survey data. Meanwhile, the national average crop production estimated by the new agricultural model has increased by 1–4 times from the 1960s to the 2010s, which is consistent with the observed trend.

(2) Both U.S. corn and soybean yields show heightened sensitivity to short-term droughts (spanning 1-3 months) and heatwaves during their critical reproductive stages, typically occurring from July to September for droughts and July to August for heatwaves. Among the extreme climate events, droughts tend to have a more detrimental impact on yields compared to heatwaves. The simultaneous occurrence of droughts and heatwaves exacerbates yield loss substantially, resulting in yield losses of 29.6% for corn and 25.4% for soybean, surpassing the effects of single extreme events. Our results also indicate a decreased sensitivity in corn and soybean yields to concurrent droughts and heatwaves from 1964 to 2018.

(3) During 1960-2018, U.S. croplands acted as a net carbon sink with an average SOC sequestration rate of $13.2 \pm 1.16 \text{ Tg C year}^{-1}$ but a net source of N_2O and CH_4 with average emission rates of $0.39 \pm 0.02 \text{ Tg N year}^{-1}$ and $0.21 \pm 0.01 \text{ Tg C year}^{-1}$, respectively. When translated into the GWP100 metric, the simulated national average net GHG emission rate of U.S. agricultural soils was $121.9 \pm 11.46 \text{ Tg CO}_2\text{-eq yr}^{-1}$. Thus, net effort of soil GHG emission during this study period was a contributor of climate warming. Sequestered SOC offset ~28% of the climate-warming effects resulting from non- CO_2 GHG emissions, and the proportion of this offset increased over time. The Midwest hub contributed ~47% of the national total net GHG balance, followed by the Northern Plains hub at ~21%. Our factorial analysis over 1960-2018 indicated that N fertilization use was the dominant factor promoting net GHG emissions from U.S. croplands and explained ~47% of the total changes, while reduced tillage and rising atmospheric

CO₂ attenuated net GHG emissions from U.S. croplands.

(4) The predicted national net GHG balance exhibited a significant increase under the SSP245 and SSP585 scenarios, with the most pronounced increase occurring under the high-emission trajectory SSP585, averaging 236 Tg CO₂-eq year⁻¹. In contrast, the net GHG balance under the 126 scenario remains relatively stable throughout the 2020-2100 period. Crop production shows significant interannual variations but does not exhibit significant trends across all climate scenarios. This imbalance, where the net GHG balance increases disproportionately compared to crop production, leads to an increased GHGI, which is estimated to be 0.26 CO₂-eq Tg⁻¹, 0.34 CO₂-eq Tg⁻¹, and 0.42 CO₂-eq Tg⁻¹ under the SSP126, SSP245, and SSP585 scenarios, respectively. Increased temperatures and atmospheric CO₂ concentrations are the primary contributors to the significant increase in net GHG balance and GHGI. The heightened GHGI raises serious concerns about deviating from the sustainable agriculture goal of mitigating climate change and ensuring food security, and underscores the urgent need for immediate intervention through CSA practices.

(5) Under future climate scenarios, the four CSA practices—no tillage, N fertilizer reduction, cover cropping (planting peas in the fallow period), and crop rotation—significantly reduced the net GHG balance in U.S. croplands, with average reductions of 18.9%, 10.3%, 28.6%, and 17.8%, respectively. Moreover, while no tillage and N fertilizer reduction only marginally impacted crop production, cover cropping and crop rotation resulted in substantial reductions, estimated at 14.7% and 18.5%, respectively, underscoring the need to consider the associated impacts on food security when implementing these CSA practices. Additionally, the variations in mitigation potential under different climate scenarios further emphasize the imperative for comprehensive, scenario-specific CSA strategies for climate change mitigation and sustainable development within the agricultural sector.

Several potential future works include:

(1) Due to the large uncertainty in model simulations, further improving key model processes is necessary. For example, the current DLEM representation of groundwater and irrigation practice (i.e., without considering irrigation amount and frequency) is relatively simple, which could lead to biased simulated soil moisture that, in turn, might affect yield and GHG emission predictions. Therefore, I plan to further improve the DLEM, especially soil-related processes, to better simulate key variables.

(2) Several other important CSA practices, such as biochar application and alternate wetting and drying irrigation practice, are not included in the DLEM. Therefore, I plan to incorporate the mechanistic representations of these CSA practices into the DLEM to analyze their impacts on crop production and the net GHG balance.

(3) Our current analysis of the climate benefits of CSA practices still lacks robust verification, which may compromise the conclusions drawn. Therefore, I plan to collect more in-situ measurements on the impacts of different CSA practices on crop production and net GHG emissions and their dependences on background environments (e.g., crop types and climates) to more accurately calibrate, validate, and corroborate model simulations.

(4) The future CSA scenarios designed in this study do not account for the complexities of real-world implementation. Hence, I plan to integrate related factors (e.g., economic factors and available agricultural resources) into the CSA scenario design and subsequent analysis to provide more practical suggestions and solutions.

(5) Currently, our evaluations primarily focus on the impacts of agricultural management practices on crop production and net GHG balance, while neglecting other environmental impacts like nutrient loading, which may lead to biased evaluation. Therefore, I plan to comprehensively

evaluate the impacts of different CSA practices to obtain more accurate and unbiased assessments, thereby providing actionable, science-based recommendations. For example, I plan to explore the optimization of N fertilization practices to obtain an optimal balance among crop yield, net GHG emissions, nutrient loading, air pollution, and economic benefits.

(6) I plan to broaden my research scope from the U.S. agricultural system to the global agricultural system. For example, I will evaluate the potential of different CSA practices and their combinations to address climate change mitigation and global food security, as well as provide science-based guidance for achieving these objectives.